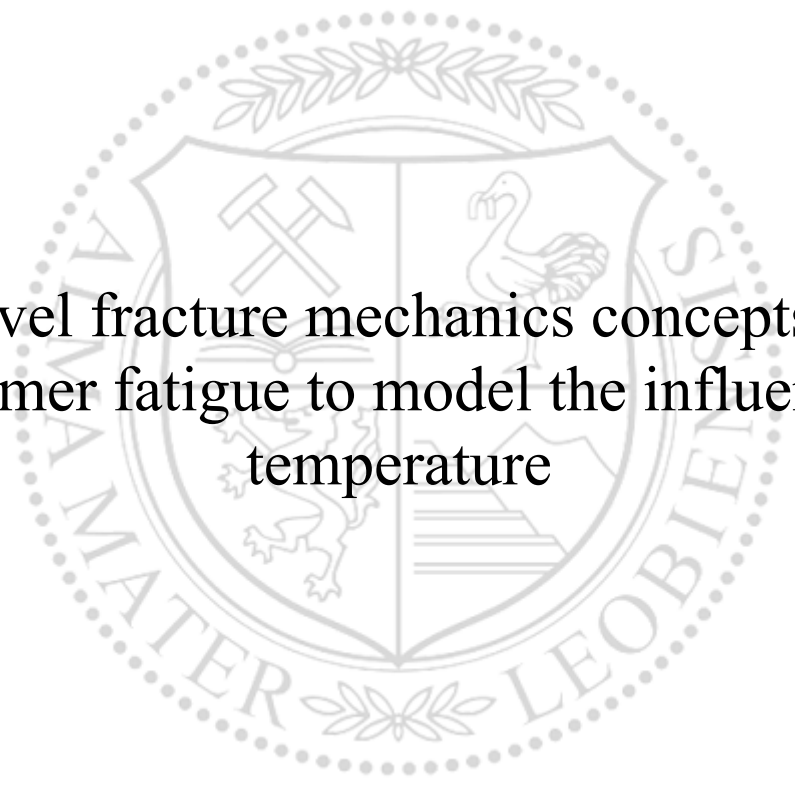Chair of Materials Science and Testing of Polymers

Doctoral Thesis

Novel fracture mechanics concepts in elastomer fatigue to model the influence of temperature

Jacopo Schieppati

July 2022

MONTANUNIVERSITÄT LEOBEN

www.unileoben.ac.at

AFFIDAVIT

I declare on oath that I wrote this thesis independently, did not use other than the specified sources and aids, and did not otherwise use any unauthorized aids.

I declare that I have read, understood, and complied with the guidelines of the senate of the Montanuniversität Leoben for "Good Scientific Practice".

Furthermore, I declare that the electronic and printed version of the submitted thesis are identical, both, formally and with regard to content.

Date 20.07.2022

_____
Signature Author
Jacopo Schieppati

"You were not made to live like brutes,

but to follow virtue and knowledge"

("Fatti non foste a viver come bruti,
ma per seguir virtute e canoscenza")

Ulysses, Inferno, Canto XXVI

Dante Alighieri, *Divine Comedy*

"That didn't hurt! 'Cause I'm made of rubber"

Monkey D Luffy, Chapt. 2

Eichiro Oda, *One Piece*

Acknowledgment

First of all, I would like to thank Dr. Bernd Schrittesser, the person who gave me the opportunity of working at PCCL GmbH and starting the adventure of my PhD. He has been a guide during this journey: without him and his trust in me, this experience would not have been possible.

I would also like to express my gratitude to my supervisor, Prof. Gerald Pinter. Over the years, he has always shown his trust and esteem for me, supporting me with his scientific opinions and advice. He has been a reference and guide as well as a source of inspiration throughout the years.

I would like to offer my thanks to the colleagues from the company Semperit Technische Produkte Gesellschafts m.b.H., ho funded the research and with whom we have fruitful scientific discussion. Special thanks go to DI Alfred Wondracek, Dr. Stefan Robin and Dr. Armin Holzner.

I would also like to thank the colleagues from PCCL and WPK, with whom I have had the pleasure of spending these years. A special thanks goes to Dr. Andreas Hausberger and Dr. Roman Kerschbaumer who allow me to prolong my experience at PCCL and supported me over the month of the PhD. Furthermore, I would like to acknowledge Dr. Winoj Balasooriya, with whom it was easy to discuss science and life but also joke together. Another mention is necessary to DI Tanja Stiller, with whom I shared much more than work and science. Without her, these years would not have been the same.

My journey into the field of rubbers would never have begun without Prof. Claudia Marano. With her I had the honor and pleasure of collaborating during my first year as a researcher. I learned a lot in those months and that experience was fundamental for my PhD. I am glad that we were able to maintain a relationship that goes beyond the professional one. Moreover, I would like to thank the entire group of the "PolyEngLab" from Politecnico di Milano from the supervisors Marta, Francesco and Luca to the colleagues and friends Stefano, Tommaso, Marco Contino, Davide, Giancarlo, Federica and Marco Brambilla. They are all a source of motivation and inspiration, and I am grateful to have shared a piece of the road together.

My sincere gratitude also goes to the friends of a lifetime: Verga, Gibo, Ricky, Vince, Fiz, Maddi, Giulia, Robi, Davide, Zanna, Eli, Dario and Kenneth. They have always made me feel like I never

left home. This is something that only special people like true friends can accomplish. Thanks for the beers, the trips, the pizzas and all the time spent together.

The deepest gratitude goes to my parents, Lino and Patrizia. They have always supported me during the good and bad times. Although far from home, I have never felt alone. Thank you for the support, the trust and the love.

A final remembrance goes to those who left us over the years - Zio Renzo, Zio Pierluigi and Nonna Gianna. I know you would have been proud.

Abstract

Failure of elastomers is often related to fatigue. In fact, the mechanical properties of these materials make them suitable in applications in which cyclic loading overlaps with large static loads. Due to the peculiar mechanical properties, namely hyperelasticity and viscoelasticity, the investigation of elastomers' mechanical and fatigue properties is not a trivial task.

Temperature strongly influences the mechanical and fatigue behavior of elastomers. Despite the awareness of the effects of temperature dating back to the early studies of rubber fatigue, only little effort has been made to rationalize this behavior and develop a systematic model that allows this effect to be taken into account.

Thus, this thesis aims to analyze the fatigue of a non-crystallizing elastomer and specifically to investigate the effect of temperature in order to create a model able to improve the fatigue predictions. At first, the influence of self-heating upon cyclic loading due to heat build-up was assessed considering different frequencies, and interesting observations about the temperature evolution during crack propagation were made. Furthermore, an equation for the evaluation of temperature in the thickness of samples was described. Second, the fatigue crack propagation of a filled elastomer was analyzed, considering several mechanical parameters and among them, the most influential for non-crystallizing elastomers was found to be frequency. Based on these findings, the influence of temperature on the mechanical behavior was investigated in terms of large and small deformations, evidencing a strong role of fillers on the overall mechanical properties. Moreover, the fatigue crack propagation at high temperatures was studied and a model to reduce the data to a fatigue master curve was developed. Finally, fatigue lifetime investigations were correlated with initial defect size and crack propagation results. This was possible by exploiting the fatigue master curve applied according to the surface temperature monitored in the fatigue tests as a consequence of heat build-up. These results were then verified through the particle size obtained from

microtomography measurements. Finally, a hyperelastic J-integral equation for notched specimens was developed, correlating the fatigue lifetime independently of the geometry.

Kurzfassung

Das Versagen von Elastomeren ist häufig auf Ermüdung zurückzuführen. Aufgrund ihrer mechanischen Eigenschaften eignen sich diese Werkstoffe für Anwendungen, bei denen sich zyklische Belastungen mit großen statischen Belastungen überlagern. Aufgrund der besonderen mechanischen Eigenschaften, nämlich der Hyperelastizität und der Viskoelastizität, ist die Untersuchung der mechanischen und Ermüdungseigenschaften von Elastomeren keine triviale Aufgabe.

Temperatur hat einen starken Einfluss auf das mechanische Verhalten und die Ermüdung von Elastomeren. Obwohl die Auswirkungen der Temperatur bereits in den ersten Studien zur Ermüdung von Elastomeren bekannt waren, wurde nur wenig Aufwand betrieben, dieses Verhalten einzuordnen und ein systematisches Modell zu entwickeln um diesen Effekt mitberücksichtigen zu können.

Daher zielt diese Arbeit darauf ab, die Ermüdung eines nicht kristallisierenden Elastomers zu analysieren und im Speziellen die Auswirkungen der Temperatur zu untersuchen, um ein Modell zu erstellen, das die Ermüdungsvorhersagen verbessert. Zunächst wurde der Einfluss der Selbsterwärmung bei zyklischer Belastung aufgrund von Wärmestau unter Berücksichtigung verschiedener Frequenzen untersucht, bei welchen interessanten Beobachtungen über die Temperaturentwicklung während der Rissausbreitung gemacht wurden. Darüber hinaus wurde die Bewertung der Temperatur über die Dicke in den Proben mit einer Gleichung beschrieben. Zweitens wurde die Ausbreitung von Ermüdungsrissen in gefüllten Elastomeren unter Berücksichtigung verschiedener mechanischer Parameter analysiert, wobei sich herausstellte, dass die Frequenz bei nicht kristallisierenden Elastomeren den größten Einfluss hat. Auf der Grundlage dieser Erkenntnisse wurde der Einfluss der Temperatur auf das mechanische Verhalten in Bezug auf große und kleine Verformungen untersucht, wo sich ein starker Einfluss der Füllstoffe auf die mechanischen Eigenschaften insgesamt zeigte. Darüber hinaus wurde das

Ermüdungsrisswachstum bei hohen Temperaturen untersucht und daraus ein Modell zur Reduzierung der Daten auf eine Ermüdungsmasterkurve entwickelt. Anschließend wurden Untersuchungen der Ermüdungslebensdauer mit der anfänglichen Defektgröße und den Ergebnissen der Rissausbreitung korreliert. Dies war möglich, indem die Ermüdungsmasterkurve entsprechend der in den Ermüdungsversuchen beobachteten Oberflächentemperatur als Folge der Wärmeentwicklung verwendet wurde. Diese Ergebnisse wurden dann anhand der aus Mikrotomographiemessungen gewonnenen Partikelgröße verifiziert. Schlussendlich wurde eine hyperelastische J-Integral-Gleichung für gekerbte Proben aufgestellt, welche mit der Ermüdungslebensdauer unabhängig von der Geometrie korreliert.

Table of Contents

Acronyms and Symbols

A	[mm^2]	area
a	[mm]	notch size
BIIR		bromobutyl rubber
BR		butadiene rubber
c	[mm]	crack length
C	[-]	Paris law parameter
c_0	[mm]	initial defect size
c_f	[mm]	final defect size
C_1	[MPa]	Mooney-Rivlin parameter
C_2	[MPa]	Mooney-Rivlin parameter
CB		Carbon Black
c_p	[J/kg·K]	specific heat
CRB		cracked round bar
D''	[Pa]	dynamic loss compliance
dc/dN	[mm/cycle]	crack growth rate
DMA		dynamic mechanical analysis
E^*	[Pa]	complex dynamic modulus
E'	[Pa]	dynamic storage modulus
E''	[Pa]	dynamic loss modulus
E_0	[Pa]	dynamic modulus in rubbery region
E_∞	[Pa]	dynamic modulus in glassy region
$E_{a,app}$	[kJ/mol]	activation energy
ECO		epichlorohydrin rubber
EPDM		ethylene-propylene-diene rubber
f	[Hz]	frequency

F	[N]	load (force)
F_{max}	[N]	maximum force
F_{min}	[N]	minimum force
G	[J/m^2]	tearing energy
G'	[Pa]	dynamic shear storage modulus
G''	[Pa]	dynamic shear loss modulus
G_0	[J/m^2]	critical tearing energy
G_{Grif}	[J/m^2]	energy release rate evaluated by Griffith
G_T	[J/m^2]	tearing energy at T
$G_{T,Tref}$	[J/m^2]	tearing energy at T shifted to T_{ref}
IR		infrared
J	[J/m^2]	J-integral
J_{max}	[J/m^2]	maximum J-integral
J_{min}	[J/m^2]	minimum J-integral
$k(\lambda)$		geometrical factor for tearing energy
L	[m]	thickness
l	[-]	deformation
LFA		laser flash analysis
m	[-]	Paris law parameter
NBR		acrylonitrile butadiene rubber
N	[-]	number of cycles
N_f	[-]	number of cycles to failure
NR		natural rubber
P	[Pa]	pressure
q	[J]	heat
R	[-]	load ratio (with respect to F or σ)
R_ε	[-]	load ratio (with respect to s or ε)
r	[mm]	distance from the crack tip
r_{out}	[mm]	external radius
S	[J/K]	entropy

s	[mm]	displacement
SBR		styrene-butadiene rubber
s_{max}	[mm]	maximum displacement
s_{min}	[mm]	minimum displacement
s_T	[-]	fatigue shift factor
T	[°C]	temperature
t	[s]	time
$\tan\delta$	[-]	loss factor
T_g	[°C]	glass transition temperature
T_{ref}	[°C]	reference temperature
T_s	[°C]	surface temperature
U	[J]	energy
U_{diss}	[J]	dissipated energy
U_{in}	[J]	input energy
U_{sto}	[J]	elastically stored energy
V	[m^3]	volume
W_0	[J/m^3]	strain energy density
ε	[%]	strain
ε_0	[%]	strain amplitude
ε_{max}	[%]	maximum strain
κ	[W/m·K]	thermal conductivity
λ	[-]	stretch ratio
μ-CT		X-ray microtomography
ρ	[kg/m^3]	density
σ	[MPa]	stress
σ_0	[MPa]	stress amplitude
σ^*	[MPa]	reduced stress
ω	[Hz]	perturbing frequency

1 Introduction

Elastomers have unique mechanical properties that make them indispensable in several applications such as tires, seals, hoses, belts, dampers, and so on. Each of the several applications in which elastomers are employed have their own specific requirements; however, bearing large strains and cyclic deformations is the main characteristic to be fulfilled. This is guaranteed by the peculiar structure of elastomers that leads to outstanding and unique elastic behavior. In fact, through the vulcanization (i.e., curing of rubbers) process, chemical crosslinks are introduced between the macromolecules of a polymer with a glass transition temperature below room temperature. The presence of chemical crosslinks hinders the possibility of sliding between the polymeric macromolecules; hence, it allows elastomers to withstand huge deformations. For this characteristic, elastomers are classified as hyperelastic materials.

The chemical structure induced by vulcanization has major consequences on the mechanical behavior of these materials, which are characterized by entropic elasticity. By using a thermodynamic approach, it is possible to demonstrate that upon stretching a rubber piece, an internal restoring force is generated. During the deformation, the macromolecules align with the loading direction, which results in a decrease of entropy. Once the external deformation is removed, the elastomer tends to recover the initial state in order to increase its entropic state. The restoring force is proportional through the temperature to the variation of entropy related to the deformation. In addition, due to the fact that elastomers' main component is the rubber matrix, their mechanical behavior is characterized by a certain degree of viscoelasticity. This is even more pronounced when considering filled elastomers: the introduction of fillers - typically the second main constituents of elastomer formulations – leads to a reduction in the mobility of macromolecules, affecting the viscoelastic response of the material.

Elastomers' components are typically subjected to cyclic loading even in the form of small vibrations. Thus, when considering the long-term behavior of structural materials, fatigue plays a major role. This process involves the repetition of loads that are smaller than the strength of the material, which leads to the accumulation of damage and the premature failure of the components. Fatigue initiates from cracks that nucleate from defects and inhomogeneities that are normally present in any materials. Subsequently, the nucleated microscopic cracks increase in size and coalesce up to failure. The analysis of rubber's fatigue started with the early work of Caldwell et al. in 1940 [1] and with the application of fracture mechanics to rubbers by Rivlin and Thomas in 1953 [2] and its successful application to fatigue [3,4]. Within these works, it was highlighted how an energetic approach based on the tearing energy is able to describe the fracture and fatigue behavior of rubbers.

Elastomers are hyperelastic materials characterized by entropic elasticity and viscoelasticity. Both of these characteristics are significantly influenced by temperature. On the one hand, the level of the entropic response of the elastomeric matrix is proportional to the temperature. On the other hand, temperature affects the degree of mobility of the polymer chains and thus the viscoelastic response of the material. Furthermore, a typical feature of viscoelastic materials is energy dissipation: upon cyclic loading, a part of the mechanical energy is dissipated and converted into heat. Due to the low thermal conductivity and large strains at which elastomer components are typically subjected, significant temperature increases are often observed. This phenomenon is known as heat build-up.

During cyclic loading, elastomers are subjected to different extents of temperature variation, either related to the environment or due to self-heating as a consequence of heat build-up. Therefore, the effect of temperature on the fatigue resistance of elastomers is extremely relevant for numerous applications. Already in 1964, Lake and Lindley [4] reported a drop of four order of magnitude of fatigue life passing from 0 °C to 100 °C for styrene-butadiene rubber (SBR), evidencing how this parameter strongly affects the fatigue resistance of elastomers. Although the influence of temperature on the fatigue of elastomers is a well-known phenomenon, little research has been focused on modeling its influence. Such a model is fundamental to increase the accuracy of lifetime predicting models for elastomer components.

2 Structure of the Thesis

The objective of the research presented in this thesis was to investigate several aspects of the fatigue of elastomers, with a particular focus on the effect of temperature. The final aim was to develop a model able to consider the effect of temperature on fatigue. To do so, several investigations were performed considering a carbon black-filled acrylonitrile butadiene rubber (NBR), and the results are presented in the framework of the state of the art. The structure of NBR makes this material resistant to fuels and oils due to its strong polarity; therefore, it is of fundamental importance in the oil and gas industry. Despite this, it has received little attention throughout the literature and this thesis aims to extend the knowledge of fatigue for this material as well.

A relevant focus was devoted to the analysis of self-heating as a consequence of heat build-up. Several aspects were considered, like the influencing parameters and how the temperature varies in the volume of the specimen. Furthermore, the investigation of heat build-up was extended to the case of a propagating crack. Subsequently, the fatigue behavior of elastomers was considered by analyzing the effect of several mechanical parameters. A particular focus was devoted to frequency, force control, waveform and load ratio and the consequences on fatigue crack propagation were described. Based on these fundamentals investigation, the effect of temperature on the mechanical behavior at both large and small deformations was analyzed, and several models to consider the impact of temperature on the fatigue of elastomers were presented. Finally, fracture mechanics-based methodologies were used to assess the lifetime of elastomers based on in-depth investigations on defect size and crack growth. In this context, a new tool for the analysis of accelerated fatigue through a J-integral approach for notched specimens was described.

The doctoral thesis is based on the following five publications that have all been published in refereed journals or refereed conference proceedings.

- *Publication 1*: Impact of temperature on the fatigue and crack growth behavior of rubbers [5]
- *Publication 2*: Heat build-up of rubbers during cyclic loading [6]
- *Publication 3*: Effect of mechanical loading history on fatigue crack growth of non-crystallizing rubber [7]
- *Publication 4*: Temperature impact on the mechanical and fatigue behavior of a non-crystallizing rubber [8]
- *Publication 5*: Fatigue analysis and critical defect size evaluation of filled NBR including temperature influence [9]

In the thesis, the methodology and the main findings are elaborated considering the state of the art and highlighting the results extending the level of existing knowledge. In the appendix, the papers are presented in their published state, including the authors, affiliations and detailed representation of the work done by the individual authors.

3 Heat Build-Up During Cyclic Loading

Rubbers subjected to cyclic loading normally show an increase in temperature as a consequence of heat build-up. In fact, during cyclic loading, part of the mechanical energy is dissipated and heat is generated within the volume of the object. This characteristic is an intrinsic property of viscoelastic materials such as the rubber matrix of elastomers. Considering a cyclic load, viscoelastic materials can be schematized as having an elastic component (Figure 3.1(a)) for which no energy is dissipated and a viscous component (Figure 3.1(b)) for which all energy is dissipated. Viscoelastic materials can be modeled as having both components (Figure 3.1(c)) and the resulting mechanical behavior is a combination of both: a fraction of the energy is stored while the rest is dissipated [10].
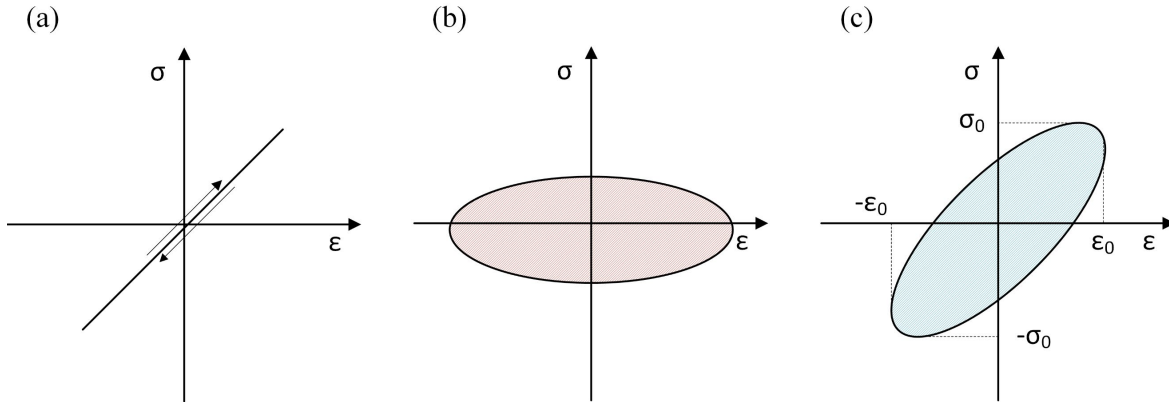

Figure 3.1 Schematic of the mechanical behavior under cyclic load for (a) elastic material, (b) viscous material and (c) viscoelastic material.

The dissipated energy in one cycle is the area below the hysteresis curve and for a viscoelastic material can be evaluated as [10,11]:

$$U = \int_0^{\frac{2\pi}{f}} \sigma \cdot d\varepsilon = \pi \varepsilon_0^2 E''(f,T) = \pi \sigma_0^2 D''(f,T) \qquad (3.1)$$

where f is the frequency, ε_0 the strain amplitude and $E''(f,T)$ the loss modulus, while σ_0 is the stress amplitude and $D''(f,T)$ the loss compliance. Therefore, at each cycle, a certain amount of energy is dissipated and (partially) converted into heat. Generally, due to non-adiabatic conditions, heat is exchanged with the surrounding environment at the specimen (or component) surface, limiting the extent of temperature rises. However, since rubbers possess low thermal conductivity [10], not all of the generated heat can be transferred fast enough to the surface and exchanged with the environment, which is why a significant increase in temperature is observed. It is worth noting that the higher the temperature the object reaches, the higher the gradient with environmental temperature will be, making it a larger driving force for the temperature reduction. A schematic of the temperature evolution as a consequence of heat build-up is reported in Figure 3.2.
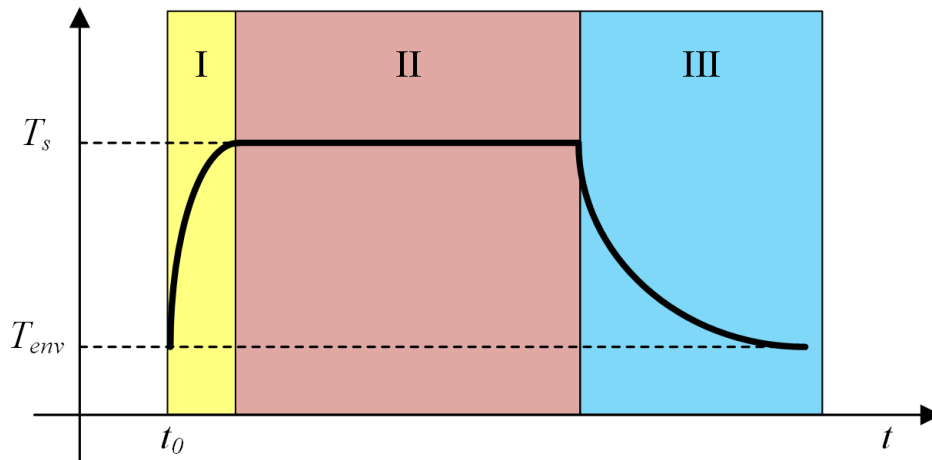

Figure 3.2 Schematic of the temperature evolution due to heat build-up upon cyclic loading.

Three phases can be evidenced:

- Phase I - transient phase of heating: immediately after the application of the load, the heat is generated in the volume due to energy dissipation and the temperature rises;
- Phase II - steady state: the temperature reaches an equilibrium since the flux of internal heat (generated heat) is the same as the external flux (heat exchanged with the environment);
- Phase III - transient phase of cooling: the load is removed and thus, the internal heat generation stops and the object starts to cool.

Generally, heat build-up is studied by measuring the temperature variation during cyclic loading and then it is analyzed by using different thermo-mechanical models [12–23]. The temperature increases due to heat build-up were also considered as predictor parameters for fatigue failure [24,25].

3.1 *Parameters influencing the heat build-up*

The extent of temperature variation depends on several parameters such as material stiffness, the frequency of oscillation, the loading amplitude and the thickness of the component [10]. These effects are well described by considering the rate of temperature increase, $\dot{\Delta T}$ [26,27]:

$$\dot{\Delta T} = \frac{\pi \cdot f \cdot \sigma_0 \cdot D''(f,T)}{4 \cdot c_p \cdot \rho} \qquad (3.2)$$

where f is the frequency, σ_0 is the stress amplitude, $D''(f,T)$ is the loss compliance, c_p is the specific heat and ρ is the density. Larger temperature increases are found with high loading amplitudes, large frequencies or for a material with large energy dissipation. On the other hand, a material with low specific heat (and thus, thermal conductivity) will result in larger rises in temperature. Kar and Bhowmick [28] verified the influences of different parameters on heat generation on both NR and SBR. They found that heat generation increases with the increase of hysteresis loss, frequency, specific heat, stress, stroke amplitude, filler loading, surface area of the filler and the temperature difference between the wall and the environment. Conversely, heat generation decreases with an increase of in temperature with respect to the T_g of the material, thermal conductivity and structure of the carbon black. Actually, when considering filled elastomers, another source of energy dissipation is represented by fillers, since they increase the friction during the stretch of the macromolecules [29]. Park et al. [30] reported that an increase of filler loading leads to larger heat generation. Considering the frequency, **Schieppati et al.** [5] examined experimentally the temperature evolution for a CB-filled NBR at different frequencies (Figure 3.3), observing that larger frequencies lead to higher temperature increases for a filled NBR, according to Equation (3.2). The effect of frequencies on temperature is clear when

considering that at higher frequencies, more energy is dissipated per second: therefore, in the same time frame, a higher amount of heat is generated.
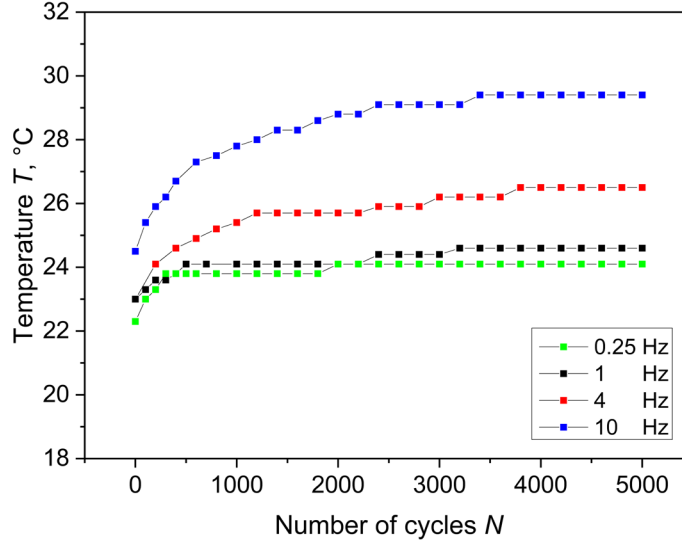

Figure 3.3 Surface temperature as a function of number of cycles at different frequencies observed during fatigue crack growth of CB-filled NBR. Reproduced from [5].

3.2 *Temperature profile in the sample thickness*

The temperature increases upon loading are evaluated using surface temperature values. However, due to the low thermal conductivity of elastomers, it is reasonable to believe that the temperature is not homogenous along the thickness. This was observed experimentally by Kerchman and Shaw [24], who reported a parabolic shape of the temperature in the thickness of a cylindrical specimen.

In order to model the internal temperature distribution, an equation for calculating the temperature profile along the thickness was obtained by **Schieppati et al.** [6] by considering the heat equation with a heating source, i.e., the internal heat generated due to heat build-up. This is described by the differential equation:

$$\rho c_p \frac{\partial T}{\partial t} - \nabla(\kappa \nabla T) = \dot{q} \tag{3.3}$$

where ρ is the density, c_p the specific heat, κ the thermal conductivity and $\dot{q}$ the internal heat generated per unit volume.

In order to achieve a simplified analytical solution, some assumptions were made. First of all, it was considered that the thermal conductivity was constant with temperature. This assumption was justified by the experimental results shown in Figure 3.4 obtained by **Schieppati et al.** [5]; the thermal conductivity was found to be substantially constant in a large range of temperature, corresponding to the range of utilization of elastomers.

Since κ is constant over temperature, Equation (3.3) becomes:

$$\rho c_p \frac{\partial T}{\partial t} - \kappa \nabla^2 T = \dot{q} \qquad (3.4)$$
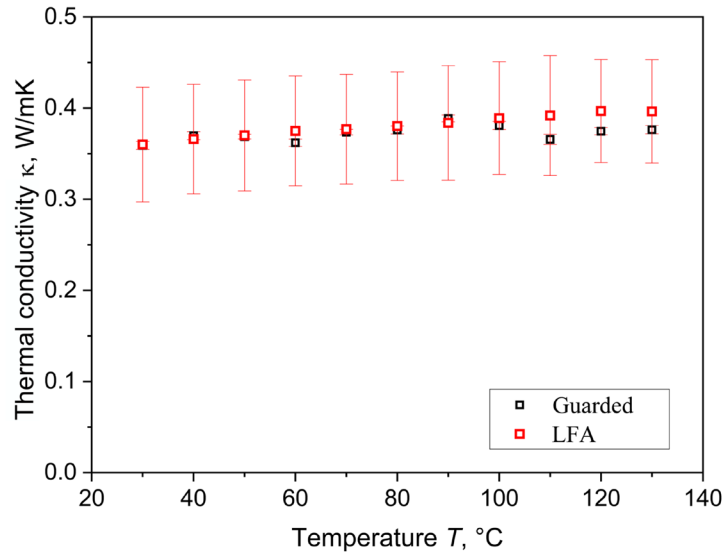

Figure 3.4 Values of thermal conductivity for the material between 30 and 130 °C measured with two different techniques: in black, the data obtained with the guarded heat method and in red, the one obtained with the Laser Flash Method (LFA). Reproduced from [5].

This equation could be used to calculate the steady state and the transient regions [31] by considering an overall energy balance [32]. However, for an accurate determination, an efficient evaluation of the external fluxes such as convection and irradiation would be required, which are often difficult to estimate with sufficient precision. Nevertheless, more accurate conclusions could be drawn by considering the temperature in the steady state. In this case, the internal and external heat flux are the same and the temperature is in equilibrium. In the steady state condition, the rate of variation of temperature is zero ($\partial T/\partial t$=0).

Considering then a rectangular plate geometry and assuming that the temperature only varies in the thickness, it was possible to simplify the problem to a one-dimensional case. Taking into account all of these considerations, Equation (3.4) can be rewritten as:

$$\frac{d^2 T}{dx^2} = -\frac{\dot{q}}{\kappa}$$

(3.5)

The analytical solution for the temperature profile along the thickness can be retrieved by considering the following boundary condition: at the surface, the temperature T_S is constant, while the continuity of the function in the center of the specimen implies that dT/dx=0. The solution to the problem is a parabolic function of the thickness L:

$$T = T_S + \frac{\dot{q}}{2\kappa}\left(\frac{L^2}{4} - x^2\right)$$

(3.6)

The temperature will be maximum in the center for $x = 0$:

$$T = T_S + \frac{\dot{q}L^2}{8\kappa}$$

(3.7)

In the case of cyclic loading, the specific energy dissipated per unit second (i.e., specific dissipated power), $\dot{q}$, can be approximated as:

$$\dot{q} = \frac{f \cdot U_{diss}}{V}$$

(3.8)

where U_{diss} is the energy dissipated per cycle, f the frequency of oscillation and V the volume of the specimen. It is worth noting that this is a simplification since not all dissipated energy is converted into heat; however, this represents an overestimation and for that reason, a conservative estimation.

Using Equation (3.6), **Schieppati et al.** [6] calculated the temperature profile along the thickness for pure shear at different frequencies (Figure 3.5). It was observed that the temperature was substantially constant along the thickness in all tested conditions, with minor variations only at higher frequencies. That was connected to the low thickness of the specimens (4 mm): the small path of the heat to the surface led to a fast exchange with the environment, limiting the temperature rises. The data suggested that for pure shear

specimens, the temperature can be considered homogenous along the thickness and can be accounted as the surface temperature.
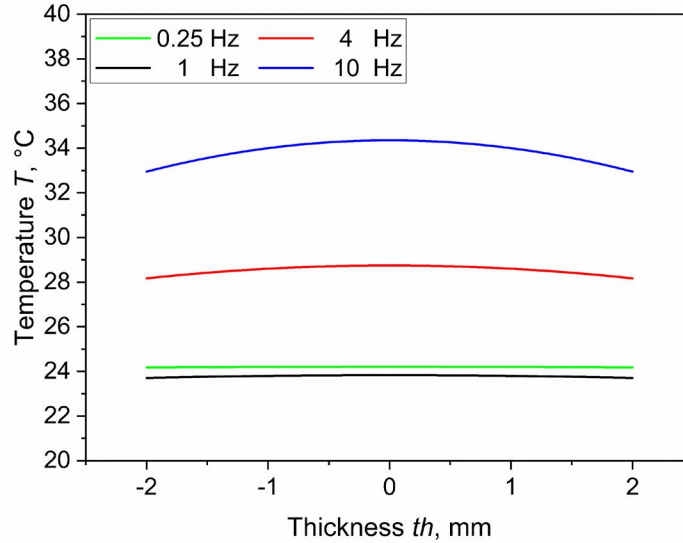

Figure 3.5 Calculated temperature profiles along the thickness of pure shear specimens of CB-filled NBR at different frequencies. Reproduced from [6].

3.3 *Temperature evolution during crack propagation*

According to Perrson and Brener [33], when considering a propagating crack in a viscoelastic material in the rubbery state, an increase in temperature in front of the crack tip is expected due to high viscoelastic dissipations in the proximity of the crack tip. Considering a propagating crack, a perturbing frequency, ω, is originated; this is proportional to the propagation speed of the crack, v, and inversely proportional to the distance from the crack tip, r (i.e., $\omega = v/r$). Therefore, three different regions can be distinguished depending on the distance from the crack tip (see Figure 3.6). In the most inner part, the perturbing frequency is so high that the material behavior is fully glass-like (E_∞), while in the outer part, the material behaves fully rubber-like (E_0). In between these extremes, the intermediate region shows high energy dissipation: the storage elastic $E(\omega)$ is in the glass transition region and thus, at the maximum of loss factor (and loss modulus).

Schieppati et al. [5] analyzed the heat build-up considering the evolution of the temperature during crack growth experiments. In particular, they measured the surface
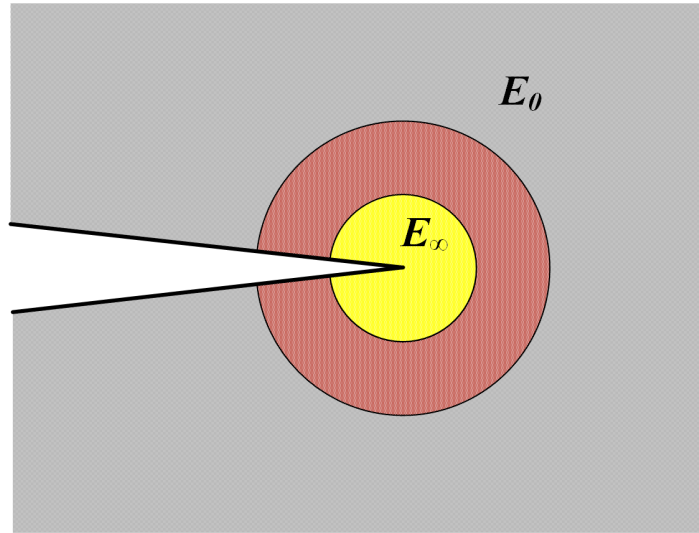
Figure 3.6 Schematic of a viscoelastic material in the vicinity of the crack tip subdivided into three regions according to [33]: the outer region (gray) behaves fully rubber-like (E_0), the inner part (yellow) behaves fully glass-like (E_∞), while the intermediate region (red) is a transition region where bulk viscoelastic energy dissipation occurs.

temperature using an IR sensor placed around 10 mm in front of the initial crack tip (i.e., notch). A general overview of the temperature evolution during these tests is reported in Figure 3.7. Once the load was applied, the temperature increased rapidly in the first cycles, while afterwards, a plateau value was observed. Since in the experiment reported in Figure 3.7 the IR sensor position was fixed, some further observations were made, also considering the temperature evolution as a function of the crack length (Figure 3.8). In both plots, the gray areas corresponded to the number of cycles and the position in which the crack was below the IR sensor. From both plots, it was possible to observe a slight increase in temperature in front of the crack tip and that when the crack length increased in size and passed the IR sensor, the surface temperature dropped, since no strain was applied in the monitored region.
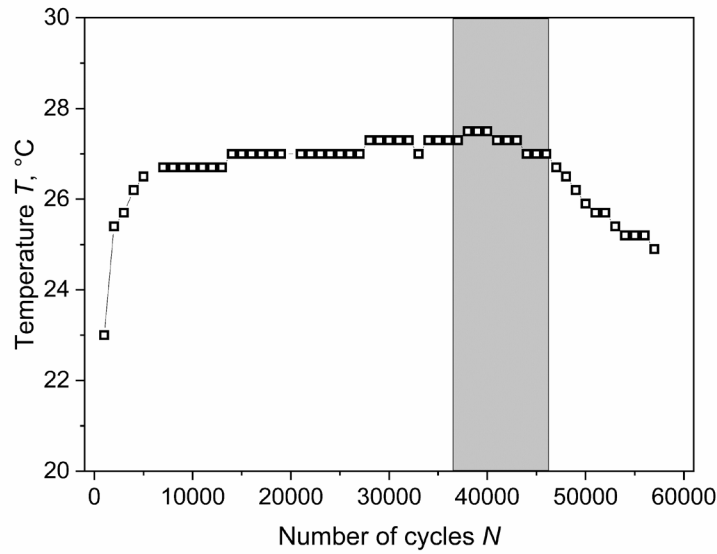
Figure 3.7 Surface temperature as a function of the number of cycles. The gray area corresponds to the number of cycles at which the crack was below the IR sensor. Reproduced from [5].
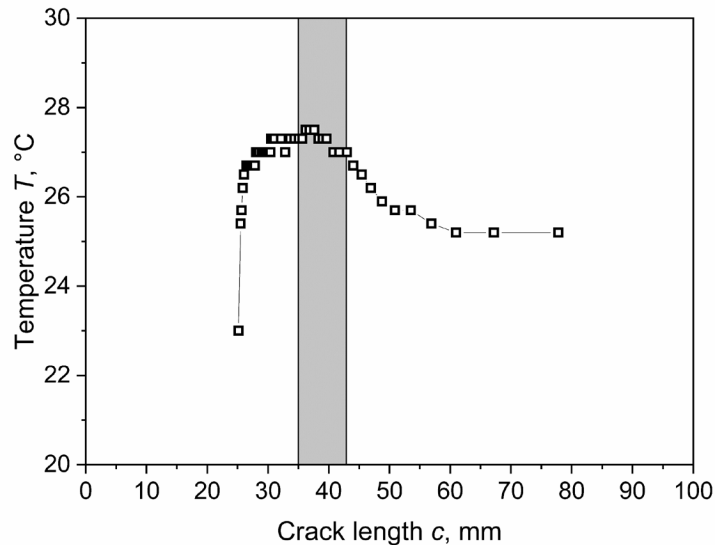

Figure 3.8 Surface temperature as a function of crack length. The gray area corresponds to the position at which the crack was below the IR sensor. Reproduced from [5].

More details about the temperature evolution during the fatigue crack growth experiment can be obtained by using an IR camera. Kerchman and Shaw [24] and **Schieppati et al.** [6] reported the temperature evolution during the propagation of a crack for different specimen geometries, Single Edge Notched Tension (SENT) and Pure Shear (Figure 3.9) specimens, respectively. In both cases, larger temperatures were observed in front of crack

tip as a consequence of stress/strain intensification and to larger dissipations in this area. Moreover, with smaller cracks, the temperature was more homogenously distributed in the specimen, while with larger cracks, the temperature rises were localized in the area closer to the crack tip. In addition, it was evidenced how the crack propagation affects the temperature distribution in the specimen: from a symmetric distribution along the height of the specimen, to an asymmetric distribution due to the crack developed towards the upper clamp (Figure 3.9).
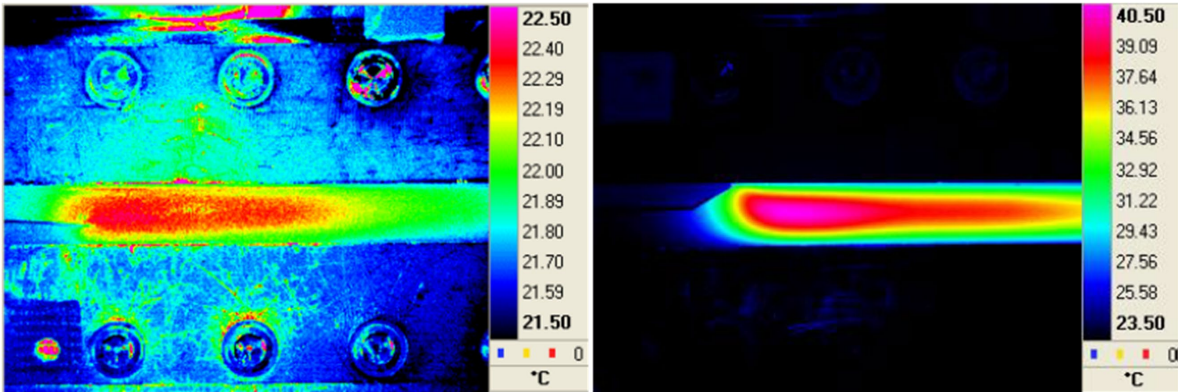

Figure 3.9 Temperature distribution recorded with an IR camera at different stages of crack propagation with a pure shear specimen. Reproduced from [6].

4 Effect of Loading Parameters on Fatigue Crack Growth

The fracture mechanics approach to study the fatigue of elastomers has its foundations in the energy balance of a body of area, A, containing a stationary crack:

$$\frac{dU_{in}}{A} - \frac{dU_{sto}}{A} = \frac{dU_{diss}}{A} \tag{4.1}$$

where U_{in} is the input energy (external forces' work), U_{sto} is the recoverable elastic strain energy and U_{diss} is the dissipated energy. From this energy balance, Griffith [34] defined the energy release rate G_{Grif} as the energy dissipated during fracture per unit of newly created area at a fixed displacement, s:

$$G_{Grif} = -\frac{dU}{dA}\bigg|_s \tag{4.2}$$

From this definition, Rivlin and Thomas [2] introduced the tearing energy of rubbers, representing the work expended irreversibly per unit area of crack advancement - the left end side of Equation (4.1) - and expressed it as function of the strain energy density, W_0:

$$G = \frac{dU_{in}}{A} - \frac{dU_{sto}}{A} = k(\lambda) \cdot W_0 \cdot c \tag{4.3}$$

where c is the crack length and $k(\lambda)$ is a function of the stretch ratio. Furthermore, they derived simplified semi-empirical equations for the evaluation of tearing energy for different specimens' geometry.

Generally, the fracture mechanics approach involves the study of the propagation of a pre-inserted crack and its behavior at different values of tearing energy. Thus, by plotting the crack growth rate against the tearing energy, it is possible to describe the fatigue behavior of elastomers. An example of such a plot is represented in Figure 4.1. As depicted, four regions with different regimes can be identified, as described by Lake and Lindley [35]:

- Regime 1: the energy is below a threshold value and the crack propagation is only due to environmental attack and independent of the mechanical loading;
- Regime 2: the energy is above the threshold and there is a transition area;
- Regime 3: the crack growth follows a power law, Paris' law [36];
- Regime 4: the energy is so high that the crack growth is unstable and substantially infinite.
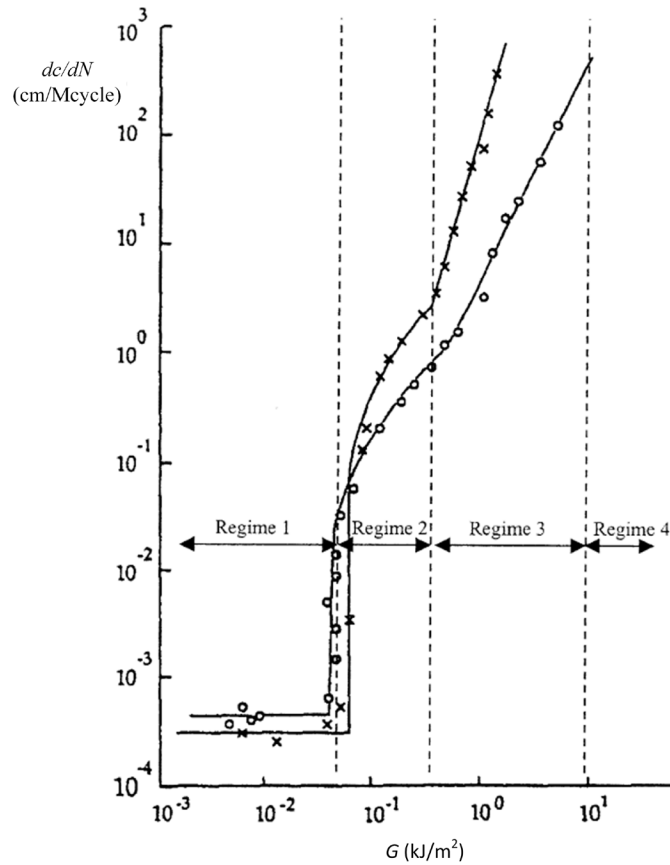

Figure 4.1 Regimes of fatigue crack growth in unfilled SBR (crosses) and NR (circles). Reproduced from [37].

This classification does not hold for all rubber compounds: either the transition region is suppressed or more complex empirical relationships are present [38]. Nevertheless, the analysis of the stable crack growth (Regime 3) involves the use of Paris' law:

$$\frac{dc}{dN} = CG^m \tag{4.4}$$

16

where *dc/dN* represents the crack growth rate per cycle and *G* the tearing energy, while *C* and *m* are material-dependent constants.

Fatigue (and thus, cyclic loading) can be characterized by several parameters that affect the fatigue resistance of rubbers. These parameters can be classified as related to the mechanical load, the environment and the composition of the elastomer [39]. Considering the mechanical load, this can be described by several parameters such as the frequency, the input load (force or displacement), the shape of the periodic function and the load ratio (and so the minimum load). Each of these parameters may affect the mechanical response of the material in a different way and therefore, its fatigue behavior.

4.1   *Frequency effect and energetic consideration of cyclic heating*

A fundamental parameter when considering polymers and rubbers undergoing cyclic loading is the frequency. In fact, viscoelastic materials are time-dependent, so frequency affects their mechanical behavior. According to viscoelastic theories, high frequencies are associated with stiffer mechanical behavior. The different mechanical response at distinct frequencies is then reflected in their fatigue resistance. On the whole, frequencies affect the fatigue behavior of rubbers to different extents depending on the ability of the material to crystallize under strain. In fact, strain crystallizing rubbers such as NR are less affected by a variation of frequency [38], even for complex compounds such as SBR/BR/NR [40]. Conversely, non-crystallizing rubbers seem to be strongly influenced by frequency. Busfield et al. [41] reported that higher frequencies induce an increase of fatigue resistance for SBR, especially at high tearing energy. Similar conclusions were drawn by Major et al. [42] on both EPDM and SBR.

Schieppati et al. [7] investigated the effect of frequency on a CB-filled NBR. As reported in Figure 4.2(a), the different frequencies influence the mechanical behavior, as evidenced by the hysteresis loop: increasing slopes were observed with increasing frequency due to stiffer mechanical behavior as a consequence of viscoelastic effects. The results in terms of fatigue crack growth as a function of tearing energy (Figure 4.2(b)) confirmed the effect of frequency on non-crystallizing rubbers: higher fatigue crack growth rates were

17

found with lower frequencies, with an increase of approximately one order of magnitude passing from 10 to 0.25 Hz.

It is worth noting that different frequencies would affect the temperature of the material due to heat build-up (see Chapter 3) and thus, indirectly, the fatigue behavior due to viscoelasticity. In fact, a viscoelastic material at a higher temperature behaves more elastically and dissipates less energy. Therefore, at low frequencies (and lower temperature increases), more energy will be dissipated and lower energy will be available for crack propagation, resulting in a lower crack growth rate.
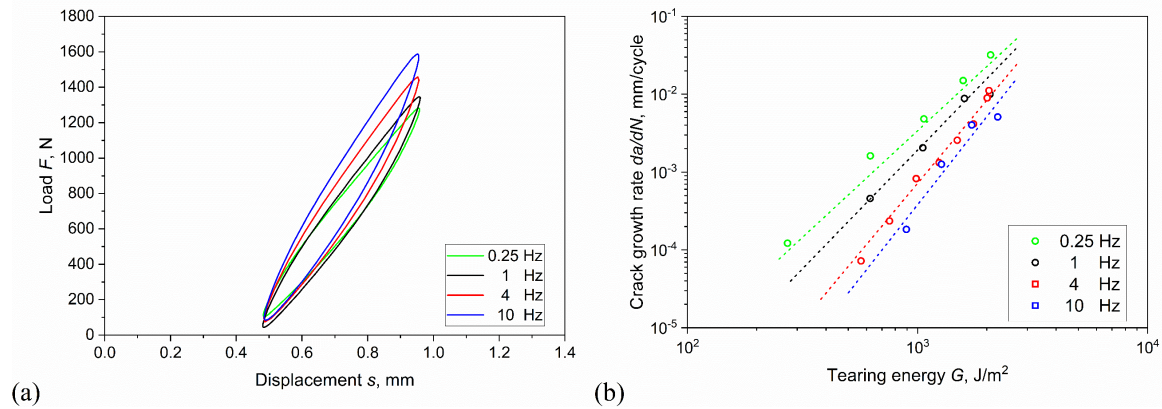

(a)

(b)

Figure 4.2 (a) Hysteresis curves obtained during fatigue crack growth measurements at the same maximum strain and (b) fatigue crack growth rate as a function of tearing energy at different frequencies for a CB-filled NBR at room temperature and load ratio R_ε of 0.5 with a sinusoidal load. Reproduced from [7].

This aspect was investigated by **Schieppati et al.** [3] by analyzing the energy during fatigue crack growth experiments at different frequencies. They evaluated the dissipated energy as the area inside the hysteresis, while the stored energy was considered as the area below the unloading curve. The dissipated and stored energies at the different frequencies were compared by normalizing with respect to the total mechanical energy (sum of both dissipated and stored energies). The resulting plot of the normalized energies as a function of the number of cycles is shown in Figure 4.3. As depicted, no differences were observed and thus, the same proportion of energy was dissipated independently of the frequencies. This evidenced that the energy dissipation is not the cause of the differences in the crack growth propagation at different frequencies. These investigations supported the idea reported by Lake and Lindley [4] and Lindley [43] in which the effect of frequency was explained

considering that the overall fatigue crack growth rate is related to a static and a dynamic growth component, which are additive as :

$$\left(\frac{dc}{dN}\right)_{overall} = \frac{1}{f} \cdot \left(\frac{dc}{dN}\right)_{static} + \left(\frac{dc}{dN}\right)_{dynamic} \tag{4.5}$$

The first component is related to the viscoelastic effect and connected to the time necessary for completing one cycle, i.e., the reciprocal of the frequency, while the dynamic component is frequency independent. The static component at small frequencies is more relevant and the overall crack growth rate results higher.
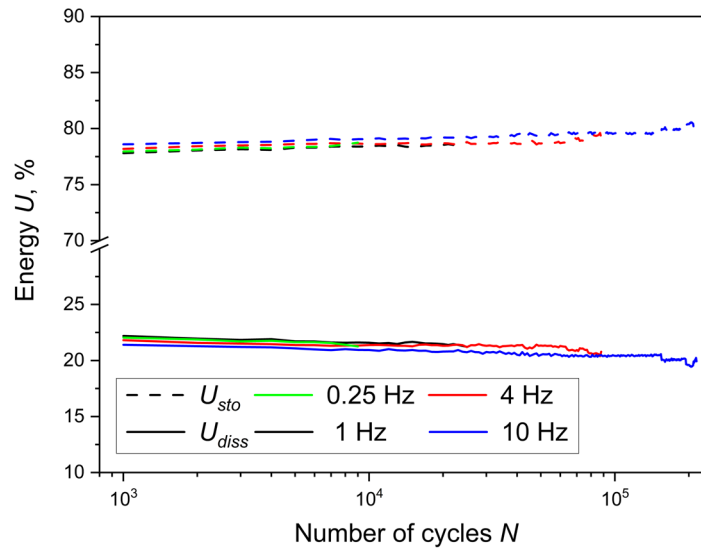

Figure 4.3 Normalized dissipated energy (full line) and elastically stored energy (dashed line) as a function of the number of cycles observed from crack growth experiments of a CB-filled NBR at different frequencies. Adapted from [5].

4.2   Force control effect

The majority of fatigue tests of rubbers and elastomers are performed using displacement (or strain) as the input load due to an easier control of this parameter as the input load. However, the knowledge of the effect of force as load parameters can be interesting for certain applications.

Schieppati et al. [7] performed tests in force control and compared the results with those obtained in displacement control. For a proper comparison, the parameters were selected to

ensure a similar load ratio R_ε (of 0.5) in order to evaluate the differences only related to the loading control mode. The hysteresis curves showed higher slopes with increasing frequencies (Figure 4.4(a)) due to stiffer mechanical behavior. The fatigue crack growth results reported in Figure 4.4(b) were compared with the fitted curves obtained in displacement control (dashed lines). The same general trend was found, i.e., higher crack growth resistance with increasing frequency. Furthermore, at all investigated frequencies, force-controlled and displacement-controlled tests produced similar outcomes, suggesting no significant influence of the choice of the input parameter on the results. Analogous conclusions were drawn by Andreini et al. [44] for SBR in stress and strain controlled tests.
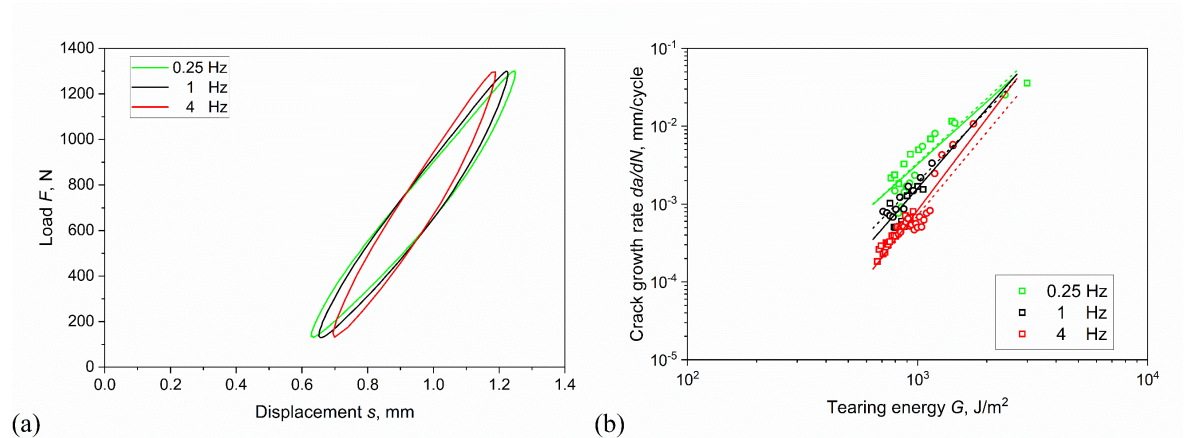

(a) (b)

Figure 4.4 (a) Hysteresis curves obtained during fatigue crack growth measurements in force control with the same number of cycles and (b) fatigue crack growth rate as a function of tearing energy in force control at different frequencies for a CB-filled NBR at room temperature and load ratio R of 0.1 with a sinusoidal load. The dashed lines correspond to fitted curves at the same frequencies in displacement control reported in Figure 4.2(b) at room temperature and load ratio R_ε of 0.5 with a sinusoidal load. Reproduced from [7].

4.3 Waveform effect

The shape of the applied cyclic load may affect the mechanical and fatigue behavior since distinct waveforms have different strain rates in different loading phases. Stadlbauer et al. [45] dealt with this topic and performed tests comparing sinusoidal and square waveforms. The results evidenced similar crack growth rates for blends of filled SBR, as exhibited in Figure 4.5. Similarly, Seichter et al. [40] reported analogous fatigue lifetime for blends of SBR/BR/NR using sinusoidal and square waveforms.
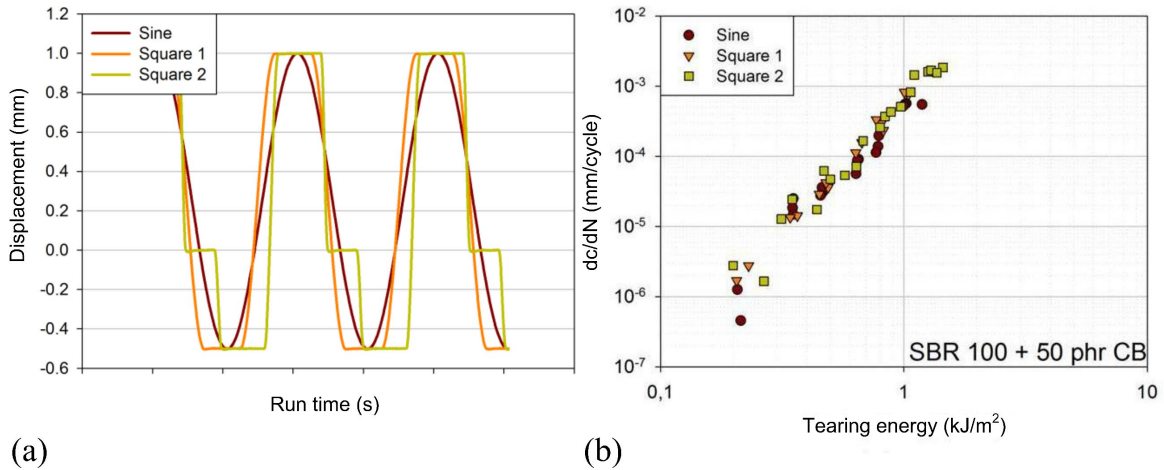
Figure 4.5 (a) Shape of the waveforms in terms of displacement against the run time and (b) fatigue crack growth rate as a function of tearing energy for filled SBR at room temperature and load ratio R_ε of -0.5 with a sinusoidal load. Adapted from [45].

Schieppati et al. [7] reported similar crack growth for sinusoidal, triangular and rectangular waveforms for filled NBR even if different hysteresis were monitored. In fact, the hysteresis curves (Figure 4.6(a)) evidenced some differences in the mechanical behavior - with the same number of cycles, higher displacement levels were monitored for the sinusoidal waveform. The rectangular waveform (red curve in Figure 4.6(a)) shows that the prescribed load was reached as a peak value, while afterwards, the load amplitude dropped by a quarter; this was connected to the limits of the machine at the frequency used to reproduce a rectangular waveform. However, the fatigue crack growth curves were quite similar, as depicted in Figure 4.6(b).

Even though the influence of waveform on the fatigue crack growth seems to be negligible, a strong influence of cyclic pulse loads – typical conditions for tires - was reported. Ghosh et al. [46] reported a higher crack growth rate for pulse than for sinusoidal loading for both NR and NR/BR blends (Figure 4.7). The reason behind the increase of crack growth seems to be related to the so-called "dwell time," which is the time at static load in between the pulses, associated with time-dependent recovery in front of crack tip [47,48]. Overall, the effect of the dwell time seemed to be material-dependent. In fact, Andreini et al. [44] reported that pulse waveforms induced a larger influence on crack growth for NR, while negligible effects were found for BR and SBR.
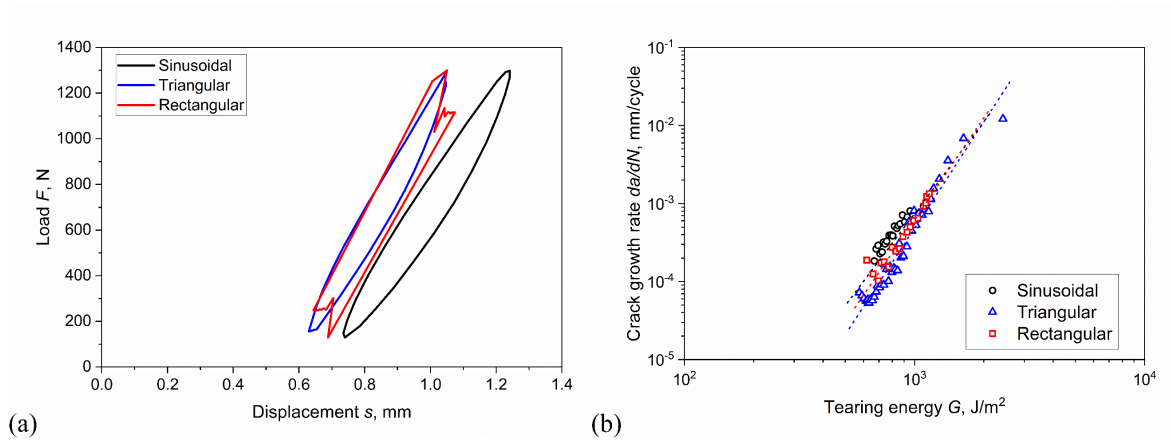
(a)   (b)

Figure 4.6 **(**a) Hysteresis curves obtained during fatigue crack growth measurements in force control with the same number of cycles and (b) fatigue crack growth rate as a function of tearing energy for different waveforms for a CB-filled NBR at room temperature, load ratio R of 0.1 and frequency of 4 Hz. Reproduced from [7].

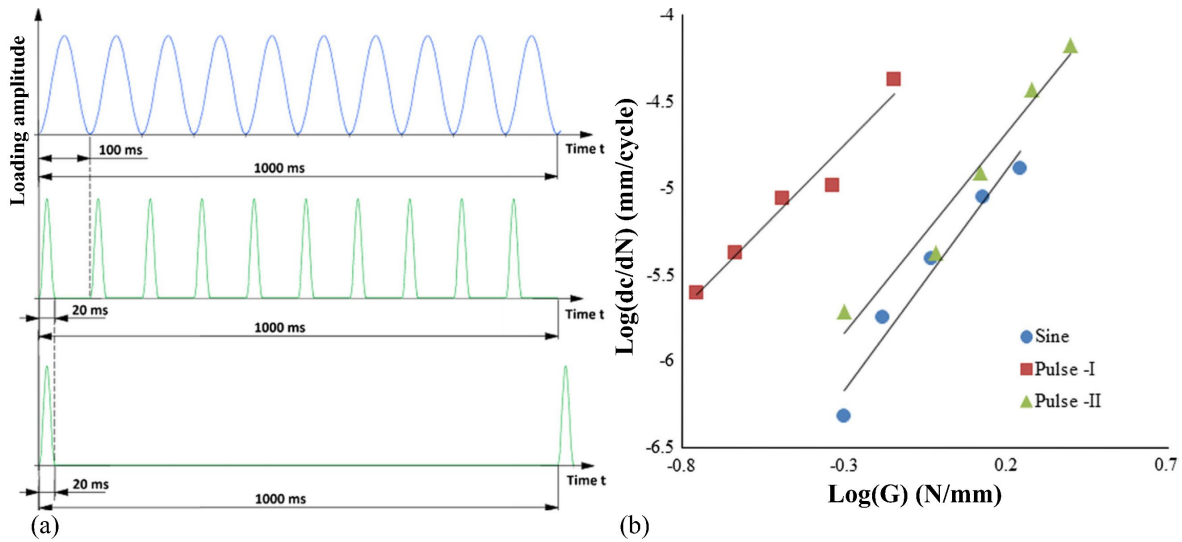(a)   (b)

Figure 4.7 (a) Schematic of the waveforms sine (upper), pulse-I (middle) and pulse-II (lower), and (b) correspondent fatigue crack growth as a function of tearing energy for NR at temperature of 28 °C and load ratio R of 0. Adapted from [46].

4.4   Load ratio effect

A further parameter that characterizes cyclic loading is the load ratio, which gives a first indication of the stress state in terms of tension and compression. According to the loading control mode, the load ratio can be defined considering the maximum and minimum values of force or displacement set in the machine. Consequently, for the force control tests, the load ratio R can be defined as:

$$R = \frac{F_{min}}{F_{max}} \tag{4.6}$$

where F_{min} is the minimum force and the F_{max} is the maximum force. Conversely, in displacement control mode, the load ratio R_ε can be written as considering the minimum displacement, s_{min}, and the maximum displacement, s_{max} as:

$$R_\varepsilon = \frac{s_{min}}{s_{max}} \tag{4.7}$$

With respect to $R = 0$ (commonly referred to elastomers' fatigue as "relaxing conditions"), non-relaxing conditions affect the fatigue behavior of some elastomers. Harbour et al. [48] verified the influence of load ratio on both crystallizing (NR) and non-crystallizing (SBR) elastomers. As depicted in Figure 4.8, with the variation of load ratio, no effect was monitored for SBR, while an increase in fatigue resistance was found for NR. Similarly, Ghosh et al. reported a reduction of fatigue crack growth with increasing load ratio not only for NR, but also for NR/BR blends [46]. Overall, the effect of the load ratio seems to be more relevant for crystallizing rubbers, with an increase in crack growth resistance for positive load ratios due to the formation of crystallites that bring beneficial reinforcing effects [49–56]. The crystallite formation leads to the formation of "sideways" cracks in the parallel direction to the load reducing the "forward" crack propagation [57,58]. Mars and Fatemi [59] developed an empirical model to take into account the effect of R for strain crystallizing rubbers. **Schieppati et al.** [7] confirmed the negligible influence of load ratio on fatigue for non-crystallizing elastomers (CB-filled NBR) even though different load ratios resulted in very different loading conditions. As shown in the hysteresis curves in Figure 4.9(a), for the lowest values of R_ε, the stress state was in a tension–compression state (the shape of the curve for $R_\varepsilon = 0$ even suggested buckling of the samples), while for $R_\varepsilon = 0.5$, the stress was in a tension–tension state. Nevertheless, the resulting fatigue crack growth curves (Figure 4.9(b)) were very similar.
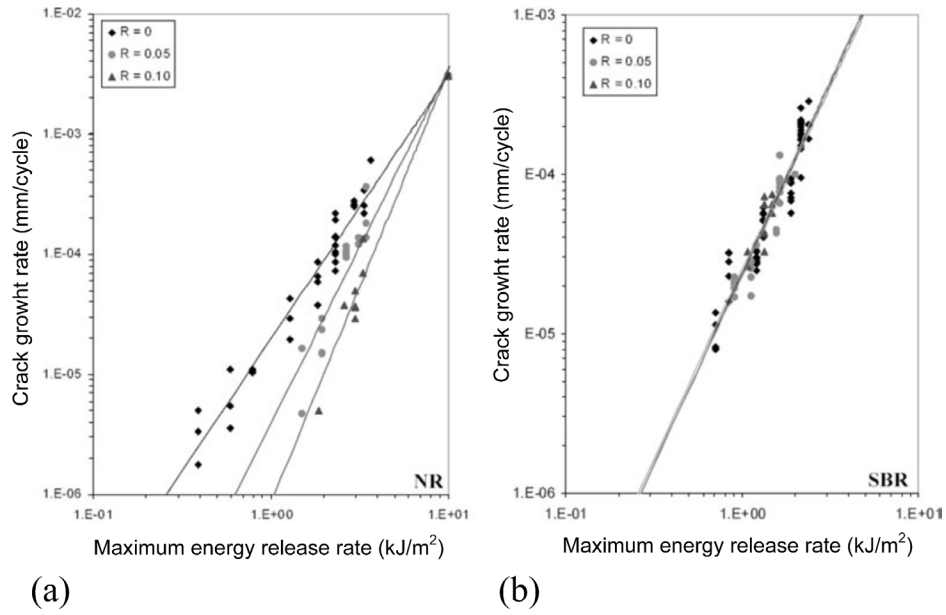
Figure 4.8 Fatigue crack growth rate as a function of tearing energy at different load ratios for (a) NR and (b) SBR. Reproduced from [48].
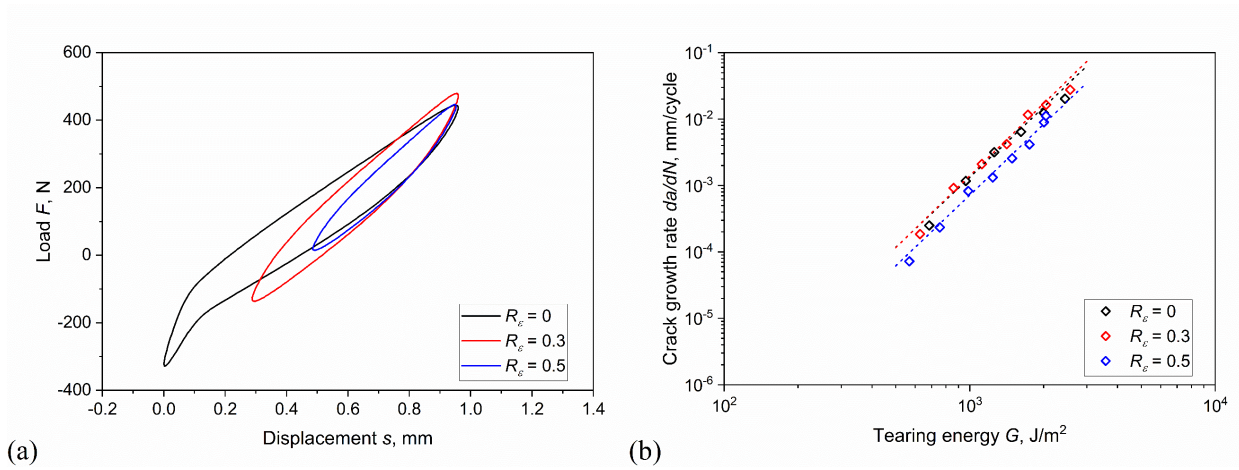

Figure 4.9 (a) Hysteresis curves obtained during fatigue crack growth measurements at the same maximum strain and (b) fatigue crack growth rate as a function of tearing energy at different load ratios for filled NBR at room temperature with a sinusoidal load and frequency of 4 Hz. Reproduced from [7].

5 Effect of Temperature on Mechanical and Fatigue Behavior

The effect of temperature on the mechanical behavior of elastomers is an intrinsic characteristic that can be traced back to the material constitution. In fact, the process of vulcanization leads to the formation of chemical crosslinks that hinder the viscous flow between the macromolecules and transform the (visco-)plastic behavior of rubbers to the (visco-)elastic behavior of elastomers. The peculiar structure of these materials is responsible for the unique elastic properties of rubber, the so-called "rubber elasticity": in these materials, the elastic behavior is governed by entropy. When stretching an elastomer, the macromolecules assume a more ordered configuration, leading to a decrease in entropy (Figure 5.1). A restoring force is created, which tends to restore the initial configuration in order to increase the entropy of the system. From a thermodynamic point of view, the restoring force f can be expressed as:

$$f = -T \left(\frac{\partial S}{\partial l} \right)_{T,P} \tag{5.1}$$

where T is the temperature, ∂S the variation of entropy, ∂l the deformation and P the pressure. Equation (5.1) not only highlights the importance of entropy in elastomers, but clearly proves that the temperature also has a strong role: the entropic response of the material is proportional to temperature. More details about rubber elasticity can be found elsewhere [60,61]. Furthermore, rubbers are polymers, so they are viscoelastic materials, showing a strong temperature dependency.
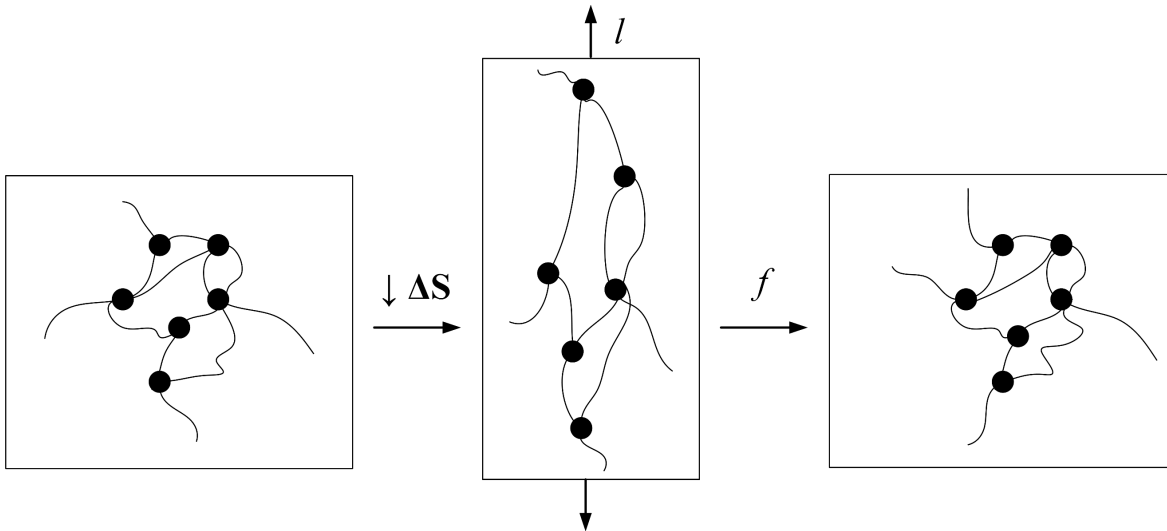
Figure 5.1 Schematic of the effect of stretching on elastomers. The deformation, *l,* causes an increase of the order in the material - the macromolecules are aligned in the stretching direction – resulting in a decrease of entropy, ΔS, that leads to a restoring force, *f.*

5.1 *Effect of temperature at large deformations*

Due to entropic elasticity, an increase in stiffness is expected for elastomers. However, the situation is more complex when considering reinforced elastomers. The interactions between polymers and fillers lead to a reduction of the mobility of macromolecules, affecting the viscoelastic response of the material. As a result, the temperature dependence derived from viscoelastic effects become more relevant for filled elastomers. For viscoelastic materials, a general reduction of stiffness is expected with increasing temperature. Therefore, the overall behavior of filled elastomers will be a tradeoff between the increase in stiffness due to entropic elasticity and a decrease in stiffness because of the viscoelastic effect. Considering a highly CB-filled NBR, **Schieppati et al.** [8] observed a reduction in the stiffness and an overall decrease in the ultimate properties (Figure 5.2).

The stress-strain data of rubbers can be analyzed using the Mooney-Rivlin equation [62,63]:

$$\sigma = 2\left(C_1 + \frac{C_2}{\lambda}\right)\left(\lambda - \frac{1}{\lambda^2}\right)$$
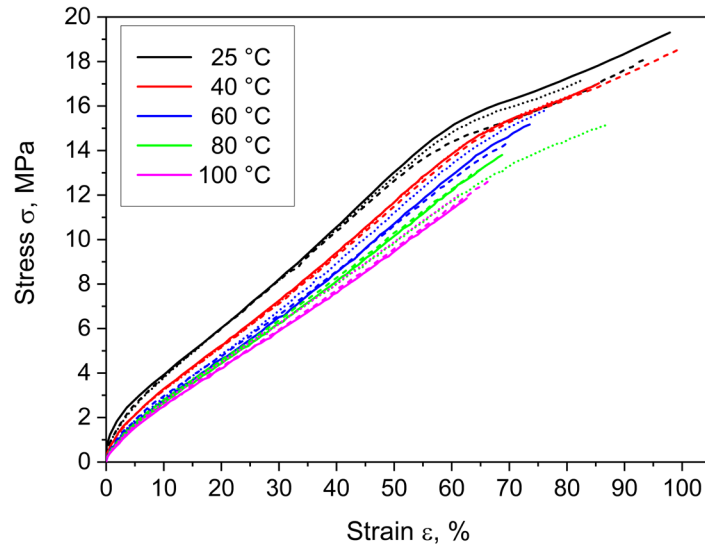(5.2)

Figure 5.2 Stress-strain curves from tensile tests of filled NBR at different temperatures. The different line styles correspond to different specimens. Reproduced from [8].

where C_1 and C_2 are material constants and λ is the stretch ratio. It is possible to consider the reduced stress, $\sigma*$:

$$\sigma^* = {}^{\sigma}\!\big/\!{}_{\lambda - \frac{1}{\lambda^2}} \tag{5.3}$$

Finally, Equation (5.2) can be rewritten as:

$$\sigma^* = 2C_1 + \frac{2C_2}{\lambda} \tag{5.4}$$

Equation (5.4) allows the reduced stress $\sigma*$ to be plotted against λ^{-1}, obtaining the so-called Mooney-Rivlin plots [64–68]. Typically, this kind of plot presents a minimum: at low strains (i.e., high value of inverse of the stretch ratio), the reduced stress decreases up to a minimum, called "upturn," after which the reduced stresses grow. The value of stretch corresponding to the upturn stress is interesting since it seems to represent the maximum chain extensibility between crosslinks for non-crystallizing rubbers [69,70]. The maximum chain extensibility for elastomers is affected by both the presence of filler and by the occluded rubber, which limits the molecules' extension. **Schieppati et al.** [8] reported the Mooney-Rivlin plots at different temperatures for a CB-filled NBR (Figure 5.3). The values of the upturn strain in Figure 5.3 are represented as the star signs. As depicted, the upturn strain (and the maximum

chain extensibility) varied with the temperature: initially, the upturn strain showed decreasing values with temperature, while it rose again at higher temperatures, showing that the limited chain extensibility has a minimum at intermediate temperatures around 40 and 80 °C. These findings were related to different enthalpic and entropic contributions to the overall elasticity and to different effects of the bound rubber at different temperatures.
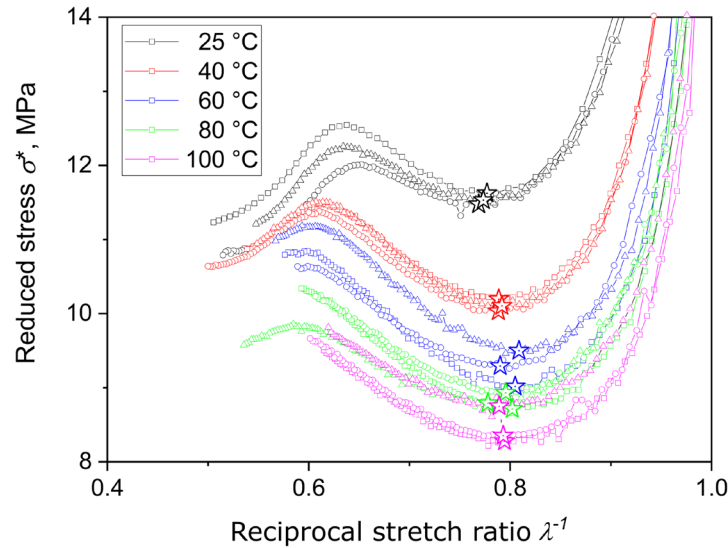

Figure 5.3 Mooney-Rivlin plot of a CB-filled NBR at different temperatures. The different symbols correspond to different specimens. The stars represent the upturn strain. Reproduced from [8].

5.2   *Effect of temperature at small deformations*

The temperature influence on the mechanical behavior at small deformation is normally investigated with DMA. The dynamic properties of rubbers are strongly influenced by the presence of fillers. An example of SBR was reported by Fritzsche and Klüppel [71], represented in Figure 5.4. Considering the storage modulus of the unfilled elastomers, the typical behavior of rubber is represented with a drop of three order of magnitude after the glass transition and a slight increase in the modulus with rising temperature above T_g due to entropic elasticity (the so-called "Joule effect"). The addition of fillers instead induces different effects: on one side, the storage modulus increased over the entire temperature range, inducing a reinforcement effect, while on the other side, the Joule effect was hindered, especially at large loadings of fillers. Considering the loss modulus (Figure 5.4(b)), a general

increase was found for larger CB loading in the whole range of temperature, evidencing an increase in energy dissipation with the presence of fillers.
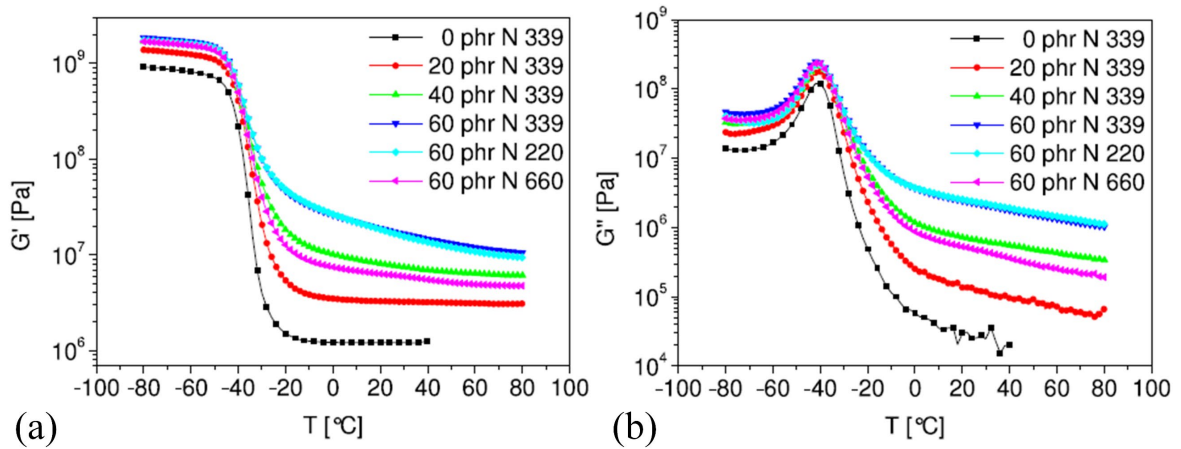

Figure 5.4 Dynamic properties of SBR with different loadings of CB: (a) shear storage modulus and (b) shear loss modulus. Reproduced from [71].

Similar findings were reported by **Schieppati et al.** for a CB-filled NBR for which the plots of storage modulus E', loss modulus E'' and the loss factor tanδ are represented in Figure 5.5. Due to the presence of fillers, above T_g, no Joule effect was observed: the storage modulus constantly decreased with increasing temperature. Moreover, a faster reduction with temperature of the loss modulus E'' was observed and it was related to the fact that at high temperatures, the viscous effects are minimized and the energy dissipation is reduced.

The dependency of the dynamic moduli at high temperature can be analyzed by using Arrhenius plots, graphing the logarithm moduli against the inverse of temperature. In this way, a linear relationship can be observed above T_g + 30 °C when the molecular motion is high and the dynamic mechanical response is fully rubberlike [10]. The decrease of moduli with rising temperatures seems to be connected to a decrease of the stiffness of the glassy polymer's bridges [71]. Such Arrhenius plots were reported by Fritzsche and Klüppel [71] for SBR with different loadings of CB, by Le Gal et al. [72] for EPDM with both CB and silica and by **Schieppati et al.** [8] for filled NBR (Figure 5.6).
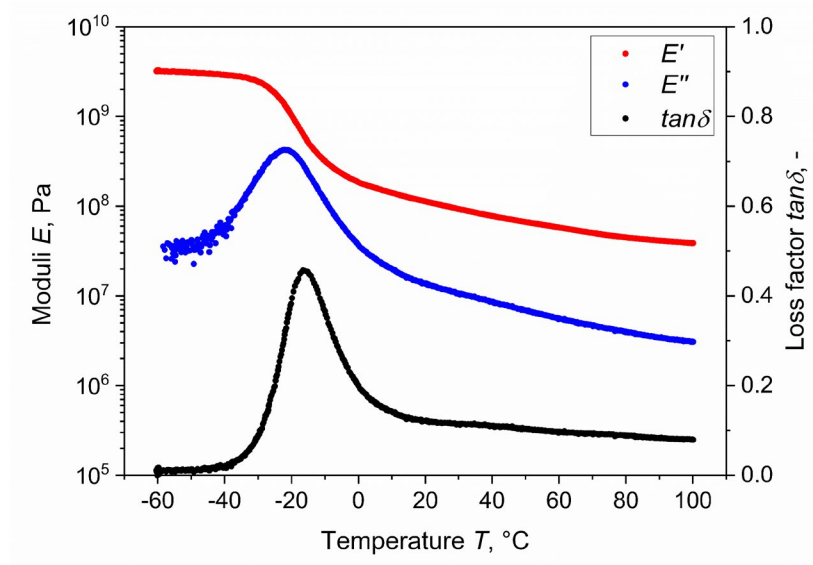
Figure 5.5 Storage modulus E' (red), loss modulus E'' (blue) and loss factor tanδ (black) as a function of temperature of a filled NBR. Reproduced from [8].
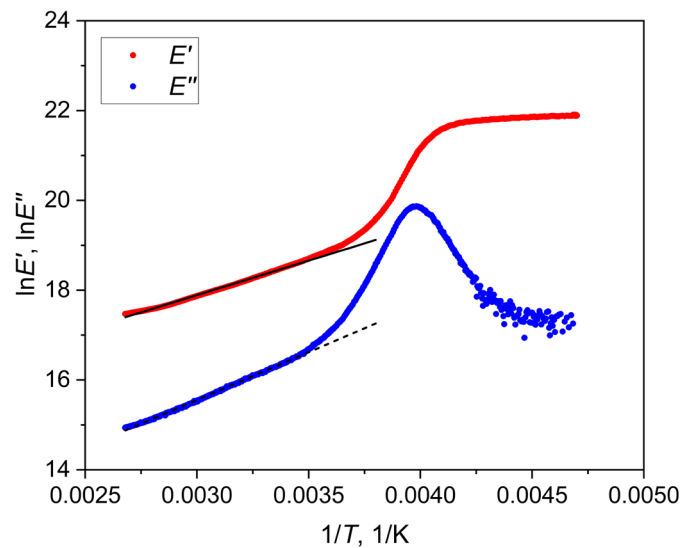

Figure 5.6 Logarithms of storage modulus E' (red) and loss modulus E'' (blue) as a function of the inverse of temperature of a filled NBR. The black lines correspond to the fitting with Arrhenius equation above $T_g + 30$ °C. Reproduced from [8].

Another aspect that can be studied using DMA at different temperatures is the construction of master curves of the dynamic properties. By exploiting the time-temperature superposition principle, isothermal frequency sweeps at different temperatures can be shifted along the frequency axis to generate master curves. The construction of these kinds of master

curves can be performed on materials that are thermorheologically simple just with horizontal shifts. However, for some filled elastomers that are not thermorheologically simple, horizontal shifts can be integrated with vertical shifts to obtain a proper master curve [11,71–74]. Therefore, at first, a material should be proven to be thermorheologically simple, as suggested in literature [75,76], by using the Cole-Cole plot [77] and wicket plot [78]. That way, the curves of the storage modulus E' can be horizontally shifted with respect to a reference temperature. Furthermore, the shift factors of E' can be applied to the isothermal plots of the loss modulus and the loss factor, obtaining master curves. This approach was employed for building master curves for blends of SBR and BR with different fillers by Wang and Mahmud [79] and for filled NBR by **Schieppati et al.** [8] (Figure 5.7). Lorenz et al. [80] compared different shifting procedures for different rubbers and they show that accurate master curves can be obtained using a causality condition.
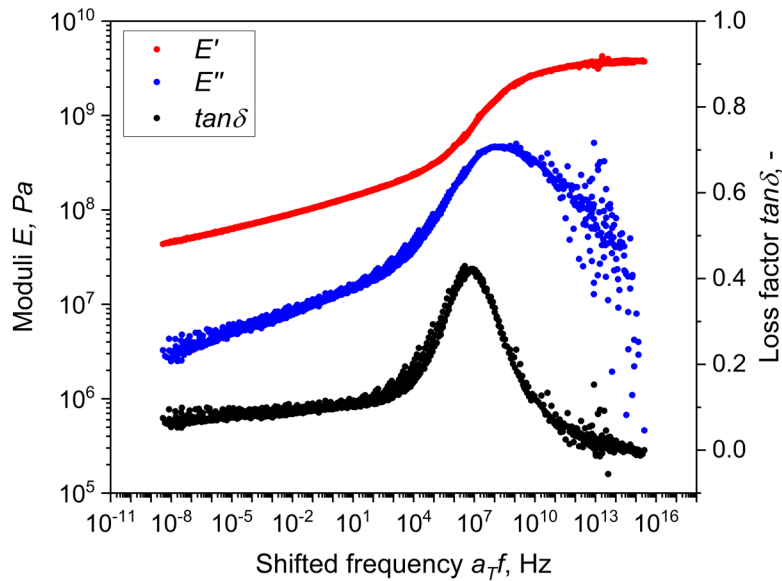
Figure 5.7 Master curves of storage modulus E' (red), loss modulus E'' (blue) and loss factor tanδ (black) as a function of frequency obtained from isothermal frequency sweeps at different temperatures of a CB-filled NBR at a reference temperature of 25 °C. Reproduced from [8].

5.3 *Effect of temperature on fatigue crack growth*

A strong influence of temperature on the fatigue of rubber is known from the seminal work of Lake and Lindley [4], who reported both higher crack growth rates and a decrease

of fatigue lifetime for NR and SBR (Figure 5.8). In particular, a decrease of four order of magnitude of fatigue lifetime was found for SBR, while a lower reduction was reported for NR.
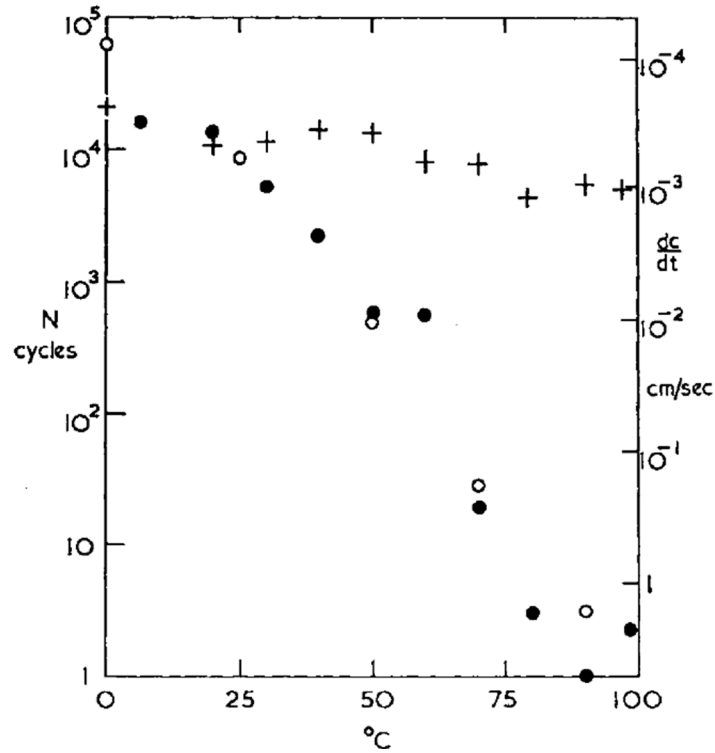

Figure 5.8 Effect of temeprature on fatigue life (left scale) for SBR (full circles) and NR (empty circles) and crack growth rates (right scale) on SBR. Reproduced from [4].

Furthermore, Asare and Busfield [81] reported a significant increase in the crack growth rate for NR passing from room temperature to 70 °C (Figure 5.9). In addition, a stronger influence of temperature at lower strain for NR was reported by Wu et al. [82]. Legorju-jago and Bathias [83] reported a decrease in the threshold for fatigue with increasing temperature for NR and they highlighted a role of the combined effect of oxygen (Figure 5.10). A contribution of the effect of high temperatures in reducing the fatigue resistance of NR was found in the reduction or even suppression of crystallite formation under strain [55,56].
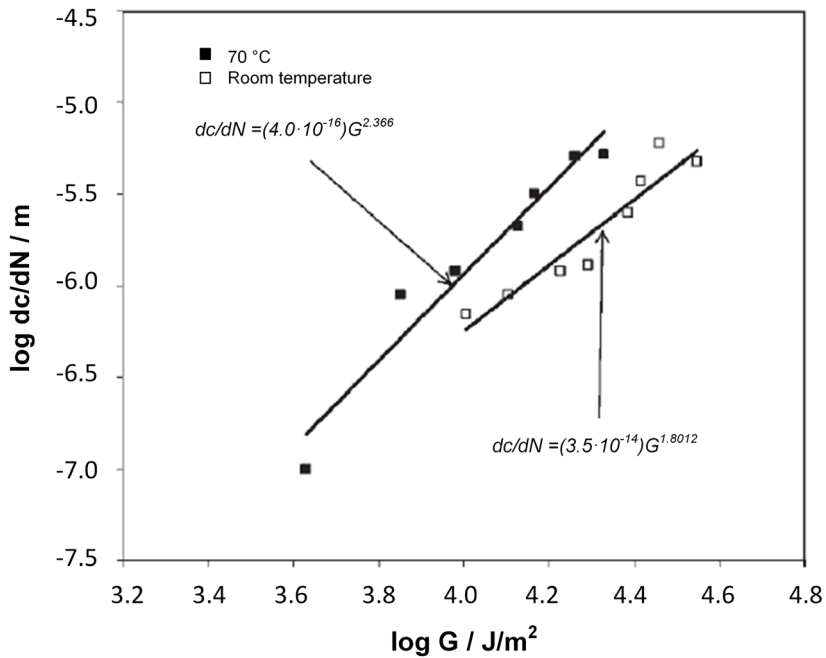
Figure 5.9 Fatigue crack growth rate as a function of tearing energy for a CB-filled NR at room temperature and at 70°C. Adapted from [81].
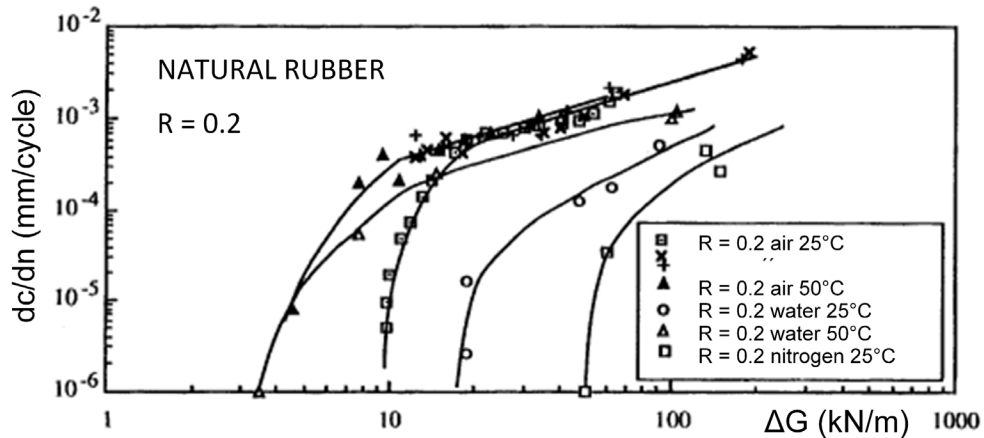
Figure 5.10 Fatigue crack growth rate as a function of tearing energy for a CB-filled NR at different temperatures (25 and 50 °C) and with different environments (air, water and nitrogen). Adapted from [83].

Nevertheless, crack propagation measurements on several carbon black-filled elastomers by Young [84] showed that not only NR, but most of the synthetic rubbers have higher rates at higher temperatures. Young and Danik [85] verified similar trends for various compounds: due to the higher T_g of compounds of ECO and SBR, they reported two order of

magnitude larger crack growth with respect to BIIR and NR, demonstrating the strong impact of viscoelasticity. Moreover, they reported higher sensitivity to temperature for under-cured rubbers. Analogously, NR and BR blends showed increasing crack growth [46] and lower fatigue lifetime [86]. An increase in crack growth rate and thus, a reduction in fatigue lifetime with higher temperatures, was reported for both NR and EPDM [87]. Bérangeret et al. [88] reported a large increase in crack growth for NBR passing from 23 to 120 °C. Similarly, **Schieppati et al.** [8] analyzed the effect of high temperature on filled NBR. The results in terms of crack growth rate as a function of tearing energy are reported in Figure 5.11. As depicted, rising temperatures lead to a higher crack growth rate: considering a constant value of the tearing energy, the crack growth rate increased by almost two orders of magnitude from 25 to 80 °C. This was justified considering that for the same value of energy, due to lower energy dissipations at high temperatures, more energy is available for crack propagation, leading to faster crack growth. On the other hand, the plot revealed that considering the same crack growth rate, the high temperature curves seemed shifted to lower tearing energies, suggesting that the crack propagation process is similar at different temperatures but occurs at lower energy values. This behavior correlates with the observation
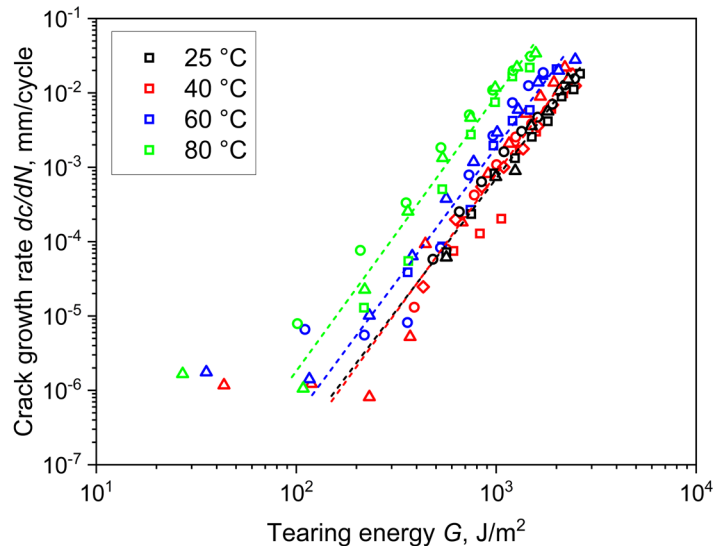

Figure 5.11 Fatigue crack growth as a function of tearing energy for a CB-filled NBR at different temperatures using a sinusoidal load at 4 Hz with load ratio R_ε of 0.5 Reproduced from [8].

made on the critical energy for tearing, G_0, which decreases with increasing temperature when viscous effects are minimized [89] and to the reduction of the threshold of fatigue for NR discussed above.

5.4   Models accounting for the temperature effect on fatigue

Overall, the results obtained with several materials evidenced the strong role of temperature on the fatigue resistance of elastomers. Nevertheless, a further step is necessary for using the results in practice for the prediction of component lifetime at high temperatures. Recently, several studies have focused on the development of a tool for considering the effect of temperature.

In general, the effect of temperature on both fracture and peeling [89,90] was considered by shifting the curves along the crack growth axis, using the same shift factors obtained from the construction of a master curve from an isothermal frequency sweep (see Chapter 5.2). A similar approach was employed by Wunde and Klüppel [91] for the fatigue crack growth curve, in which they shifted the crack growth curve of both unfilled and filled SBR using the shift factors taken from the unfilled material. However, **Schieppati et al.** [8] reported that an analogous approach did not provide satisfactory results for NBR.

El Maanaoui and Meier [87] developed an empirical model considering the temperature dependence of the coefficient *C* of the Paris law for EPDM and NR (Figure 5.12); the *m* coefficient was considered constant, since they found that the slopes of the curves were not affected by the temperature. Using this model, they were able to make an accurate prediction of the fatigue crack growth curves at different temperatures (Figure 5.13). Similarly, Luo et al. [92] developed an empirical model by considering the temperature dependence of the critical tearing energy in order to shift the crack growth curve at higher temperatures.

Schieppati et al. [8] reported a different approach based on energy dissipations. It is known that the propagation of cracks in viscoelastic solid is strongly influenced by dissipative mechanisms, especially in front of crack tip. A proportionality of the tearing energy with loss modulus was found for different non-crystallizing elastomers [93].

Generally, the strength of elastomers can be characterized by the amount of energy required for crack propagation: this includes the energy required for bond breaking and the energy
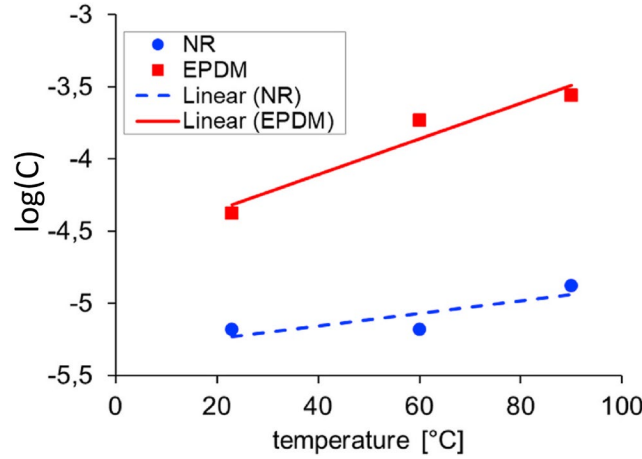
Figure 5.12 Parameter *C* of the Paris law from crack growth propagation as a function of temperature for EPDM and NR. Adapted from [87].

(a)   (b)
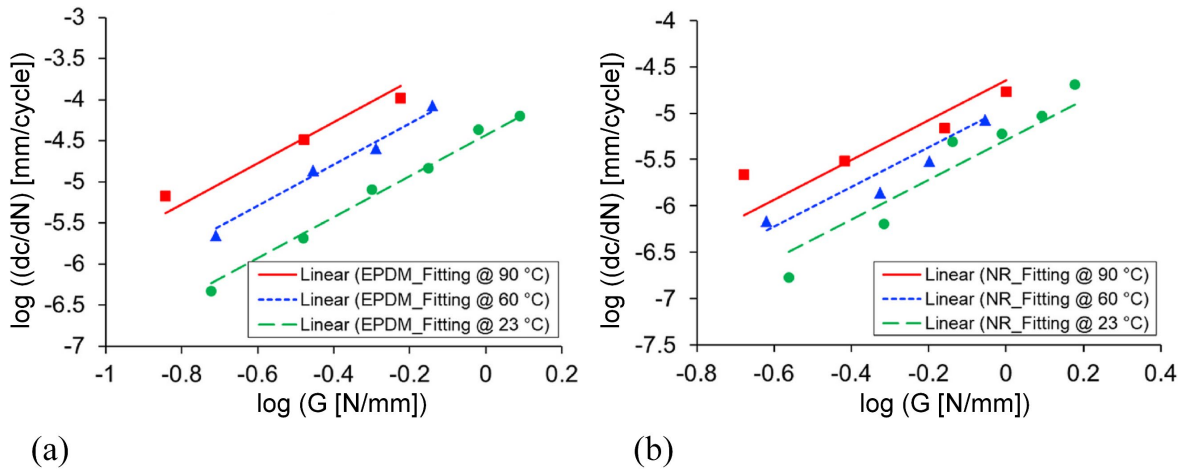
Figure 5.13 Comparison of experimental results (symbols) and predicted fatigue crack growth rate (lines) as a function of tearing energy at different temperatures using an empirical model for accounting of the Paris coefficient *C* (Figure 5.12) and for (a) EPDM and (b) NR. Adapted from [87].

dissipated in front of the crack tip [94]. According to Persson and Brener's theory [33,94], the tearing energy as a function of the crack speed *v* is given by:

$$G = G_0 \left[1 - \frac{2}{\pi} E_0 \int_0^{\frac{2\pi v}{a}} d\omega \frac{F(\omega)}{\omega} Im \frac{1}{E^*(\omega)} \right]^{-1} \tag{5.5}$$

36

where G_0 is the critical tearing energy, E_0 is the modulus in the rubbery region, a is the crack tip diameter, ω is the perturbing frequency, which is defined as v/r (r is the distance from the crack tip), and E^* is the complex modulus, while the function $F(\omega)$ is given by:

$$F(\omega) = \left[1 - \left(\frac{\omega a}{2\pi v}\right)^2\right]^{\frac{1}{2}} \tag{5.6}$$

The last term of Equation (5.5) can be expressed as:

$$Im\frac{1}{E^*(\omega)} = -\frac{E''}{|E^*|^2} \tag{5.7}$$

where E'' is the loss modulus. These relations have been used in different [95–97] studies to analyze qualitatively the crack growth resistance of different rubbers. Equations (5.5) and (5.7) correlate the tearing energy to the energy dissipation through the loss modulus. Sustained by the aforementioned theory, **Schieppati et al.** [8] considered the temperature dependence of the tearing energy by correlating it to the temperature dependence of the loss modulus. In particular, for temperatures above $T_g + 30\ °C$, the loss modulus exhibited an Arrhenius dependence (Figure 5.6) from which they evaluated an apparent activation energy. Using this value, shift factors s_T were evaluated with respect to the reference temperature (set at 25 °C) using an Arrhenius form:

$$s_T = \frac{\ln E''_T}{\ln E''_{T_{ref}}} = \frac{E_{a,app}}{R}\left(\frac{1}{T} - \frac{1}{T_{ref}}\right) \tag{5.8}$$

The shift factors evaluated were then used to horizontally shift the fatigue crack growth curves along the tearing energy axis by evaluating the tearing energy at the temperature T (denoted as G_T) and shifting it with respect to the reference temperature T_{ref}, resulting in the value $G_{T,Tref}$ given by:

$$G_{T,Tref} = \frac{G_T}{s_T} \tag{5.9}$$

By doing so, the curves at higher temperatures (Figure 5.11) were shifted towards higher values of tearing energy, and they achieved a fatigue crack growth master curve (Figure 5.14).
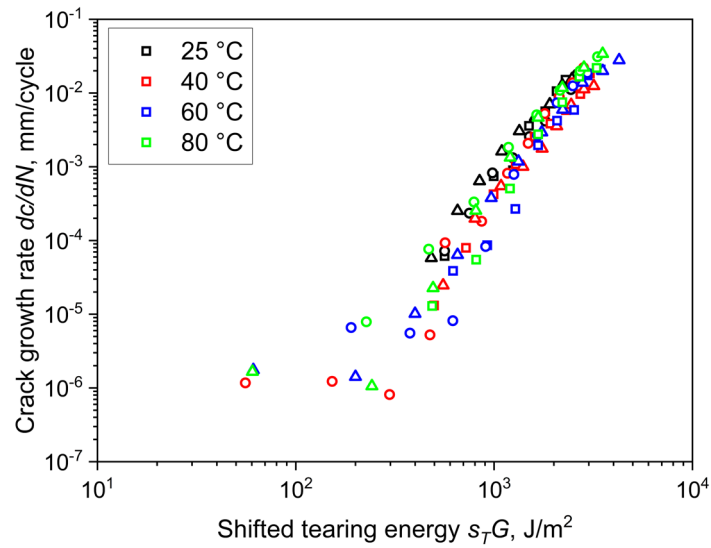
Figure 5.14 Master curves of fatigue crack growth as a function of tearing energy for a CB-filled NBR obtained by shifting the curves at different temperatures (Figure 5.11) using shift factor s_T evaluated through temperature dependence of the dynamic loss modulus. Reproduced from [8].

6 Application of Fracture Mechanics to the Determination of Fatigue Lifetime

The analysis of the fatigue lifetime of rubbers is generally based on the construction of Wöhler curves [98]. A typical example was reported by **Schieppati et al.** [9], who observed that the fatigue lifetime of CB-filled NBR showed large scattering and a power law dependency (Figure 6.1).
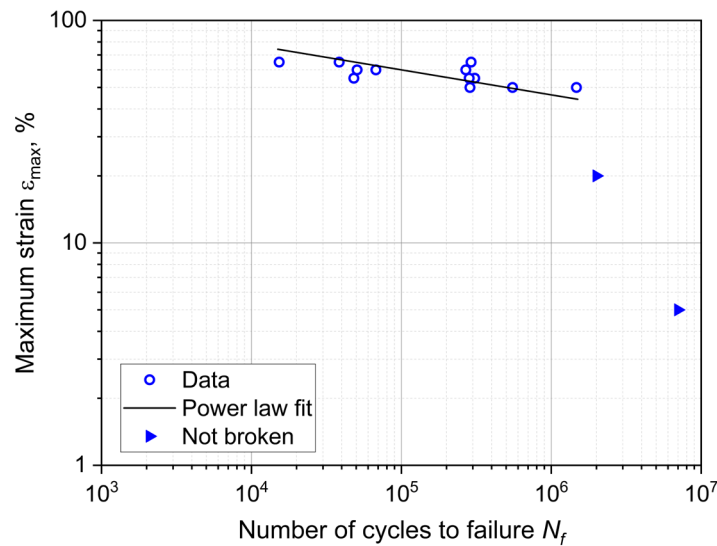
Figure 6.1 Wöhler curve obtained from axisymmetric dumbbell of a CB-filled NBR. The fitting power law (Equation (4.4)) was obtained using ASTM E739 – 10. Reproduced from [9].

If the effect of the mean load is more relevant, Haigh diagrams [99] are employed for the analysis of the fatigue of elastomers. By plotting iso-lifetime curves, Ruellan et al. [56] distinguished four regions (Figure 6.2) depending on the load ratio and thus, the mean load.

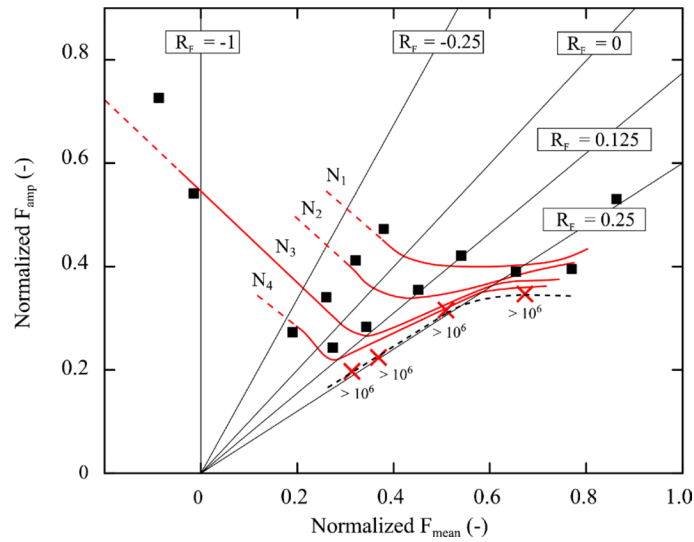Figure 6.2 Haigh diagram for different load ratios for a CB-filled NR. Reproduced from [56].

Fatigue cracks are generally initiated from defects and inhomogeneities in materials which then over repeated loads grow and coalesce up to failure. Due to the high number of components in elastomer blends, these materials exhibit a high level of inhomogeneity. In fact, besides the rubber matrix, elastomers typically contain fillers, plasticizers, processing aids, antioxidants, ozone protectors, vulcanization systems, accelerators and activators. All of these constituents may represent a defect in the rubber matrix from which cracks can nucleate as a result of high local stress intensifications. The typical dimension of defects for different elastomers was found to be of a few tens of µm [3,4,35,37,38,100,101]. Huneau et al. [102] investigated samples of a CB-filled NR subjected to fatigue through SEM and reported that fatigue damage initially occurs mainly from CB agglomerates or oxides (such as ZnO). Nevertheless, a large scatter in the fatigue life of elastomers is normally expected. A clear example of the level of scattering of the fatigue lifetime in elastomers was reported by Balutch et al. [103]: from the analysis of the fatigue life of an industrial EPDM, they highlighted the results at a specific strain from 25 samples, showing huge scattering up to almost three orders of magnitude (Figure 6.3).
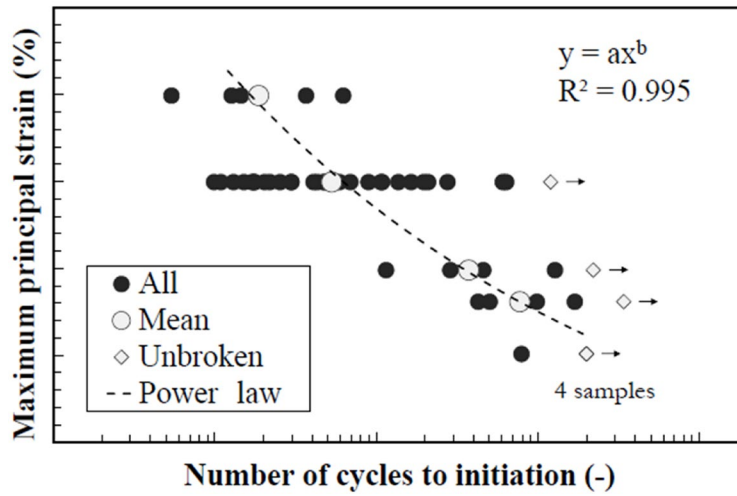
Figure 6.3 Wöhler curve for an industrial CB-filled EPDM with large scattering. Reproduced from [103].

6.1 Evaluation of defect size

The application of fracture mechanics to elastomers helps in the definition of the fatigue life by knowing the initial defect size. In fact, by integrating the crack growth characteristic over time (i.e., number of cycles) and summing the initiation time, it is possible to obtain the overall lifetime. On the other hand, by knowing the fatigue lifetime, it is possible to estimate the defect size that caused fracture. Normally, the use of this approach for elastomers neglects the initiation time. This could be justified considering the outcome observed by the analysis of the evolution of defects during the fatigue of elastomers, through μ-CT [104,105] and SEM analysis [102,106]. It was shown that cracks are initiated in the early stages of fatigue and that the number of defects mainly increases within the first 10 % of the overall fatigue life. Thus, during cyclic loading, the majority of the lifetime of rubbers is governed by crack growth. Therefore, the initiation time can be neglected and it is possible to obtain the initial size of defects, c_0, by the integration of Paris' law (Equation (4.4)). For small cracks, the energy release rate (i.e., tearing energy) can be factored into the strain energy density and the crack size [37] and its estimation can be given by:

$$G = 2 \cdot k(\lambda) \cdot W_0 \cdot c \qquad (6.1)$$

where W_0 is the strain energy density and c is the crack length; $k(\lambda)$ is a function of the stretch ratio [64]. By combining Paris' law (Equation (4.4)) and Equation (6.1) and integrating, the following can be retrieved:

$$N_f = \frac{1}{(m-1) \cdot C(2kW_0)^m} \cdot \left(\frac{1}{c_0^{m-1}} - \frac{1}{c_f^{m-1}} \right) \tag{6.2}$$

By considering that the initial defect size c_0 is much smaller than the final crack length c_f, this last contribution can be neglected, and Equation (6.2) reduces to:

$$N_f = \frac{1}{(m-1) \cdot C(2kW_0)^m} \cdot \frac{1}{c_0^{m-1}} \tag{6.3}$$

In general, this equation can be used to calculate the number of cycles to failure as a consequence of the growth of a pre-existing defect of dimension c_0, in order to obtain fatigue life predictions [3,4,107–115]. On the other hand, Equation (6.3) can be reversed to find the defect size, c_0 [9,100,101]:

$$c_0 = \left[\frac{1}{(m-1) \cdot N_f \cdot C(2kW)^m} \right]^{\frac{1}{m-1}} \tag{6.4}$$

By looking at Equations (6.3) and (6.4), the critical parameters for a correct evaluation of either the fatigue life or the defect size are the estimation of the strain energy density W_0 and the crack growth parameters (m and C). In particular, the estimation of these last parameters is affected by several factors such as frequency (see Chapter 4.1) and temperature (see Chapter 5.3). As discussed in Chapter 3, upon cyclic loading, a change of temperature is often found in rubber specimens and components, especially for significant thickness of the object under loading. Therefore, the inclusion of the influence of temperature has to be considered for a correct evaluation of lifetime prediction - or an accurate estimation of the defect dimension. El Maanaoui and Meier [87] developed a model (see Chapter 5.4) to account for temperature for the prediction of fatigue lifetime at high temperatures. On the other hand, **Schieppati et al.** [9] retrieved the dimension of initial size by considering the temperature effect. They reported remarkable temperature increases for axisymmetric dumbbells undergoing cyclic loading (Figure 6.4) and they accounted for the temperature using the model described by **Schieppati et al.** [8] (see Chapter 5.4). In this way, they

calculated critical defect sizes which were independent from the strain, as displayed in Figure 6.5.

The analysis of particle size and fatigue damage in elastomers is performed through techniques such as Scanning Electron Microscopy (SEM) [102,106,116–124] and X-ray microtomography [87,104,105,114,124–126]. The latter can give an overview of the distribution of the inhomogeneities in the entire sample and has thus been employed to estimate the defect size to be inserted in Equation (6.3) to calculate the fatigue lifetime predictions [87,114,125]. **Schieppati et al.** [9] evaluated the initial defect dimensions through the reconstruction of μ-CT evaluated from axisymmetric dumbbell samples in the undamaged state (Figure 6.6(a)). From the reconstructed volume, defects due to inhomogeneities and processing were identified (Figure 6.6(b)) and their volumes were estimated. The particles were approximated as spheres and from their radius, the initial particle size distribution was obtained (Figure 6.7).
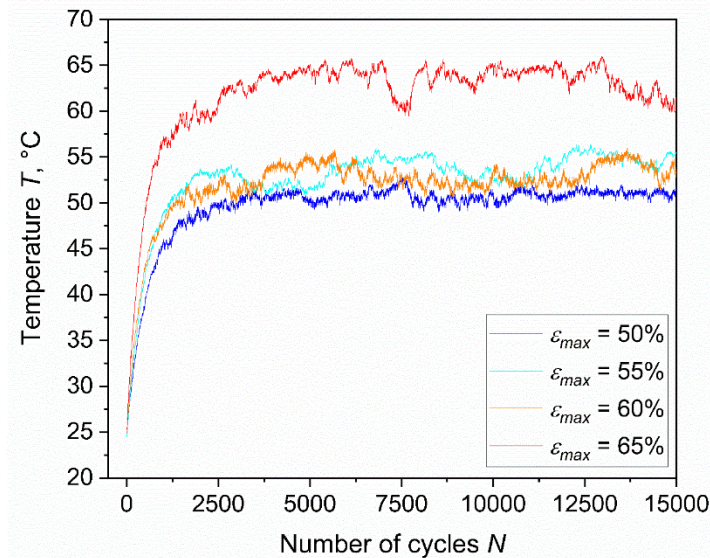
Figure 6.4 Surface temperature evolution at different strains of the fatigue experiments with axisymmetric dumbbell of a CB-filled NBR. Reproduced from [9].

In this way, it was possible to compare the initial particle size distribution with the calculations performed through Equation (6.4) – results in Figure 6.5. In general, they reported that the sizes of the detected defects were in the same range as the calculation and

the majority of them measured under 5 μm, smaller than the calculated critical defect size (9 μm).
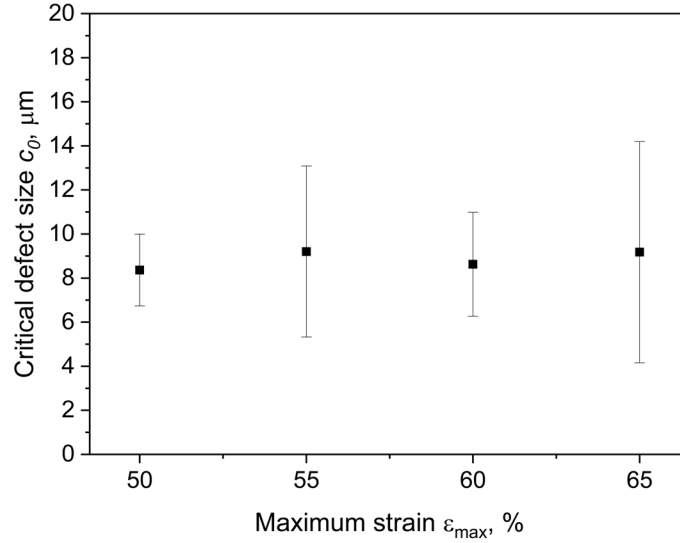
Figure 6.5 Critical defect size c_0 at different strains evaluated from fatigue data using Equation (6.3). The fatigue tests were implemented on axisymmetric dumbbell specimens of a CB-filled NBR. The average of all strains was 9 ±3 μm. Reproduced from [9].
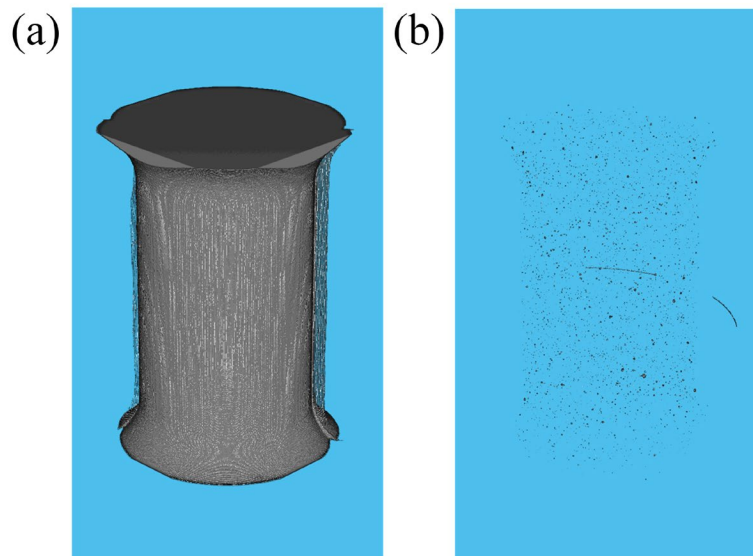
Figure 6.6 (a) Volume reconstruction of an undamaged axisymmetric dumbbell specimen of CB-filled NBR obtained from μ-CT and (b) cavity distribution in the reconstructed volume acquired from μ-CT. Reproduced from [9].
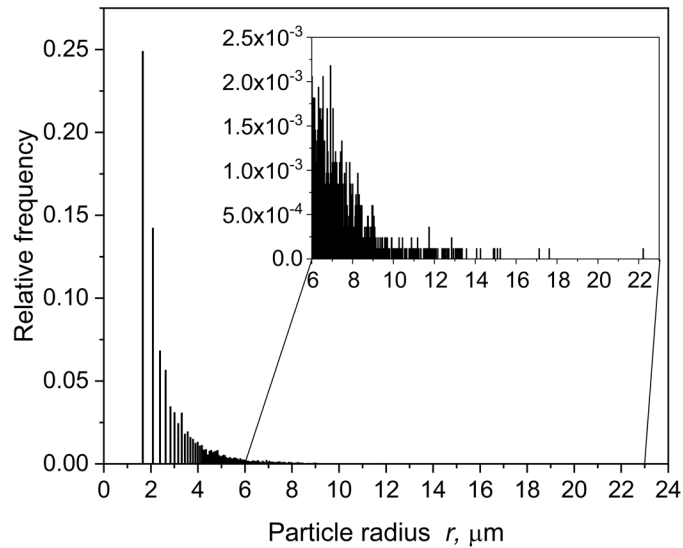
Figure 6.7 Particle size distribution of an undamaged axisymmetric dumbbell specimen of CB-filled NBR considered as spherical radius of the cavities. Reproduced from [9].

6.2 *J-integral evaluation of fatigue lifetime*

The introduction of a notch into samples leads to a reduction of both testing time and scattering of the results. In fact, the notch is an initial defect larger than the typical inhomogeneities in elastomers, reducing the initiation time as a result; moreover, being a reproducible initial defect, the scattering of the results is reduced. When considering cylindrical specimens, the introduction of a circumferential notch gives rise to the geometry referred to as Crack Round Bar (CRB). This allows a fast fatigue ranking by inducing a quasi-brittle failure on polymers, elastomers and thermoplastic elastomers [127,128]. **Schieppati et al.** [9] analyzed the results of fatigue tests achieved with both standard dumbbells and CRB, and the respective Wöhler curve is reproduced in Figure 6.8. As depicted, a general reduction of the lifetime of about four orders of magnitude was found for CRB as a consequence of the introduction of the notch. The induced stress intensification led to the failure at a level of strain for which no failure was observed for unnotched samples.

Furthermore, **Schieppati et al.** [9] attempted to find an approach for the determination of the fatigue life of elastomers that was independent from the geometry of the sample. To

do so, they developed a J-integral hyperelastic model in order to describe the CRB specimens from an energetic point of view. In particular, *J* was evaluated with:

$$J = \frac{F^2}{\pi(r_{out} - a)^2} \cdot f\left(\frac{a}{r_{out}}\right)$$

(6.5)
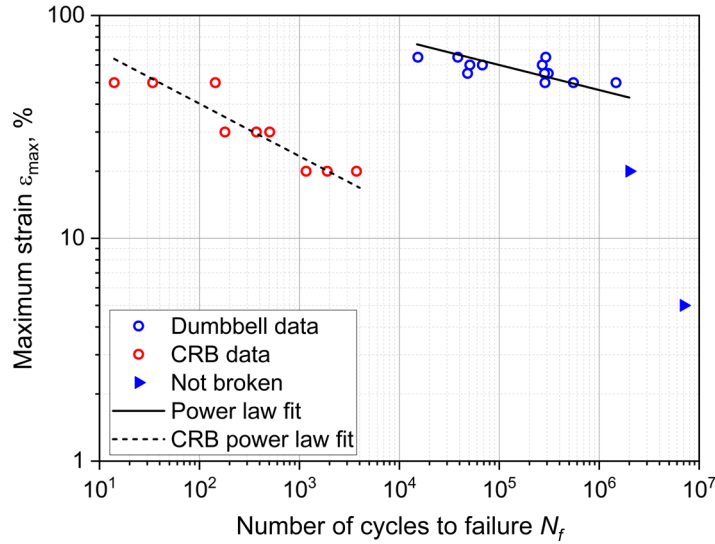
Figure 6.8 Wöhler curve obtained from axisymmetric dumbbell specimens (blue) and CRB (red) of filled NBR. The fitting power laws are represented as the continuous line for the dumbbells and the dashed lined for CRB. Reproduced from [9].

where *F* is the force, r_{out} the external radius of the CRB and *a* the size of the notch inserted in the CRB. *f(a/r_{out})* is a geometric factor of the form:

$$f\left(\frac{a}{r_{out}}\right) = 11.190\left(\frac{a}{r_{out}}\right)^4 - 3.766\left(\frac{a}{r_{out}}\right)^3 - 1.072\left(\frac{a}{r_{out}}\right)^2 + 3.615\left(\frac{a}{r_{out}}\right) + 0.012.$$

(6.6)

Equation (6.5) was used to evaluate J_{max} and J_{min}, using F_{max} and F_{min}, respectively. The difference between J_{max} and J_{min} was then evaluated to compare the CRB results with those of the unnotched dumbbell samples. The J-integral of the axisymmetric dumbbell was evaluated considering that *J* can be approximated as the energy release rate *G* [129]; this can be evaluated according to (6.1). The comparison of the J-integral as a function of the number of cycles to failure for the two geometries is represented in Figure 6.9. As shown, a unique fitting curve was found for both geometries, demonstrating that independently of the specimen geometry, it is possible to evaluate the fatigue lifetime based on the J-integral.

Figure 6.9 Wöhler curves in terms of the J-integral for the 3D dumbbell (blue) and CRB (red) specimens. A unique fitting line was found correlating the two geometries. Reproduced from [9].

7 Summary and Conclusions

In this thesis, the focus was devoted to the fatigue behavior of elastomers. In particular, special attention was dedicated to the influence of temperature with the final objective to develop a model able to consider its effect on fatigue. The results con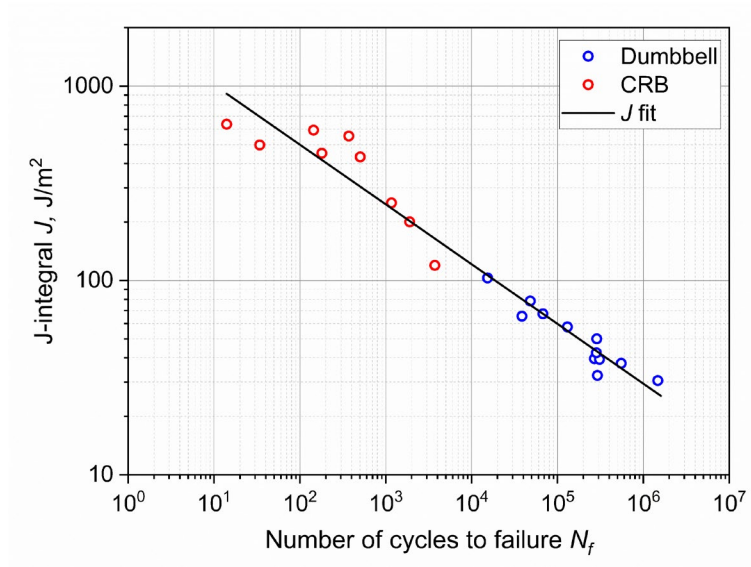cerning a carbon black (CB) filled non-crystallizing rubber (NBR) were presented in the framework of the fracture mechanics of elastomers.

First, heat build-up due to cyclic loading was studied. When studying fatigue, heat build-up represents an important aspect to consider since, due to the viscoelastic nature of elastomers, upon cyclic loading, part of the mechanical energy is converted into heat. Within the parameters influencing the extent of temperature variation, stress (or strain), frequency, material dissipation and thermal conductivity were highlighted as making a major contribution. Small variations of frequency were demonstrated to have a significant impact on the temperature increase. Moreover, due to the low thermal conductivity of elastomers - which was verified to be low and constant over the range of elastomer use - local differences in temperature within the volume are expected. This was confirmed by considering a simplified model based on the heat equation to analyze the temperature profile along the thickness: a parabolic equation able to describe the temperature profile was presented. Furthermore, according to the theory of crack propagation in viscoelastic materials in the rubbery state, higher temperatures were observed in front of a growing crack tip during fatigue loading.

The presence of heat build-up during cyclic load affects elastomer crack growth, but various other parameters also influence the fatigue process and crack propagation. Several loading parameters were considered in the framework of the state of the art and their effect was verified with the material under study. Fatigue crack growth measurement at different frequencies revealed that lower frequencies induced higher fatigue crack growth rates and that the difference was not related to energy dissipation, but due to static contribution to the

crack growth rates. Tests in force control evidenced similar trends with frequency and negligible differences in the crack growth, demonstrating no influences of the control mode of the input load. Investigations with different waveforms confirmed no effects on the fatigue crack propagation: only pulse loading affects the fatigue resistance of elastomers. In contrast to the results of crystallizing elastomers, no effect of the load ratio was observed, highlighting the role of strain-induced crystallization in determining a higher fatigue resistance with positive load ratios.

Once the aspects related to heat build-up and the effect of loading parameters on fatigue crack propagation were clarified, the effect of temperature on the mechanical and fatigue behavior was analyzed in order to develop a model to describe its influence on fatigue. Tests at large deformation evidenced a decrease in the ultimate properties and stiffness. This was related to a larger contribution of viscoelastic effects that overcame the entropic response. Moreover, Mooney- Rivlin plots revealed that the maximum chain extensibility, connected with the upturn strain, decreases with temperature and possesses a minimum at intermediate temperature while it increases at higher temperatures. DMA in terms of temperature sweeps showed an Arrhenius dependence of the dynamic properties in the rubbery state (above T_g + 30 °C). Furthermore, isothermal frequency sweeps were horizontally shifted along the frequency axis and a master curve of the dynamic properties was obtained. Fatigue crack growth measurements at high temperatures revealed that higher temperatures resulted in higher crack growth rates with the same tearing energy. On the other hand, the curves had the same slopes but they were shifted towards lower tearing energies, suggesting that similar processes were involved but at lower energies. This effect was modeled by considering an Arrhenius equation and the temperature dependence of the loss modulus. With this model, a fatigue master curve was obtained by shifting the curves on the tearing energy axis.

Fracture mechanics was applied to correlate fatigue crack growth to fatigue lifetime. Specifically, the defect size was calculated from fatigue data by neglecting initiation and integrating the crack growth characteristics. To do so, the temperature rise due to heat built-up was considered and through the application of the fatigue master curve developed led to an accurate calculation of the defect size. The flaw dimension was found to be independent of the strain level and with an average value of 9 ± 3 μm. The value obtained was also

compared with the initial defect size established by X-ray μ-CT, confirming similar size and a good accuracy of the calculations. In addition, an equation to evaluate the J-integral of the notched specimens allowed the results of unnotched specimens to be compared, verifying a geometry independency of the J-integral formulation for the assessment of fatigue life.

8 Outlook

Although the study of fatigue and fracture mechanics of elastomers is quite a recent science, several aspects have been investigated and understood in the last 80 years. A major focus has been dedicated to elastomers used in the tire industry, namely NR and SBR. Nevertheless, several aspects are not yet fully understood and further investigations are required.

The mechanical behavior of elastomers is quite complex and characterized by entropic elasticity and viscoelastic effects. Even though the theory of entropic elasticity is established for rubbers, when considering more complex compounds used in the rubber industry, this general approach is not applicable. This is believed to be related to a different mobility of the polymer chains due to the presence of fillers and the formation of the so-called "bound rubber," which strongly affects the mechanical behavior of elastomers by also influencing its viscoelastic response. As the technologies of characterization methods and in-situ measurements advance, a deeper understanding of the phenomena involved during the deformation of complex elastomeric compounds could lead to more accurate modeling of their mechanical behavior. In addition, a more profound understanding of the duality of entropic elasticity and viscoelasticity concerning their contributions at different temperatures would be needed. In fact, their trends are opposite with respect to temperature and the overall behavior is a tradeoff of these two components, making it difficult to predict the actual behavior. Furthermore, although the detrimental effect of temperature on fatigue seems established, tools that consider this influence should be extended to other elastomers and approaches should be generalized to develop a formal theory.

Another aspect related to viscoelasticity that should be investigated is the amount of dissipated energy that is actually converted into heat during cyclic loading. It is established that the conversion is not complete and that further dissipative mechanisms are involved. However, clear evidence of which mechanism dissipates energy and the rate of conversions

of mechanical energy into heat are still obscure. As highlighted in this thesis work, the internal temperature of elastomer products subjected to cyclic loading is often higher than the surface temperature and it can be so high as to affect fatigue but can also lead to thermal damage or even thermal failure. A more thorough understanding of the dissipative mechanisms in elastomers would be beneficial for an accurate estimation of the internal temperature of components subjected to cyclic loadings in order to have an appropriate component design as a result.

Finally, very little has been understood about the crack initiation process in elastomers.. Generally, cracks nucleate starting from inhomogeneities and defects present in the materials. The complex formulations of elastomers lead to a significant level of inhomogeneities, making it complicated to determine the origin of fatigue cracks. More investigations in this regard should be performed to identify the time for initiation. Though initiation is often neglected, the recognition of the initiation time would improve the accuracy of models even more for the fatigue lifetime prediction.

References

1. Cadwell, S.M.; Merril, R.A.; Sloman, C.M.; Yost, F.L. Dynamic fatigue life of rubber. *Ind. Eng. Chem. Anal. Ed.* **1940**, *23*, 19–23, doi:10.1021/ac50141a006.

2. Rivlin, R.S.; Thomas, A.G. Rupture of rubber. I. Characteristic energy for tearing. *Journal of Polymer Science* **1953**, *10*, 291–318, doi:10.1002/pol.1953.120100303.

3. Gent, A.N.; Lindley, P.B.; Thomas, A.G. Cut growth and fatigue of rubbers. I. The relationship between cut growth and fatigue. *Journal of Applied Polymer Science* **1964**, *8*, 455–466, doi:10.1002/app.1964.070080129.

4. Lake, G.J.; Lindley, P.B. Cut growth and fatigue of rubbers. II. Experiments on a noncrystallizing rubber. *Journal of Applied Polymer Science* **1964**, *8*, 707–721, doi:10.1002/app.1964.070080212.

5. Schieppati, J.; Schrittesser, B.; Wondracek, A.; Robin, S.; Holzner, A.; Pinter, G. Impact of temperature on the fatigue and crack growth behavior of rubbers. *Procedia Structural Integrity* **2018**, *13*, 642–647, doi:10.1016/j.prostr.2018.12.106.

6. Schieppati, J.; Schrittesser, B.; Wondracek, A.; Robin, S.; Holzner, A.; Pinter, G. Heat build-up of rubbers during cyclic loading. In *Proceedings of the 11th European Conference on Constitutive Models for Rubber (ECCMR 2019), June 25-27, 2019, Nantes, France*; Huneau, B., Le Cam, J.B., Marco, Y., Verron, E., Eds., 2019.

7. Schieppati, J.; Schrittesser, B.; Wondracek, A.; Robin, S.; Holzner, A.; Pinter, G. Effect of mechanical loading history on fatigue crack growth of non-crystallizing rubber. *Engineering Fracture Mechanics* **2021**, *257*, 108010, doi:10.1016/j.engfracmech.2021.108010.

8. Schieppati, J.; Schrittesser, B.; Wondracek, A.; Robin, S.; Holzner, A.; Pinter, G. Temperature impact on the mechanical and fatigue behavior of a non-crystallizing

rubber. *International Journal of Fatigue* **2021**, *144*, 106050, doi:10.1016/j.ijfatigue.2020.106050.

9. Schieppati, J.; Schrittesser, B.; Tagliabue, S.; Andena, L.; Holzner, A.; Poduška, J.; Pinter, G. Fatigue Analysis and Defect Size Evaluation of Filled NBR including Temperature Influence. *Materials (Basel)* **2022**, *15*, 3745, doi:10.3390/ma15113745.

10. Gent, A.N.; Scott, K.W. Dynamic mechanical properties. In *Engineering with Rubber*: *How to Design Rubber Components,* 3rd Edition; Gent, A.N., Ed.; Hanser Publications, 2012.

11. Riande, E.; Diaz-Calleja, R.; Prolongo, M.; Masegosa, R.; Salom, C. *Polymer Viscoelasticity*: *Stress and Strain in Practice*, 1st Edition; CRC Press: Boca Raton, 2000, ISBN 9780429175534.

12. Dippel, B.; Johlitz, M.; Lion, A. Thermo-mechanical couplings in elastomers - experiments and modelling. *Z. Angew. Math. Mech.* **2015**, *95*, 1117–1128, doi:10.1002/zamm.201400110.

13. Li, F.; Liu, J.; Yang, H.; Lu, Y.; Zhang, L. Numerical simulation and experimental verification of heat build-up for rubber compounds. *Polymer* **2016**, *101*, 199–207, doi:10.1016/j.polymer.2016.08.065.

14. Guo, Q.; Zaïri, F.; Ovalle Rodas, C.; Guo, X. Constitutive modeling of the cyclic dissipation in thin and thick rubber specimens. *Z. Angew. Math. Mech.* **2018**, *98*, 1878–1899, doi:10.1002/zamm.201800087.

15. Guo, Q.; Zaïri, F.; Guo, X. A thermo-viscoelastic-damage constitutive model for cyclically loaded rubbers. Part I: Model formulation and numerical examples. *International Journal of Plasticity* **2018**, *101*, 106–124, doi:10.1016/j.ijplas.2017.10.011.

16. Guo, Q.; Zaïri, F.; Guo, X. A thermo-viscoelastic-damage constitutive model for cyclically loaded rubbers. Part II: Experimental studies and parameter identification. *International Journal of Plasticity* **2018**, *101*, 58–73, doi:10.1016/j.ijplas.2017.10.009.

17. Cruanes, C.; Deffarges, M.-P.; Lacroix, F.; Méo, S. Modeling of the thermomechanical behavior of rubbers during fatigue tests from infrared measurements. *International Journal of Fatigue* **2019**, *126*, 231–240, doi:10.1016/j.ijfatigue.2019.04.035.

18. Ovalle Rodas, C.; Zaïri, F.; Naït-Abdelaziz, M.; Charrier, P. A thermo-visco-hyperelastic model for the heat build-up during low-cycle fatigue of filled rubbers: Formulation, implementation and experimental verification. *International Journal of Plasticity* **2016**, *79*, 217–236, doi:10.1016/j.ijplas.2015.01.001.

19. Le Saux, V.; Marco, Y.; Calloch, S.; Taveau, D. Heat build-up of rubber under cyclic loadings: validation of an efficient demarch to predict the temperature fields. *Rubber Chemistry and Technology* **2013**, *86*, 38–56, doi:10.5254/rct.13.88912.

20. Wollscheid, D.; Lion, A. Predeformation- and frequency-dependent material behaviour of filler-reinforced rubber: Experiments, constitutive modelling and parameter identification. *International Journal of Solids and Structures* **2013**, *50*, 1217–1225, doi:10.1016/j.ijsolstr.2012.12.015.

21. Johnson, A.R.; Chen, T.-K. Approximating thermo-viscoelastic heating of largely strained solid rubber components. *Computer Methods in Applied Mechanics and Engineering* **2005**, *194*, 313–325, doi:10.1016/j.cma.2004.03.014.

22. Luo, W.; Yin, B.; Hu, X.; Zhou, Z.; Deng, Y.; Song, K. Modeling of the heat build-up of carbon black filled rubber. *Polymer Testing* **2018**, *69*, 116–124, doi:10.1016/j.polymertesting.2018.05.017.

23. Zhi, J.; Wang, S.; Zhang, M.; Wang, H.; Lu, H.; Lin, W.; Qiao, C.; Hu, C.; Jia, Y. Numerical analysis of the dependence of rubber hysteresis loss and heat generation on temperature and frequency. *Mech Time-Depend Mater* **2019**, *23*, 427–442, doi:10.1007/s11043-018-9398-8.

24. Kerchman, V.; Shaw, C. Experimental Study and Finite Element Simulation of Heat Build-Up in Rubber Compounds with Application to Fracture. *Rubber Chemistry and Technology* **2003**, *76*, 386–405.

25. Le Saux, V.; Marco, Y.; Calloch, S.; Doudard, C.; Charrier, P. Fast evaluation of the fatigue lifetime of rubber-like materials based on a heat build-up protocol and micro-tomography measurements. *International Journal of Fatigue* **2010**, *32*, 1582–1590, doi:10.1016/j.ijfatigue.2010.02.014.

26. Ferry, J.D. *Viscoelastic properties of polymers*, 3rd ed.; Wiley: New York, Chichester, 1980, ISBN 978-0-471-04894-7.

27. Hertzberg, R.W.; Manson, J.A. *Fatigue of engineering plastics;* Academic Press: New York, London, 1980, ISBN 0123435501.

28. Kar, K.K.; Bhowmick, A.K. Hysteresis loss in filled rubber vulcanizates and its relationship with heat generation. *Journal of Apllied Polymer Science* **1997**, *64*, 1541–1555, doi:10.1002/(SICI)1097-4628(19970523)64:8<1541:AID-APP12>3.0.CO;2-0.

29. Medalia, A.I. Heat generation in elastomer compounds: causes and effects. *Rubber Chemistry and Technology* **1991**, *64*, 481–492, doi:10.5254/1.3538565.

30. Park, D.M.; Hong, W.H.; Kim, S.G.; Kim, H.J. Heat generation of filled rubber vulcanizates and its relationship with vulcanizate network structures. *European Polymer Journal* **2000**, *36*, 2429–2436, doi:10.1016/S0014-3057(00)00020-3.

31. Jungk, J.; Klüppel, M. Simulation of the internal sample temperature of rubber components during cyclic deformation authors. *KGK. Kautschuk, Gummi, Kunststoffe* **2011**, *64*, 44–51.

32. Dedova, S.; Schneider, K.; Heinrich, G. Influence of dissipative specimen heating on the tearing energy of elastomers estimated by global adn local characterization methods. In *Constitutive Models for Rubber X*: *Proceedings of the 10th European Conference on Constitutive Models for Rubber (ECCMR), Munich, Germany, 28-31 August 2017*; Lion, A., Johlitz, M., Eds.; CRC Press Taylor & Francis Group: London, 2017; pp 219–224, ISBN 9781138030015.

33. Persson, B.N.J.; Brener, E.A. Crack propagation in viscoelastic solids. *Phys. Rev. E Stat. Nonlin. Soft Matter Phys.* **2005**, *71*, 36123, doi:10.1103/PhysRevE.71.036123.

34. Griffith, A.A. The phenomena of rupture and flow in solids // VI. The phenomena of rupture and flow in solids. *Phil. Trans. R. Soc. Lond. A* **1921**, *221*, 163–198, doi:10.1098/rsta.1921.0006.

35. Lake, G.J.; Lindley, P.B. The mechanical fatigue limit for rubber. *J. Appl. Polym. Sci.* **1965**, *9*, 1233–1251, doi:10.1002/app.1965.070090405.

36. Paris, P.; Erdogan, F. A Critical Analysis of Crack Propagation Laws. *Journal of Basic Engineering* **1963**, *85*, 528–533, doi:10.1115/1.3656900.

37. Mars, W.V.; Fatemi, A. A literature survey on fatigue analysis approaches for rubber. *International Journal of Fatigue* **2002**, *24*, 949–961, doi:10.1016/S0142-1123(02)00008-7.

38. Ellul, M.D. Mechanical fatigue. In *Engineering with Rubber*: *How to Design Rubber Components,* 3rd Edition; Gent, A.N., Ed.; Hanser Publications, 2012.

39. Mars, W.V.; Fatemi, A. Factors that affect the fatigue life of rubber: a literature survey. *Rubber Chemistry and Technology* **2004**, *77*, 391-412, doi:10.5254/1.3547831.

40. Seichter, S.; Archodoulaki, V.-M.; Koch, T.; Holzner, A.; Wondracek, A. Investigation of different influences on the fatigue behaviour of industrial rubbers. *Polymer Testing* **2017**, *59*, 99–106, doi:10.1016/j.polymertesting.2017.01.018.

41. Busfield, J.J.C.; Tsunoda, K.; Davies, C.K.; Thomas, A.G. Contributions of Time Dependent and Cyclic Crack Growth to the Crack Growth Behavior of Non Strain-Crystallizing Elastomers. *Rubber Chemistry and Technology* **2002**, *75*, 643–656, doi:10.5254/1.3544991.

42. *The test frequency dependence of the fatigue behavior of elastomers;* Major, Z.; Feichter, C.; Steinberger, R.; Lang, R., Eds. Fracture of Nano and Engineering Materials and Structures - Proceedings of the 16th European Conference of Fracture, 2006.

43. Lindley, P.B. Non-relaxing crack growth and fatigue in a non-crystallizing rubber. *Rubber Chemistry and Technology* **1974**, *47*, 1253–1264, doi:10.5254/1.3540497.

44. Andreini, G.; Straffi, P.; Cotugno, S.; Gallone, G.; Polacco, G. Comparison of sine versus pulse waveform effects on fatigue crack growth behavior of NR, SBR, and BR compounds. *Rubber Chemistry and Technology* **2010**, *83*, 391–403.

45. Stadlbauer, F.; Koch, T.; Archodoulaki, V.-M.; Planitzer, F.; Fidi, W.; Holzner, A. Influence of Experimental Parameters on Fatigue Crack Growth and Heat Build-Up in Rubber. *Materials* **2013**, *6*, 5502–5516, doi:10.3390/ma6125502.

46. Ghosh, P.; Stocek, R.; Gehde, M.; Mukhopadhyay, R.; Krishnakumar, R. Investigation of fatigue crack growth characteristics of NR/BR blend based tyre tread compounds. *Int J Fract* **2014**, *188*, 9–21, doi:10.1007/s10704-014-9941-9.

47. Harbour, R.J.; Fatemi, A.; Mars, W.V. The effect of a dwell period on fatigue crack growth rates in filled SBR and NR. *Rubber Chemistry and Technology* **2007**, *80*, 838–853, doi:10.5254/1.3539420.

48. Harbour, R.J.; Fatemi, A.; Mars, W.V. Fatigue crack growth of filled rubber under constant and variable amplitude loading conditions. *Fat Frac Eng Mat Struct* **2007**, *30*, 640–652, doi:10.1111/j.1460-2695.2007.01143.x.

49. Saintier, N.; Cailletaud, G.; Piques, R. Cyclic loadings and crystallization of natural rubber: An explanation of fatigue crack propagation reinforcement under a positive loading ratio. *Materials Science and Engineering: A* **2011**, *528*, 1078–1086, doi:10.1016/j.msea.2010.09.079.

50. Beurrot-Borgarino, S.; Huneau, B.; Verron, E.; Rublon, P. Strain-induced crystallization of carbon black-filled natural rubber during fatigue measured by in situ synchrotron X-ray diffraction. *International Journal of Fatigue* **2013**, *47*, 1–7, doi:10.1016/j.ijfatigue.2012.07.001.

51. Brüning, K.; Schneider, K.; Roth, S.V.; Heinrich, G. Strain-induced crystallization around a crack tip in natural rubber under dynamic load. *Polymer* **2013**, *54*, 6200–6205, doi:10.1016/j.polymer.2013.08.045.

52. Rublon, P.; Huneau, B.; Saintier, N.; Beurrot, S.; Leygue, A.; Verron, E.; Mocuta, C.; Thiaudière, D.; Berghezan, D. In situ synchrotron wide-angle X-ray diffraction

investigation of fatigue cracks in natural rubber. *J. Synchrotron Radiat.* **2013**, *20*, 105–109, doi:10.1107/S0909049512044457.

53. Candau, N.; Chazeau, L.; Chenal, J.-M.; Gauthier, C.; Ferreira, J.; Munch, E.; Thiaudière, D. Strain induced crystallization and melting of natural rubber during dynamic cycles. *Phys. Chem. Chem. Phys.* **2015**, *17*, 15331–15338, doi:10.1039/c5cp00384a.

54. Champy, C.; Le Saux, V.; Marco, Y.; Glanowski, T.; Charrier, P.; Hervouet, W. Fatigue of crystallizable rubber: Generation of a Haigh diagram over a wide range of positive load ratios. *International Journal of Fatigue* **2021**, *150*, 106313, doi:10.1016/j.ijfatigue.2021.106313.

55. Ruellan, B.; Le Cam, J.-B.; Robin, E.; Jeanneau, I.; Canévet, F.; Mauvoisin, G.; Loison, D. Fatigue crack growth in natural rubber: The role of SIC investigated through post-mortem analysis of fatigue striations. *Engineering Fracture Mechanics* **2018**, *201*, 353–365, doi:10.1016/j.engfracmech.2018.07.001.

56. Ruellan, B.; Le Cam, J.-B.; Jeanneau, I.; Canévet, F.; Mortier, F.; Robin, E. Fatigue of natural rubber under different temperatures. *International Journal of Fatigue* **2019**, *124*, 544–557, doi:10.1016/j.ijfatigue.2018.10.009.

57. Marano, C.; Calabrò, R.; Rink, M. Effect of molecular orientation on the fracture behavior of carbon black-filled natural rubber compounds. *J. Polym. Sci. B Polym. Phys.* **2010**, *48*, 1509–1515, doi:10.1002/polb.22054.

58. Xiang, F.; Schneider, K.; Heinrich, G. New observations regarding fatigue crack paths and their fracture surfaces in natural rubber: Influences of R-ratio and pre-load. *International Journal of Fatigue* **2020**, *135*, 105508, doi:10.1016/j.ijfatigue.2020.105508.

59. Mars, W.V.; Fatemi, A. A Phenomenological Model for the Effect of R-ratio on Fatigue in Strain Crystallizing Rubbers. *Rubber Chemistry and Technology* **2003**, *76*, 1241–1258, doi:10.5254/1.3547800.

60. Gent, A.N. Elasticity. In *Engineering with Rubber*: *How to Design Rubber Components,* 3rd Edition; Gent, A.N., Ed.; Hanser Publications, 2012.

61. Gent, A.N. Rubber Elasticity: Basic Concepts and Behavior. In *The Science and Technology of Rubber*; Mark, J.E., Erman, B., Roland, C.M., Eds.; Academic Press, 2013, ISBN 978-0-12-394584-6.

62. Mooney, M. A theory of large elastic deformation. *Journal of Applied Physics* **1940**, *11*, 582.

63. Rivlin, R.S. Large elastic deformations of isotropic materials IV. Further developments of the general theory. *Phil. Trans. R. Soc. Lond. A* **1948**, *241*, doi:10.1098/rsta.1948.0024.

64. Gao, Y.; Liu, J.; Shen, J.; Zhang, L.; Guo, Z.; Cao, D. Uniaxial deformation of nanorod filled polymer nanocomposites: A coarse-grained molecular dynamics simulation. *Phys. Chem. Chem. Phys.* **2014**, *16*, 16039–16048, doi:10.1039/c4cp01555j.

65. Tzounis, L.; Debnath, S.; Rooj, S.; Fischer, D.; Mäder, E.; Das, A.; Stamm, M.; Heinrich, G. High performance natural rubber composites with a hierarchical reinforcement structure of carbon nanotube modified natural fibers. *Materials & Design* **2014**, *58*, 1–11, doi:10.1016/j.matdes.2014.01.071.

66. Fu, X.; Huang, G.; Xie, Z.; Xing, W. New insights into reinforcement mechanism of nanoclay-filled isoprene rubber during uniaxial deformation by in situ synchrotron X-ray diffraction. *RSC Adv.* **2015**, *5*, 25171–25182, doi:10.1039/C5RA02123E.

67. Peddini, S.K.; Bosnyak, C.P.; Henderson, N.M.; Ellison, C.J.; Paul, D.R. Nanocomposites from styrene–butadiene rubber (SBR) and multiwall carbon nanotubes (MWCNT) part 2: Mechanical properties. *Polymer* **2015**, *56*, 443–451, doi:10.1016/j.polymer.2014.11.006.

68. He, F.; Yuan, T.; Li, C.; Sun, L.; Liao, S. Interfacial interactions and properties of natural rubber-silica composites with liquid natural rubber as a compatibilizer and

prepared by a wet-compounding method. *J. Appl. Polym. Sci.* **2018**, *135*, 46457, doi:10.1002/app.46457.

69. Furukawa, J.; Onouchi, Y.; Inagaki, S.; Okamoto, H. Rubber elasticity at very large elongation. *Polymer Bulletin* **1982**, *6*, 381–387, doi:10.1007/BF00959847.

70. Bokobza, L.; Rapoport, O. Reinforcement of natural rubber. *Journal of Applied Polymer Science* **2002**, *85*, 2301–2316.

71. Fritzsche, J.; Klüppel, M. Structural dynamics and interfacial properties of filler-reinforced elastomers. *Journal of physics: Condensed matter* **2011**, *23*, 35104, doi:10.1088/0953-8984/23/3/035104.

72. Le Gal, A.; Yang, X.; Klüppel, M. Evaluation of sliding friction and contact mechanics of elastomers based on dynamic-mechanical analysis. *J. Chem. Phys.* **2005**, *123*, 14704, doi:10.1063/1.1943410.

73. Klüppel, M. Evaluation of viscoelastic master curves of filled elastomers and applications to fracture mechanics. *J. Phys. Condens. Matter* **2009**, *21*, 35104, doi:10.1088/0953-8984/21/3/035104.

74. Isono, Y.; Aoyama, T. Filler Effects on Temperature Shift Factors in Viscoelastic Properties of Carbon Black Filled Rubbers. *Nihon Reoroji Gakkaishi* **2013**, *41*, 137–144.

75. Rouleau, L.; Deü, J.-F.; Legay, A.; Le Lay, F. Application of Kramers–Kronig relations to time–temperature superposition for viscoelastic materials. *Mechanics of Materials* **2013**, *65*, 66–75, doi:10.1016/j.mechmat.2013.06.001.

76. Butaud, P.; Placet, V.; Klesa, J.; Ouisse, M.; Foltete, E.; Gabrion, X. Investigations on the frequency and temperature effects on mechanical properties of a shape memory polymer (Veriflex). *Mechanics of Materials* **2015**, *87*, 50–60, doi:10.1016/j.mechmat.2015.04.002.

77. Han, C.D.; Kim, J.K. On the use of time-temperature superposition in multicomponent/multiphase polymer systems. *Polymer* **1993**, *34*, 2533–2539, doi:10.1016/0032-3861(93)90585-X.

78. van Gurp, M.; Palmen, J. Time-Temperature Superposition for Polymer Blends. *Rheology Bullettin* **1998**, *67*, 5–8.

79. Wang, M.-J.; Lu, S.X.; Mahmud, K. Carbon–silica dual-phase filler, a new-generation reinforcing agent for rubber. Part VI. Time–temperature superposition of dynamic properties of carbon–silica-dual-phase-filler-filled vulcanizates. *J. Polym. Sci. B Polym. Phys.* **2000**, *38*, 1240–1249, doi:10.1002/(SICI)1099-0488(20000501)38:9<1240:AID-POLB15>3.0.CO;2-Q.

80. Lorenz, B.; Pyckhout-Hintzen, W.; Persson, B. Master curve of viscoelastic solid: Using causality to determine the optimal shifting procedure, and to test the accuracy of measured data. *Polymer* **2014**, *55*, 565–571, doi:10.1016/j.polymer.2013.12.033.

81. Asare, S.; Busfield, J.J.C. Fatigue life prediction of bonded rubber components at elevated temperature. *Plastics, Rubber and Composites* **2011**, *40*, 194–200, doi:10.1179/1743289810Y.0000000044.

82. Wu, J.; Chen, L.; Li, H.H.; Su, B.L.; Wang, Y.S. Effect of Temperature on Tensile Fatigue Life of Natural Rubber. *IOP Conf. Ser.: Mater. Sci. Eng.* **2018**, *389*, 12024, doi:10.1088/1757-899X/389/1/012024.

83. Legorju-jago K.; Bathias, C. Fatigue initiation and propagation in natural and synthetic rubbers. *International Journal of Fatigue* **2002**, *24*, 85–92, doi:10.1016/S0142-1123(01)00062-7.

84. Young, D.G. Fatigue crack propagation in elastomer compounds: effects of strain rate, temperature, strain level, and oxidation. *Rubber Chemistry and Technology* **1986**, *59*, 809–825.

85. Young, D.G.; Danik, J.A. Effect of temperature on fatigue and fracture. *Rubber Chemistry and Technology* **1994**, *67*, 137–147, doi:10.5254/1.3538660.

86. Neuhaus, C.; Lion, A.; Johlitz, M.; Heuler, P.; Barkhoff, M.; Duisen, F. Fatigue behaviour of an elastomer under consideration of ageing effects. *International Journal of Fatigue* **2017**, *104*, 72–80, doi:10.1016/j.ijfatigue.2017.07.010.

87. El Maanaoui, H.; Meier, J. Lifetime prediction with temperature dependence for EPDM and NR elastomers based on fatigue crack growth mechanical measurements and filler distribution. *Polymer* **2021**, *228*, 123909, doi:10.1016/j.polymer.2021.123909.

88. Béranger, A.S.; Qin, J.; Heuillet, P.; Baurier, H. Fatigue crack growth behavior of NBR, HNBR, HNBR ZSC compounds. *Procedia Engineering* **2018**, *213*, 145–152, doi:10.1016/j.proeng.2018.02.016.

89. Gent, A.N.; Lai, S.M. Interfacial bonding, energy dissipation, and adhesion. *Journal of Polymer Science Part B: Polymer Physics* **1994**, *32*, 1543–1555, doi:10.1002/polb.1994.090320826.

90. Gent, A.N. Adhesion and strength of viscoelastic solids. Is there a relationship between adhesion and bulk properties? *Langmuir* **1996**, *12*, 4492–4496.

91. Wunde, M.; Klüppel, M. Viscoelastic response during crack propagation of unfilled and filled SBR. *Rubber Chemistry and Technology* **2018**, *91*, 668–682, doi:10.5254/rct.18.81537.

92. Luo, W.; Li, M.; Huang, Y.; Yin, B.; Hu, X. Effect of temperature on the tear fracture and fatigue life of carbon-black-filled rubber. *Polymers (Basel)* **2019**, *11*, doi:10.3390/polym11050768.

93. Lake, G.J.; Thomas, A.G. Strength. In *Engineering with Rubber*: *How to Design Rubber Components,* 3rd Edition; Gent, A.N., Ed.; Hanser Publications, 2012.

94. Persson, B.N.J.; Albohr, O.; Heinrich, G.; Ueba, H. Crack propagation in rubber-like materials. *J. Phys.: Condens. Matter* **2005**, *17*, R1071-R1142, doi:10.1088/0953-8984/17/44/R01.

95. Nie, Y.; Wang, B.; Huang, G.; Qu, L.; Zhang, P.; Weng, G.; Wu, J. Relationship between the material properties and fatigue crack-growth characteristics of natural rubber filled with different carbon blacks. *Journal of Apllied Polymer Science* **2010**, *24*, 3341-3347, doi:10.1002/app.32098.

96. Nie, Y.; Qu, L.; Huang, G.; Wang, B.; Weng, G.; Wu, J. Improved resistance to crack growth of natural rubber by the inclusion of nanoclay. *Polym. Adv. Technol.* **2012**, *23*, 85–91, doi:10.1002/pat.1826.

97. Rooj, S.; Das, A.; Morozov, I.A.; Stöckelhuber, K.W.; Stocek, R.; Heinrich, G. Influence of "expanded clay" on the microstructure and fatigue crack growth behavior of carbon black filled NR composites. *Composites Science and Technology* **2013**, *76*, 61–68, doi:10.1016/j.compscitech.2012.12.020.

98. Wöhler, A. Wöhler's experiments on the strength of metals. *Engineering* **1867;**, *2*.

99. Haigh, B.P. Experiments on the fatigue of brasses. *Journal of the Institute of Metal* **1917**.

100. Choi, I.S.; Roland, C.M. Intrinsic defects and the failure properties of cis-1,4-polyisoprenes. *Rubber Chemistry and Technology* **1996**, *69*, 591–599, doi:10.5254/1.3538386.

101. Guo, H.; Li, F.; Wen, S.; Yang, H.; Zhang, L. Characterization and Quantitative Analysis of Crack Precursor Size for Rubber Composites. *Materials (Basel)* **2019**, *12*, doi:10.3390/ma12203442.

102. Huneau, B.; Masquelier, I.; Marco, Y.; Le Saux, V.; Noizet, S.; Schiel, C.; Charrier, P. Fatigue crack initiation in a carbon black-filled natural rubber. *Rubber Chemistry and Technology* **2016**, *89*, 126–141.

103. Balutch, T.; Huneau, B.; Marco, Y.; Charrier, P.; Champy, C.; Hénaff, G. Fatigue behaviour of an industrial synthetic rubber. *MATEC Web Conf.* **2018**, *165*, 22004, doi:10.1051/matecconf/201816522004.

104. Marco, Y.; Le Saux, V.; Calloch, S.; Charrier, P. X-ray computed µ-tomography: a tool for the characterization of fatigue defect population in a polychloroprene rubber. *Procedia Engineering* **2010**, *2*, 2131–2140, doi:10.1016/j.proeng.2010.03.229.

105. Le Saux, V.; Marco, Y.; Calloch, S.; Charrier, P. Evaluation of the fatigue defect population in an elastomer using X-ray computed micro-tomography. *Polym Eng Sci* **2011**, *51*, 1253–1263, doi:10.1002/pen.21872.

106. Marco, Y.; Huneau, B.; Masquelier, I.; Le Saux, V.; Charrier, P. Prediction of fatigue properties of natural rubber based on the descriptions of the cracks population and of the dissipated energy. *Polymer Testing* **2017**, *59*, 67–74, doi:10.1016/j.polymertesting.2017.01.015.

107. Fielding-Russell, G.S.; Rongone, R.L. Fatiguing of rubber-rubber interfaces. *Rubber Chemistry and Technology* **1983**, *56*, 838–844, doi:10.5254/1.3538158.

108. Royo, J. Fatigue testing of rubber materials and articles. *Polymer Testing* **1992**, *11*, 325–344, doi:10.1016/0142-9418(92)90002-S.

109. Lake, G.J. Fatigue and fracture of elastomers. *Rubber Chemistry and Technology* **1995**, *68*, 435–460, doi:10.5254/1.3538750.

110. Mars, W.V.; Fatemi, A. Fatigue crack nucleation and growth in filled natural rubber. *Fatigue and Fracture of Engineering Materials and Structures* **2003**, *26*, 779–789, doi:10.1046/j.1460-2695.2003.00678.x.

111. Zarrin-Ghalami, T.; Fatemi, A. Fatigue life predictions of rubber components: Applications to an automobile cradle mount. *Proceedings of the Institution of Mechanical Engineers, Part D: Journal of Automobile Engineering* **2012**, *227*, 691–703, doi:10.1177/0954407012461863.

112. Zarrin-Ghalami, T.; Fatemi, A. Material deformation and fatigue behavior characterization for elastomeric component life predictions. *Polym Eng Sci* **2012**, *52*, 1795–1805, doi:10.1002/pen.23125.

113. Kim, H.J.; Song, M.W.; Moon, H.I.; Kim, H.; Kim, H.Y. Fatigue life prediction of a rubber material based on dynamic crack growth considering shear effect. *Int.J Automot. Technol.* **2014**, *15*, 317–324, doi:10.1007/s12239-014-0032-8.

114. El Yaagoubi, M.; Juhre, D.; Meier, J.; Kröger, N.; Alshuth, T.; Giese, U. Lifetime prediction of filled elastomers based on particle distribution and the J-integral evaluation. *International Journal of Fatigue* **2018**, *112*, 341–354, doi:10.1016/j.ijfatigue.2018.03.024.

115. Gehrmann, O.; El Yaagoubi, M.; El Maanaoui, H.; Meier, J. Lifetime prediction of simple shear loaded filled elastomers based on the probability distribution of particles. *Polymer Testing* **2019**, *75*, 229–236, doi:10.1016/j.polymertesting.2019.02.025.

116. Le Cam, J.-B.; Huneau, B.; Verron, E.; Gornet, L. Mechanism of fatigue crack growth in carbon black filled natural rubber. *Macromolecules* **2004**, *37*, 5011–5017.

117. Mars, W.V.; Fatemi, A. Nucleation and growth of small fatigue cracks in filled natural rubber under multiaxial loading. *J Mater Sci* **2006**, *41*, 7324–7332, doi:10.1007/s10853-006-0962-2.

118. Hainsworth, S.V. An environmental scanning electron microscopy investigation of fatigue crack initiation and propagation in elastomers. *Polymer Testing* **2007**, *26*, 60–70, doi:10.1016/j.polymertesting.2006.08.007.

119. Saintier, N.; Cailletaud, G.; Piques, R. Crack initiation and propagation under multiaxial fatigue in a natural rubber. *International Journal of Fatigue* **2006**, *28*, 61–72, doi:10.1016/j.ijfatigue.2005.03.006.

120. Le Cam, J.-B.; Toussaint, E. The mechanism of fatigue crack growth in rubbers under severe loading: The Effect of Stress-Induced Crystallization. *Macromolecules* **2010**, *43*, 4708–4714, doi:10.1021/ma100042n.

121. Weng, G.; Huang, G.; Lei, H.; Qu, L.; Nie, Y.; Wu, J. Crack initiation and evolution in vulcanized natural rubber under high temperature fatigue. *Polymer Degradation and Stability* **2011**, *96*, 2221–2228, doi:10.1016/j.polymdegradstab.2011.09.004.

122. Le Cam, J.-B.; Huneau, B.; Verron, E. Fatigue damage in carbon black filled natural rubber under uni- and multiaxial loading conditions. *International Journal of Fatigue* **2013**, *52*, 82–94, doi:10.1016/j.ijfatigue.2013.02.022.

123. Le Cam, J.-B.; Huneau, B.; Verron, E. Failure analysis of carbon black filled styrene butadiene rubber under fatigue loading conditions. *Plastics, Rubber and Composites* **2014**, *43*, 187–191, doi:10.1179/1743289814Y.0000000089.

124. Federico, C.E.; Padmanathan, H.R.; Kotecky, O.; Rommel, R.; Rauchs, G.; Fleming, Y.; Addiego, F.; Westermann, S. Cavitation Micro-mechanisms in Silica-Filled Styrene-Butadiene Rubber Upon Fatigue and Cyclic Tensile Testing. In *Fatigue Crack Growth in Rubber Materials*: *Experiments and Modelling*; Heinrich G., Kipscholl R., Stoček R., Ed.; Springer, Cham., 2020, ISBN 978-3-030-68919-3.

125. El Yaagoubi, M.; El Maanaoui, H.; Meier, J. New fatigue test sample: Lifetime prediction of carbon black filled elastomers based on the probability distribution of particles. *Polymer* **2020**, *208*, 122973, doi:10.1016/j.polymer.2020.122973.

126. Euchler, E.; Bernhardt, R.; Schneider, K.; Heinrich, G.; Tada, T.; Wießner, S.; Stommel, M. Cavitation in Rubber Vulcanizates Subjected to Constrained Tensile Deformation. In *Fatigue Crack Growth in Rubber Materials*: *Experiments and Modelling*; Heinrich G., Kipscholl R., Stoček R., Ed.; Springer, Cham., 2020, ISBN 978-3-030-68919-3.

127. Arbeiter, F.; Schrittesser, B.; Frank, A.; Berer, M.; Pinter, G. Cyclic tests on cracked round bars as a quick tool to assess the long term behaviour of thermoplastics and elastomers. *Polymer Testing* **2015**, *45*, 83–92, doi:10.1016/j.polymertesting.2015.05.008.

128. Wang, C.; Stiller, T.; Hausberger, A.; Pinter, G.; Grün, F.; Schwarz, T. Correlation of Tribological Behavior and Fatigue Properties of Filled and Unfilled TPUs. *Lubricants* **2019**, *7*, 60, doi:10.3390/lubricants7070060.

129. El Yaagoubi, M.; Juhre, D.; Meier, J.; Alshuth, T.; Giese, U. Tearing energy and path-dependent J-integral evaluation considering stress softening for carbon black

reinforced elastomers. *Engineering Fracture Mechanics* **2018**, *190*, 259–272, doi:10.1016/j.engfracmech.2017.12.029.

List of Publications

Publication 1

Impact of temperature on the fatigue and crack growth behavior of rubbers

Jacopo Schieppati [a], Bernd Schrittesser [a], Alfred Wondracek [b], Stefan Robin [b], Armin Holzner [b] and Gerald Pinter [c]

[a]   Polymer Competence Center Leoben GmbH, Roseggerstrasse 12, 8700 Leoben, Austria
[b]   Semperit Technische Produkte Gesellschaft m.b.H., Triester Bundesstrasse 26, 2632 Wimpassing, Austria
[c]   Department of Polymer Engineering and Science – Material Science and Testing of Polymers, Montanuniversität, Otto Glöckel-Strasse 2, 8700 Leoben, Austria

Relevant contributions to this publication:

Conceptualization:	Jacopo Schieppati, Bernd Schrittesser, Alfred Wondracek, Stefan Robin, Armin Holzner, Gerald Pinter
Methodology:	Jacopo Schieppati, Bernd Schrittesser
Investigation:	Jacopo Schieppati
Writing - Original Draft:	Jacopo Schieppati
Writing - Review & Editing:	Jacopo Schieppati; Bernd Schrittesser, Alfred Wondracek, Gerald Pinter

ECF22 - Loading and Environmental effects on Structural Integrity

Impact of temperature on the fatigue and crack growth behavior of rubbers

Jacopo Schieppati[a]*, Bernd Schrittesser[a], Alfred Wondracek[b], Stefan Robin[b], Armin Holzner[b], Gerald Pinter[c]

[a]Polymer Competence Center Leoben GmbH, Roseggerstrasse 12, 8700 Leoben, Austria
[b]Semperit Technische Produkte Gesellschaft m.b.H., Triester Bundesstrasse 26, 2632 Wimpassing, Austria
[c]Department of Polymer Engineering and Science,, Montanuniversitaet, Otto Glöckel-Strasse 2, 8700 Leoben, Austria

Abstract

Elasticity and chemical resistance are only two of outstanding properties of elastomers and make them applicable in a broad field of cyclic loaded components. During the cyclic loading, the failure is mainly related to crack growth mechanism. For the description and prediction of the material failure, fracture mechanics concepts represent a valid tool. In the field of elastomer failure under cyclic loading, two main approaches have been developed: (1) the crack nucleation dealing with the lifetime of rubber, due to a specific number of cycles until appearance of a specific crack size and (2) the crack growth approach, devoting the attention to the growth of pre-existing defects. Although both approaches represent effective instruments for fatigue analysis, only little attention has been drawn on the impact of temperature on the failure behavior. Moreover, scientific publications report that temperature influences the fatigue life of rubbers by decreasing the magnitude by four orders. Therefore, a focus on the impact of temperature on the crack growth behavior seems indispensable to rise knowledge in this field. For the evaluation of influence of temperature on the fatigue performance, crack growth tests were implemented. For the characterization of crack growth behavior, pure shear specimens equipped with a camera system to measure the crack growth behavior and the temperature were monitored with contactless thermo-couples to measure the surface temperature during the cyclic loading. Furthermore, the thermal conductivity was measured at different temperatures to allow an accurate evaluation of temperature influence. With the obtained data, a further description of the failure could be provided to extend the fracture mechanics approach through the implementation of the temperature effect within different fatigue models for elastomers.

Keywords: rubber; fatigue; temperature; crack growth; thermal conductivity.

* Corresponding author. Tel.: +43 3842 42962 94.
    E-mail address: jacopo.schieppati@pccl.at

1. Introduction

The unique mechanical properties of rubbers make them suitable for applications in which cyclic loadings are involved. In this loading condition, failure is mainly related to fatigue phenomena, Gent (2012), and therefore the study of the fatigue behaviour of materials is of great practical importance in the rubber industry. The ultimate task of fatigue analysis is to estimate the lifetime of components, hence the prediction of fatigue life of materials is of critical importance in this frame. Mars and Fatemi (2002) reported that in the field of elastomers, two main approaches are followed for fatigue life prediction: (i) crack nucleation and (ii) crack growth. The first one deals with the nucleation and growth of cracks up to a certain limit and is based on a continuum mechanics approach. The second one is based on the study of the growth of pre-existing cracks up to end of service life using fracture mechanical approaches.

The fatigue behaviour of rubbers is influenced by a large number of parameters, which can be related to the mechanical history, environmental conditions and rubber formulation as pointed out by Mars and Fatemi (2004). Among them, temperature has a relevant effect on the fatigue properties of rubbers: Lake and Lindley (1964) reported a drop of 4 order of magnitude of fatigue life passing from 0 °C to 100 °C. Further analysis on the effect of temperature can be found in Young (1986), Young & Danik (1994), Legorju-Jago & Bathias (2002).

Even though an increase in temperature is considered to cause a decrease in the fatigue properties of rubbers, this effect has not been yet proved. The aim of this work is to have a better comprehension of the impact of temperature on the fatigue properties of elastomers. In order to do this, crack growth measurements have been established measuring the surface temperature and studying the effect of frequency on the crack growth rate and on temperature variation. Moreover, the impact of temperature has been assessed through thermal conductivity measurements. The measurements were carried out at different temperatures, from 30 to 130°C, in order to have a better description of the impact of temperature on the material properties. This study represents a basis to extend the fracture mechanics approach, by implementing the temperature effect in common used models for fatigue life prediction.

2. Experimental part

2.1. Materials

The material used for this research is a commercial acrylonitrile butadiene rubber (NBR) filled with 42 phr of carbon black. Due to confidentially, no additional information about the precise formulation can be given.

2.2. Crack growth measurements

For the implementation of the crack growth measurements, a pure shear specimen geometry was used. The height of the specimen was 16 mm, the width 200 mm (width to height ratio 1/12.5) and the thickness 4 mm. The samples were mounted on special clamps, preloaded to 20 N and notched. The initial notch was introduced using a razor blade, mounted on a customized tool guided on the clamping system, for an initial notch of about 25 mm. The tests were carried out using an MTS 858 Table Top System testing machine and the crack length was monitored through a camera system CV-5701P by Keyence. In order to avoid light reflections the specimens were sprayed with a white powder coating. The tests were utilized in force control mode with a load ratio of 0.1 and a maximum load of 1300 N. The surface temperature was monitored using an IR sensor placed around 10 mm in front of the initial crack tip.

From the position of the crack tip, evaluated through the pictures recorded with the camera system, the crack growth rate was calculated. The hysteresis were monitored during the cyclic loading through the MTS test device and the tearing energy G was calculated dynamically, i.e. during testing on the same specimen. For pure shear geometry, G can be calculated with equation 1, Rivlin and Thomas (1953):

$$G = W_0 \cdot h_0 = {}^{U}/_{A_{uncr}} \tag{1}$$

where W_0 is the elastically stored energy and h_0 the height of the specimen in the unstrained condition. For practical purpose, it is easier to calculate the tearing energy using the mechanical energy U calculated from the load-displacement curve divided by the uncracked area A_{uncr}. Further explanations of the procedure can be found in Stadlbauer et al. (2013).

2.3. Thermal conductivity

Thermal conductivity measurements were carried out using two different methods. In a first step, a guarded heat method was conducted using a DTD300 machine by TA instruments. Secondly, a laser flash method (LFA) was implemented with a LFA467 Hyperflash by Netzsch. However, the actual measurement from the LFA method is thermal diffusivity. The thermal conductivity can be retrieved by knowing the density and specific heat. The specific heat was measured with a DSC6000 by Perkin Elmer while the density was measured using a XS205 Dual Range Analytical Balance by Mettler Toledo. The measurements for thermal conductivity were carried out between 30 °C and 130 °C, for every 10 °C. For the measurements carried out with the first method, specimens with thickness of 2 mm were used, while for the second method 1 mm thick samples provided a higher reproducibility.

3. Results and discussion

3.1. Fatigue crack growth

Rubbers subjected to cyclic loading present high-energy dissipation due to molecular frictions, which results in a significant heat generation in the material as reported by Medalia (1991). This effect, in combination with the low thermal conductivity of elastomers, leads to a considerable increase of temperature of rubber components. The temperature could reach regions leading even to thermal failure. The degree of heat build-up strongly depends on the stiffness of the material, on the frequency of oscillation and on the loading amplitude, Gent (2012).

During fatigue crack growth tests, the evolution of the surface temperature was monitored and the results of one of the tests are reported in Fig. 1. From the plots in Fig. 1(a), it is possible to notice that the temperature increased fast in the first six thousand cycles, while afterwards a plateau value was reached around 27 °C. It is worth to notice that a slight increase of the temperature was recorded around the crack tip (grey area in the plots), which is more evident in Fig. 1(b). This increase in temperature is related to higher viscoelastic dissipations near the crack tip as suggested by Persson and Brener (2005). With increasing crack length and passing the IR sensor, the surface temperature dropped since no strain is applied in the monitored region. Even though the temperature variation is limited, the small changes reported should be considered relevant since they originated from specimens with low thickness (4 mm).

To measure the fatigue crack growth rate, tests were carried out at different frequencies in order to verify the impact of this parameter on both, surface temperature and crack growth rate. As depicted in Fig. 2(a) higher frequencies result in a rising surface temperature. As reported by Gent (2012), the heat generated per second is given by the energy dissipated per cycle multiplied by the frequency. Therefore, the increasing frequency leads to a higher amount of heat, which cannot be transferred to the surrounding environment, resulting in a rising temperature. Moreover, the frequency also impacts the crack growth rate as depicted in Fig. 2(b), with faster crack growth rates for lower frequency. Gent (2012) reported that for non-crystallizing rubbers as NBR, the frequency has a stronger effect than for crystallizing rubbers, especially at a frequency lower than 0.2 Hz. The reported results reveal a variation of one order of magnitude in the crack growth rate with a change of frequency of one order of magnitude even at frequencies higher than 0.2 Hz. Therefore, further analyses of these results were implemented to characterize this specific behavior in detail.

In a first step, the reported behavior was explained considering the rising temperature at higher frequency suggesting a higher energy dissipation, resulting in a lower available energy for crack propagation, i.e. lower crack growth rate. For the verification of this hypothesis, the dissipated and the elastically stored energy during cycling loading were analyzed. Fig. 3(a) summarizes the hysteresis curves at 1000 cycles for different frequencies. The curve shapes seem similar and the only evident variation is the increasing slope with higher frequencies, correlating to a stiffer material behavior at higher strain rates. In order to compare the dissipated and stored energies at the different frequencies, their percentages with respect to the input of mechanical energy were calculated and plotted as a function of the number of cycles in Fig. 3(b). As depicted, the differences in the percentage of dissipated energy are very small and they maintain constant along the duration of the tests at different frequencies. This fact suggests that the energy dissipation is not responsible for the observed differences in the crack growth rate.
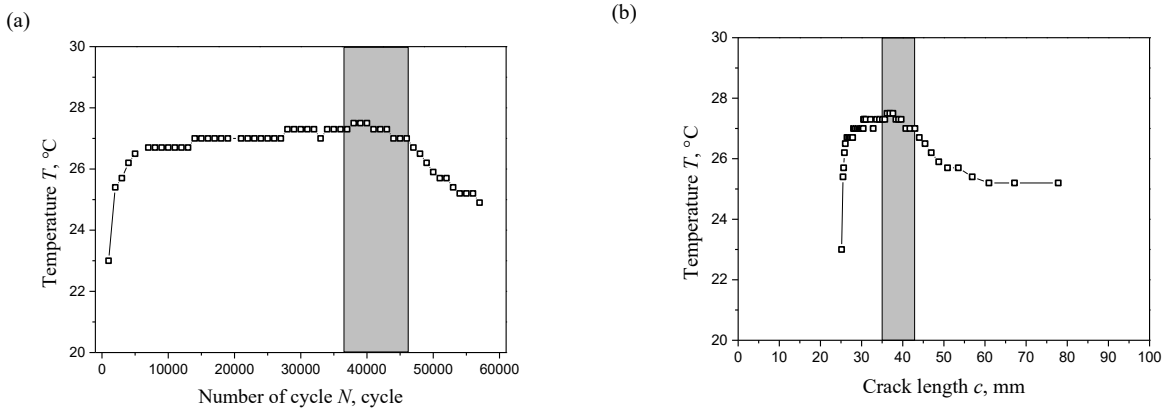
Fig. 1. (a) Surface temperature as a function of number of cycle and (b) surface temperature as a function of crack length. The plots refer to a test carried out at 4 Hz; the grey area corresponds to the number of cycle (a) and the position (b) at which the crack was below the IR sensor.
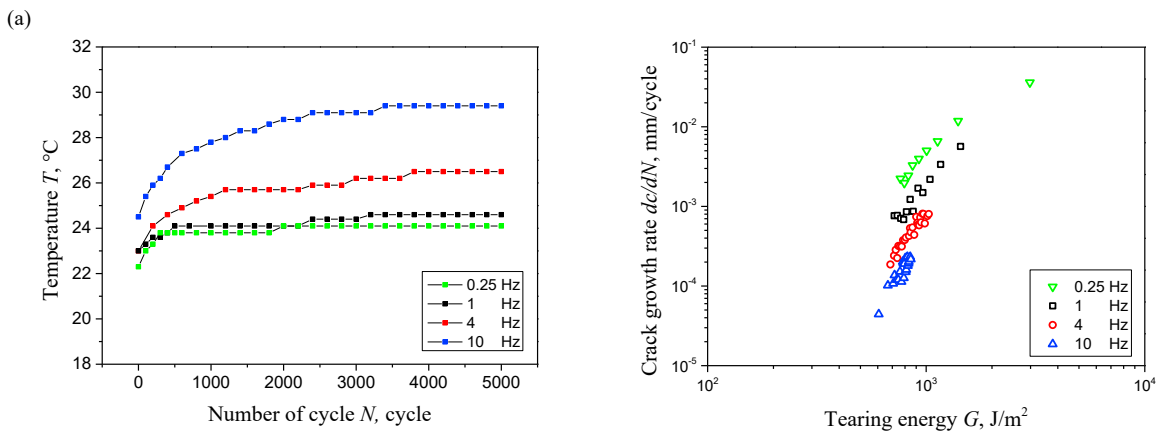

Fig. 2. (a) Surface temperature as a function of number of cycle and (b) crack growth rate as a function of tearing energy at different frequencies.
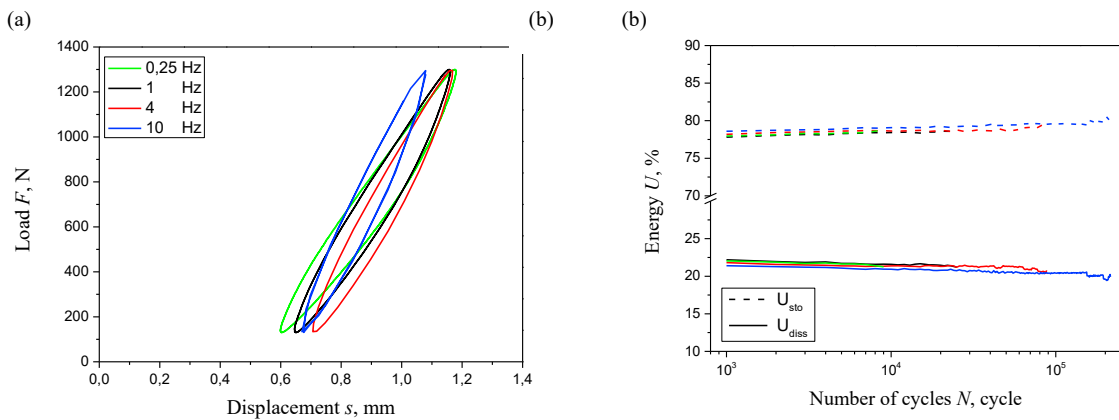

Fig. 3. Energy evaluation from crack growth experiments at different frequencies: (a) hysteresis loops recorded at 1000 cycles; (b) percentage of dissipated energy (full line) and elastically stored energy (dashed line) as a function of the number of cycle.

Lake and Lindley (1964) and Lindley (1974) reported that the fatigue crack growth rate is related to a static growth and a dynamic growth component, which are additive. The first component is related to the viscoelastic effect and connected to the time necessary for completing one cycle, i.e. the reciprocal of the frequency, while the dynamic

component is frequency independent. Therefore, the static component at small frequencies is more relevant and the overall crack growth rate results higher. This theory is not related to the energy dissipation and therefore seems to represent a proper explanation to our results. Analogous trend of increasing crack growth rate with lower frequencies were also reported by Busfield et al. (2002) by testing a styrene-butadiene copolymer.

3.2. Thermal conductivity

Rubbers are poor thermal conductors and this characteristic associated with considerable internal heat generation, leads to consistent increase in temperature in thick rubber components. Therefore, thermal conductivity was measured in the range of possible utilization of the rubber components with two different techniques. Fig. 4 summarizes the thermal conductivity as a function of temperature for both measurement techniques (guarded heat and laser flash). Both methods reveal results in very good agreement along the investigated temperature range. Moreover, it is worth notice that the values remain almost constant along the tested range of temperature. The average values across all the range of temperature for the two methods are reported in Table 1. Compared to the guarded heated method the results for the laser flash method are more scattered.

Table 1. Average values of thermal conductivity obtained with two techniques.

Measurement method	L (W/m·K)	Error (W/m·K)
Guarded heat	0,372	± 0,004
Laser flash	0,380	± 0,061

4. Conclusion

Measurements to determine the fatigue crack growth rate and thermal conductivity were implemented in order to study the impact of temperature on the fatigue properties of rubbers. Through the monitoring of the surface temperature during crack growth experiments a further increase of the temperature at the crack tip was observed, which was related to higher local strain in the region. The temperature increase during cyclic loading dependents on the testing frequency, resulting in higher temperatures with higher frequencies. These differences can be explained with higher energy dissipations at high frequencies. Moreover, by varying the loading frequency variations of the crack growth rates were found as well. The differences were not connected to higher energy dissipations during cyclic loading, but to the viscoelastic contribution due to the static growth component of the overall crack growth rate, Lake and Lindley (1964). Furthermore, the thermal conductivity was measured and seems constant along the considered temperature range. The reported work represents a first step towards a better comprehension of the impact of temperature on the fatigue properties of rubbers. These basic concepts will be taken into account for further characterizations at different environmental
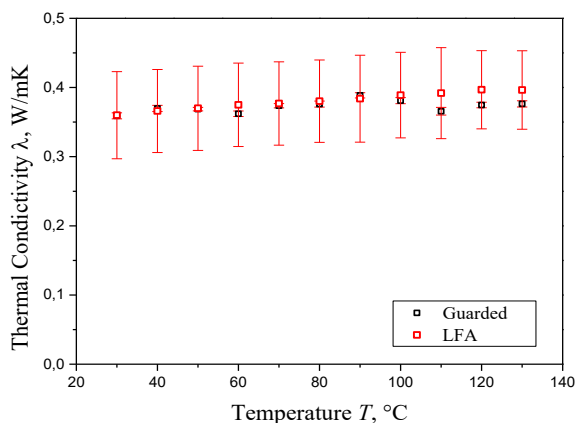

Fig. 4. Values of thermal conductivity for the material between 30 and 130 °C measured with two different techniques: in black the data obtained with the guarded heat method and in red the one obtained with the laser flash method.

temperatures. A detailed understanding of the temperature influence on the fatigue behavior finally allows the adaption of commonly used models to predict the lifetime of rubber components.

Acknowledgements

References

Busfield, J. J. C., Tsunoda, K., Davies, C. K. L., & Thomas, A. G. (2002). Contributions of time dependent and cyclic crack growth to the crack growth behavior of non strain-crystallizing elastomers. *Rubber Chemistry and Technology*, *75*(2), 643–656. https://doi.org/10.5254/1.3544991

Gent, A. N. (2012). *Engineering with Rubber* (3rd ed.). Carl Hanser Verlag GmbH Co KG. https://doi.org/10.5254/1.3538214

Lake, G. J., Lindley, P. B. (1964). Cut growth and fatigue of rubbers. II Experimetns on a noncrzstalliying rubber. *Journal of Applied Polymer Science*, *8*, 707–721.

Legorju-Jago, K., & Bathias, C. (2002). Fatigue initiation and propagation in natural and synthetic rubbers. *International Journal of Fatigue*, *24*(2–4), 85–92. https://doi.org/10.1016/S0142-1123(01)00062-7

Lindley, P. B. (1974). Non-Relaxing Crack Growth and Fatigue in a Non-Crystallizing Rubber. *Rubber Chemistry and Technology*. https://doi.org/10.5254/1.3540497

Mars, W. V., & Fatemi, A. (2004). Factors that Affect the Fatigue Life of Rubber: A Literature Survey. *Rubber Chemistry and Technology*, *77*(3), 391–412. https://doi.org/10.5254/1.3547831

Mars, W., & Fatemi, a. (2002). A literature survey on fatigue analysis approaches for rubber. *International Journal of Fatigue*, *24*(9), 949–961. https://doi.org/10.1016/S0142-1123(02)00008-7

Medalia, A. I. (1991). Heat Generation in Elastomer Compounds: Causes and Effects. *Rubber Chemistry and Technology*. https://doi.org/10.5254/1.3538565

Persson, B. N. J., & Brener, E. A. (2005). Crack propagation in viscoelastic solids. *Physical Review E - Statistical, Nonlinear, and Soft Matter Physics*, *71*(3), 1–8. https://doi.org/10.1103/PhysRevE.71.036123

Rivlin, R. S., & Thomas, A. G. (1953). Rupture of rubber. I. Characteristic energy for tearing. *Journal of Polymer Science*, *10*(3), 291–318. https://doi.org/10.1002/pol.1953.120100303

Stadlbauer, F., Koch, T., Archodoulaki, V. M., Planitzer, F., Fidi, W., & Holzner, A. (2013). Influence of experimental parameters on fatigue crack growth and heat build-up in rubber. *Materials*, *6*(12), 5502–5516. https://doi.org/10.3390/ma6125502

Young, D. G. (1986). Dynamic Property and Fatigue Crack Propagation Researchon Tire Sidewall and Model Compounds.pdf. *Rubber Chemistry and Technology*, *59*, 785–805.

Young, D. G., & Danik, J. A. (1994). Effects of temperature on fatigue and fracture. *Rubber Chemistry and Technology*, *67*(1), 137–147.

Publication 2

Heat build-up of rubbers during cyclic loading

Jacopo Schieppati [a], Bernd Schrittesser [a], Alfred Wondracek [b], Stefan Robin [b], Armin Holzner [b] and Gerald Pinter [c]

[a]   Polymer Competence Center Leoben GmbH, Roseggerstrasse 12, 8700 Leoben, Austria
[b]   Semperit Technische Produkte Gesellschaft m.b.H., Triester Bundesstrasse 26, 2632 Wimpassing, Austria
[c]   Department of Polymer Engineering and Science – Material Science and Testing of Polymers, Montanuniversität, Otto Glöckel-Strasse 2, 8700 Leoben, Austria

Relevant contributions to this publication:

Conceptualization:	Jacopo Schieppati, Bernd Schrittesser, Alfred Wondracek, Stefan Robin, Armin Holzner, Gerald Pinter
Methodology:	Jacopo Schieppati, Bernd Schrittesser
Investigation:	Jacopo Schieppati
Writing - Original Draft:	Jacopo Schieppati
Writing - Review & Editing:	Jacopo Schieppati; Bernd Schrittesser, Alfred Wondracek, Gerald Pinter

Heat build-up of rubbers during cyclic loading

J. Schieppati & B. Schrittesser
Polymer Competence Center Leoben GmbH, Roseggerstrasse 12, 8700 Leoben, Austria

A. Wondracek & St. Robin & A. Holzner
Semperit Technische Produkte Gesellschaft m.b.H., Triester Bunderstrasse 26, 2632 Wimpassing, Austria

G. Pinter
Department of polymer Engineering and science – Material Science and Testing of Plastic, Montanuniversitaet, Otto Glöckel-Strasse 2, 8700 Leoben, Austria

ABSTRACT: The unique mechanical properties of rubbers make them suitable for applications in which cyclic loadings are involved and hence, fatigue characterization represents a fundamental requirement for these materials. However, due to the high hysteretic losses present in such materials, a significant heat generation is present. This effect in combination with the low thermal conductivity, leads to a considerable increase of temperature in the rubber components, which is commonly referred as heat build-up. In order to avoid such temperature rises, low frequencies or small thickness can be used during material characterization. However, in real applications, limiting these two parameters it is not always possible and hence, a proper analysis of this phenomenon is required. In order to have more details about heat build-up, two different rubbers were tested under cyclic loading and surface temperatures were evaluated and compared taking into account the energy dissipation involved in the loading processes. In particular two specimen geometries were considered, one used for the characterization of fatigue crack nucleation and one used for fatigue crack growth analysis. For the first case, 3D dumbbell specimens were cyclically loaded with a sine wave at different testing conditions and the surface temperatures were monitored with an IR sensor. For the second case, pure shear specimens were cyclically loaded and the surface temperatures were monitored using both an IR sensor and an IR camera. In this latter case, the impact of the presence of a crack on the surface temperature was also considered. Moreover, starting from the heat equation, the temperature profiles along the thickness for both specimen geometries were considered. In order to have a proper description of the temperature distribution, thermal conductivity for both materials were evaluated as well using two different techniques. The analysis of the temperature distribution in the volume is important to distinguish between fatigue and thermal failure. With the obtained data, a further description of heat build-up in rubbers can be provided, contributing in the differentiation between failures related to fatigue and the ones related to local temperature increase.

1 INTRODUCTION

Fatigue characterization is of fundamental importance when dealing with rubbers. In fact, due to their mechanical behavior, rubber products are used in applications in which cyclic loadings are involved and therefore, fatigue represents one of the most common reason of failure for these components (Gent, 2012). The fatigue analyses of rubbers are usually carried out exploiting two different approaches: crack nucleation and crack growth. The first one is based on continuum mechanics and deals with the nucleation and growth of cracks, while the second is focused on the growth of pre-existing cracks making use of fracture mechanics tools (Mars & Fatemi, 2002).

Under cyclic loadings, rubbers show high level of heat generation as a consequence of dissipation mechanisms due to the viscoelastic nature of elastomers and due to the presence of fillers (Medalia, 2011). However, the dissipated heat cannot be transferred fast enough to the surrounding environment due to the low thermal conductivity of rubbers (Gschwandl et al., 2019), inducing a temperature increase in the rubber components. This phenomenon is commonly referred as heat build-up and its degree strongly depends on the material stiffness, on the frequency of oscillation, on the loading amplitude and on the thickness of the component (Gent, 2012).

Due to heat build-up, the temperature of the specimen under cyclic loading could reach high levels even for tests performed at room temperature, affecting the results of the fatigue characterization. In fact, temperature has a relevant effect on fracture (Schrittesser et al., 2012) and on the fatigue properties of rubber: it has been shown that higher temperatures result in faster crack growth and lower fatigue life (Lake & Lindley, 1964; Young, 1986). It seems

therefore indispensable for a proper material characterization, the analysis of heat build-up and its consequences in terms of temperature increases. In order to achieve these goals, two different rubbers were tested under cyclic loading using two geometries and their surface temperatures were monitored. The chosen geometries were 3D dumbbell, used for crack nucleation approach (Arbeiter et al., 2015) and pure shear geometry, used for crack growth approach (Schieppati et al., 2018). Moreover, for pure shear geometry, the temperature was monitored with an IR camera. Finally, the thermal conductivity of the materials were tested using two different techniques, giving the possibility to estimate the temperature profile along the thickness, providing further insights in the self-heating of rubbers.

2 EXPERIMENTAL PART

2.1 *Material*

The materials used for this research are acrylonitrile butadiene rubber (NBR) highly filled with carbon black and a blend of styrene butadiene rubber (SBR), butadiene rubber (BR) and natural rubber (NR), highly filled with two grades of carbon black. Due to confidentially, no additional information about the formulations can be given. For sake of simplicity, from now on the first material will be called Material A and the second Material B.

2.2 *Thermal conductivity*

Thermal conductivity measurements of both materials were carried out using two different methods: a guarded heat method using a DTD300 machine by TA instruments and a laser flash method (LFA) with a LFA467 Hyperflash machine by Netzsch. It is worth noting that the actual measurement from the LFA method is thermal diffusivity. The thermal conductivity can be retrieved by knowing the density and specific heat of the material. The specific heat was measured with a DSC6000 by Perkin Elmer while the density was measured using a XS205 Dual Range Analytical Balance by Mettler Toledo. The measurements for thermal conductivity were carried out between 30 °C and 130 °C, every 10 °C. For the measurements carried out with the first method, specimens with thickness of 2 mm were used, while for the second method specimens 1 mm thick were chosen.

2.3 *Surface temperature*

The evolution of surface temperature during cyclic loading was measured using a CT IR sensor by Optris. The measurements were recorded during fatigue characterization using two different specimen geometry, pure shear and 3D dumbbell. These geometries are normally used for fatigue characterization of crack growth and crack nucleation respectively. The dimension of the pure shear specimens were 16 mm of height, 200 mm of width (width to height ratio 1/12.5) and thickness of 4 mm. The dumbbell specimens were cylindrical with a diameter of 15 mm and a gauge height of 20 mm. Fatigue tests were implemented using a MTS 858 Table Top System testing machine. Both materials were tested using a 3D dumbbell geometry at 1 and 4 Hz; the tests were conducted in force control using a load ratio of 0.1 and a maximum force of 560 N. For pure shear geometry, both materials were tested in displacement control using a load ratio $R_\varepsilon = 0.5$ at a maximum strain of 10 %; the used frequencies were 0.25, 1, 4 and 10 Hz. Surface temperatures for pure shear specimen at different strain level were recorded also with an infrared camera by FLIR Titanium SC750).

3 RESULTS AND DISCUSSION

3.1 *Thermal conductivity*

Rubbers are poor conductors of heat and the low thermal conductivity greatly determines the temperature rise upon loading. Therefore, the values of thermal conductivity of both materials were characterized by means of two different techniques in the range of possible utilization of rubber components. In Figure 1 and 2 are reported the thermal conductivity as a function of temperature and for both measurement techniques for material A and Material B respectively. Both methods reveal results in very good agreement along the investigated temperature range. Compared to the guarded heated method the results for the laser flash method are more scattered, since more measurements are necessary for obtaining these results. Moreover, it is worth notice that
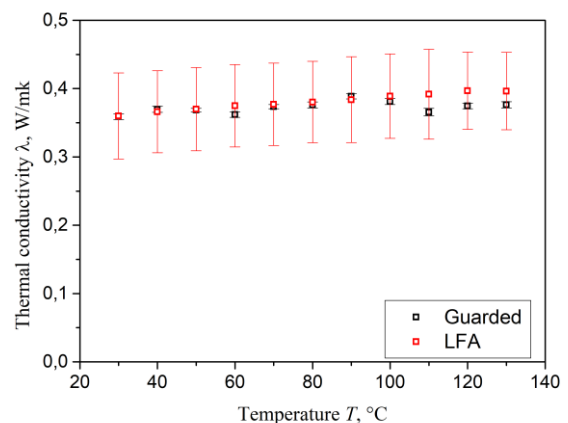

Figure 1 Values of thermal conductivity for Material A between 30 and 130 °C measured with two different techniques: in black the data obtained with the guarded heat method and in red the one obtained with the laser flash method.

the values remain almost constant along the tested range of temperature. The average values across all the range of temperature for the two methods are reported in Table 1.
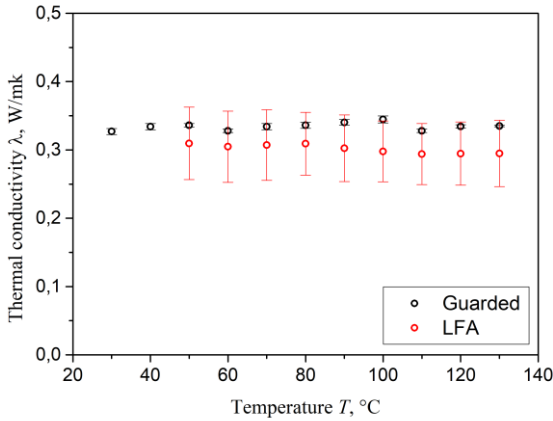

Figure 2 Values of thermal conductivity for Material B between 30 and 130 °C measured with two different techniques: in black the data obtained with the guarded heat method and in red the one obtained with the laser flash method.

Table 1. Average values of thermal conductivity of both materials along the temperature range obtained with guarded heat and laser flash methods.

Method	Material A		Material B	
	λ (W/mK)		λ (W/mK)	
Guarded heat	0.372	±0.004	0.381	±0.061
Laser flash	0.334	±0.004	0.302	±0.048

3.2 Surface temperature

As discussed in the previous paragraph, rubbers possess low thermal conductivity and therefore the heat generated under cyclic loading cannot be transferred fast enough to the surrounding environment, resulting in an increase in temperature. The temperature increase is a function of the stiffness of the material and of the characteristic of the oscillating loading, i.e. frequency and amplitude. Moreover, an increase in the thickness of the components will result in higher heat build-up and temperature. In Figure 3, the hysteresis curves are reported for both materials at a cycle number of 10000 cycles. From the curves, it is possible to see the difference in the material behavior: material A (black) is much more stiff with a relative small hysteresis while material B (red) show a much softer behavior and high dissipated energy (area inside the curve). In Figure 4 are reported the plots of the surface temperature evolution upon loading as a function of number of cycles for all tested conditions. During the first cycles, the temperature raised due to the internal heat generation, which is higher than the rate of cooling due to the external environment. As the temperature increased, the driving force for cooling increased until the rate of cooling became equal to the rate of inter-

nal heat generation. As a result, the temperature showed a plateau value, which was stable during cycles. Similar results were found for pure shear geometry. (Schieppati et al., 2018). As expected, the plateau temperatures for material B were higher for both frequencies, since the dissipation of energy was higher for this compound. In Table 2, the values of the plateau surface temperature and the relative temperature increases are reported. As expected, higher frequencies resulted in higher surface temperature. However, it is evident that even a small change of frequency results in big differences of temperature increase for dumbbell specimens. Beside the test of material A at 1 Hz, the increase in temperature for the other testing conditions is high and therefore it is not possible to neglect the temperature effect during fatigue analysis.
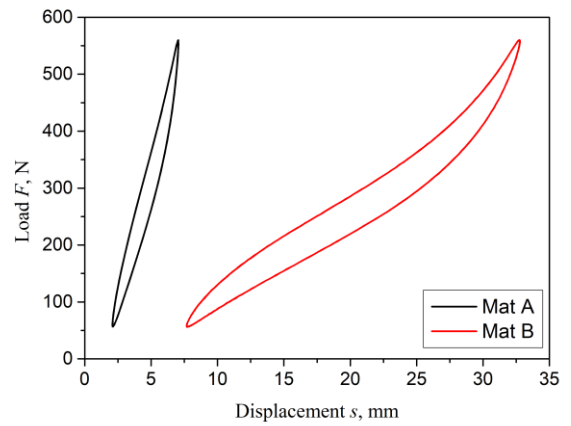

Figure 3 Hysteresis curves of Material A (black) and Material B (red). The data shown were recorded at 10000 cycles in force control with F_{max} = 560 N and R = 0.1, with f = 4 Hz.
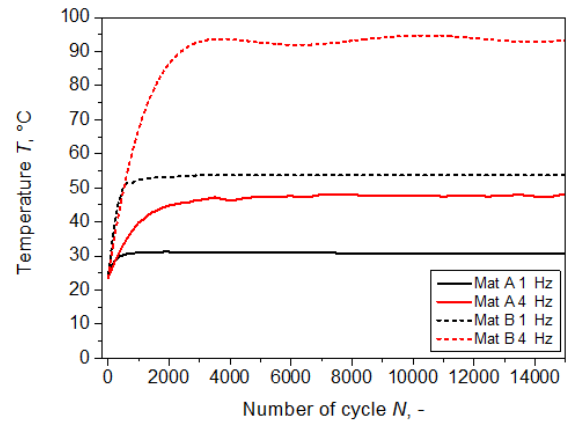

Figure 4 Temperature evolution of 3D dumbbell specimens for material A (black) and Material B (red). The tests were performed in force control with F_{max} = 560 N and R = 0.1, at frequency of 1 (full lines) and 4 Hz (dashed lines).

In Figure 5 and 6 two pictures obtained with IR camera during testing of pure shear specimens of material A are reported. From Figure 5 it is possible to observe that the temperature was symmetrically distributed along the height of the specimen while it

became asymmetric when the crack developed towards one of the clamps as show in Figure 6. It is important then to consider the position of the measurement of surface temperature

Table 2. Plateau surface temperature T_S and temperature increase with respect to the specimen in the unload state ΔT for both material using dumbbell geometry. The test were performed in load control using a load ratio R = 0.1 and a maximum force F_{max} = 560 N.

f (Hz)	Material A		Material B	
	T_S (°C)	ΔT (°C)	T_S (°C)	ΔT (°C)
1	31	6	54	29
4	49	24	94	70
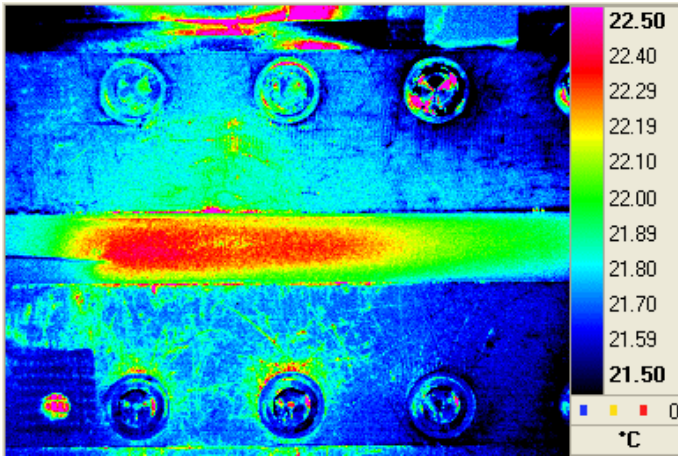
Figure 5 Picture recorded with an IR camera during testing of a pure shear specimen. The temperature is symmetrically distributed along the height of the specimen.
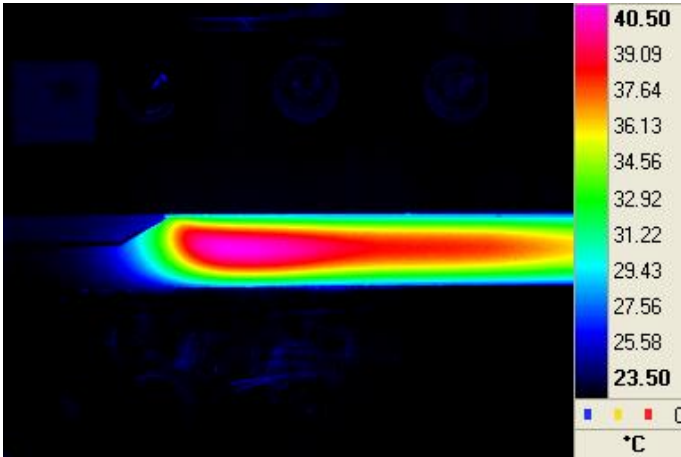

Figure 6 Picture recorded with an IR camera during testing of a pure shear specimen. The temperature is asymmetrically distributed along the height of the specimen due to crack development towards the upper clamp.

3.3 Temperature profile

The temperature increases upon loading are evaluated using surface temperature values. However, due to the low thermal conductivity, it is reasonable to believe that the temperature is not homogenous in the thickness. In order to get an idea of the internal temperature distribution, an equation for retrieving

the temperature profile along the thickness can be obtained considering the heat equation with a heating source

$$\rho \, C_P \frac{\partial T}{\partial t} - \nabla(\lambda \nabla \mathrm{T}) = \dot{q} \qquad (1)$$

where ρ is the density, C_P the specific heat, λ the thermal conductivity and $\dot{q}$ is the internal heat generated per unit volume, which is given by

$$\dot{q} = \frac{f \cdot U_{dis}}{V} \qquad (2)$$

where U_{dis} is the energy dissipated per cycle, f the frequency and V the volume. In order to get a solution, some assumptions could be done. Considering the equilibrium condition when the temperature show a plateau value, the rate of variation of temperature is zero $\partial T/\partial t = 0$. By considering a rectangular plate (useful for pure shear specimens), it is possible to consider that the temperature is homogenous along the width and the height and that it varies only in the thickness, allowing to simplify the problem to a 1D case. Moreover, it is possible to consider the thermal conductivity constant with temperature; this assumption is justified by the experimental results shown in section 3.1. Taking into account all these considerations, equation (1) can be simplify into

$$\frac{d^2 T}{dx^2} = -\frac{\dot{q}}{\lambda} \qquad (3)$$

The solution can be retrieved then by considering the following boundary condition: at the surface, the temperature T_S is constant, while the continuity of the function in the center imply that $dT/dx = 0$. The solution of the problem is a parabolic function of the thickness L

$$T = T_S + \frac{\dot{q}}{2\lambda} \cdot \left(\frac{L^2}{4} - x^2\right) \qquad (4)$$

In the center, for $x = 0$ the temperature is

$$T = T_S + \frac{\dot{q}L^2}{8\lambda} \qquad (5)$$

Similar arguments could be considered for the cylindrical case (useful for dumbbell specimens) of radius R, obtaining

$$T = T_S + \frac{\dot{q}R^2}{4\lambda} \cdot \left(1 - \frac{r^2}{R^2}\right) \qquad (6)$$

and in the center, for $r = 0$

$$T = T_S + \frac{\dot{q}R^2}{4\lambda} \qquad (7)$$

The treatment above can be found in literature (Holman, 2010). By using this treatment, it was possible to evaluate the temperature distribution along the thickness for both pure shear and 3D dumbbell specimens, by making use of equations 4 and 6 respectively.

In Figure 7 and 8 the calculated temperature profile along the thickness for pure shear for material A

and B are reported, respectively. In Figure 9 and 10 the calculated temperature profile along the thickness for dumbbell specimens for material A and B are reported, respectively. The value of surface temperature T_S and the temperature in the center T_C are reported in table 3 and 4.
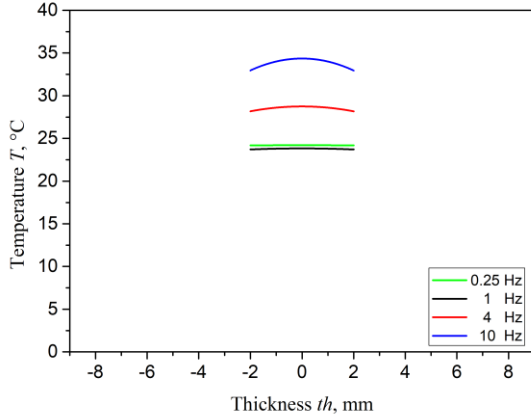

Figure 7 Temperature profile along the thickness of pure shear specimen of Material A. The tests were performed in displacement control with $R\varepsilon= 0.5$ with $\varepsilon_{max} = 10$ % at different frequencies.
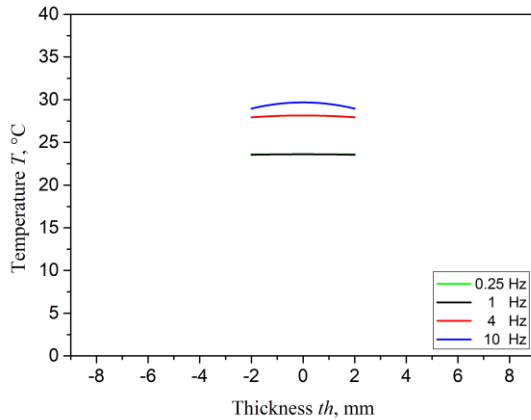

Figure 8 Temperature profile along the thickness of pure shear specimen of Material B. The tests were performed in displacement control with $R\varepsilon= 0.5$ with $\varepsilon_{max} = 10$ % at different frequencies.

Even for pure shear specimens, the surface temperature was higher for higher frequencies for both material, as depicted in Figure 7 and 8 and reported in Table 3. Moreover, it is possible to observe that the temperature is substantially constant along the thickness in all tested conditions. This is related to the low thickness (4 mm) of the specimens: the small path of the heat to surface lead to a fast exchange with the environment, limiting the temperature increase. The data suggest that for pure shear specimens, the temperature can be considered homogenous along the thickness and will be accounted as the surface temperature.
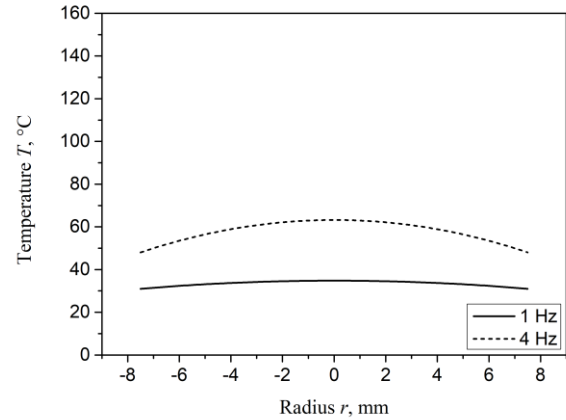

Figure 9 Temperature profile along the thickness of 3D dumbbell specimen of Material A. The tests were performed in force control with $F_{max} = 560$ N and $R = 0.1$, at frequency of 1 and 4 Hz.
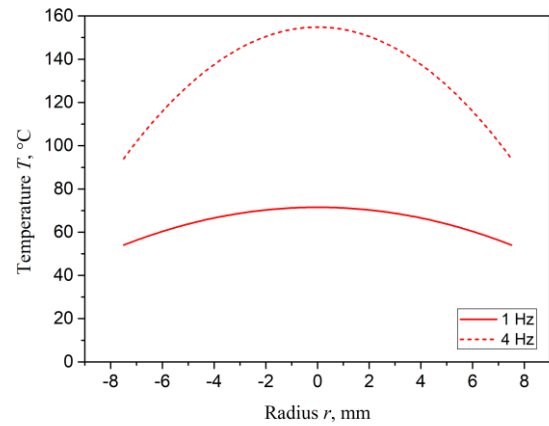

Figure 10 Temperature profile along the thickness of 3D dumbbell specimen of Material A. The tests were performed in force control with $F_{max} = 560$ N and $R = 0.1$, at frequency of 1 and 4 Hz.

Table 3. Plateau surface temperature T_S and temperature in the center T_C for pure shear geometry of both material at different frequencies.

f (Hz)	Material A		Material B	
	T_S (°C)	T_C (°C)	T_S (°C)	T_C (°C)
0.25	24	24	24	24
1	24	24	24	24
4	28	29	28	28
10	33	34	29	30

Table 4. Plateau surface temperature T_S and temperature in the center T_C for 3D dumbbell geometry of both material at different frequencies.

f (Hz)	Material A		Material B	
	T_S (°C)	T_C (°C)	T_S (°C)	T_C (°C)
1	31	35	54	62
4	49	73	94	162

As depicted in Figure 9 and 10 and the data reported in Table 4, the higher thickness of 3D dumbbell specimens (15 mm of diameter) leads to much higher temperature increases and very high values in the center of the specimen. For 1 Hz the temperature in the center was higher than the surface one of 4 °C for Material A and 8 °C for Material B. For 4 Hz the temperature in the middle resulted higher in the center of 24 °C for material A and 68 °C for material B. Such temperatures inside the specimen, not only could influence the fatigue properties but they could also lead to thermal failure. When dealing with fatigue testing, for dumbbell specimens it is therefore necessary to try to avoid such temperature increases by using low testing frequency or, when it is not possible, to take into account the temperature evolution especially in the core of the specimen. By doing so, the discrimination between fatigue and thermal failures could be possible.

4 CONCLUSIONS

In order to have more insights of heat build-up during fatigue testing, several tests were performed for two different rubbers. Thermal conductivity of both materials was measured using two techniques along the range of possible utilization of rubber components and it was found that the thermal conductivity was low for both materials and it remained constant along the temperature range. The surface temperature evolution during loading was monitored for 3D dumbbell specimens, revealing that even a small variation of frequency could result in much higher temperature increases. The surface temperature of pure shear specimens was recorded also with an IR camera, revealing that the temperature distribution along the height of the specimens is affected by the position of the crack tip. Moreover, an equation for calculating the temperature profile along the thickness was retrieved from the heat equation and the temperature profiles were calculated for both dumbbell and pure shear specimens. Based on the calculations, the temperature for pure shear specimen could be considered as homogenous in the specimen thickness, while the higher temperatures in the center should be taken into account for 3D dumbbell specimen during fatigue analysis.

REFERENCES

Arbeiter, F., Schrittesser, B., Frank, A., Berer, M., & Pinter, G. (2015). Cyclic tests on cracked round bars as a quick tool to assess the long term behaviour of thermoplastics and elastomers. *Polymer Testing*, *45*, 83–92.

Gent, A. N. (2012). *Engineering with Rubber* (3rd ed.). Carl Hanser Verlag GmbH Co KG.

Gschwandl, M., Kerschbaumer, R. C., Schrittesser, B., Fuchs, P. F., Stieger, S., & Meinhart, L. (2019). Thermal conductivity measurement of industrial rubber compounds using laser flash analysis: Applicability, comparison and evaluation. *AIP Conference Proceedings*, *2065*.

J. P. Holman. (2010). Heat Transfer (10th Edition). *The McGraw-Hill Companies*.

Lake, G. J. & Lindley, P. B. (1964). Cut growth and fatigue of rubbers. II Experiments on a noncrystalizing rubber. *Journal of Applied Polymer Science*, *8*, 707–721.

Mars, W. & Fatemi, A. (2002). A literature survey on fatigue analysis approaches for rubber. *International Journal of Fatigue*, *24*(9), 949–961.

Medalia, A. I. (2011). Heat Generation in Elastomer Compounds: Causes and Effects. *Rubber Chemistry and Technology*.

Schieppati, J., Schrittesser, B., Wondracek, A., Robin, S., Holzner, A., & Pinter, G. (2018). Impact of temperature on the fatigue and crack growth behavior of rubbers. *Procedia Structural Integrity*, *13*, 642–647.

Schrittesser, B., Pinter, G., & Major, Z. (2012). Temperature dependent fracture behavior of Rubbers used in the oil and gas industry. In *19th European Conference on Fracture: Fracture Mechanics for Durability, Reliability and Safety*.

Young, D. G. (1986). Dynamic Property and Fatigue Crack Propagation Research on Tire Sidewall and Model Compounds. *Rubber Chemistry and Technology*, *59*, 785–805.

Publication 3

Effect of mechanical loading history on fatigue crack growth of non-crystallizing rubber

Jacopo Schieppati [a], Bernd Schrittesser [a], Alfred Wondracek [b], Stefan Robin [b], Armin Holzner [b] and Gerald Pinter [c]

[a]   Polymer Competence Center Leoben GmbH, Roseggerstrasse 12, 8700 Leoben, Austria
[b]   Semperit Technische Produkte Gesellschaft m.b.H., Triester Bundesstrasse 26, 2632 Wimpassing, Austria
[c]   Department of Polymer Engineering and Science – Material Science and Testing of Polymers, Montanuniversität, Otto Glöckel-Strasse 2, 8700 Leoben, Austria

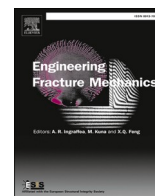### *Relevant contributions to this publication:*

Conceptualization:	Jacopo Schieppati, Bernd Schrittesser, Alfred Wondracek, Stefan Robin, Armin Holzner, Gerald Pinter
Methodology:	Jacopo Schieppati, Bernd Schrittesser
Investigation:	Jacopo Schieppati
Writing - Original Draft:	Jacopo Schieppati
Writing - Review & Editing:	Jacopo Schieppati; Bernd Schrittesser, Alfred Wondracek, Gerald Pinter

Effect of mechanical loading history on fatigue crack growth of non-crystallizing rubber

Jacopo Schieppati [a],[*], Bernd Schrittesser [a], Alfred Wondracek [b], Stefan Robin [b], Armin Holzner [b], Gerald Pinter [c]

[a] *Polymer Competence Center Leoben GmbH, Roseggerstrasse 12, 8700 Leoben, Austria*
[b] *Semperit Technische Produkte Gesellschaft m.b.H., Triester Bunderstrasse 26, 2632 Wimpassing, Austria*
[c] *Department of Polymer Engineering and Science – Material Science and Testing of Polymers, Montanuniversitaet, Otto Glöckel-Strasse 2, 8700 Leoben, Austria*

A B S T R A C T

Rubbers possess unique mechanical properties that make them indispensable for technological products such as seals and tires, which are normally subjected to quasi-static loading conditions which superimposes cyclic loads; their failure is mainly related to fatigue. In this study the focus is on the effect on fatigue of parameters connected to the mechanical history. Fatigue crack growth of a non-crystallizing rubber was investigated using cyclically loaded pure shear specimens considering different loading conditions. In a first step, the geometry of the specimens, in terms of width to height ratios and notch length, was considered to avoid specimen-influences on the results. Subsequently, several tests were implemented using both force and displacement control with different loading histories. Finally, the effect on the fatigue crack growth of parameters such as waveform, frequency and load ratio was investigated. In general, no significant influence of load or displacement control was found. Among the loading parameters, waveform and load ratio seem not to have a marked effect on the fatigue behavior of the material. In contrast, decreasing values of frequency were found to increase the crack growth rate.

1. Introduction

Several technological applications require materials that can bear large static strains and cyclic loads and rubbers represent a fundamentally suitable material for these applications. In these loading conditions, the failure of rubbers is mainly related to fatigue. Therefore, the analysis of fatigue and the lifetime prediction of these materials is of primary importance for rubbers industry.

In the field of rubber fatigue, two main approaches are used for the evaluation of fatigue lifetime: crack nucleation and crack growth. The first one deals with the nucleation and growth of cracks up to a certain limit and is based on a continuum mechanics approach. Conversely, the second one is based on the study of the growth of pre-existing cracks using a fracture mechanical approach [1].

The fatigue behavior of rubbers is influenced by several parameters, which can be related to the mechanical history, environmental conditions and rubber formulation [2]. Several studies have analyzed the influence of parameters such as load ratio [3–5], frequency [6–9], waveform [10–12] and temperature [8,13–17] for different rubbers. However, little attention has been devoted to the study of

---

* Corresponding author.
E-mail address: jacopo.schieppati@pccl.at (J. Schieppati).

fracture fatigue behavior of acrylonitrile butadiene rubber (NBR) [17–27]. This elastomer is used in several applications in which also a good chemical resistance is required, having excellent fuel and oil resistance. In fact, NBR is an amorphous rubber with high polarity that makes it the ideal candidate for fuel and oil hoses, and seals. Furthermore, NBR is referred to as non-crystallizing since it does not show crystallization even under strain. Strain-induced crystallization is a reinforcing mechanism that leads to the formation of a crystalline structure upon stretching as a consequence of the alignment of the macromolecules and a higher degree of order. Therefore, in order to achieve good mechanical properties, NBR is normally filled with a medium to high content of reinforcing fillers (typically carbon black), which should be small enough to induce a reinforcing effect: small particles possess high surface areas that lead to more interactions with the polymer chains. The addition of carbon black induces increases of stiffness, strength and resistance to fatigue crack growth. On the other hand, the introduction of fillers leads to the enhancement of hysteresis, which causes a greater temperature increases due to heat- build up [28].

In this study the focus was devoted to the effect of parameters related to the mechanical history on the fatigue crack growth of a non-crystallizing rubber (NBR). Pure shear specimens were tested under cyclic loadings and different configurations were evaluated, in terms of width to height ratios and notch length. Afterwards the influence of several parameters was accessed using both force and displacement control with different loading histories. The effect of parameters such as frequency, input loading control, loading history, waveform and load ratio on the fatigue crack growth of a filled NBR was investigated.

2. Material and methods

2.1. Materials

The material used for this research is a commercial acrylonitrile butadiene rubber (NBR) filled with 42 phr of carbon black (CB). Due to confidentially, no additional information about the precise formulation can be given. Nevertheless, preliminary results showed a relatively homogenous filler distribution with typical aggregations of CB primary particles with only rare micrometric agglomerates.

2.2. Fatigue crack growth

Fatigue crack growth measurements were implemented using a pure shear geometry (Fig. 1a) in order to obtain Paris plots (crack
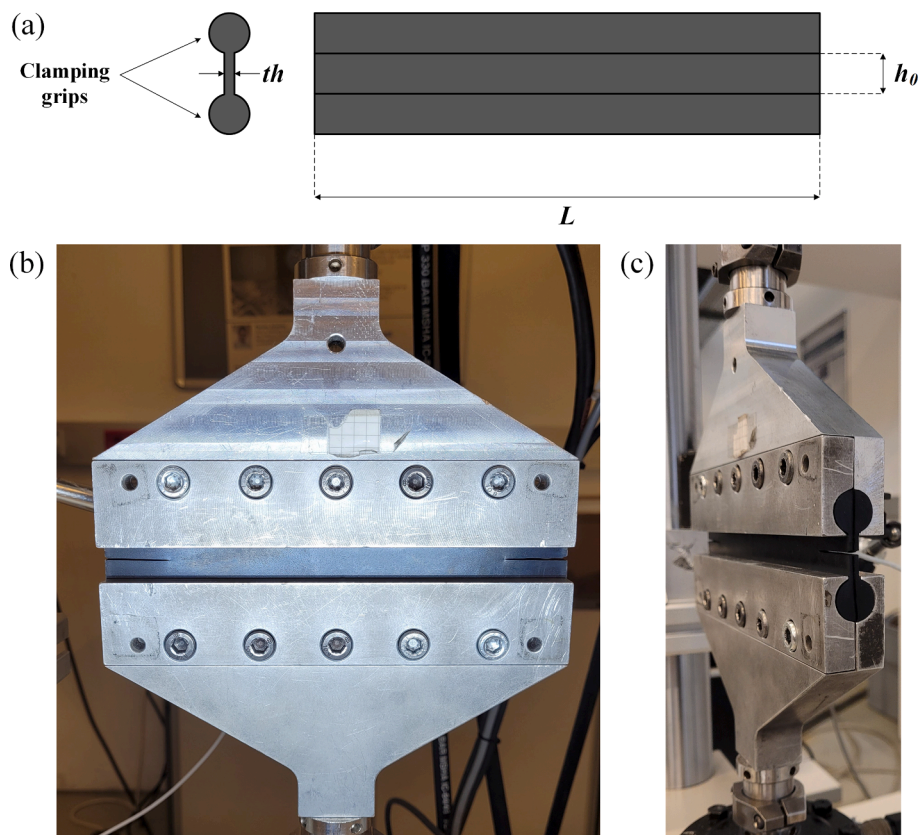

Fig. 1. (a) Sketch of the pure shear specimen used during fatigue crack growth measurements. (b) Picture of a notched pure shear specimen notched on both sides mounted on custom clamping system. (c) Lateral view of the clamping system.

growth rate vs tearing energy) exploiting different conditions to study the influence of several parameters. The actual testing conditions will be stated in the results section. In general, pure shear specimens with height h_0 of 16 mm, initial width L of 200 mm and thickness th of 4 mm were examined. The pure shear geometry is characterized by a dimension much larger than the other two dimensions, in order to ensure a pure shear state in the specimen thickness. The samples were mounted on special clamps, preloaded to 20 N and notched on both sides (unless differently stated). A view of a clamped specimen with two notches is shown in Fig. 1b, while the lateral view is displayed in Fig. 1c. The initial notches were made using a razor blade (thickness = 0.1 mm, tip-radius < 5 μm), mounted on a customized tool guided on the clamping system and by cutting the specimen in its entire thickness (see Fig. 1c) at half of the height of the specimen (see Fig. 1b). Generally, the initial notches were about 25 mm in length; the initial notch tip radius was not considered since, due to the large strains involved during the loading, significant blunting of the notch tip occurred. The tests were carried out using a MTS 858 Table Top System servohydraulic testing machine (MTS Systems GmbH, Minnesota, USA) and the crack length was monitored through a camera system CV-5701P by Keyence (Osaka, Japan). In order to avoid light reflections, the specimens were sprayed with a white powder coating. The set-up for the measurements leads to a picture's resolution of 50–70 μm/pixel; the pictures were recorded every 1000 cycles.

Furthermore, the tests were performed both in force and displacement control. The tests in force control were performed by cyclically loading at maximum force of 1300 N, monitoring the crack growth up to the failure of the specimen. The tests in displacement control were performed with increasing strain steps with maximum strain ranging from 4 to 16% in order to vary the tearing energy and to obtain different crack growth rates with one specimen. Each strain step lead to a constant crack growth and by plotting the crack length against the number of cycles, the crack growth rate was determined by linear fitting of each strain step. Each step was kept for a predetermined number of cycles, tuned with preliminary tests depending on the frequency. From every crack growth rate, associated to the tearing energy of the correspondent strain step, one data point of the Paris plot was determined.

Furthermore, according to the loading control mode, the load ratios were defined considering the maximum and minimum values of force or displacement set in the machine. Consequently, for the force control tests the load ratio R was defined as:

$$R = \frac{F_{min}}{F_{max}} \tag{1}$$

where F_{min} is the minimum force and the F_{max} is the maximum force. Conversely, in displacement control mode the load ratio R_ε was considered as:

$$R_\varepsilon = \frac{s_{min}}{s_{max}} \tag{2}$$

where s_{min} is the minimum displacement and the s_{max} is the maximum displacement.

The hysteresis was monitored during the cyclic loading through the MTS test device and the tearing energy G was calculated with the data obtained from the specimen under testing. For pure shear geometry, the tearing energy can be calculated with Eq. (3) [29]:

$$G = W_0 \cdot h_0 = \frac{U}{A_{uncr}} \tag{3}$$

where W_0 is the strain energy density and h_0 the height of the specimen in the unstrained condition. For practical purposes, it is easier to calculate the tearing energy using the mechanical energy U calculated from the load–displacement curve divided by the uncracked area A_{uncr}. Under non-relaxing condition, the mechanical energy was evaluated according to the following convention. For the positive load ratio, the static contribution was considered and added to the mechanical energy obtained by the area under the load–displacement curve. Therefore, the static contribution U_{static} was considered as:

$$U_{static} = F_{min} \cdot s_{min} \tag{4}$$

where F_{min} and s_{min} are the minimum force and the minimum displacement in the hysteresis curve. For the negative load ratio, only the positive part of the area under the loading curve was taken into account. Using this approach, the tearing energy was evaluated at the maximum strain and corresponded to G_{max} reported in the literature [3]. More details about the procedure and the evaluation of the tearing energy are reported in [17].

In the stable crack growth region, the curves were fitted using the Paris law [30]:

$$\frac{da}{dN} = CG^m \tag{5}$$

where da/dN represents the crack growth rate per cycle, G the tearing energy, while C and m are material dependent constants.

In addition, for the tests at different frequencies, the surface temperature was monitored during the loading through a CT LT22 infrared sensor (Optris GmbH, Berlin, Germany).

3. Results and discussion

3.1. Geometry influence

3.1.1. Notch length

Different configurations of the pure shear specimen have been investigated in order to find the configuration that could reveal reproducible results without an effect from the test setup. In fact, the presence of one crack could lead to a bending moment during the crack opening phase - when the crack is long enough - and therefore, the double edge notch configuration was considered. As a matter of fact, the growth of cracks on both sides of the specimen lead to the same loading direction during all the tests and the bending moment was avoided. The use of two cracks was considered by Harbour et al. [12,31] and by Weng et al. [32]. Moreover, finite element analysis of this configuration was investigated by Yeoh [33] and it was demonstrated that two edge cracks configuration of twin cracks growing simultaneously is equivalent to a single edge crack configuration, as long as the two cracks did not interfere with each other.

The influence of the notching length was assessed using three configurations: single notch ($a_0 = 25$ mm), single notch with double length ($2 \cdot a_0 = 50$ mm) and a double edge notch configuration with two notches on both sides of the specimen ($a_0 = 25$ mm). A schematic of the three configurations is shown in Fig. 2. The single notch with double length configuration has been analyzed to verify the results using the same total notch length (i.e., same ligament length) as the double notch configuration. The fatigue tests were carried out in displacement control at a frequency of 4 Hz, load ratio R_ε of 0.5 and maximum strain ranging between 4 and 16%. In Fig. 3a, the hysteresis curves for the three configurations at a maximum strain of 6% are displayed. The force levels results were dissimilar as a result of the different compliance of the specimens, due to the distinct ligaments' lengths. Anyway, the highest loads were found for the single notch configuration, while the lowest loads were for the single long notch configuration; intermediate load values were found for the double notch configuration. Nevertheless, the plots of fatigue crack growth as a function of the tearing energy of the different configurations (Fig. 3b) show that the curves are very similar to each other as displayed also by the parameters from the curves fitting with Eq. (5), reported in Table 1. It is worth noting that the results for the double notched configuration are intended as the sum of the crack growth on the two sides. These results demonstrate that the notch effect is not relevant and the results are independent of the configuration. The double edge configuration is to be preferred for a proper material characterization, due to the stability of loading direction provided during the testing.

3.1.2. Width to height ratio

With the established double edge configuration, pure shear specimens with different widths were analyzed in order to study the influence of the width to height ratio. The width of the specimen may influence the pure shear state in the specimen. In fact, the pure shear state ensures the independence of the tearing energy from the crack length and therefore, the tearing energy can be estimated with Eq. (3) [29]. This is guaranteed with a value of width to height ratio L/h_0 above 5 [33]. Three widths were considered: starting from the initial width $L = 200$ mm, the specimens were cut in half and to one third of the initial width (designated as $L/2$ and $L/3$ respectively) resulting in widths of approximately 100 mm and 66 mm. The reduction of the width of the specimen was analyzed in order to verify the possibility of having a better resolution of the crack, due to the reduced area of interest. With the three widths, the width to height ratio L/h_0 were of 12.5, 6.25 and 4 for the length L, $L/2$ and $L/3$, respectively. It is worth noting that the case $L/3$ does not fulfill the aforementioned requirement of $L/h_0 = 5$.

Fatigue crack growth tests were carried out using the same parameters as in section 3.1.1. The hysteresis curves (Fig. 4a) reveal
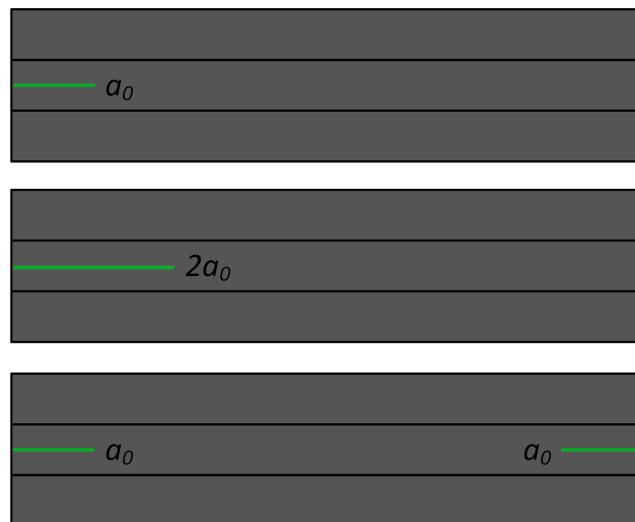

Fig. 2. Sketch of the different configurations used for testing the influence of notch length. From the top: single notch, single long notch and double notch.
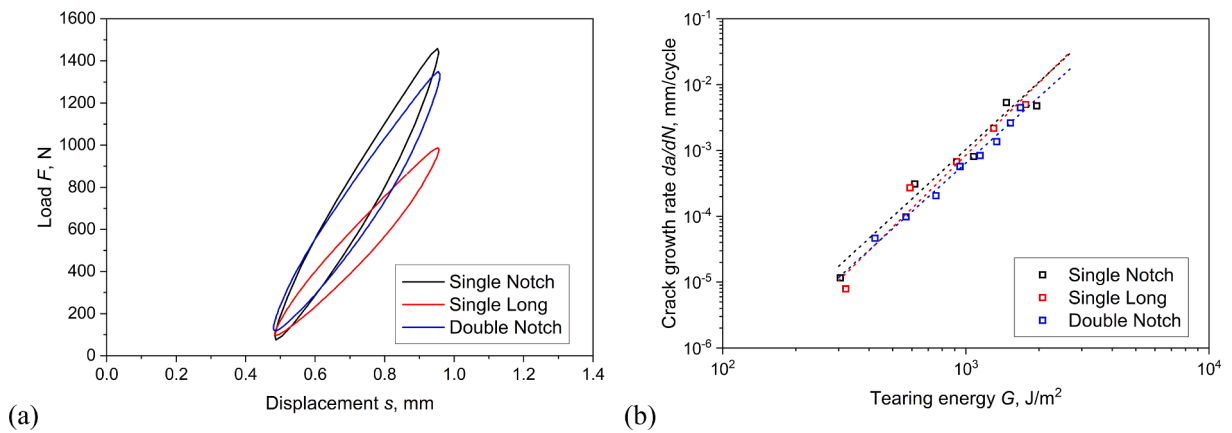
Fig. 3. (a) Hysteresis curves obtained during fatigue crack growth measurements at maximum strain of 6% for single notch (black), single long notch (red) and double notch (blue). **(b)** Fatigue crack growth rate as a function of tearing energy of filled NBR considering different notch configurations: single notch (black), single long notch (red) and double notch (blue). The measurements were performed with a specimen width L of 200 mm in displacement control at 4 Hz, with load ratio R_ε of 0.5 and maximum strain ranging between 4 and 16%. Three specimens were evaluated and only one of them has been reported for clarity reasons. The curves were fitted in the stable crack growth region with Eq. (5); the reported curve is the average from three specimens. (For interpretation of the references to colour in this figure legend, the reader is referred to the web version of this article.)

Table 1
Values of the power law coefficients obtained from fitting the fatigue crack growth curves for different notch configurations (Fig. 3b) with Paris law (Eq. (5)). The values correspond to the mean value of the fitting of three tests under the same conditions.

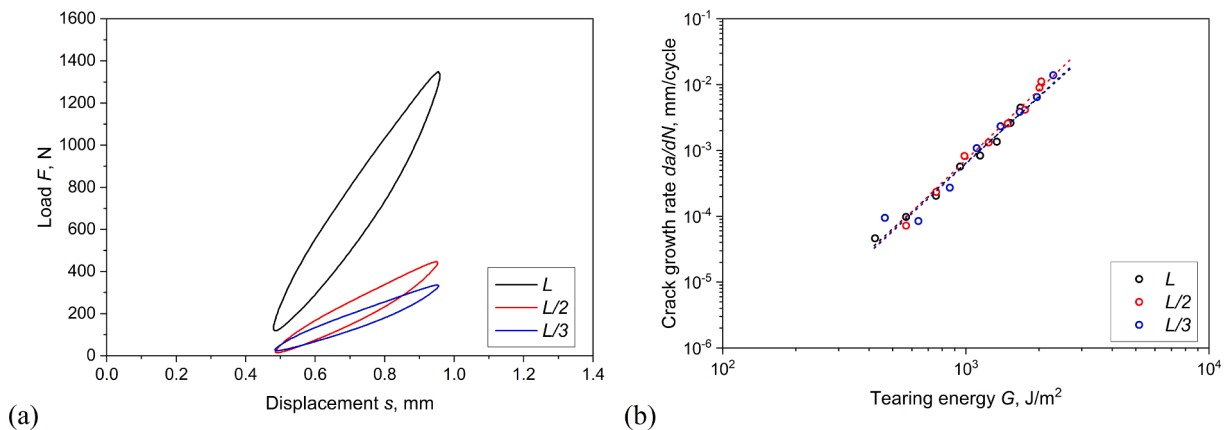|	m	$\log C$
Single Notch	3.3 ± 0.1	-13.2 ± 0.2
Single Long	3.7 ± 0.2	-14.0 ± 0.2
Double Notch	3.4 ± 0.2	-13.2 ± 0.3

Fig. 4. (a) Hysteresis curves obtained during fatigue crack growth measurements at maximum strain of 6% for width to height ratio of 12.5 (L - black), 6.25 (L/2 - red) and 4 (L/3 - blue). **(b)** Fatigue crack growth rate as a function of tearing energy of filled NBR considering different width to height ratios of 12.5 (L - black), 6.25 (L/2 - red) and 4 (L/3 - blue). The measurements were performed in displacement control at 4 Hz, with load ratio R_ε of 0.5 and maximum strain ranging between 4 and 16%. Three specimens were evaluated and only one of them has been reported for clarity reasons. The curves were fitted in the stable crack growth region using Eq. (5); the reported curve is the average from three specimens. (For interpretation of the references to colour in this figure legend, the reader is referred to the web version of this article.)

decreasing loads with decreasing width to height ratios, due to a higher specimen compliance. The outcomes in terms of fatigue crack growth as a function of the tearing energy are reported in Fig. 4b. As depicted, the considered width to height ratios have no effect on the results. This is confirmed even from the coefficients retrieved from the curves fitting with Eq. (5) (Table 2). Therefore, all considered cases show the same fatigue behavior and the choice of an optimal dimension must be a trade-off between a better crack

Table 2
Values of the power law coefficients obtained from fitting the fatigue crack growth curves for different width to height ratio (Fig. 4b) with Paris law (Eq. (5)). The values correspond to the mean value of the fitting of three tests under the same conditions.

Width to height ratio L/h_0	m	$\log C$
12. 5 (L)	3.3 ± 0.1	−13.2 ± 0.2
6.25 (L/2)	3.3 ± 0.1	−13.8 ± 1.1
4 (L/3)	3.4 ± 0.4	−13.4 ± 1.0

resolution (due to a reduced area of interest) and sufficient room for the growth of the cracks, so as to avoid any possible influence of cracks on each other. A width $L/2$ of 100 mm with a L/h_0 of 6.25 is suggested as the right compromise. It is worth noting that the reported absolute value of 100 mm is case-specific and refers to the considered h_0 of 16 mm. Nevertheless, the ratio L/h_0 of 6.25 could be transferred to other cases.

3.2. Parameters effect

3.2.1. Frequency

The effect of different frequencies has been assessed by exploiting fatigue crack growth measurements in displacement control, with a load ratio R_ε of 0.5 and a maximum strain ranging between 4 and 16%. The frequencies were 0.25, 1, 4 and 10 Hz. The different frequencies influence the hysteretic behavior as depicted in Fig. 5a: increasing slopes were seen with increasing frequency due to higher material stiffness as a consequence of viscoelastic effects in the elastomer matrix. The results in terms of fatigue crack growth as a function of tearing energy are reported in Fig. 5b. In contrast to the increase of material stiffness with higher frequencies, higher fatigue crack growth rates were found with lower frequencies, with an increase of approximately one order of magnitude passing from 10 to 0.25 Hz. This effect seems related to a higher contribution of the static component to the overall crack growth rate [6,8]. The values of the coefficients obtained from the curves fitting with Eq. (5) are reported in Table 3. As depicted in the plots and in the values reported in Table 1, the slope of the curves varies at different frequencies, rising with increasing frequencies. This effect may be associated with increasing temperatures related to heat build-up during the cyclic loading. Generally, temperature affects the mechanical behavior of rubbers in both small and large deformations. Specifically, a reduction of stiffness, elongation at break and fatigue crack growth resistance was observed passing from 25 to 80 °C [17]. The temperature increases due to heat build-up strongly depends on the stiffness of the material, on the thickness of the component and on the loading parameters such as the frequency of oscillation and the loading amplitude [34]; in particular, larger frequencies would result in higher temperature increases. This was observed for force control tests for the same material, in which almost no variation of surface temperature was detected for frequencies of 0.25 and 1 Hz, while increases of up to 8 °C were monitored for 10 Hz [7]. For the tests in displacement control, the extent of the temperature increases depended on the strain level: increasing temperatures were monitored at higher strains. In particular, at the highest strains (specifically 14 and 16%), the variation of temperature at 0.25 Hz was of approximately 2 °C, whereas temperature increases up to 18 °C (leading to absolute values of approximately 40 °C) were observed at 10 Hz. Therefore, at higher frequencies and at high strains (i.e., high tearing energies), such temperatures were large enough to affect both the mechanical and the crack growth behavior - even
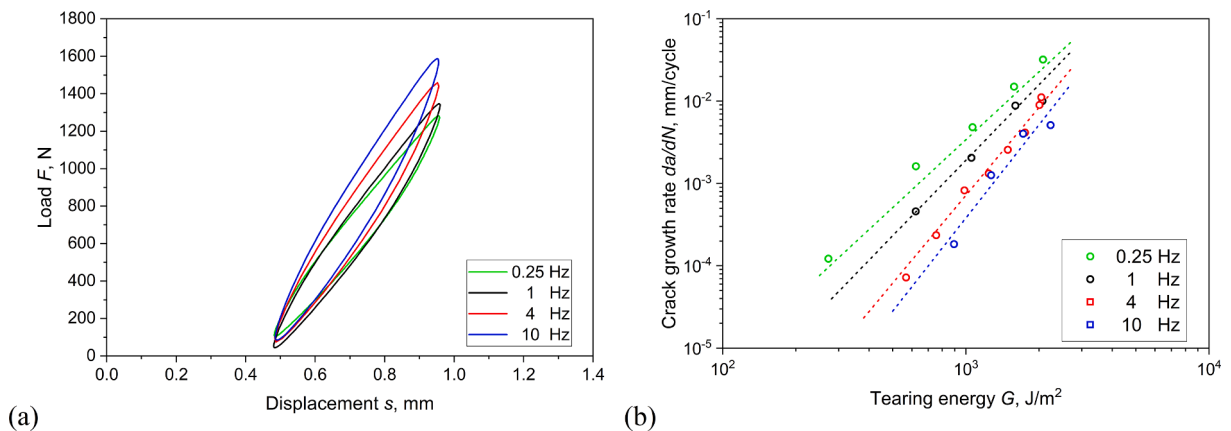

(a)   **(b)**

Fig. 5. **(a)** Hysteresis curves obtained during fatigue crack growth measurements at maximum strain of 6% for different frequencies of 0.25 (green), 1 (black), 4 (red) and 10 Hz (blue). **(b)** Fatigue crack growth rate as a function of tearing energy of filled NBR at different frequencies of 0.25 (green), 1 (black), 4 (red) and 10 Hz (blue). The measurements were performed with a specimen width L of 200 mm in displacement control with load ratio R_ε of 0.5 and maximum strain ranging between 4 and 16%. Three specimens were evaluated and only one of them has been reported for clarity reasons. The curves were fitted in the stable crack growth region using Eq. (5); the reported curve is the average from three specimens. (For interpretation of the references to colour in this figure legend, the reader is referred to the web version of this article.)

Table 3
Values of the power law coefficients obtained from fitting the fatigue crack growth curves for different frequencies (Fig. 5b) with Paris law (Eq. (5)). The values correspond to the mean value of the fitting of three tests under the same conditions.

Frequency f [Hz]	m	$logC$
0.25	2.7 ± 0.2	-10.7 ± 0.7
1	3.0 ± 0.2	-11.9 ± 0.7
4	3.5 ± 0.3	-13.8 ± 1.1
10	3.8 ± 0.4	-14.7 ± 0.8

within the limited number of cycles used in the experiments. Hence, the temperature rises due to heat build-up at higher strain seemed to cause an increase of the crack growth rate, which lead to a steeper slope of the curves.

3.2.2. Force control

Several tests were carried out in force control at different frequencies and the results were compared with the ones obtained in displacement control. The tests were implemented at frequencies of 0.25, 1 and 4 Hz using a maximum force of 1300 N and a load ratio $R = 0.1$. For a proper comparison, the parameters were selected to ensure an approximate strain load ratio R_ε of 0.5, in order to evaluate the differences only related to the loading control mode. Similar to the displacement control mode, higher slopes of the hysteresis curves were monitored with increasing frequencies, as depicted in Fig. 6a. The fatigue crack growth results of force-controlled tests are reported in Fig. 6b, in which fitted curves obtained in displacement control are represented by the dashed lines. The parameters from the curves fitting with Eq. (5) are reported in Table 4. For a proper statistical analysis, further measurements would be required, however, the same general trend of higher crack growth resistance with increasing frequency was found and it seems that at all investigated frequencies the choice of using loading displacement or force control amplitude as input does not have a significant impact on the final results, provided that loading conditions are similar. Analogous conclusions were drawn for SBR considering stress and strain control tests [10]. Only the case of 4 Hz shows a slightly different slope; however, at this frequency the force-controlled results are in a limited range of tearing energy, decreasing the accuracy of a proper fitting. Generally, force control and displacement control tests reveal similar results, but due to the broader tearing energy range, displacement control testing mode should be preferred.

3.2.3. Loading history

Different mechanical loading histories have been investigated, implementing tests in displacement control at a frequency of 4 Hz and load ratio R_ε of 0.5. The principle of the tests using displacement control is to vary the strain level in order to obtain the corresponding values of tearing energies and crack growth rates, which is constant in the stable crack propagation regime. Therefore, a single fatigue crack growth curve can be constructed with one specimen. In order to verify the effect of the initial strain level on the final results, four different load histories were exploited by varying the initial maximum strain. A full statistical analysis was not performed, since in principle the results were expected to be already repetitions of the results shown in Section 3.2.1 at 4 Hz. The results were compared, considering both the hysteresis curves and fatigue crack growth as a function of tearing energy. In particular
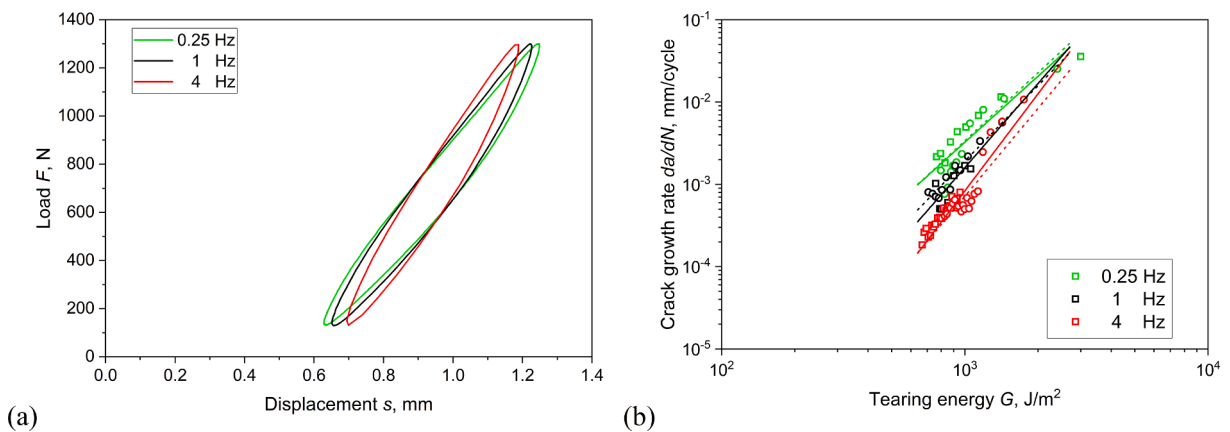

(a)

(b)

Fig. 6. (a) Hysteresis curves obtained during fatigue crack growth measurements in force control at 2000 cycles for different frequencies of 0.25 (green), 1 (black) and 4 (red). (b) Fatigue crack growth rate as a function of tearing energy of filled NBR in force control at different frequencies of 0.25 (green), 1 (black) and 4 (red); the different symbols (squares and circles) correspond to different specimens. The measurements were performed with a specimen width L of 200 mm using a maximum force of 1300 N and a load ratio R of 0.1. The parameters were selected to obtain a load ratio R_ε of 0.5. The curves were fitted in the stable crack growth region using Eq. (5); the reported curve is the average from two specimens. The dashed line corresponds to the fitted curves at the same frequencies in displacement control reported in Fig. 5. (For interpretation of the references to colour in this figure legend, the reader is referred to the web version of this article.)

Table 4
Values of the power law coefficients obtained from fitting the fatigue crack growth curves for different frequencies in force control (Fig. 6b) with Paris law (Eq. (5)). The values correspond to the mean value of the fitting of two tests under the same conditions.

Frequency f [Hz]	m	$\log C$
0.25	2.7 ± 0.5	-10.5 ± 1.7
1	3.4 ± 0.2	-13.0 ± 0.6
4	3.9 ± 0.2	-14.8 ± 0.6

the histories were:

1. Load history 1: increasing maximum strain: $4 - 6 - 8 - 10 - 12\%$
2. Load history 2: increasing maximum strain: $8 - 10 - 12\%$
3. Load history 3: decreasing maximum strain: $12 - 10 - 8 - 6 - 4\%$
4. Load history 4: decreasing maximum strain: $10 - 8 - 6 - 4\%$

Figs. 7-10 show sketches of the maximum strain as a function of the number of cycle (a) and the hysteresis curves (b) for the different loading histories. As depicted in the plots, the hysteresis curves have different shapes. Load history 1 (Fig. 7) shows the increasing size of the hysteretic curves for the first 4 steps and at the fourth step the majority of damage occurs leading to a different slope of the hysteresis in the last stage. In load history 2 (Fig. 8), the first step is at intermediate strain of 8% and it already exhibits heavy damaging; furthermore, the hysteresis curves in subsequent steps show a different slope, maintaining however a similar shape. Conversely, for load history 3 (Fig. 9) and load history 4 (Fig. 10) with decreasing load amplitude, the curves show in the first step major damage while the subsequent load steps display hysteresis curves with similar slopes, suggesting slight damaging in the successive steps. Moreover, the hysteretic curves at similar strain are much smaller than the ones with increasing loading. It is worth noting that in load history 3, the hysteresis curve at the last step (i.e., smallest maximum strain) show the presence of a compression state which leads to a different shape of the hysteresis loops.

The different loading histories possess distinct hysteretic behavior and these deviations are reflected even in the fatigue crack growth curves, reported in Fig. 11, and in the Paris coefficients from the curve fitting, reported in Table 5. In fact, considering the increasing loading histories 1 and 2, the crack growth curves are substantially the same. The differences between the two histories lay in the difference in the initial maximum strain (4 and 8%); however, although the hysteretic curves are different, the crack growth curve is the same. Therefore, the initial level of strain does not affect the resulting fatigue crack growth curves, which are then only material dependent. In principle, these results are valid as long as the microstructure ahead of the crack tip does not change as a consequence of the load. Therefore, it holds for non-crystallizing elastomers and in given conditions, even for crystallizing elastomers. In fact, the formation of crystallites ahead of the crack tip would affect or even hinder crack propagation; it is known, in fact, that the strain-induced crystallization depends on minimum strain (i.e., load ratio), frequency and temperature [35,36].

On the other hand, slight differences can be observed when considering the unloading histories (3 and 4) that show slightly faster crack propagation. Even though at higher tearing energies (i.e., high strain) the crack growth is quite similar to the increasing load cases, the main differences can be found at lower strains (and tearing energies) where the crack growth rates cannot be fitted with Paris law: those data do not correspond to the stable crack growth and cannot be described through Paris law, but rather they represent a transition phase. As a matter of fact, at these levels of strain even the hysteretic curves were different, suggesting the existence of
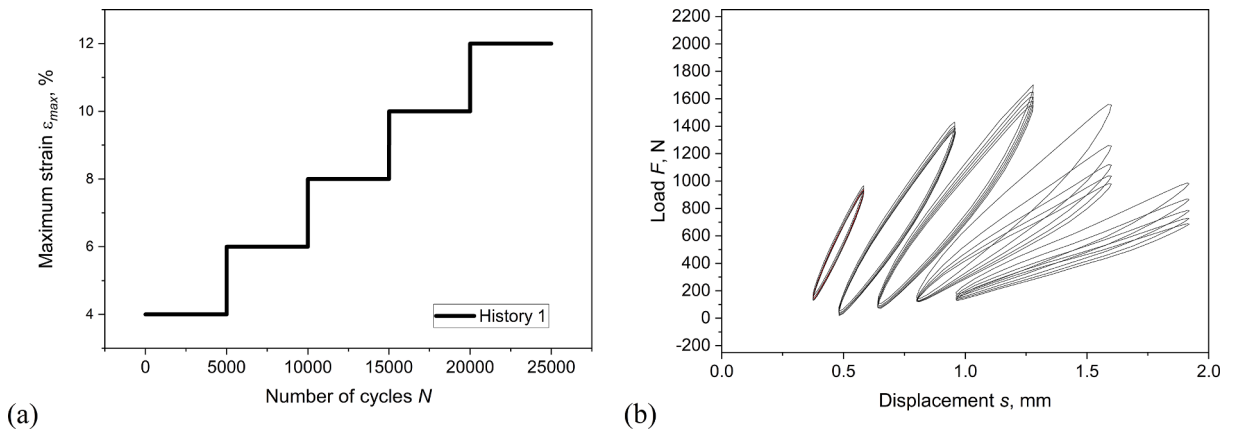

(a)   (b)

Fig. 7. (a) Graph of the maximum strain used during fatigue crack growth measurements for load history 1. **(b)** Hysteresis curves obtained during fatigue crack growth measurements every 1000 cycles related to load history 1. The measurements were performed with a specimen width L of 200 mm in displacement control at 4 Hz, with load ratio R_ε of 0.5 and maximum strain ranging between 4 and 12%.

Fig. 8. (a) Graph of the maximum strain used during fatigue crack growth measurements for load history 2. **(b)** Hysteresis curves obtained during fatigue crack growth measurements every 1000 cycles related to load history 2. The measurements were performed with a specimen width *L* of 200 mm in displacement control at 4 Hz, with load ratio R_e of 0.5 and maximum strain ranging between 8 and 12%.
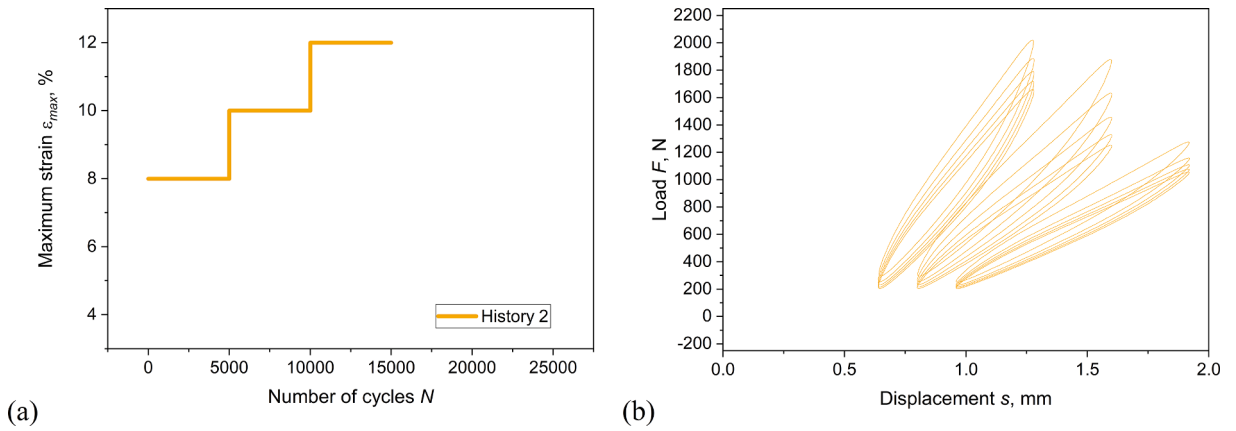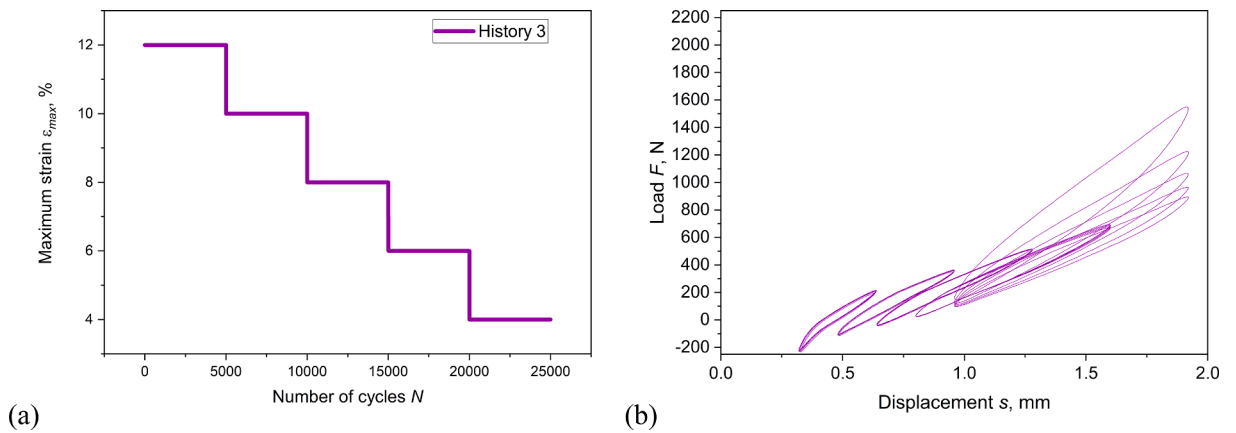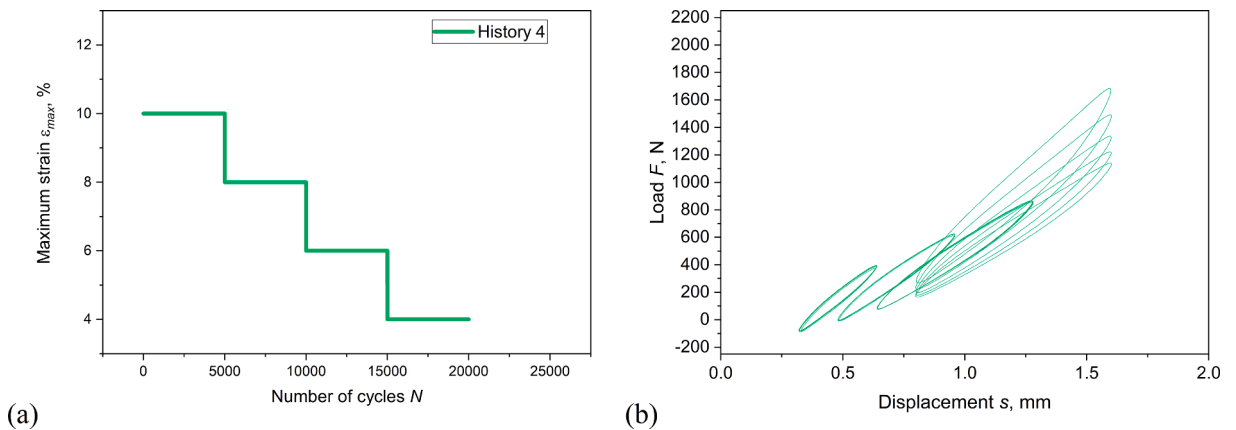

Fig. 9. (a) Graph of the maximum strain used during fatigue crack growth measurements for load history 3. **(b)** Hysteresis curves obtained during fatigue crack growth measurements every 1000 cycles related to load history 3. The measurements were performed with a specimen width *L* of 200 mm in displacement control at 4 Hz, with load ratio R_e of 0.5 and maximum strain ranging between 12 and 4%.

Fig. 10. (a) Graph of the maximum strain used during fatigue crack growth measurements for load history 4. **(b)** Hysteresis curves obtained during fatigue crack growth measurements every 1000 cycles related to load history 4. The measurements were performed with a specimen width *L* of 200 mm in displacement control at 4 Hz, with load ratio R_e of 0.5 and maximum strain ranging between 10 and 4%.
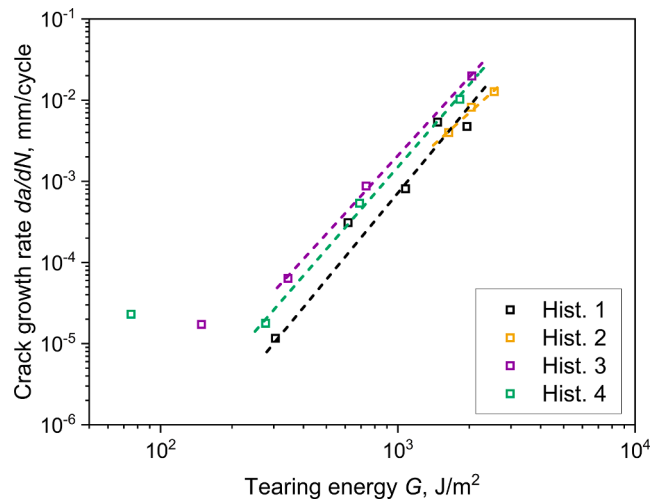
Fig. 11. Fatigue crack growth rate as a function of tearing energy of filled NBR at different load history: Load history 1 (black), Load history 2 (orange), Load history 3 (purple) and Load history 4 (green). The measurements were performed with a specimen width *L* of 200 mm in displacement control at 4 Hz and load ratio R_ε of 0.5. The curves were fitted in the stable crack growth region using Eq. (5). (For interpretation of the references to colour in this figure legend, the reader is referred to the web version of this article.)

Table 5
Values of the power law coefficients obtained from fitting the fatigue crack growth curves for different loading histories (Fig. 11) with Paris law (Eq. (5)).

Load history	*m*	log*C*
History 1	3.5	−13.8
History 2	2.6	−10.8
History 3	3.2	−12.3
History 4	3.4	−12.9

residual stress, which has a hindering effect on crack propagation. Overall, the crack growth rate for decreasing loading is slightly higher than the one with increasing loading. Therefore, precautions should be taken when considering loading histories with decreasing loading level.
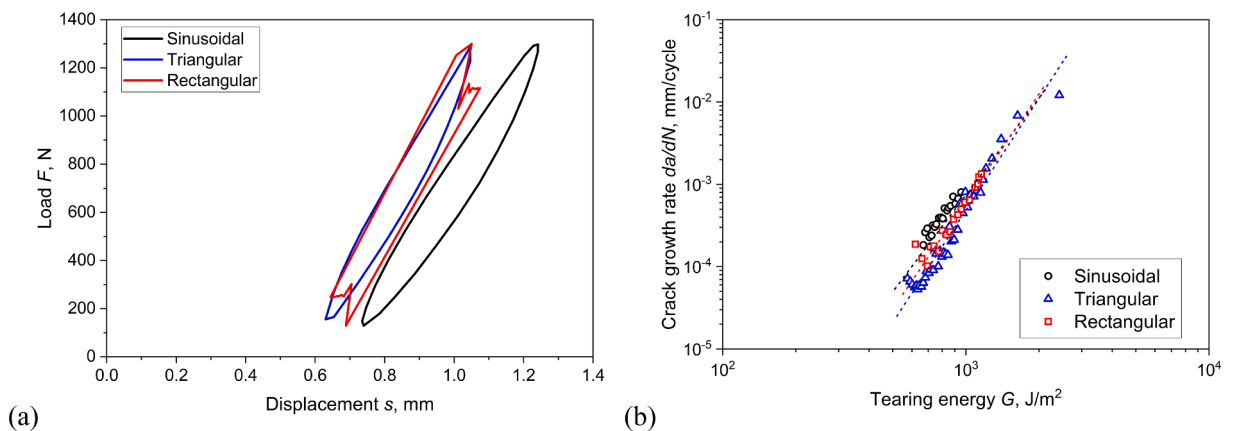

Fig. 12. (a) Hysteresis curves obtained during fatigue crack growth measurements in force control at 10,000 cycles for different waveforms: sinusoidal (black), triangular (blue) and rectangular (red). **(b)** Fatigue crack growth rate as a function of tearing energy of filled NBR using different waveforms: sinusoidal (black), triangular (blue) and rectangular (red). The measurements were performed with a specimen width *L* of 200 mm in force control at 4 Hz, with load ratio *R* of 0.1 and maximum force of 1300 N. The curves were fitted in the stable crack growth region using Eq. (5); the reported curve is the average from two specimens. (For interpretation of the references to colour in this figure legend, the reader is referred to the web version of this article.)

3.2.4. Waveform

The effect of waveform has been assessed exploiting sinusoidal, triangular and rectangular shape load. The tests were carried out in force control with a maximum force of 1300 N, load ratio R of 0.1 and frequency of 4 Hz. Considering the results shown above, the results would be the same in displacement control. The hysteresis curves reported in Fig. 12a highlight some differences in the mechanical behavior. In fact, at the same number of cycles, higher displacement levels were monitored for the sinusoidal waveform. Moreover, the different waveforms resulted in different shapes of the hysteresis curves. In particular, the rectangular waveform (red curve in Fig. 12a) shows that the prescribed load was reached as a peak value, while afterwards the load amplitude fell by approximately 25%; this is related to limitations of the machine at the frequency used to reproduce a rectangular waveform. Nevertheless, the resulting fatigue crack growth curves are quite similar as illustrated in Fig. 12(b). Even though the curves' slopes seem to increase passing from sinusoidal to rectangular and then to triangular, this variation is within the scattering error of the measurements. This is also confirmed from the coefficients of the curves fitting displayed in Table 6. Actually, the effect of waveform seems to be mostly related to pulse waveforms [10] and in particular to the time at static load in between the pulses, which is referred as "dwell time" [12]. Therefore, the reported results confirmed previous reports for other rubbers that the shape of the waveform has only a small influence on the fatigue behavior of filled elastomers.

3.2.5. Load ratio

The effect of the load ratio was investigated exploiting three different load ratios R_ε of 0, 0.3 and 0.5. The measurements were implemented in displacement control mode at a frequency of 4 Hz with strains ranging between 4 and 16%. As depicted in the hysteresis curve from Fig. 13(a), the different load ratios lead to different loading conditions: for the lowest value of R_ε the stress state was in a tension–compression state (lower for $R_\varepsilon = 0$), while for $R_\varepsilon = 0.5$ the stress was mainly in tension–tension state. The results in terms of fatigue crack growth as a function of tearing energy are reported in Fig. 13 (b). As depicted the fatigue curves are very similar, even though the lowest curve is the one with $R_\varepsilon = 0.5$, corresponding to a tension–tension state with the smallest hysteresis loop. Nevertheless, considering the scattering of typical fatigue experiments and the coefficients of Paris law reported in Table 7, it is possible to state that the load ratio has only a negligible influence on the fatigue crack growth of this material. The effect of the load ratio is mainly present for crystallizing rubbers, with a beneficial increase of crack growth resistance for positive load ratios [5].

4. Summary and conclusions

In this work, the focus was devoted to the effect of different parameters related to the mechanical history on the fatigue behavior of a filled NBR. The fatigue behavior was investigated through the crack growth approach using pure shear specimens.

The specimen configuration was analyzed considering single notch, single notch with double length and double edge notch configuration. The results were independent of the configuration demonstrating that the notch has no effect on the fatigue crack growth of the material. However, the double edge configuration assures more stable loading direction during testing. Moreover, different width to height ratios (12.5, 6.25 and 4 for the specimen lengths L, $L/2$ and $L/3$) were tested and no significant influences of this parameter were observed on the fatigue crack behavior of the material.

After the analysis of the influence of the specimen geometry on the fatigue behavior of the material, the effect of several parameters was investigated. Fatigue crack growth measurement at different frequencies (0.25, 1, 4 and 10 Hz) were implemented demonstrating that lower frequencies results in higher fatigue crack growth, with a difference of approximately one order of magnitude between 0.25 and 10 Hz. Furthermore, several tests were carried out in force control and the results were compared with the results obtained in displacement control mode at 0.25, 1 and 4 Hz. At all investigated frequencies, the use of the displacement or force as input parameter of the load had negligible influence on the final results. Different loading histories were tested in displacement control and it was found that the crack growth rate for decreasing loading steps is slightly higher than the one with increasing load, especially at low tearing energies. The effect of waveforms has been assessed by investigating the fatigue crack growth, examining sinusoidal, triangular and rectangular shapes. The waveform was found to have only a minor influence on the fatigue crack growth curves. Finally, the effect of the load ratio on the fatigue crack growth was investigated using load ratios R_ε of 0, 0.3 and 0.5. The resulting fatigue crack showed no significant influence on the fatigue behavior of this material.

The results shown in this work represent a further step forward in understanding the fatigue behavior of non-crystallizing rubbers and in particular of NBR for which there are few studies in the literature. Furthermore, this comprehensive investigation of the fatigue crack resistance of the same material provided a global overview that has allowed the authors to state that frequency is one of the most influential parameters as it has a strong influence on crack growth and high temperature development as a consequence of heat build-up. A better comprehension of the effect of different parameters on fatigue is important to develop more accurate models that consider

Table 6
Values of the power law coefficients obtained from fitting the fatigue crack growth curves for different waveforms (Fig. 12b) with Paris law (Eq. (5)). The values correspond to the mean value of the fitting of two tests under the same conditions.

Waveform	m	$\log C$
Sinusoidal	3.9 ± 0.5	-14.9 ± 0.7
Triangular	4.5 ± 0.4	-16.9 ± 1.0
Rectangular	4.3 ± 0.4	-16.2 ± 1.2

(a)

(b)

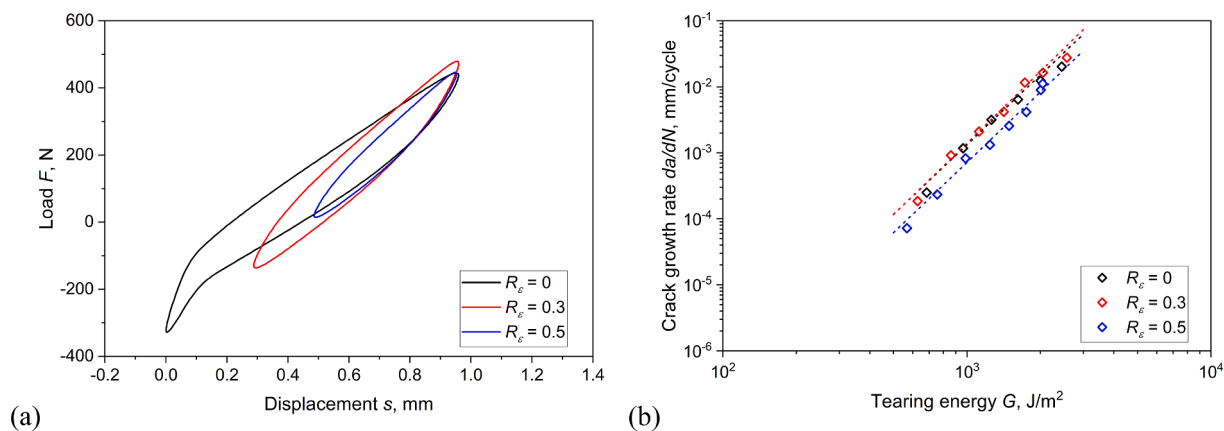**Fig. 13.** (a) Hysteresis curves obtained during fatigue crack growth measurements at maximum strain of 6% for different load ratios R_ε of 0 (black), 0.3 (red) and 0.5 (blue). (b) Fatigue crack growth rate as a function of tearing energy of filled NBR at different load ratios R_ε of 0 (black), 0.3 (red) and 0.5 (blue). The measurements were performed with a specimen width L of 100 mm in displacement control at 4 Hz and maximum strain ranging between 4 and 16%. Three specimens were evaluated and only one of them has been reported for clarity reasons. The curves were fitted in the stable crack growth region using Eq. (5); the reported curve is the average from three specimens. (For interpretation of the references to colour in this figure legend, the reader is referred to the web version of this article.)

Table 7
Values of the power law coefficients obtained from fitting the fatigue crack growth curves for different load ratios R_ε (Fig. 13b) with Paris law (Eq. (5)). The values correspond to the mean value of the fitting of three tests at the same conditions.

Load Ratio R_ε	m	$\log C$
0	3.5 ± 0.2	-13.4 ± 0.5
0.3	3.6 ± 0.1	-13.7 ± 0.1
0.5	3.5 ± 0.3	-13.8 ± 1.1

the influence and interactions of different parameters in order to obtain a more accurate prediction of durability.

Declaration of Competing Interest

The authors declare that they have no known competing financial interests or personal relationships that could have appeared to influence the work reported in this paper.

Acknowledgements

References

[1] Mars WV, Fatemi A. A literature survey on fatigue analysis approaches for rubber. Int J Fatigue 2002;24(9):949–61. https://doi.org/10.1016/S0142-1123(02)00008-7.

[2] Mars WV, Fatemi A. Factors that affect the fatigue life of rubber: a literature survey. Rubber Chem Technol 2004;77(2):391–412. https://doi.org/10.5254/1.3547831.

[3] Lindley PB. Non-relaxing crack growth and fatigue in a non-crystallizing rubber. Rubber Chem Technol 1974;47(5):1253–64. https://doi.org/10.5254/1.3540497.

[4] Mars WV, Fatemi A. A phenomenological model for the effect of r-ratio on fatigue in strain crystallizing rubbers. Rubber Chem Technol 2003;76(5):1241–58. https://doi.org/10.5254/1.3547800.

[5] Saintier N, Cailletaud G, Piques R. Cyclic loadings and crystallization of natural rubber: An explanation of fatigue crack propagation reinforcement under a positive loading ratio. Mater Sci Engng, A 2011;528(3):1078–86. https://doi.org/10.1016/j.msea.2010.09.079.

[6] Busfield JJC, Tsunoda K, Davies CKL, Thomas AG. Contributions of time dependent and cyclic crack growth to the crack growth behavior of non strain-crystallizing elastomers. Rubber Chem Technol 2002;75(4):643–56. https://doi.org/10.5254/1.3544991.

[7] Schieppati J, Schrittesser B, Wondracek A, Robin S, Holzner A, Pinter G. Impact of temperature on the fatigue and crack growth behavior of rubbers. Procedia Struct Integrity 2018;13:642–7. https://doi.org/10.1016/j.prostr.2018.12.106.

[8] Lake GJ, Lindley PB. Cut growth and fatigue of rubbers. II. Experiments on a noncrystallizing rubber. J Appl Polym Sci 1964;8(2):707–21. https://doi.org/10.1002/app.1964.070080212.

[9] Young DG. Dynamic property and fatigue crack propagation research on tire sidewall and model compounds. Rubber Chem Technol 1985;58(4):785–805. https://doi.org/10.5254/1.3536093.

[10] Andreini G, Straffi P, Cotugno S, Gallone G, Polacco G. Comparison of sine versus pulse waveform effects on fatigue crack growth behavior of NR, SBR, and BR compounds. Rubber Chem Technol 2010;83(4):391–403.

[11] Ghosh P, Stocek R, Gehde M, Mukhopadhyay R, Krishnakumar R. Investigation of fatigue crack growth characteristics of NR/BR blend based tyre tread compounds. Int J Fract 2014;188(1):9–21. https://doi.org/10.1007/s10704-014-9941-9.

[12] Harbour RJ, Fatemi A, Mars WV. The effect of a dwell period on fatigue crack growth rates in filled SBR and NR. Rubber Chem Technol 2007;80(5):838–53. https://doi.org/10.5254/1.3539420.

[13] Young DG. Fatigue crack propagation in elastomer compounds: effects of strain rate, temperature, strain level, and oxidation. Rubber Chem Technol 1986;59(5):809–25.

[14] Young DG, Danik JA. Effect of temperature on fatigue and fracture. Rubber Chem Technol 1994;67(1):137–47. https://doi.org/10.5254/1.3538660.

[15] Luo W, Li M, Huang Y, Yin B, Hu X. Effect of temperature on the tear fracture and fatigue life of carbon-black-filled rubber. Polymers (Basel) 2019;11(5):768. https://doi.org/10.3390/polym11050768.

[16] Ruellan B, Le Cam J-B, Jeanneau I, Canévet F, Mortier F, Robin E. Fatigue of natural rubber under different temperatures. Int J Fatigue 2019;124:544–57. https://doi.org/10.1016/j.ijfatigue.2018.10.009.

[17] Schieppati J, Schrittesser B, Wondracek A, Robin S, Holzner A, Pinter G. Temperature impact on the mechanical and fatigue behavior of a non-crystallizing rubber. Int J Fatigue 2021;144:106050. https://doi.org/10.1016/j.ijfatigue.2020.106050.

[18] Agnelli S, Balasooriya W, Bignotti F, Schrittesser B. On the experimental measurement of fracture toughness in SENT rubber specimens. Polym Test 2020;87:106508. https://doi.org/10.1016/j.polymertesting.2020.106508.

[19] Benkahla J, Baranger TN, Issartel J. Fatigue life estimation for an NBR rubber and an expanded polyurethane. Exp Mech 2013;53(8):1383–93. https://doi.org/10.1007/s11340-013-9749-y.

[20] Béranger AS, Qin J, Heuillet P, Baurier H. Fatigue crack growth behavior of NBR, HNBR. HNBR ZSC compounds Procedia Engineering 2018;213:145–52. https://doi.org/10.1016/j.proeng.2018.02.016.

[21] Cho K, Jang WJ, Lee D, Chun H, Chang Y-W. Fatigue crack growth of elastomers in the swollen state. Polymer 2000;41(1):179–83. https://doi.org/10.1016/S0032-3861(99)00142-1.

[22] Cho K, Lee D. Effect of molecular weight between cross-links on the abrasion behavior of rubber by a blade abrader. Polymer 2000;41(1):133–40. https://doi.org/10.1016/S0032-3861(99)00111-1.

[23] Kim JK. Fracture behavior of crumb rubber-filled elastomers. J Appl Polym Sci 1999;74(13):3137–44. https://doi.org/10.1002/(SICI)1097-4628(19991220)74:13<3137::AID-APP16>3.0.CO;2-0.

[24] Mahmoud WE, Mansour SA, Hafez M, Salam MA. On the degradation and stability of high abrasion furnace black (HAF)/acrylonitrile butadiene rubber (NBR) and high abrasion furnace black (HAF)/graphite/acrylonitrile butadiene rubber (NBR) under cyclic stress–strain. Polym Degrad Stab 2007;92(11):2011–5. https://doi.org/10.1016/j.polymdegradstab.2007.08.005.

[25] Major Z, Lang RW. Characterization of the fracture behavior of NBR and FKM grade elastomers for oilfield applications. Engng Fail Anal 2010;17(3):701–11. https://doi.org/10.1016/j.engfailanal.2009.08.004.

[26] Mohammed A, Nemat-Alla MM, Emara KM. Influence of cyclic loading on fatigue behavior of SBR and NBR compounds with different contents of carbon black. Journal of Engineering Science, Assiut University, Faculty of Engineering 2013;42(2):365–84.

[27] Najipoor M, Haroonabadi L, Dashti A. Assessment of failures of nitrile rubber vulcanizates in rapid gas decompression (RGD) testing: Effect of physico-mechanical properties. Polym Test 2018;72:377–85. https://doi.org/10.1016/j.polymertesting.2018.11.002.

[28] Hamed GR. Materials and compounds. In: Gent AN, editor. Engineering with Rubber: How to Design Rubber Components. 3rd ed. Hanser Publications.

[29] Rivlin RS, Thomas AG, Thomas AG. Rupture of rubber. I. Characteristic energy for tearing. Journal of Polymer Science 1953;10(3):291–318. https://doi.org/10.1002/pol.1953.120100303.

[30] Lake GJ, Lindley PB. The mechanical fatigue limit for rubber. J Appl Polym Sci 1965;9(4):1233–51. https://doi.org/10.1002/app.1965.070090405.

[31] Harbour RJ, Fatemi A, Mars WV. Fatigue crack growth of filled rubber under constant and variable amplitude loading conditions. Fatigue Fract Engng Mater Struct 2007;30(7):640–52. https://doi.org/10.1111/j.1460-2695.2007.01143.x.

[32] Weng G, Chang A, Fu K, Kang J, Ding Y, Chen Z. Crack growth mechanism of styrene-butadiene rubber filled with silica nanoparticles studied by small angle X-ray scattering. RSC Adv 2016;6(10):8406–15. https://doi.org/10.1039/C5RA26238K.

[33] Yeoh OH. Analysis of deformation and fracture of 'pure shear' rubber testpiece. Plast, Rubber Compos 2013;30(8):389–97. https://doi.org/10.1179/146580101101541787.

[34] Gent AN, Scott KW. Dynamic mechanical properties. In: Gent AN, editor. Engineering with Rubber: How to Design Rubber Components. 3rd ed. Hanser Publications.

[35] Huneau B. Strain-induced crystallization of natural rubber: a review of x-ray diffraction investigations. Rubber Chem Technol 2011;84(3):425–52. https://doi.org/10.5254/1.3601131.

[36] Candau N, Chazeau L, Chenal J-M, Gauthier C, Ferreira J, Munch E, et al. Strain induced crystallization and melting of natural rubber during dynamic cycles. Phys Chem Chem Phys 2015;17(23):15331–8. https://doi.org/10.1039/C5CP00384A.

Publication 4

Temperature impact on the mechanical and fatigue behavior of a non-crystallizing rubber

Jacopo Schieppati [a], Bernd Schrittesser [a], Alfred Wondracek [b], Stefan Robin [b], Armin Holzner [b] and Gerald Pinter [c]

[a]   Polymer Competence Center Leoben GmbH, Roseggerstrasse 12, 8700 Leoben, Austria
[b]   Semperit Technische Produkte Gesellschaft m.b.H., Triester Bundesstrasse 26, 2632 Wimpassing, Austria
[c]   Department of Polymer Engineering and Science – Material Science and Testing of Polymers, Montanuniversitaet, Otto Glöckel-Strasse 2, 8700 Leoben, Austria

Relevant contributions to this publication:

Conceptualization: Jacopo Schieppati, Bernd Schrittesser, Alfred Wondracek, Stefan Robin, Armin Holzner, Gerald Pinter

Methodology: Jacopo Schieppati, Bernd Schrittesser

Investigation: Jacopo Schieppati

Writing - Original Draft: Jacopo Schieppati

Writing - Review & Editing: Jacopo Schieppati; Bernd Schrittesser, Alfred Wondracek, Gerald Pinter

Temperature impact on the mechanical and fatigue behavior of a non-crystallizing rubber

Jacopo Schieppati [a,*], Bernd Schrittesser [a], Alfred Wondracek [b], Stefan Robin [b], Armin Holzner [b], Gerald Pinter [c]

[a] *Polymer Competence Center Leoben GmbH, Roseggerstrasse 12, 8700 Leoben, Austria*
[b] *Semperit Technische Produkte Gesellschaft m.b.H., Triester Bunderstrasse 26, 2632 Wimpassing, Austria*
[c] *Department of Polymer Engineering and Science – Material Science and Testing of Plastic, Montanuniversitaet, Otto Glöckelstrasse 2, 8700 Leoben, Austria*

ARTICLE INFO

ABSTRACT

Temperature is one of the main parameters affecting the mechanical behavior of rubbers. The impact of this parameter is particularly important in the case of cyclic loads. In this study the mechanical and fatigue behavior of a carbon filled acrylonitrile butadiene rubber (NBR) was investigated. Tensile tests revealed a general decrease of the ultimate properties with temperature. Moreover, the maximum chain extensibility, evaluated through Mooney-Rivlin plots, showed a similar trend and a minimum at intermediate temperature. The dynamic properties of the material were investigated through DMA measurements. Temperature sweep revealed an Arrhenius dependence of the dynamic moduli for temperatures above $T_g + 30\,°C$. Master curves of the dynamic properties were generated through the application of the time-temperature superposition principle, by shifting horizontally the isothermal frequency sweeps. The fatigue behavior at different temperature was assessed through the crack growth approach and a lower crack growth resistance was found at higher temperatures. Finally, a new procedure for building fatigue master curves has been investigated by exploiting the temperature dependence of the loss modulus.

1. Introduction

Due to their outstanding mechanical properties, rubbers have a relevant importance in applications involving cyclic loads, which are normally superimposed to a large static load. In this loading conditions, fatigue is the main cause of failure and therefore, the fatigue characterization is of primary importance for rubber industry. The prediction of the lifetime during rubber fatigue is mainly assessed using two approaches, crack nucleation and crack growth [1]. The latter is focused on the growth of preexisting cracks making use of a fracture mechanical approach, based on a tearing energy criterion developed for rubbers by Rivlin and Thomas [2].

Because of the presence of fillers and of the viscoelastic nature of the elastomer matrix [3], temperature strongly influences the mechanical and failure behavior of rubbers. In an early work Lake and Lindley [4] reported that styrene-butadiene rubber (SBR) showed a drop of 4 order of magnitude of fatigue life passing from 0 to 100 °C. Several studies focus on the impact of temperature on fracture and fatigue of different

rubbers [5–13] underlining the importance of this parameters for the analysis of the failure of these materials. In fact, during working conditions the rubber products may be subjected to high temperatures not only related to the environment but even due to temperature increases as a consequence of heat build-up during cyclic loading. Even though the role of temperature is known to be relevant for rubbers failure, further researches are necessary for the comprehension of the processes involved in high temperature fatigue.

In this study, the impact of temperature has been assessed implementing different mechanical characterization techniques. Tensile tests at different temperatures allowed to monitor the variation of the ultimate properties with the temperature. Moreover, through the use of Mooney-Rivlin plots, the maximum chain extensibility was verified at different temperature. Dynamic mechanical analysis (DMA) resulted in the evaluation of the temperature dependence of the material under cyclic loading and to construct master curves. Furthermore, fatigue crack growth measurements were performed on pure shear specimens at different temperatures. Finally, the effect of temperature was considered

by using a novel procedure to construct a master curve based on the fatigue crack growth performance.

2. Material and methods

2.1. Materials

The material used for this research is a commercial acrylonitrile butadiene rubber (NBR) filled with 42 phr of carbon black. Due to confidentially, no additional information about the precise formulation can be given.

2.2. Tensile tests

Tensile measurements were performed at different temperatures (25, 40, 60, 80 and 100 °C) using a universal testing machine by Zwick GmbH & Co. (Ulm, Germany) equipped with a temperature chamber. According to DIN 53504 [14], the specimens (S2 geometry) were cut from 2 mm thick rubber plates. Three specimens were tested at each temperature, using a rate of 200 mm/min (corresponding to a strain rate of 0.1167 s^{-1}). The local strain was monitored with Digital Image Correlation (DIC), using two cameras and Mercury RT software (Sobriety s. r.o., Kuřim, Czech Republic) for the analysis. In particular, the strains were evaluated following the distance of two markers placed on the specimens. Before testing, the specimens were inserted in the oven at the corresponding temperature and kept there for approximately one hour in order to reach a homogenous temperature distribution in the specimens. Each specimen was then clamped in the upper clamp and it was kept further 15 min in this state before clamping the lower part. In this way, no stresses related to thermal expansion were introduced.

2.3. Dynamic mechanical analysis (DMA)

Dynamic mechanical analysis tests were implemented in tension mode using a rubber strip (1 mm thick, 10 mm and 5 mm of length and width respectively) with a DMA 8000 Dynamic Mechanical Analyzer by PerkinElmer. A temperature sweep was implemented in the temperature range between −60 and 100 °C (heating rate of 3 K/min) with a strain amplitude of 0.05%. Furthermore, the tests were carried out at different frequencies of 1 and 4 Hz. For creating the master curve, isothermal frequency sweeps were performed in the temperature range −60 and 100 °C (5 K steps), at a strain amplitude of 0.03%. The used frequency range was between 0.1 and 50 Hz. Both strains lay in the linear viscoelastic region: this was determined with a preliminary strain sweep whereat the linear region extended to approximately 0.1%.

2.4. Fatigue crack growth

Fatigue crack growth measurements were implemented using a pure shear specimen geometry. The height of the specimens was 16 mm, the width 100 mm (width to height ratio 6.25) and the thickness 4 mm. Specifically, the samples were mounted on special clamps, preloaded to 20 N and notched on both sides. As a matter of fact, the double edge notched configuration was considered to avoid tilting of the loading direction during the crack opening phase. A study by Yeoh [15] indicated the equivalence between one and two edge cracks; moreover, several preliminary tests have been conducted to analyze the impact of different configurations and the double edge notched configuration provided more reproducible results. Consequently, two initial notches (25 mm each) were introduced on both sides using a razor blade, mounted on a customized tool guided on the clamping system. The tests were carried out using a MTS 858 Table Top System testing machine and the crack length was monitored through a camera system CV-5701P by Keyence; the final crack growth rate was considered to be the sum of the crack growth rates on the two sides of the specimen. In order to avoid light reflections, the specimens were sprayed with a white powder

coating. Specifically, the tests were performed in displacement control mode with increasing strain steps with maximum strain ranging between 1 and 12%; a similar approach can be found in literature [16]. A sinusoidal waveform was used at frequency of 4 Hz and with load ratio R_ε of 0.5. Moreover, the tests were performed in a temperature chamber at temperatures of 25, 40, 60 and 80 °C. Nevertheless, the specimens were notched, sprayed and clamped at room temperature. After the clamping, the temperature was raised and the force was constrained to zero, so that the distance between the clamps could adapt to balance the thermal expansion until an equilibrium was reached; this was established after about one hour.

During the cyclic loading, the hysteresis was monitored through the MTS test device and the tearing energy G was calculated with the data obtained from the specimen under testing in the beginning of each strain step. As described by Agnelli et al. [17], the fracture mechanics approach developed for rubbers has its foundations in the energy balance of a body of area A containing a stationary crack:

$$\frac{dU_{in}}{A} - \frac{dU}{A} = \frac{dU_{diss}}{A} \tag{1}$$

where U_{in} is the input energy (external forces' work), U is the recoverable elastic strain energy, and U_{diss} is the dissipated energy. From this energy balance, Griffith [18] defined the energy release rate G_{Grif} as the energy dissipated during fracture per unit of newly created area at a fixed displacement s:

$$G_{Grif} = -\frac{dU}{dA}\bigg|_s \tag{2}$$

From this definition, Rivlin and Thomas [2] introduced the tearing energy G, representing the work expended irreversibly per unit area of crack advancement (so the left end side of Eq. (1)) and expressed it as function of the strain energy density W_0:

$$G = \frac{dU_{in}}{A} - \frac{dU}{A} = k(\lambda) \cdot W_0 \cdot c \tag{3}$$

where c is the crack length and $k(\lambda)$ is a function of the stretch ratio. Furthermore, they derived a simplified semi-empirical form for the evaluation of tearing energy for Pure Shear (PS) specimen geometries as [2]:

$$G = W_0 \cdot h_0 \tag{4}$$

where h_0 the height of the specimen in the unstrained condition. As reported in several works [19–23], it is possible to consider the definition of strain energy in terms of engineering stress and strain. Therefore, it is possible to obtain a formula in terms of force F and displacement s that for a Pure Shear specimen gives:

$$W_0 = \int \sigma \cdot d\varepsilon = \int \frac{F}{A_{uncr}} \cdot \frac{1}{h_0} \cdot ds = \frac{1}{h_0 A_{uncr}} \int F \cdot ds = \frac{U_{load}}{h_0 A_{uncr}} \tag{5}$$

where U_{load} is the energy under the load-displacement curve and A_{uncr} is the uncracked area. This leads to the final formula for the tearing energy:

$$G = \frac{U_{load}}{A_{uncr}} \tag{6}$$

In non-relaxing condition, the mechanical energy was evaluated according to the following convention. For positive load ratio, the static contribution was considered and added to U_{load} [24–26]. Therefore, the static contribution U_{static} was considered as:

$$U_{static} = F_{min} \cdot s_{min} \tag{7}$$

where F_{min} and s_{min} are the minimum force and the minimum displacement in the hysteresis curve. For negative load ratio, only the positive part of the area under the loading curve was taken into account. Using

this approach, the tearing energy was evaluated at the maximum strain and corresponded to G_{max} reported in literature [27].

3. Results and discussion

3.1. Stress-strain behavior

Fig. 1 summarizes the stress-strain curves evaluated through tensile tests at different temperatures. As depicted, an increase in temperature results in a reduction of the stiffness of the material. Moreover, the ultimate properties decreased with rising temperature as well. The plot in Fig. 2 shows that the stress at break σ_b, decreases almost linearly with temperature. Conversely, the strain at break ε_b (Fig. 3) remains constant passing from 25 to 40 °C, while at higher temperature it decreases, with a significant drop passing from 40 to 60 °C.

The fracture energy W_f, evaluated as the area below the stress–strain curves up to the failure point, reflects the behavior of stress and strain at break. As it is reported in Fig. 4, the fracture energy decreases with temperature, showing a small variation from 25 to 40 °C and a major drop passing from 40 to 60 °C, similarly to the trend of the strain at break.

Additionally, the stress-strain data were analyzed using the Mooney-Rivlin equation [28,29]:

$$\sigma = 2\left(C_1 + \frac{C_2}{\lambda}\right)\left(\lambda - \frac{1}{\lambda^2}\right) \tag{8}$$

where C_1 and C_2 are material constants and λ is the stretch ratio. The Mooney-Rivlin equation describes the general mechanical behavior of rubbers and has been successfully used for the evaluation of the cross-linking density [30]. It is worth noting, that this description cannot be applied for crack propagation and ahead crack tip, for which a fracture mechanical approach has to be adopted.

Furthermore, Eq. (8) can be rewritten considering the reduced stress σ^*:

$$\sigma^* = \frac{\sigma}{\lambda - \frac{1}{\lambda^2}} \tag{9}$$

In this way, by plotting the reduced stress σ^* against λ^{-1}, the so-called Mooney-Rivlin plots [31–35] can be obtained. The Mooney-Rivlin plots at different temperatures are reported in Fig. 5. This graph shows that at low strains (i.e. high value of inverse of the stretch ratio) the reduced stresses decrease up to an upturn value after which the reduced stresses grow. As a matter of fact, the upturn in the reduced stress is connected to
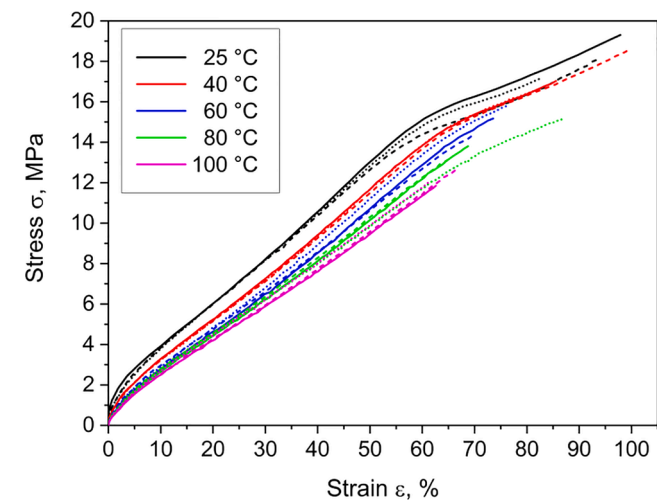

Fig. 2. Stress at break as a function of temperature from tensile tests of filled NBR at a displacement rate of 200 mm/min. The reported results correspond to the average of the values and the corresponding error obtained from three specimens.

Fig. 3. Strain at break as a function of temperature from tensile tests of filled NBR at a displacement rate of 200 mm/min. The reported results correspond to the average of the values and the corresponding error obtained from three specimens.

the limited chain extensibility between crosslinks [36,37]. It is worth noting that the limited chain extensibility is affected by the presence of filler and by the occluded rubber, which limits the molecules extension. The values of the upturn strain, defined as the strain corresponding to the minimum in the reduced stress after the initial decrease, are represented in Fig. 5 as the star signs, analyzed at different temperatures. As depicted in Fig. 6, the upturn strain (and the maximum chain extensibility) varies with the temperature. Similarly to the ultimate properties, the upturn strain shows decreasing values with temperature; however, it rises at high temperatures. Hence, it seems that the limited chain extensibility has a minimum at intermediate temperatures around 40 and 80 °C. This can be related to the entropic nature of rubbers elasticity: at different temperatures, the enthalpic and entropic contributions to the overall elasticity are different. Moreover, at different temperature the effect of the bound rubber on the materials property will be different. Even though we believed that the reported trend is reliable, further tests and testing methods should be employed to verify the absolute value of the strain for maximum chain extensibility and to understand the

Fig. 1. Stress-strain curves from tensile tests of filled NBR at different temperatures at a displacement rate of 200 mm/min. The different line styles correspond to different specimens.
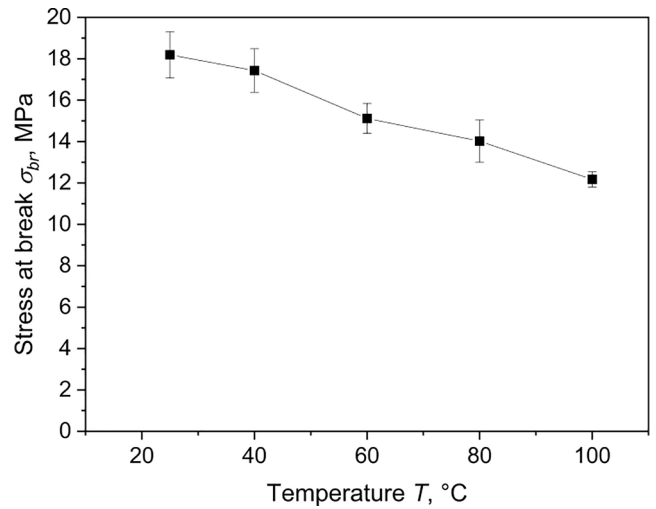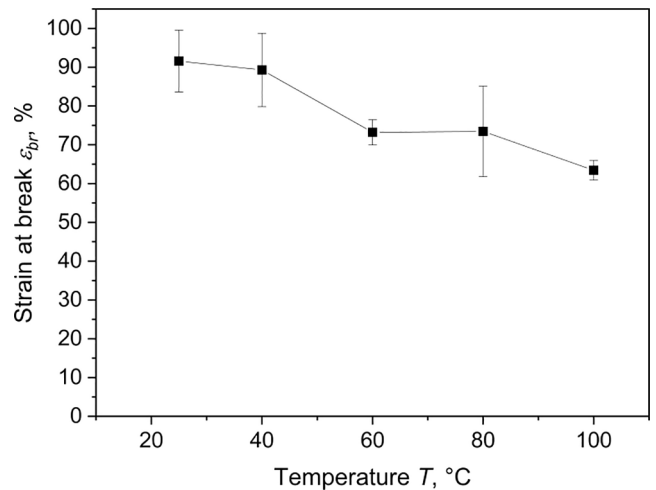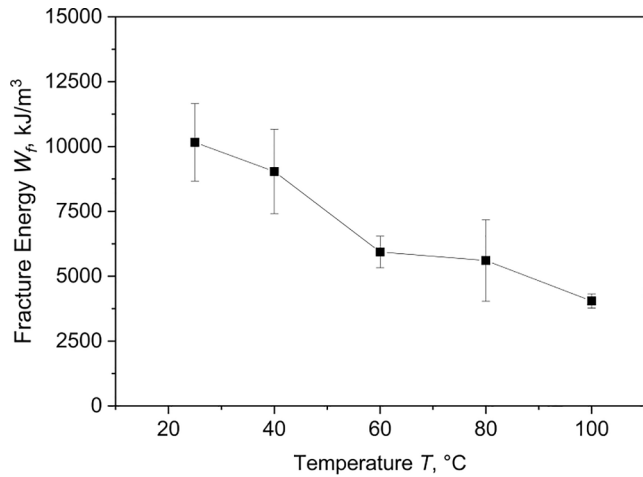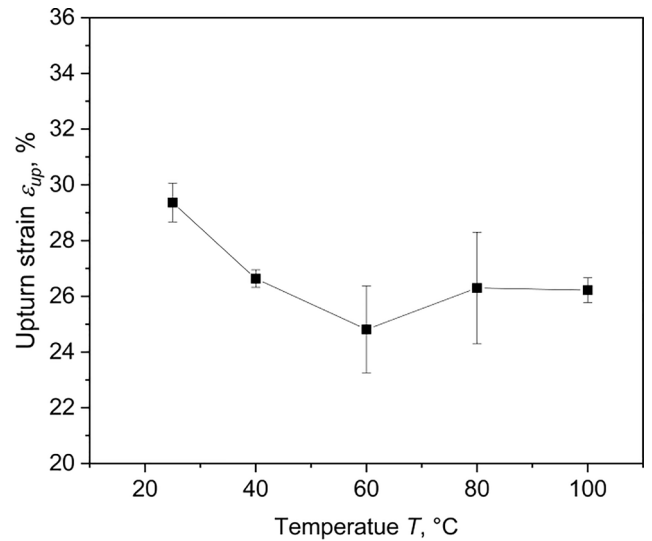
Fig. 4. Fracture energy as a function of temperature from tensile tests of filled NBR at a displacement rate of 200 mm/min. The reported results correspond to the average of the values and the corresponding error obtained from three specimens.
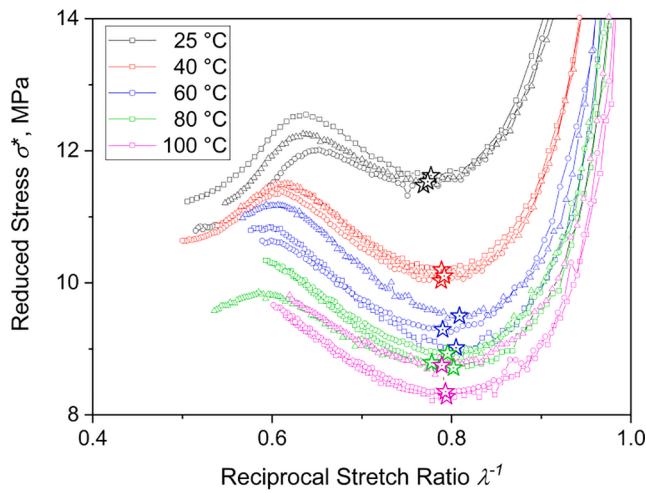

Fig. 6. Upturn strain as a function of temperature obtained from Mooney-Rivlin plots of filled NBR from tensile tests at different temperatures at a displacement rate of 200 mm/min. The reported results correspond to the average of the values and the corresponding error obtained from three specimens.

Fig. 5. Mooney-Rivlin plot of filled NBR at different temperature obtained from the data of tensile tests with a displacement rate of 200 mm/min. The different symbols correspond to different specimens. The stars represent the upturn strain.

physical phenomena connected to its variation with temperature.

3.2. Dynamic mechanical analysis (DMA)

The plots of storage modulus E', loss modulus E'' and the loss factor tanδ obtained from the temperature sweep at 4 Hz are reported in Fig. 7. Actually, the results of temperature sweep at 1 Hz are qualitatively very similar to the one obtained at 4 Hz and are not reported. From the measurement at 1 Hz, the glass transition temperature T_g, evaluated as the peak of the loss modulus, was determined at -19 °C. No significant variation due to the change of frequency was monitored: at 4 Hz a glass transition temperature of -22 °C was monitored. From the plot in Fig. 7, it is possible to observe that the storage modulus did not show a plateau after the glass transition temperature and it constantly decreased with increasing temperature. A similar behavior can be noted for the loss modulus E'', which show an even faster decrease with temperature: at high temperature, the viscous effects are minimized and the energy dissipation is reduced.

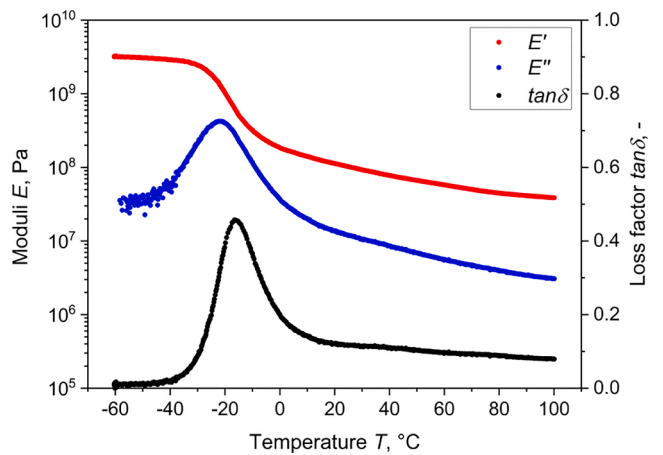To study the dependence of the dynamic moduli at high temperature,

Fig. 7. Storage modulus E' (red), loss modulus E'' (blue) and loss factor tanδ (black) as a function of temperature. The data were evaluated from DMA tests of filled NBR at 4 Hz and strain of 0.05%. (For interpretation of the references to colour in this figure legend, the reader is referred to the web version of this article.)

an Arrhenius plot of the logarithm moduli against the inverse of temperature was constructed. A similar approach was used to evaluate the temperature dependence of a rubber filled with different carbon black concentration, in which the Arrhenius dependence of the moduli was connected to the viscoelastic response of the glassy polymeric interphases between adjacent particles of the filler network. In particular, the different temperature dependence of storage and loss modulus was described as consequence of different polymer bridges: stiffer filler-filler bond in a virgin state connected to the storage modulus, while softer filler-filler bond in a damaged state - resulting from breakdown and reaggregation of the filler-filler bonds during cyclic deformation - related to loss modulus. Furthermore, the decrease of moduli with raising temperatures seems to be a connected to a decrease of the stiffness of the glassy polymers bridges [38]. The Arrhenius plots of the moduli are reported in Fig. 8. A linear relationship could be observed above $T_g + 30$ °C. This value corresponds approximately to the temperature at which the molecular motion is high and the dynamic
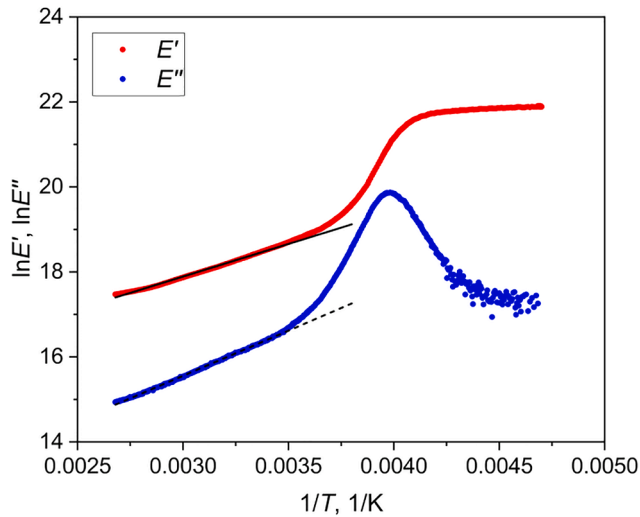
Fig. 8. Logarithms of storage modulus E' (red) and loss modulus E'' (blue) as a function of the inverse of temperature. The data were evaluated from DMA tests of filled NBR at 4 Hz and strain of 0.05%. The black lines correspond to the fitting with Arrhenius equation above $T_g + 30\ °C$. (For interpretation of the references to colour in this figure legend, the reader is referred to the web version of this article.)

mechanical response is fully rubberlike [39]. From the slopes, the apparent activation energies could be obtained; the values are reported in Table 1. These values are comparable to activation energies of highly carbon black filled SBR and EPDM [38,40].

Isothermal frequency sweeps were implemented at different temperatures. The plot of storage moduli as a function of frequency at different temperatures are reported in Fig. 9. As expected, higher values were found for lower temperatures and a major drop was found around the glass transition region. As reported in literature [41,42], the material has been proven to be thermorheologically simple by using Cole-Cole plot [43] and wicket plot [44], and therefore, by exploiting the time-superposition principle, master curves of the dynamic properties could be constructed. Accordingly, the curves of the storage modulus E' were horizontally shifted considering a reference temperature of 25 °C, obtaining the master curve for the storage modulus and the shift factors at different temperatures. The shift factors as a function of temperature (Fig. 10) showed values higher than 1 for temperature below the reference temperature of 25 °C, leading to shifts towards the high frequency range, and values lower than 1 at high temperature, producing shifts towards the low frequency region. Subsequently, the shift factors were fitted using the *WLF* equation [45] as well as the Arrhenius equation, by linearizing their formulations and applying a linear regression based on the least squares method; both equations reveal reliable results above the glass transition temperature (see caption in Fig. 10). The *WLF* coefficients and the activation energy of the Arrhenius equation - associated to the activation barrier for molecular rearrangements during relaxation processes - obtained from the two fitting procedures are reported in Table 2. Afterwards, the shift factors were applied to the isothermal plots of the loss modulus and the loss factor, obtaining master curves (Fig. 11). Similar approaches for filled elastomers can be found in literature [46,47].

Table 1
Values of apparent activation energy obtained by fitting the storage and loss modulus with Arrhenius equation for temperature above $T_g + 30\ °C$.

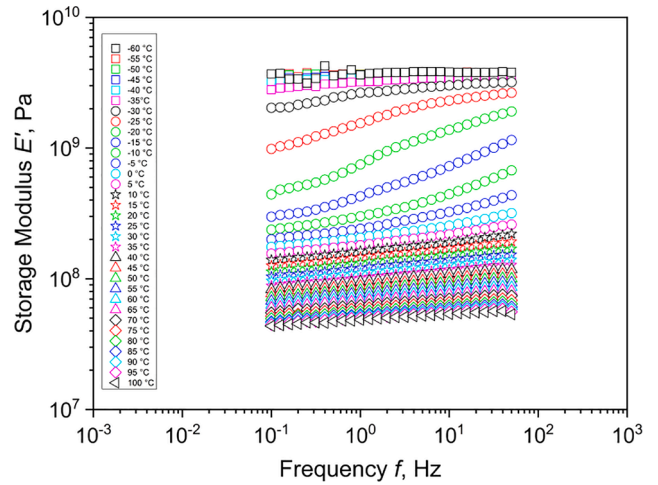|	Apparent activation energy, $E_{a,app}$ [kJ/mol]
Storage modulus, E' [Pa]	12.8
Loss modulus, E'' [Pa]	17.7

Fig. 9. Isothermal frequency sweeps of storage modulus E' of filled NBR at different temperatures at a strain of 0.03%.
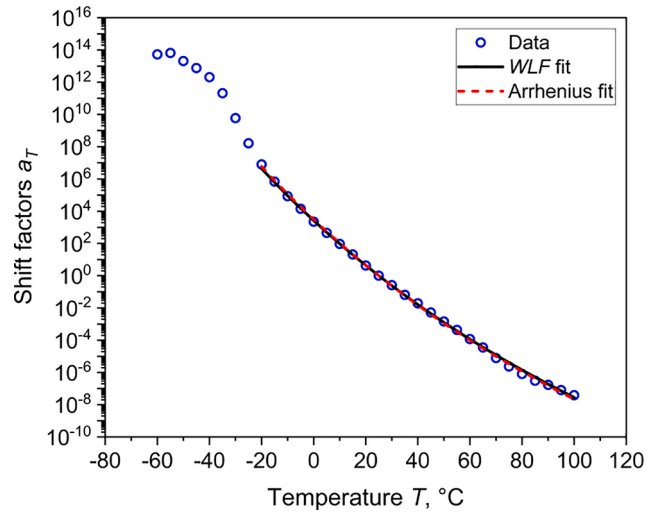

Fig. 10. Shift factors a_T as a function of temperature evaluated from the horizontal shift of the storage modulus E' obtained from isothermal frequency sweeps at different temperatures of filled NBR at a strain of 0.03% and a reference temperature of 25 °C. The shift factors are fitted with *WLF* (black line) and Arrhenius (red dashed lined) equations in their linearized form using a least squares method; the R-squared values of the two fits are of 0.94199 and 0.99891 respectively. (For interpretation of the references to colour in this figure legend, the reader is referred to the web version of this article.)

Table 2
Values of the coefficients of *WLF* equation and activation energy obtained by fitting the shift factor reported in Fig. 10 with *WLF* and Arrhenius equations in their linearized form. The fit was performed with a least squares method; the R-squared values of the two fits are of 0.94199 and 0.99891 respectively.

WLF		Arrhenius
c_1	c_2 [K]	E_a [kJ/mol]
87.64	302.95	217.4

3.3. Fatigue crack growth

Pure shear specimens were tested at different temperatures, corresponding to a possible application temperature of the compound. The results in terms of crack growth rate as a function of tearing energy are reported in Fig. 12. In all cases, a stable crack growth was monitored and
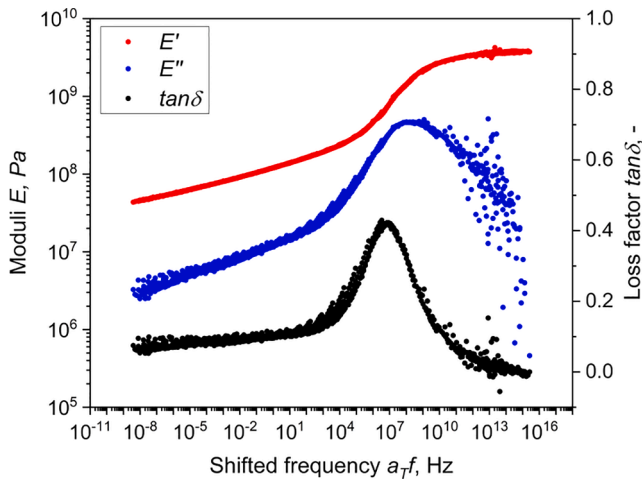
Fig. 11. Master curves of storage modulus E' (red), loss modulus E'' (blue) and loss factor $\tan\delta$ (black) as a function of frequency obtained from isothermal frequency sweeps at different temperatures of filled NBR at a strain of 0.03% at a reference temperature of 25 °C. All curves were shifted using the shift factors of the storage modulus reported in Fig. 10. (For interpretation of the references to colour in this figure legend, the reader is referred to the web version of this article.)
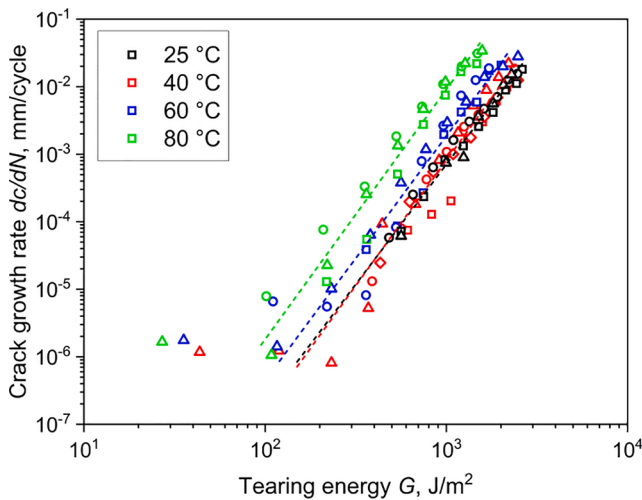
Fig. 12. Crack growth rate as a function of tearing energy of filled NBR at different temperatures. The measurements were performed at 4 Hz, with load ratio R_ε of 0.5 and maximum strain ranging between 1 and 12%. The different symbols correspond to different specimens. The curves were fitted in the stable crack growth region with Eq. (10).

the curves were fitted using Paris law; the power law was of the form [48]:

$$\frac{dc}{dN} = CG^m \tag{10}$$

where dc/dN represents the crack growth rate per cycle, G the tearing energy and C and m are constants. The values of the parameters obtained from the fitted curves using Eq. (10), are reported in Table 3.

As depicted in Fig. 12, a rising temperature leads to a higher crack growth rate. Considering a constant value of the tearing energy, the crack growth rate increased by almost two orders of magnitude from 25 to 80 °C. This is justified by the fact, that for the same value of energy, at high temperatures more energy is available for crack propagation due to lower energy dissipations, leading to faster crack growth. On the other hand, the plot reveals that, considering the same crack growth rate, the

Table 3
Values of the power law coefficients obtained from the fitting of fatigue crack growth curves from Fig. 12 in the stable region with Eq. (10). The values correspond to the mean value of the fitting of three tests at the same conditions.

Temperature, T [°C]	m	logC
25	3.55 ± 0.26	-13.80 ± 0.83
40	3.71 ± 0.20	-14.22 ± 0.55
60	3.62 ± 0.26	-13.59 ± 0.85
80	3.70 ± 0.43	-13.14 ± 1.37

high temperature curves seem shifted to lower tearing energies, suggesting that the crack propagation process is similar at different temperatures but occurs at lower energy values. This behavior is correlated to the reported results of the critical energy for tearing G_0, which decreases with increasing temperature when viscous effects are minimized [11].

It is worth noting that similar values of crack growth were found passing from 25 to 40 °C even though the fitted values are slightly different. On one hand, this can be correlated to the results of the strain at break and the fracture energy obtained from tensile tests (see Figs. 3 and 4). In fact, a similar trend was found between the two temperatures with no substantial differences of the values. On the other hand, at 25 °C higher energy dissipations were present, leading to a variation of the sample temperature due to heat build-up, especially at the highest strains. The analysis of temperature increase due to heat build-up for the same material was already reported [49].

Subsequently, the obtained data were further analyzed in order to construct a master curve for fatigue. In literature, the curves has been shifted along the crack growth axis for both fracture and peeling [10,11] and fatigue [50] using the same shift factors obtained from DMA analysis. However, a similar approach for the material under study did not provided satisfactory results.

It is known that crack propagation in viscoelastic solid is strongly influenced by dissipative mechanisms. In fact, a proportionality of the tearing energy with loss modulus was found for different non-crystallizing elastomers [51]. The strength of elastomers can be characterized by the amount of energy required for crack propagation: this includes the energy required for bond breaking and the energy dissipated ahead the crack tip [52]. According to the theory from Persson and Brener [52,53], the tearing energy as a function of the crack speed v is given by:

$$G(v) = G_0 \left[1 - \frac{2}{\pi} E_0 \int_0^{\frac{2\pi v}{a}} d\omega \frac{F(\omega)}{\omega} Im \frac{1}{E^*(\omega)} \right]^{-1} \tag{11}$$

where G_0 is the critical tearing energy, E_0 is the modulus in the rubbery region, a is the crack tip diameter, ω is the perturbing frequency, which is defined as v/r (r is the distance from the crack tip), while the function $F(\omega)$ is given by:

$$F(\omega) = \left[1 - \left(\frac{\omega a}{2\pi v} \right)^2 \right]^{\frac{1}{2}} \tag{12}$$

and $Im(1/E^*(\omega))$ represents the imaginary part of inverse of the complex modulus. This last component can be expressed as:

$$Im \frac{1}{E^*(\omega)} = -\frac{E''}{E^{*2}} \tag{13}$$

where E'' is the loss modulus. Eqs. (11) and (13) show the dependence of the tearing energy on the energy dissipation. This relation has been considered in other studies to analyze qualitatively the crack growth resistance of different rubbers [54–56].

In order to consider the temperature effect on the fatigue crack growth measurements, sustained by the aforementioned theory, the temperature dependence of the tearing energy G was considered by

Table 4
Values of the shift factor s_T obtained by applying Eq. (14) at different temperatures with the apparent activation energy obtained from the loss modulus reported in Table 1.

Temperature, T [°C]	Shift factors, s_T
25	1
40	0.78
60	0.58
80	0.45

correlating it to the temperature dependence of the loss modulus. In the previous section, it was shown that the loss modulus exhibited an Arrhenius dependence above $T_g + 30\ °C$ (Fig. 8) from which an apparent activation energy $E_{a,app}$ of 17.7 kJ/mol was evaluated. Using this value, shift factors s_T were evaluated with respect to the reference temperature (set at 25 °C) using an Arrhenius form:

$$s_T = \frac{lnE''_T}{lnE''_{T_{ref}}} = \frac{E_{a,app}}{R}\left(\frac{1}{T} - \frac{1}{T_{ref}}\right) \qquad (14)$$

The calculated values evaluated at the temperature used for crack growth measurements are reported in Table 4.

The evaluated shift factors were then used to shift the fatigue crack growth curves along the tearing energy axis by evaluating the tearing energy at the temperature T (denoted as G_T) and shifting it with respect to the reference temperature T_{ref}, resulting in the value $G_{T,Tref}$ given by:

$$G_{T,T_{ref}} = \frac{G_T}{s_T} \qquad (15)$$

By doing so, the curves at higher temperature were shifted towards higher values of tearing energy resulted in the fatigue crack growth master curve reported in Fig. 13.

A good correlation can be observed from the plot, in which all the curves converge into a unique master curve, even at the lowest values of tearing energy. The scattering that can be observed is typical for fatigue measurements of polymers. Comparable error ranges have been reported for NR and SBR [24] and NMR and HNBR [42]. Moreover, similar scatterings have been reported for differently built fatigue master curve of SBR [50]. These results evidence once again that the crack propagation is similar at different temperatures and that the main role of temperature is to decrease the energy barriers required for the fracture processes, leading to similar tearing at lower energies. Furthermore, these results seem promising for the estimation of the fatigue behavior at
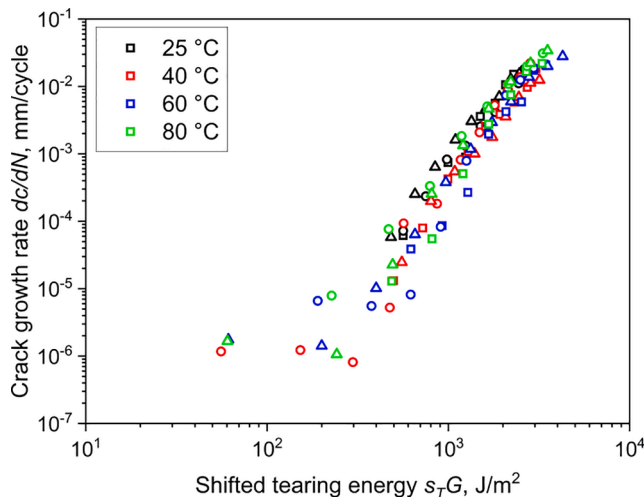
higher temperature of rubbers: the results of fatigue measurement at room temperature can be shifted only with the temperature dependence of the loss modulus, obtained from just a temperature sweep DMA test at the same frequency. A deeper examination of this procedure has to be performed and the use of it with further materials has been already planned within our research plan. Even though the application of this procedure has to be verified on different crystallizing and non-crystallizing rubbers with different fillers, this methodology represents a new tool for analyzing and understanding the complex phenomena involved in high temperature fatigue of rubbers.

4. Conclusion

In this work, the focus was devoted on the temperature effect on the mechanical and fatigue behavior of a filled NBR. Tensile tests revealed that the ultimate properties between 25 and 40 °C are similar, while they are decreasing monotonically with higher temperatures. The Mooney-Rivlin plots showed that the upturn strain, connected to the maximum chain extensibility, decreases with temperature, having a minimum around 40 and 80 °C, while it increases at 100 °C. Dynamic Mechanical Analysis (DMA) was exploited through temperature sweep and isothermal frequency sweep. Temperature sweeps gave the temperature dependence of dynamic properties of the material and an Arrhenius dependence was found for temperatures above $T_g + 30$ °C. The isothermal frequency sweeps were horizontally shifted along the frequency axis obtaining master curves of the dynamic properties. Both *WLF* and Arrhenius equation provided good fit of the shift factors. Fatigue crack growth measurements at high temperatures revealed that higher temperature resulted in higher crack growth rate, with small variation passing from 25 to 40 °C. A fatigue master curve was obtained by shifting the tearing energy using shift factors evaluated considering the temperature dependence of the loss modulus. This method represents a new tool for accounting on the temperature impact on the fatigue crack growth. The application of this procedure to other materials could provide further insights on the crack propagation during cyclic loading at different temperatures.

Declaration of Competing Interest

The authors declare that they have no known competing financial interests or personal relationships that could have appeared to influence the work reported in this paper.

Fig. 13. Master curves of fatigue crack growth as a function of tearing energy. The curves were obtained by shifting the curves from Fig. 12 using the shift factor s_T reported in Table 4. The measurements were performed at 4 Hz, with load ratio R_ε of 0.5 and maximum strain ranging between 1 and 12%.

References

[1] Mars WV, Fatemi A. A literature survey on fatigue analysis approaches for rubber. Int J Fatigue 2002;24(9):949–61. https://doi.org/10.1016/S0142-1123(02)00008-7.

[2] Rivlin RS, Thomas AG, Thomas AG. Rupture of rubber. I. Characteristic energy for tearing. J Polym Sci 1953;10(3):291–318. https://doi.org/10.1002/pol.1953.120100303.

[3] Stieger S, Kerschbaumer RC, Mitsoulis E, Fasching M, Berger-Weber GR, Friesenbichler W, et al. Contraction and capillary flow of a carbon black filled rubber compound. Polym Eng Sci 2019;60(1):32–43. https://doi.org/10.1002/pen.25256.

[4] Lake GJ, Lindley PB. Cut growth and fatigue of rubbers. II. Experiments on a noncrystallizing rubber. J Appl Polym Sci 1964;8(2):707–21. https://doi.org/10.1002/app.1964.070080212.

[5] Young DG. Fatigue crack propagation in elastomer compounds: effects of strain rate, temperature, strain level, and oxidation. Rubber Chem Technol 1986;59(5):809–25.

[6] Ruellan B, Le Cam J-B, Jeanneau I, Canévet F, Mortier F, Robin E. Fatigue of natural rubber under different temperatures. Int J Fatigue 2019;124:544–57. https://doi.org/10.1016/j.ijfatigue.2018.10.009.

[7] Luo W, Li M, Huang Y, Yin B, Hu X. Effect of temperature on the tear fracture and fatigue life of carbon-black-filled rubber. Polymers (Basel) 2019;11(5). https://doi.org/10.3390/polym11050768.

[8] Young DG, Danik JA. Effect of temperature on fatigue and fracture. Rubber Chem Technol 1994;67(1):137–47. https://doi.org/10.5254/1.3538660.

[9] Schrittesser B, Pinter G, Major Z (eds.). Temperature dependent fracture behavior of rubbers used in the oil and gas industry; 2012.

[10] Gent AN. Adhesion and strength of viscoelastic solids. Is there a relationship between adhesion and bulk properties? Langmuir 1996;12:4492–6.

[11] Gent AN, Lai SM. Interfacial bonding, energy dissipation, and adhesion. J Polym Sci, Part B: Polym Phys 1994;32(8):1543–55. https://doi.org/10.1002/polb.1994.090320826.

[12] Asare S, Busfield JJC. Fatigue life prediction of bonded rubber components at elevated temperature. Plast, Rubber Compos 2013;40(4):194–200. https://doi.org/10.1179/1743289810Y.0000000044.

[13] Sakulkaew K, Thomas AG, Busfield JJC. The effect of temperature on the tearing of rubber. Polym Test 2013;32(1):86–93. https://doi.org/10.1016/j.polymertesting.2012.09.002.

[14] DIN 53504;83.060(53504): Deutsches Institut für Normung E.V. (DIN).

[15] Yeoh OH. Analysis of deformation and fracture of 'pure shear' rubber testpiece. Plast, Rubber Compos 2013;30(8):389–97. https://doi.org/10.1179/146580101101541787.

[16] Major Z, Feichter C, Steinberger R, Lang RW (eds.). The test frequency dependence of the fatigue behavior of elastomers; 2006.

[17] Agnelli S, Balasooriya W, Bignotti F, Schrittesser B. On the experimental measurement of fracture toughness in SENT rubber specimens. Polym Test 2020;87:106508. https://doi.org/10.1016/j.polymertesting.2020.106508.

[18] Griffith AA. The phenomena of rupture and flow in solids // VI. The phenomena of rupture and flow in solids. Phil. Trans. R. Soc. Lond. A 1921;221(582–593):163–98. https://doi.org/10.1098/rsta.1921.0006.

[19] Mars WV, Fatemi A. Fatigue crack nucleation and growth in filled natural rubber. Fatigue Fract Eng Mater Struct 2003;26(9):779–89. https://doi.org/10.1046/j.1460-2695.2003.00678.x.

[20] Weng G, Yao H, Chang A, Fu K, Liu Y, Chen Z. Crack growth mechanism of natural rubber under fatigue loading studied by a real-time crack tip morphology monitoring method. RSC Adv 2014;4(83):43942–50. https://doi.org/10.1039/C4RA06518B.

[21] Weng G, Chang A, Fu K, Kang J, Ding Y, Chen Z. Crack growth mechanism of styrene-butadiene rubber filled with silica nanoparticles studied by small angle X-ray scattering. RSC Adv. 2016;6(10):8406–15. https://doi.org/10.1039/C5RA26238K.

[22] Stadlbauer F, Koch T, Archodoulaki V-M, Planitzer F, Fidi W, Holzner A. Influence of experimental parameters on fatigue crack growth and heat build-up in rubber. Materials 2013;6(12):5502–16. https://doi.org/10.3390/ma6125502.

[23] Stadlbauer F, Koch T, Planitzer F, Fidi W, Archodoulaki V-M. Setup for evaluation of fatigue crack growth in rubber: Pure shear sample geometries tested in tension-compression mode. Polym Test 2013;32(6):1045–51. https://doi.org/10.1016/j.polymertesting.2013.06.003.

[24] Harbour RJ, Fatemi A, Mars WV. Fatigue crack growth of filled rubber under constant and variable amplitude loading conditions. Fat Frac Eng Mat Struct 2007;30(7):640–52. https://doi.org/10.1111/j.1460-2695.2007.01143.x.

[25] Harbour RJ, Fatemi A, Mars WV. The effect of a dwell period on fatigue crack growth rates in filled SBR and NR. Rubber Chem Technol 2007;80(5):838–53. https://doi.org/10.5254/1.3539420.

[26] Zarrin-Ghalami T, Fatemi A. Material deformation and fatigue behavior characterization for elastomeric component life predictions. Polym Eng Sci 2012;52(8):1795–805. https://doi.org/10.1002/pen.23125.

[27] Lindley PB. Non-relaxing crack growth and fatigue in a non-crystallizing rubber. Rubber Chem Technol 1974;47(5):1253–64. https://doi.org/10.5254/1.3540497.

[28] Mooney M. A theory of large elastic deformation. J Appl Phys 1940;11:582.

[29] Rivlin RS. Large elastic deformations of isotropic materials IV. Further developments of the general theory. Phil. Trans. R. Soc. Lond. A 1948;241 (379–397). https://doi.org/10.1098/rsta.1948.0024.

[30] Sombatsompop N. Investigation of swelling behavior of NR Vulcanisates. Polym-Plast Technol Eng 1998;37(1):19–39. https://doi.org/10.1080/03602559808006910.

[31] Gao Y, Liu J, Shen J, Zhang L, Guo Z, Cao D. Uniaxial deformation of nanorod filled polymer nanocomposites: A coarse-grained molecular dynamics simulation. Phys Chem Chem Phys 2014;16(30):16039–48. https://doi.org/10.1039/c4cp01555j.

[32] Tzounis L, Debnath S, Rooj S, Fischer D, Mäder E, Das A, et al. High performance natural rubber composites with a hierarchical reinforcement structure of carbon

[33] nanotube modified natural fibers. Mater Des 2014;58:1–11. https://doi.org/10.1016/j.matdes.2014.01.071.

[33] Fu X, Huang G, Xie Z, Xing W. New insights into reinforcement mechanism of nanoclay-filled isoprene rubber during uniaxial deformation by in situ synchrotron X-ray diffraction. RSC Adv. 2015;5(32):25171–82. https://doi.org/10.1039/C5RA02123E.

[34] Peddini SK, Bosnyak CP, Henderson NM, Ellison CJ, Paul DR. Nanocomposites from styrene–butadiene rubber (SBR) and multiwall carbon nanotubes (MWCNT) part 2: Mechanical properties. Polymer 2015;56:443–51. https://doi.org/10.1016/j.polymer.2014.11.006.

[35] He F, Yuan T, Li C, Sun L, Liao S. Interfacial interactions and properties of natural rubber-silica composites with liquid natural rubber as a compatibilizer and prepared by a wet-compounding method. J Appl Polym Sci 2018;135(30):46457. https://doi.org/10.1002/app.46457.

[36] Furukawa J, Onouchi Y, Inagaki S, Okamoto H. Rubber elasticity at very large elongation. Polym Bull 1982;6:381–7. https://doi.org/10.1007/BF00959847.

[37] Bokobza L, Rapoport O. Reinforcement of natural rubber. J Appl Polym Sci 2002;85:2301–16.

[38] Fritzsche J, Klüppel M. Structural dynamics and interfacial properties of filler-reinforced elastomers. J Phys: Condens Matter 2011;23(3):35104. https://doi.org/10.1088/0953-8984/23/3/035104.

[39] Gent AN, Scott KW. Dynamic mechanical properties. In: Gent AN, editor. Engineering with Rubber: How to Design Rubber Components. Hanser Publications.

[40] Le Gal A, Yang X, Klüppel M. Evaluation of sliding friction and contact mechanics of elastomers based on dynamic-mechanical analysis. J Chem Phys 2005;123(1):14704. https://doi.org/10.1063/1.1943410.

[41] Rouleau L, Deü J-F, Legay A, Le Lay F. Application of Kramers-Kronig relations to time–temperature superposition for viscoelastic materials. Mech Mater 2013;65:66–75. https://doi.org/10.1016/j.mechmat.2013.06.001.

[42] Butaud P, Placet V, Klesa J, Ouisse M, Foltete E, Gabrion X. Investigations on the frequency and temperature effects on mechanical properties of a shape memory polymer (Veriflex). Mech Mater 2015;87:50–60. https://doi.org/10.1016/j.mechmat.2015.04.002.

[43] Han CD, Kim JK. On the use of time-temperature superposition in multicomponent/multiphase polymer systems. Polymer 1993;34(12):2533–9. https://doi.org/10.1016/0032-3861(93)90585-X.

[44] van Gurp M, Palmen J. Time-temperature superposition for polymer blends. Rheol Bull 1998;67(1):5–8.

[45] Williams ML, Landel RF, Ferry JD. The temperature dependence of relaxation mechanism in amorphous polymers and other glass-forming liquids. J Am Chem Soc 1955;77(14):3701–7.

[46] Wang M-J, Lu SX, Mahmud K. Carbon–silica dual-phase filler, a new-generation reinforcing agent for rubber. Part VI. Time–temperature superposition of dynamic properties of carbon–silica-dual-phase-filler-filled vulcanizates. J Polym Sci B Polym Phys 2000;38(9):1240–9. https://doi.org/10.1002/(SICI)1099-0488(20000501)38:9<1240:AID-POLB15>3.0.CO;2-Q.

[47] Lorenz B, Pyckhout-Hintzen W, Persson BNJ. Master curve of viscoelastic solid: Using causality to determine the optimal shifting procedure, and to test the accuracy of measured data. Polymer 2014;55(2):565–71. https://doi.org/10.1016/j.polymer.2013.12.033.

[48] Lake GJ, Lindley PB. The mechanical fatigue limit for rubber. J Appl Polym Sci 1965;9(4):1233–51. https://doi.org/10.1002/app.1965.070090405.

[49] Schieppati J, Schrittesser B, Wondracek A, Robin S, Holzner A, Pinter G. Impact of temperature on the fatigue and crack growth behavior of rubbers. Procedia Struct Integrity 2018;13:642–7. https://doi.org/10.1016/j.prostr.2018.12.106.

[50] Wunde M, Klüppel M. Viscoelastic response during crack propagation of unfilled and filled SBR. Rubber Chem Technol 2018;91(4):668–82. https://doi.org/10.5254/rct.18.81537.

[51] Lake GJ, Thomas AG. Strength. In: Gent AN, editor. Engineering with Rubber: How to Design Rubber Components. Hanser Publications.

[52] Persson BNJ, Albohr O, Heinrich G, Ueba H. Crack propagation in rubber-like materials. J Phys: Condens Matter 2005;17(44):R1071–142. https://doi.org/10.1088/0953-8984/17/44/R01.

[53] Persson BNJ, Brener EA. Crack propagation in viscoelastic solids. Phys Rev E Stat Nonlin Soft Matter Phys 2005;71(3 Pt 2A):36123. https://doi.org/10.1103/PhysRevE.71.036123.

[54] Nie Y, Wang B, Huang G, Qu L, Zhang P, Weng G, et al. Relationship between the material properties and fatigue crack-growth characteristics of natural rubber filled with different carbon blacks. J Appl Polym Sci 2010;24:3341–7. https://doi.org/10.1002/app.32098.

[55] Nie Y, Qu L, Huang G, Wang B, Weng G, Wu J. Improved resistance to crack growth of natural rubber by the inclusion of nanoclay. Polym Adv Technol 2012;23(1):85–91. https://doi.org/10.1002/pat.1826.

[56] Rooj S, Das A, Morozov IA, Stöckelhuber KW, Stocek R, Heinrich G. Influence of "expanded clay" on the microstructure and fatigue crack growth behavior of carbon black filled NR composites. Compos Sci Technol 2013;76:61–8. https://doi.org/10.1016/j.compscitech.2012.12.020.

Publication 5

<u>Fatigue analysis and critical defect size evaluation of filled NBR including temperature influence</u>

Jacopo Schieppati [a], Bernd Schrittesser [a,b], Stefano Tagliabue [c], Luca Andena [c], Armin Holzner [d], Jan Poduška [e] and Gerald Pinter [f]

[a]   Polymer Competence Center Leoben GmbH, Roseggerstrasse 12, 8700 Leoben, Austria
[b]   SCIOFLEX GmbH, Opernring 1/R/748, 1010 Wien, Austria
[c]   Dipartimento di Chimica, Materiali e Ingegneria Chimica "G. Natta", Politecnico di Milano, Piazza Leonardo da Vinci 32, Milano, 20133, Italy
[d]   Semperit Technische Produkte Gesellschaft m.b.H., Triester Bundesstrasse 26, 2632 Wimpassing, Austria
[e]   Institute of Physics of Materials of the Academy of Sciences of the Czech Republic, Brno, Czech Republic
[f]   Department of Polymer Engineering and Science – Material Science and Testing of Polymers, Montanuniversität Leoben, Otto Glöckel-Strasse 2, 8700 Leoben, Austria

Relevant contributions to this publication:

Conceptualization:	Jacopo Schieppati, Bernd Schrittesser, Stefano Tagliabue, Luca Andena; Armin Holzner, Gerald Pinter
Methodology:	Jacopo Schieppati, Bernd Schrittesser; Gerald Pinter
Investigation:	Jacopo Schieppati, Stefano Tagliabue, Luca Andena, Jan Poduška
Writing - Original Draft:	Jacopo Schieppati
Writing - Review & Editing:	Jacopo Schieppati; Bernd Schrittesser, Stefano Tagliabue, Luca Andena; Armin Holzner, Jan Poduška, Gerald Pinter

Article

Fatigue Analysis and Defect Size Evaluation of Filled NBR including Temperature Influence

Jacopo Schieppati [1,*] **, Bernd Schrittesser** [1,2] **, Stefano Tagliabue** [3] **, Luca Andena** [3] **, Armin Holzner** [4] **, Jan Poduška** [5] **and Gerald Pinter** [6]

1. Polymer Competence Center Leoben GmbH, Roseggerstrasse 12, 8700 Leoben, Austria; b.schrittesser@scioflex.com
2. SCIOFLEX GmbH, Opernring 1/R/748, 1010 Wien, Austria
3. Dipartimento di Chimica, Materiali e Ingegneria Chimica "G. Natta", Politecnico di Milano, Piazza Leonardo da Vinci 32, 20133 Milano, Italy; stefano.tagliabue@polimi.it (S.T.); luca.andena@polimi.it (L.A.)
4. Semperit Technische Produkte GmbH, Triester Bundesstrasse 26, 2632 Wimpassing, Austria; armin.holzner@semperitgroup.com
5. Institute of Physics of Materials, Czech Academy of Sciences, 61662 Brno, Czech Republic; poduska@ipm.cz
6. Department of Polymer Engineering and Science—Material Science and Testing of Polymers, Montanuniversität Leoben, Otto Glöckel-Strasse 2, 8700 Leoben, Austria; gerald.pinter@unileoben.ac.at
* Correspondence: jacopo.schieppati@pccl.at

Abstract: The fatigue behavior of a filled non-crystallizing elastomer was investigated on axisymmetric dumbbell specimens. By plotting relevant Wöhler curves, a power law behavior was found. In addition, temperature increases due to heat build-up were monitored. In order to distinguish between initiation and crack growth regimes, hysteresis curves, secant and dynamic moduli, dissipated and stored energies, and normalized minimum and maximum forces were analyzed. Even though indications related to material damaging were observed, a clear trend to recognize the initiation was not evident. Further details were revealed by considering a fracture mechanics. The analysis of the fracture surfaces evidenced the presence of three regions, associated to initiation, fatigue striation, and catastrophic failure. Additional fatigue tests were performed with samples in which a radial notch was introduced. This resulted in a reduction in lifetime by four orders of magnitude; nevertheless, the fracture surfaces revealed similar failure mechanisms. A fracture mechanics approach, which considered the effect of temperature, was adopted to calculate the critical defect size for fatigue, which was found to be approximately 9 μm. This value was then compared with the particle size distribution obtained through X-ray microcomputed tomography (μ-CT) of undamaged samples and it was found that the majority of the initial defects were indeed smaller than the calculated one. Finally, the evaluation of J-integral for both unnotched and notched dumbbells enabled the assessment of a geometry-independent correlation with fatigue life.

Keywords: fatigue; fracture mechanics; filled rubber; X-ray microtomography; defect size; temperature; J-integral

1. Introduction

Fatigue is one of the most common causes of the failure of elastomer components such as tires, dampers, seals, hydraulic hoses, and conveyor belts. In fact, rubber articles are commonly subjected to cyclic loads that may lead to the accumulation of damage and to the development and growth of cracks, which then lead to failure. Generally speaking, materials are assumed to naturally contain flaws and inhomogeneities that can lead, under specific loading conditions, to localized stress concentrations promoting the nucleation of cracks [1]. Indeed, fracture occurs due to defects, which may nucleate from inhomogeneities that grow when subjected to repeated loads and subsequently coalesce up to failure.

Continuum mechanics models can describe fatigue at a macroscopic scale, by considering the fatigue life exhibited at different stress or strain levels; however, obtaining the data necessary for the correct application of this approach is time-consuming, not to mention the large scatter in the data occurring due to the stochastic nature of the initiation.

An alternative approach is to consider stress intensification arising from the defects, using a fracture mechanics-based approach. The introduction of a dominant reproducible initial defect (i.e., notch) leads to the reduction of both scattering and testing time. Fatigue lifetime predictions can be obtained by summing up the initiation time and the integration over time (i.e., number of cycles) of the crack growth characteristic, by considering the initial defect size [1–19]. Inversely, knowing the fatigue lifetime, it is possible to estimate the size of the critical defect from which the failure started.

The typical dimension of the critical defects for different elastomers was found to be a few tens of μm [1–5,10,17]. Due to the complex formulations of typical rubber compounds, the identification of the origin of the critical defects that lead to failure is challenging. Commonly, the analysis of fatigue damage in rubbers is performed through techniques such as Scanning Electron Microscopy (SEM) [20–30] or X-ray microtomography (μ-CT) [18,30–33]. These methods represent powerful tools for the investigation of interrupted fatigue tests or for post-mortem analysis, giving insight to the defect population and its evolution during fatigue. A correct evaluation of defect size is fundamental for the accuracy of fatigue life prediction models.

In this study, the fatigue behavior of a filled acrylonitrile butadiene rubber (NBR) has been examined. This elastomer is particularly suitable for applications in the oil and gas industry due to its polarity, which makes it resistant to fuels. In such applications, the components are subject to alternating pressures that can cause fatigue damage and failure. Thus, the fatigue lifetimes of unnotched and notched axisymmetric dumbbell specimens were measured, and the behavior was further investigated by analyzing the evolution of surface temperatures, hysteresis curves, dynamic and secant moduli, and dissipated and stored energies. The fracture surfaces were also thoroughly analyzed.

Then, the assessment of the critical defect size for fatigue failure was performed using the fracture mechanics approach. This was done by considering the material fatigue crack growth [34] and taking into account the effect of temperature [35]. The calculated critical defect size was then compared with the dimensions of defects present in the undamaged specimen, which was evaluated through a μ-CT analysis. Finally, an equation for the evaluation of the J-integral was computed using a finite element method (FEM) simulation of the notched specimens, allowing to determine fatigue lifetime independently on the geometry.

2. Materials and Methods

2.1. Materials

The material used for this research is a commercial acrylonitrile butadiene rubber (NBR) filled with 42 parts per hundred rubber (phr) of carbon black (CB). Due to confidentiality agreements with the supplier, no further details about the formulation can be given.

2.2. Fatigue

Fatigue tests were conducted on axisymmetric dumbbell specimens (Figure 1a) on an MTS 858 Table Top System servohydraulic testing machine (MTS Systems GmbH, Eden Prairie, MN, USA). Hysteresis data were acquired every 100 cycles, and the force and displacement peaks were recorded on every cycle. A sinusoidal displacement waveform was used at a frequency of 4 Hz, with a load ratio R_ε of 0.5. The maximum strains ε_{max} were 5, 20, 50, 55, 60, and 65%. Complete failure of the specimen was considered as a lifetime criterion. Furthermore, the evolution of the surface temperature during the tests was monitored through a CT LT22 infrared sensor (Optris GmbH, Berlin, Germany) and recorded every 1 s.
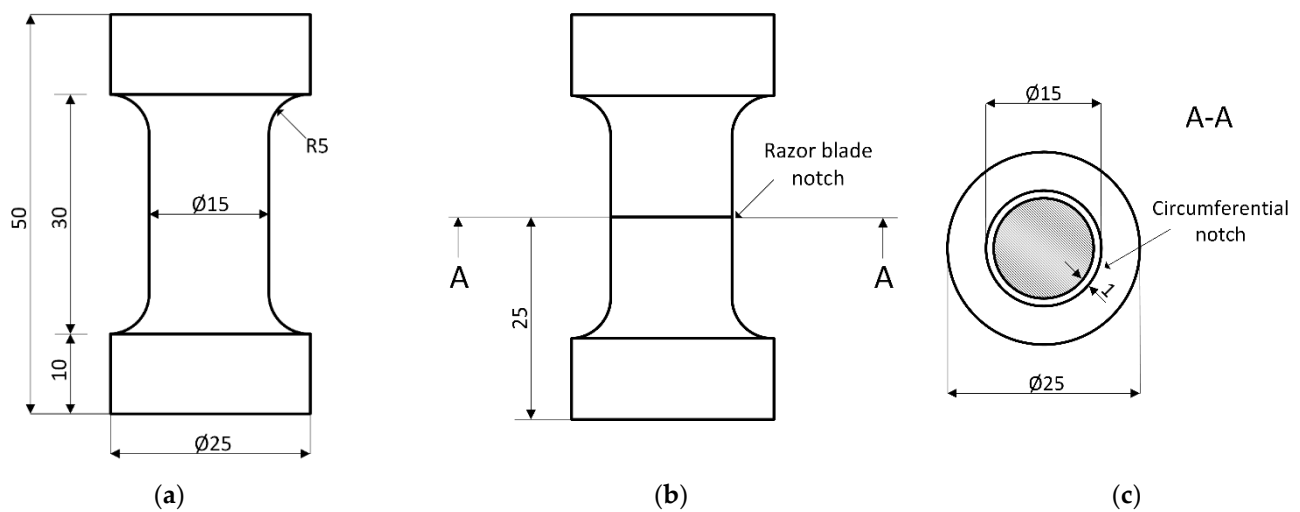
Figure 1. (**a**) Geometry and dimensions of the axisymmetric dumbbell specimens used in the fatigue experiments; (**b**) geometry of the Cracked Round Bar (CRB) specimen; (**c**) Section A-A of the CRB specimen with the circumferential notch.

Similarly, cyclic tests were performed on notched circular dumbbell specimens, denoted as Crack Round Bars—CRB (Figure 1b). According to ISO 18489 [36], an initial circumferential notch of approximately 1 mm depth (Figure 1c) was inserted at mid-height using a razor blade (thickness = 0.1 mm, tip-radius < 5 μm) mounted on a lathe rotating at 80 rpm. The specimens were cyclically loaded at maximum strains of 20, 30, and 50%, using the same frequency and load ratio used for the unnotched samples. Furthermore, the tests were monitored using a camera system CV-5701P by Keyence (Osaka, Japan) and pictures were recorded at every cycle.

2.3. Fracture Surface Analysis

An optical microscope Zeiss Stemi 2000C (Carl Zeiss AG, Oberkochen, Germany) was used for the fracture surface analysis.

2.4. X-ray Microtomography (μ-CT)

μ-CT scans of the dumbbell samples were acquired on a NSI X-25 inspection system (North Star Imaging, High Wycombe, UK). The X-ray source was operated at 40 kV and 100 μA, granting a magnification factor of 3.88 and a voxel resolution of 19 μm. It should be considered that the apparatus is capable of a nominal certified resolution of 2 μm [37]. The set of images was processed with a custom-made Matlab code (*Matlab R2020b*), performing binarization based on a combined global/local algorithm procedure [38] as a first step. The global algorithm adopted is the one developed by Otsu [39,40], which is able to distinguish between measurement artefacts and particles that are actually present inside the inspected specimen. Then, a local gradient-based watershed algorithm [41] was employed to better define the contour of the inspected particles. Following successful segmentation (i.e., separation of the voxels representing rubber and void, with Boolean values of 1 and 0, respectively), the code allowed particle detection by exploiting a spatial connectivity equal to 26, which means that two or more voxels belong to the same particle if they are in contact with at least one vertex. Each particle was then labelled, and its volume was computed as the sum of the connected full voxels (Boolean value equal to 1).

2.5. Evalaution of J-Integral Using Finite Element Method (FEM)

FEM simulation of the CRB specimen behavior was carried out using a 2D axisymmetric model created in Ansys Parametric Design Language (APDL). The element type PLANE 183 was used, which is a higher order 2D, 8-node, or 6-node element [42]. Mapped mesh was used where possible. The mesh was made very fine in the vicinity of the crack

tip with elements as small as 0.01 mm in the area closest to the crack tip. Moreover, special wedge-shaped crack tip elements were used at the crack tip. The rest of the model was meshed with a coarser mesh, with the largest elements up to 1.2 mm. The total number of elements was approximately 7000 for each of the modelled crack lengths. See Figure 2 where the mesh of the model for the crack length of 2.5 mm is depicted. A neo-Hookean incompressible hyperelastic solid was chosen for the material model; the shear modulus—obtained by fitting the uniaxial tensile test data—was 12.3 MPa, whereas the bulk modulus was not acquired as the material was assumed to be incompressible. Even though the rubbers are not strictly incompressible, this simplification does not make a big difference for the intended analysis. The goal of the simulation was to calculate values of the J-integral for various crack lengths and various loads. The calculation of the non-linear J-integral was performed through closed path integral calculation (CINT function in APDL).
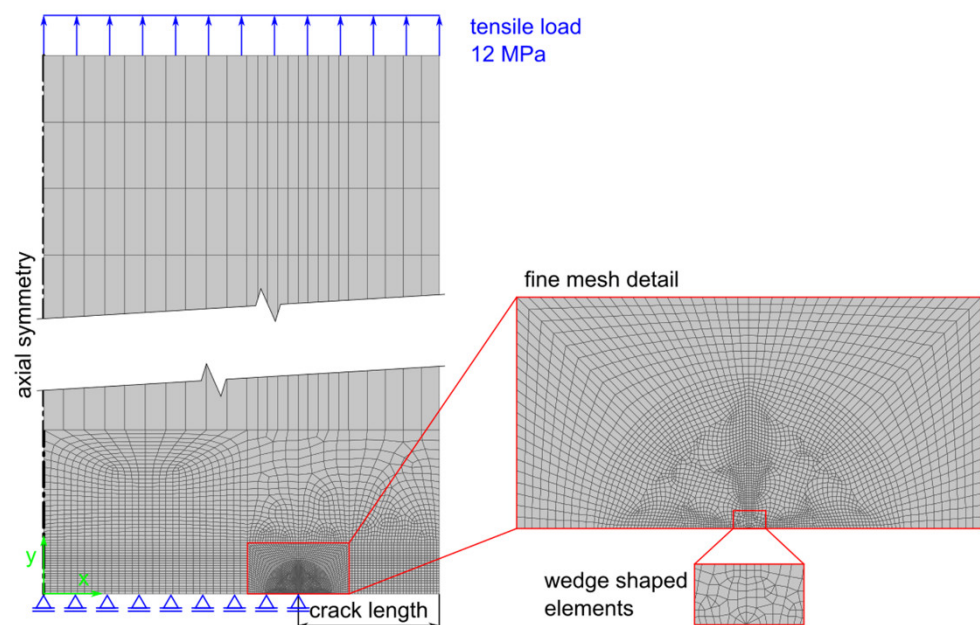

Figure 2. Mesh of the model used for the FEM calculation of the J-integral for CRB specimens.

3. Results

3.1. Fatigue of the Unnotched Dumbbell Specimens

The fatigue lifetime of the specimens subjected to cyclic loading is reported in Figure 3, in which the relevant ε-N or Wöhler curve [43] is represented. In particular, the maximum engineering strain ε_{max} was selected as the representative loading parameter and plotted in double logarithmic scale against the number of cycles to failure, N_f.

As depicted in the plot, a certain scattering of the results was found, which is typical for the fatigue of polymers and rubbers. The statistical analysis of the results was performed through the ASTM E739–10 [44], and the resulting fitting power law was found to be:

$$\varepsilon_{max} = 219 \cdot N_f^{-0.11}. \tag{1}$$

Furthermore, two interrupted tests, for which no failure was recorded, are shown in Figure 3, and they correspond to ε_{max} of 5% and 20%. In these two cases, the loads were so low that the failure would occur at a number of cycles that is well beyond the experimental window.

An alternative criterion for studying the fatigue nucleation of rubbers is to consider N_i, corresponding to the number of cycles for the transition between the phase of initiation and crack growth. This is normally related to an abrupt variation of force (or stiffness) [45]. By applying this concept to the results previously shown, it was found that qualitatively, the plot was almost identical to the one reported in Figure 3 (provided in

the Supplementary Material, Figure S1). In fact, the abrupt variation of force took place only in the last cycles (approximately 10 to 20 cycles). In actuality, this crack propagation phase corresponds to the macroscopic crack growth, which is visible to the naked eye. Generally, after the initial formation of cracks from inhomogeneities in the material, a small-scale growth of microcracks is present until macroscopic crack growth occurs, leading to a reduction of the ligament area and rapid failure.
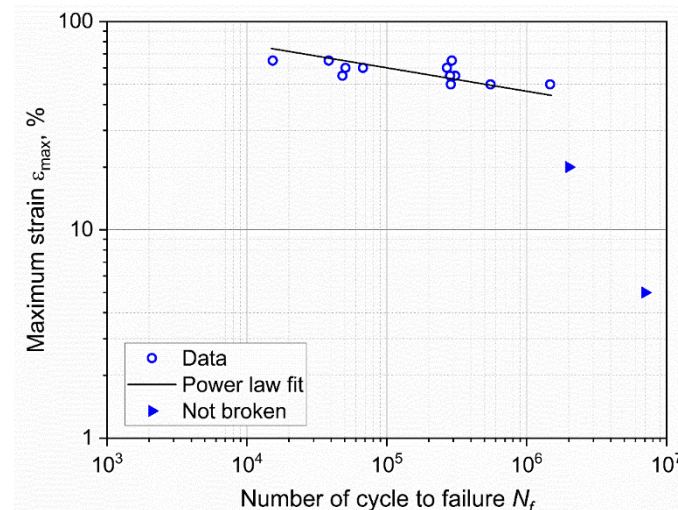

Figure 3. Wöhler curve obtained from axisymmetric dumbbell specimens of CB filled NBR at a frequency of 4 Hz and a load ratio R_ε of 0.5. The fitting power law (Equation (1)) was obtained using ASTM E739–10.

Further analysis of the fatigue tests led to the inspection of temperature evolution upon cyclic loading. In Figure 4a, the variation of the surface temperature for the first 15,000 cycles is shown. The temperature variation is a consequence of heat build-up; during every loading cycle, part of the mechanical energy is dissipated in the specimen volume and converted into heat. Due to the low thermal conductivity of rubbers [46,47], the internally generated heat slowly flows to the surrounding environment, and therefore, the temperature of the specimen significantly increases. This phenomenon strongly depends on the material compliance, on the frequency of oscillation, on the loading amplitude, and on the thickness of the component [48]. In fact, the rate of temperature variation $\dot{\Delta T}$ can be described as [49,50]:

$$\dot{\Delta T} = \frac{\pi \cdot f \cdot \Delta \sigma^2 \cdot D''(f, T)}{4 \cdot c_p \cdot \rho}, \tag{2}$$

where f is the frequency, $\Delta \sigma$ is the stress amplitude, D'' is the loss compliance, c_p is the specific heat and ρ is the density; therefore, larger load amplitudes and frequencies will result in larger temperature increases. Indeed, the effect of increasing the loading amplitude is confirmed by the results reported in Figure 4a,b. The monitored temperature increases are consequences of the geometry of the specimen (i.e., the thickness) and the used frequency (4 Hz). In actuality, a decrease of these two variables could lead to the reduction of the temperature increase; however, thicker specimens are more representative for certain applications, and the axisymmetric dumbbell samples (or slight variations of it) represent a well-established geometry for fatigue characterization of rubbers [14,15,18,51–62]. The choice of the frequency has to match the requirement of being representative for the material application, and it is a tradeoff between testing time and temperature increases. Overall, with the used loading conditions, the surface temperatures increased in a range between 20 and 40 °C. Generally, the temperatures showed fluctuations related to the cooling system of the laboratory. Nevertheless, after approximately 2500–3000 cycles, the surface temperature became stable. As depicted in Figure 4b, higher maximum strains corresponded to higher temperatures in an almost linear relationship. The monitored

temperature increases were so relevant that they must be considered during the analysis of fatigue results since such temperatures would affect the mechanical behavior of the material. In general, due to the entropic elasticity of the rubber matrix, an increase of stiffness would be expected; however, due to the presence of fillers and due to viscoelastic effects, the material would become softer at higher temperatures. Thus, the overall trend would be a trade-off between these opposite trends, and it would depend on the material composition. A reduction of stiffness at a higher temperature was previously reported for the material under investigation [35]. Nevertheless, the mechanical behavior is expected to be constant after reaching the plateau temperature.
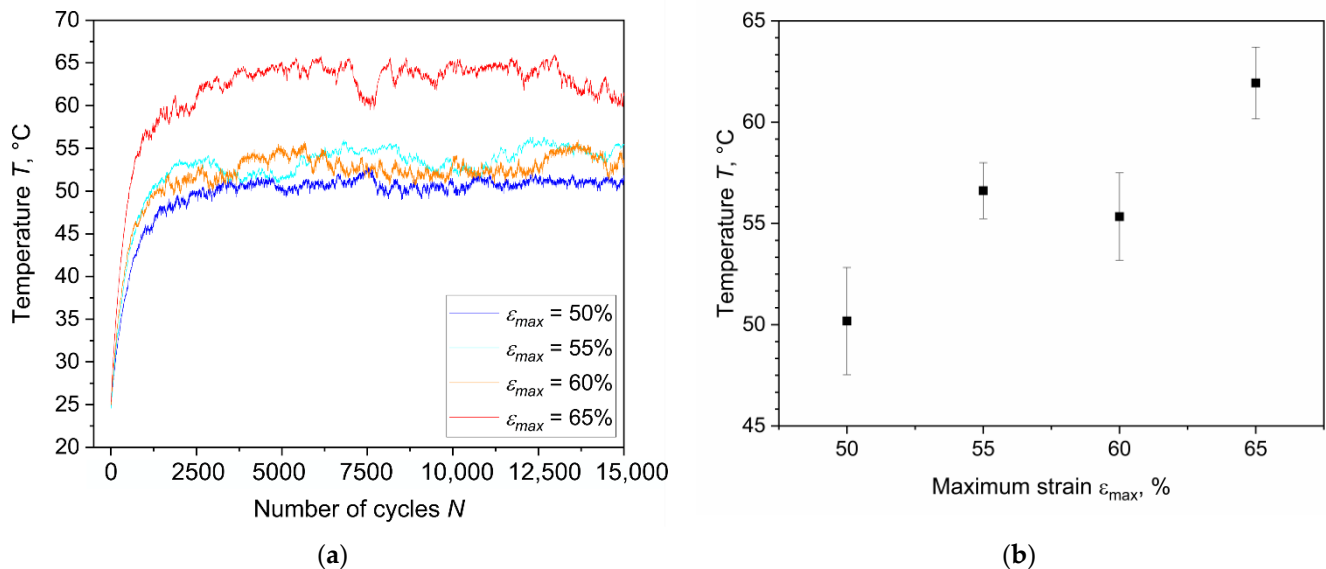

Figure 4. (**a**) Surface temperature evolution at different strains in the first 15,000 cycles of the fatigue experiments; (**b**) average values of plateau temperatures at different strains obtained during fatigue experiments from three samples per condition. The fatigue tests were implemented on axisymmetric dumbbell specimens of CB filled NBR at a frequency of 4 Hz and load ratio R_ε of 0.5.

Further analyses of the fatigue data were implemented to investigate the distinct regimes of fatigue, namely, crack initiation and crack propagation. The hysteresis curves during fatigue tests for different strain levels are reported in Figure 5a, in terms of engineering stress and engineering strain at 3000 cycles. As depicted, higher strains corresponded to larger hysteresis. In Figure 5b, the evolution of the hysteresis curves during the tests is shown for a particular specimen (ε_{max} = 55%) for a different number of cycles. A big variation of the hysteresis is present in the beginning of the test as a consequence of stress relaxation. The hysteresis seems to stabilize after approximately 3000 cycles, which corresponds to the stabilization of the surface temperatures. During the successive lifetime, the hysteresis variation was much smaller, which was a consequence of the combination of both stress relaxation and material damage accumulation.
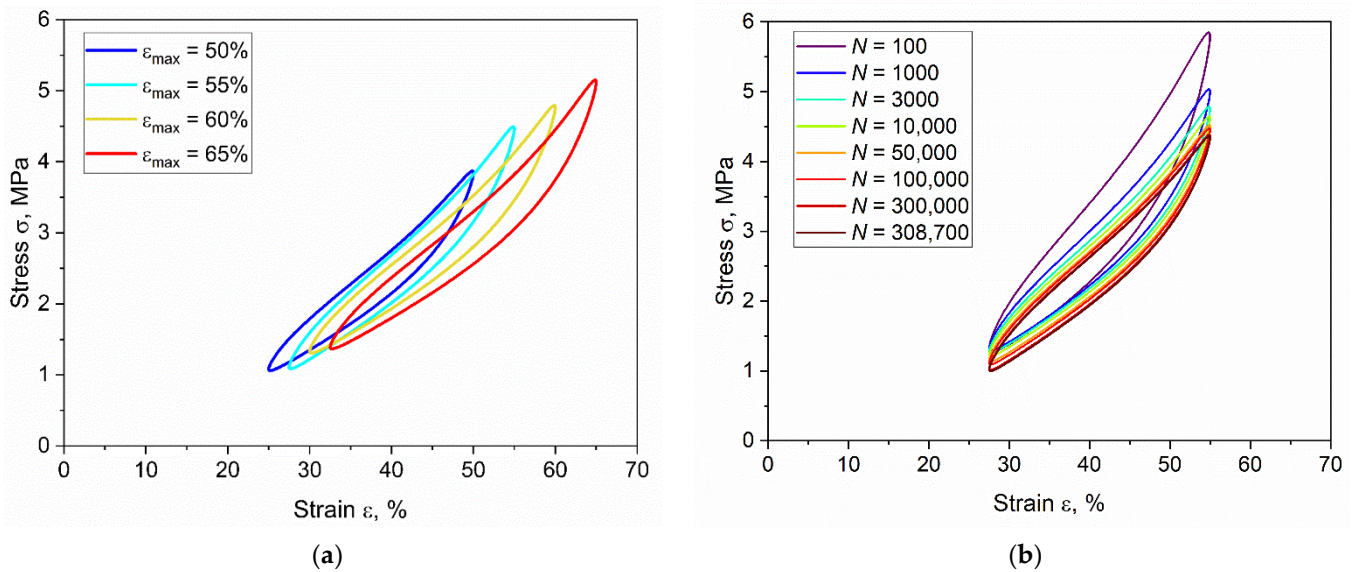
Figure 5. (**a**) Hysteresis curves at different maximum strains at 3000 cycles; (**b**) evolution of hysteresis curve at different number of cycles for maximum strain ε_{max} of 55%. The fatigue tests were implemented on axisymmetric dumbbell specimens of CB filled NBR at frequency of 4 Hz and load ratio R_ε of 0.5.

For a better understanding of the results, the hysteresis curves were analyzed considering two parameters, the secant E_{sec} and the dynamic E_{dyn} modulus that can be calculated according to Equations (3) and (4) [63,64]:

$$E_{sec} = \frac{\sigma_{max}}{\varepsilon_{max}}, \tag{3}$$

$$E_{dyn} = \left| \frac{\sigma_{max} - \sigma_{min}}{\varepsilon_{max} - \varepsilon_{max}} \right|, \tag{4}$$

where σ_{max} and σ_{min} represent the maximum and minimum stresses and ε_{max} and ε_{min} are the maximum and minimum strain, respectively. Although the dynamic modulus is correlated with the instantaneous material response, the variation of the secant modulus is related to viscoelastic effects and to the accumulation of damage in the material [64,65]. Equations (3) and (4) are probably not able to fully describe the highly non-linear mechanical behavior of elastomers; however, for a first approximation, their trends for the number of cycles may provide interesting insights about fatigue. Due to the large variation in temperature at the beginning of the tests, both moduli initially showed large drops. For a better comparison, the values were normalized with respect to those at 2500 cycles (i.e., once temperature and mechanical behavior became stable). The results at the different strains are reported in Figure 6. In all cases, it is possible to observe a similar initial drop for both moduli. Subsequently, E_{dyn} showed a lower rate of reduction and became more stable—even slight increases were monitored; therefore, the material stiffness remained essentially constant in the last stages of fatigue. The initial decrease and the successive stabilization were associated with cyclic stress softening [66], which seems to be connected to the breakdown and reformation of filler–molecule interactions [67]. On the other hand, E_{sec} shows a steady drop for the entire test duration, as a consequence of the continuous stress relaxation and accumulation of damage during the test.
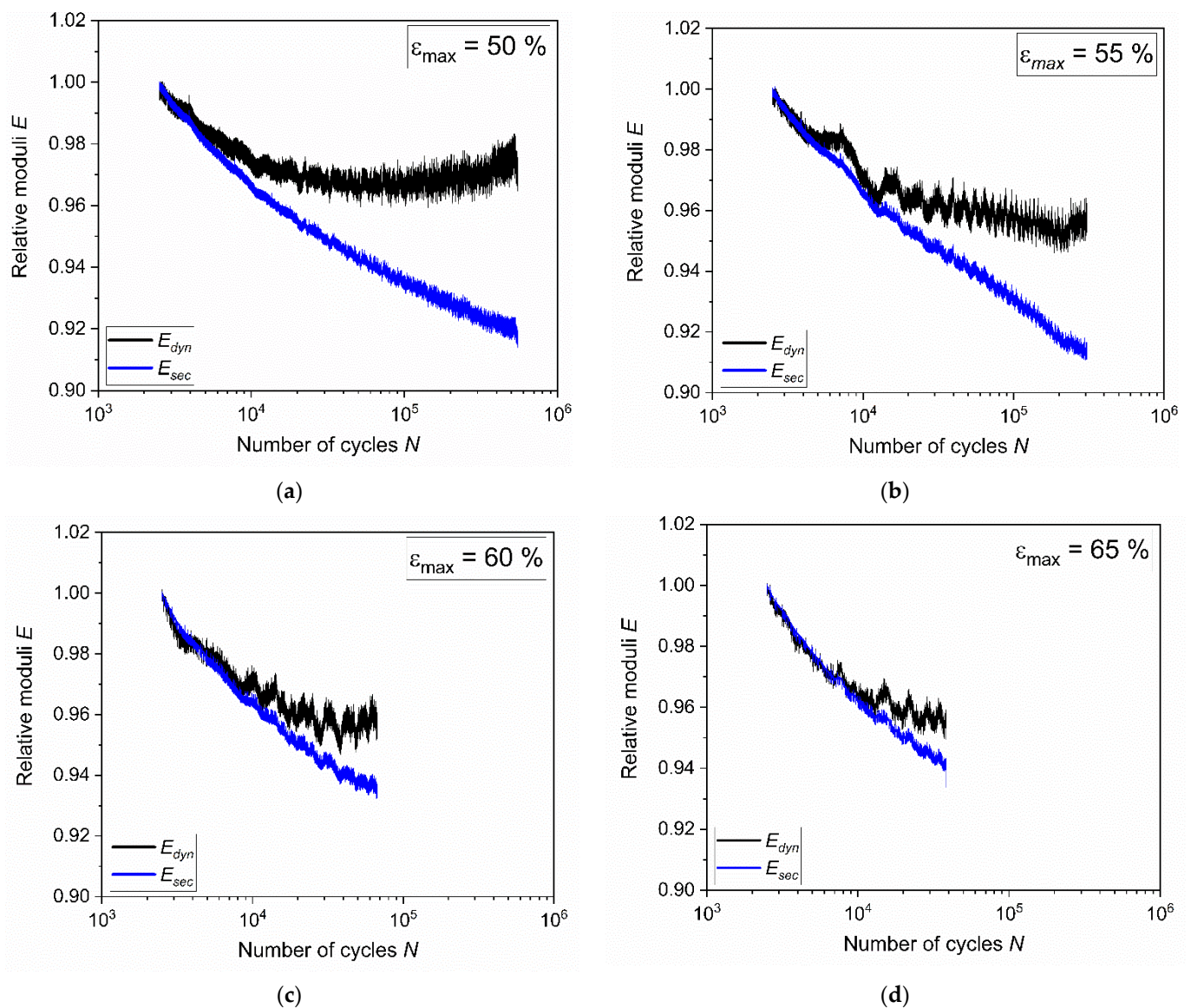
Figure 6. Dynamic (E_{dyn}) and secant (E_{sec}) moduli evaluated from hysteresis at maximum strain of (**a**) 50%, (**b**) 55%, (**c**) 60%, and (**d**) 65%, respectively. The fatigue tests were implemented on axisymmetric dumbbell specimens of CB filled NBR at a frequency of 4 Hz and a load ratio R_ε of 0.5.

Subsequently, the energies were analyzed by integrating the area of the force-displacement curves from the hysteresis curves previously discussed. In this sense, it was possible to distinguish between the dissipated energy, U_{dis}, as the area inside the hysteresis loop, and the stored energy, U_{sto}, as the area below the unloading curve. For a proper comparison, the evolution of the energies was plotted as a function of the normalized number of cycles (currently elapsed number of cycles, N, divided by the number of cycles to failure, N_f) as reported in Figure 7a. These results originate from the behavior already described for the hysteresis curves: in all the testing configurations, a drop in both energies was observed during the first cycles. As previously discussed, this effect is mainly a consequence of stress relaxation. After the drop, the values of U_{dis} are then substantially stabilized for plateau values. The stored energy U_{sto} instead kept decreasing with the number of cycles, albeit slightly, due to energy dissipation caused by material damage. On the other hand, the dissipated energies moderately increased, evidencing the increase in damage in the material. Moreover, a clear trend with respect to the maximum strains is present: both dissipated and stored energies were higher for higher strains; however, this description

is different when considering the percentage of energy, which is the normalization with respect to the total energy, U_{tot}, calculated as the sum of U_{dis} and U_{sto}. In fact, as reported in Figure 7b, the percentage energies were very similar for different strain levels and for the whole duration of the tests, maintaining values of approximately 20% for the dissipated energy and 80% for the stored one.
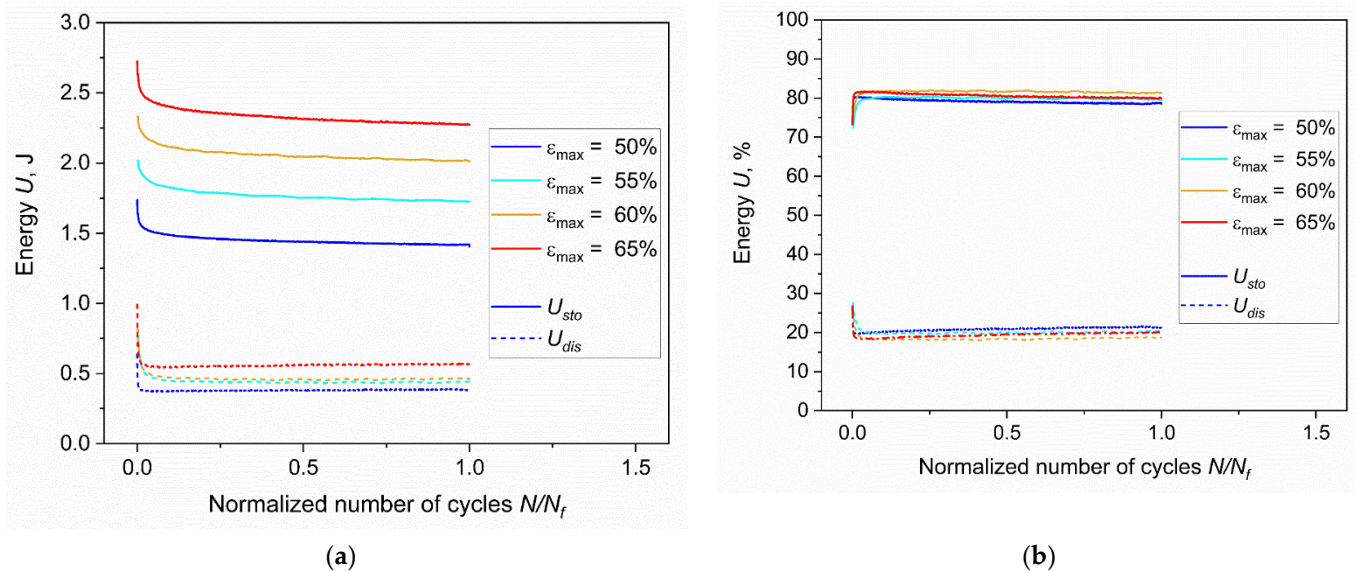

(a)   (b)

Figure 7. (**a**) Stored (U_{sto}) and dissipated (U_{dis}) energies at different strains against the normalized number of cycles; (**b**) percentage stored and dissipated energies at different strains against the normalized number of cycles. The fatigue tests were implemented on axisymmetric dumbbell specimens of CB filled NBR at a frequency of 4 Hz and a load ratio R_ε of 0.5.

Fatigue data were further analyzed by considering the peak values of the forces detected during the measurements. For a clearer comparison at different loading conditions, the maximum force, F_{max}, and the minimum force, F_{min}, were normalized with respect to their respective initial values and they were plotted against the normalized number of cycles (Figure 8a,b). Due to stress relaxation, the maximum and minimum forces showed a considerable variation in the first cycles, until consistent stress relaxation occurs in the specimen. After the initial drop, the values were constantly decreasing as a consequence of both stress relaxation and damage accumulation. In this region, the reduction extent depended on the loading conditions, but it was generally limited. Ultimately, a final major drop was present, which was related to the macroscopic crack growth and consequence of the reduction of the specimens' ligament section. As depicted in Figure 8a, the maximum forces decreased at the very beginning of the tests by about one third and stabilized up to the final failure of the specimen, regardless of the strain level. Conversely, a different behavior was found for the minimum force. It is evident from the plot in Figure 8b that after the initial drop, the minimum forces are different for distinct strain levels: larger drops were monitored for lower values of maximum strain. Furthermore, small peaks were observed after the initial drop, which are more evident for larger maximum strains in particular.

Therefore, several parameters showed a reduction during the cycles, which was related to relaxation and material damage. These changes could be observed from the early stages of fatigue, suggesting a slow crack growth process; however, clear evidence to identify a transition between the regimes of crack initiation and crack growth were not found. Thus, further investigations were performed considering a fracture mechanics-based approach.
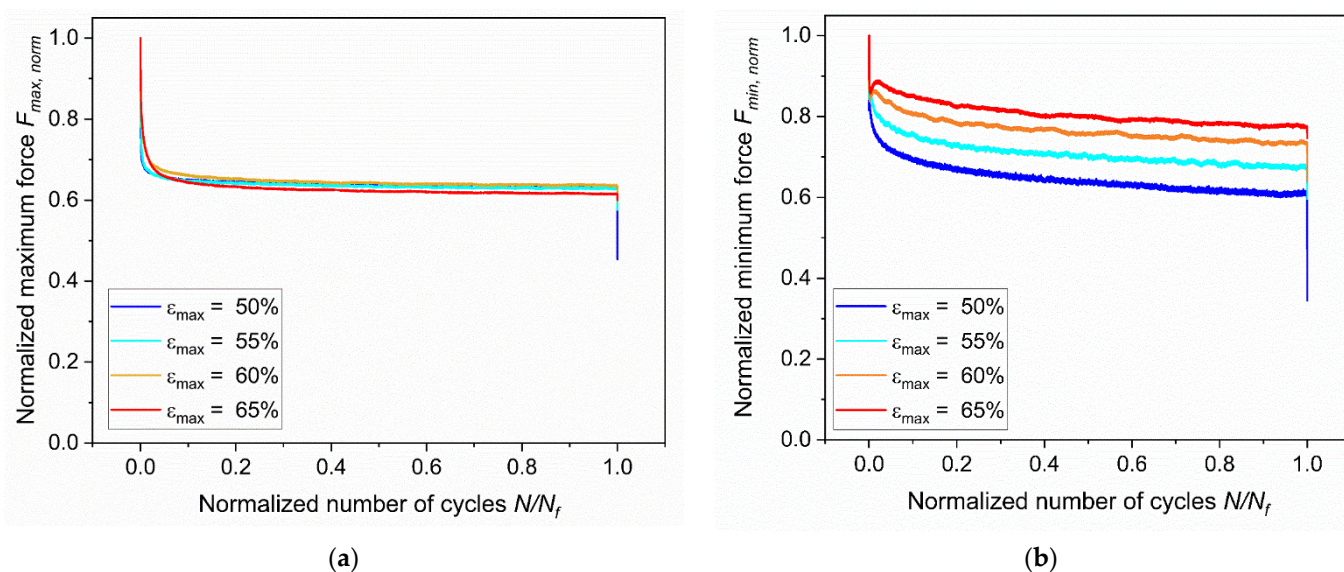
(**a**)   (**b**)

Figure 8. (**a**) Normalized maximum force at different strains against normalized number of cycles. (**b**) Normalized minimum force at different strains against the normalized number of cycles. The fatigue tests were implemented on axisymmetric dumbbell specimens of CB filled NBR at a frequency of 4 Hz and a load ratio R_ε of 0.5.

3.2. Fracture Surface Analysis of the Unnotched Dumbbell Specimens

Subsequently, the fracture surfaces of the specimens were observed under the light microscope. The typical appearance of the fracture surfaces is shown and described in Figure 9. The most evident characteristic is the presence of fatigue striations which display an increasing distance from each other as they move farther from the initiation area. Normally, fatigue striations were observed for up to half of the surface area, whereas the remaining section corresponded to the catastrophic failure. An overview of the fracture surfaces at different strains is reported in Figure 10. Generally, failure occurred perpendicularly to the loading direction, with quite flat fracture surfaces, and the features displayed in Figure 9 were the most frequently observed with evident fatigue striation in all cases; however, in some cases, the fracture surfaces results were more complex, with evident macroscopic cracks out of the plane of the fracture surface at ε_{max} of 50% and 60%. Such kinds of crack deviation could be related to local inhomogeneities in the material such as large agglomerates of carbon black. Moreover, at the lowest strain (ε_{max} of 50%), fatigue striations in two opposite directions were observed (Figure 11), suggesting that the initiation is taking place independently in different areas and that at lower strains, macroscopic crack growth took place in different directions. The single crack direction at larger strains suggests that due to the larger energy and stress intensification involved, once the crack began to form, it became the predominant crack.
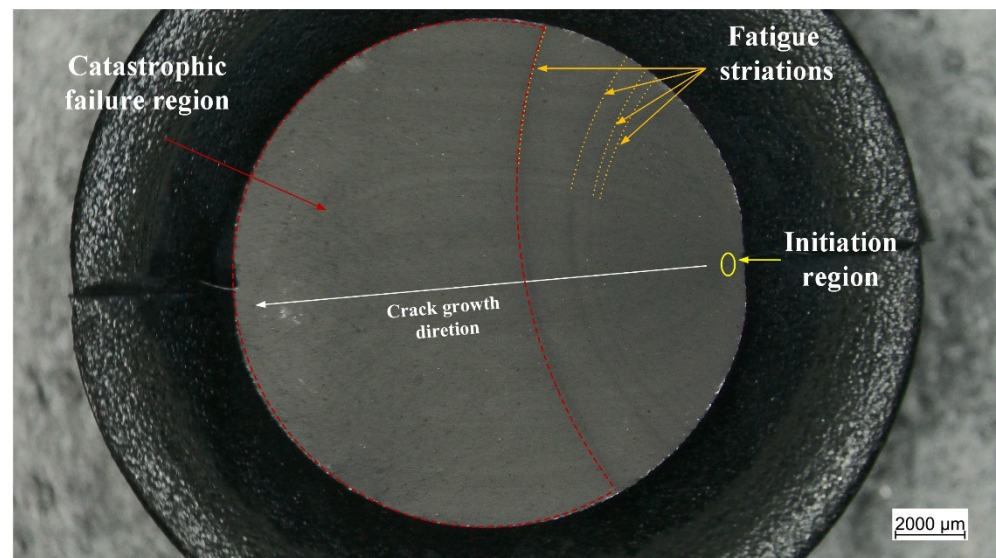
Figure 9. Light microscope picture of the fracture surface of an axisymmetric dumbbell specimen of CB filled NBR after fatigue testing. Three regions are displayed: initiation region (yellow), fatigue striation (orange), and catastrophic failure (red). The test was performed at a frequency of 4 Hz and a load ratio R_ε of 0.5.
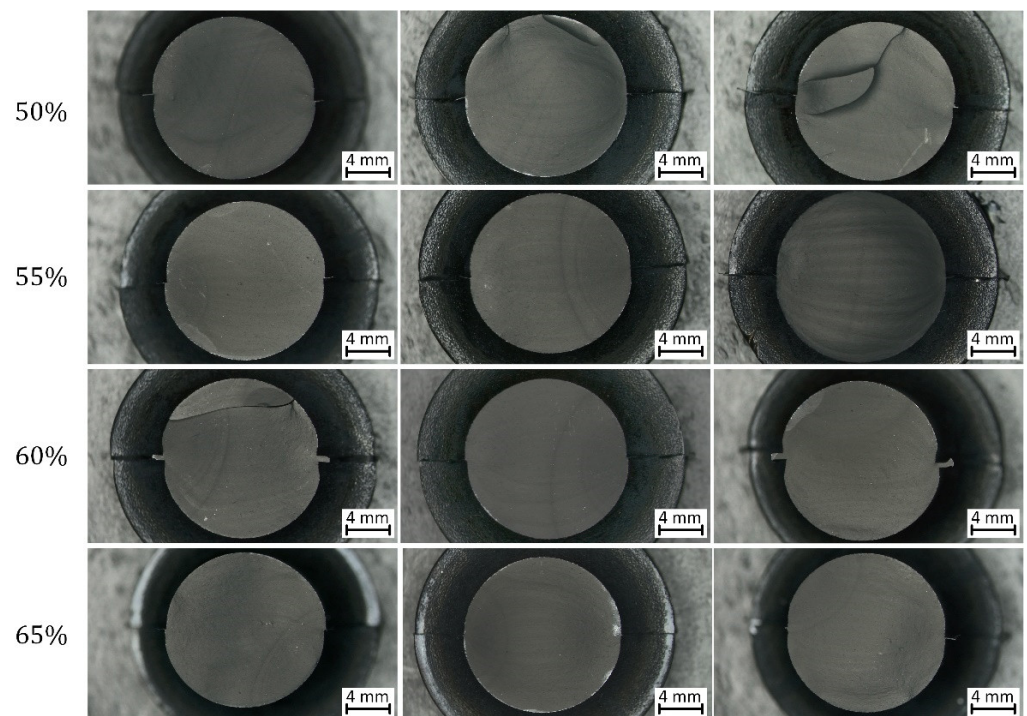

Figure 10. Light microscope pictures of fracture surfaces of axisymmetric dumbbell specimens of CB with NBR at different strains (the correspondent maximum strain is reported on the left). The tests were performed at a frequency of 4 Hz and a load ratio R_ε of 0.5.
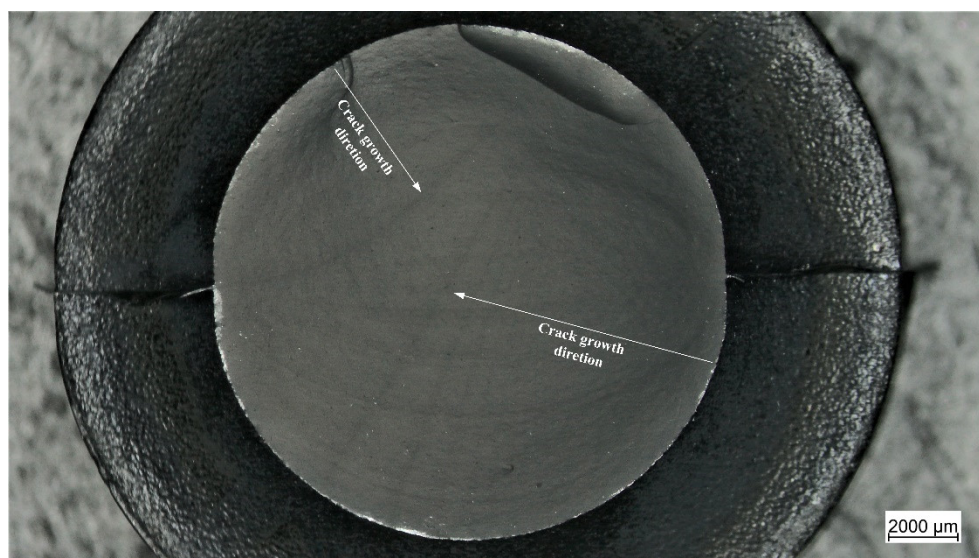
Figure 11. Light microscope picture of the fracture surface of an axisymmetric dumbbell specimen of CB filled NBR after fatigue testing in which two fronts of macroscopic fatigue crack growth are present (displayed by the arrows). The test was performed at a frequency of 4 Hz and a load ratio $R\varepsilon$ of 0.5.

3.3. Fatigue of the Cracked Round Bar Specimens

Furthermore, fatigue measurements on the Crack Round Bar (CRB) were conducted. The CRB geometry (a dumbbell with a circumferential notch in the middle) was developed for accelerated testing of quasi-brittle failure resistance of polymers, elastomers, and thermoplastic elastomers [68–70]. In principle, due to the presence of the notch, this specimen geometry would allow the crack length and crack growth rate to be measured using a Paris approach, focusing on the crack propagation regime; however, due to the cylindrical geometry, the crack front results are complex, and it is difficult to assess crack length measurements through optical methods. More accurate results could be obtained by using extensometers and retrieving the crack length through a calibration between Crack Opening Displacement (COD) and the actual crack length [71]; however, due to the large strain involved, this approach has limitations for elastomers.

The results of fatigue tests obtained on CRB specimens in comparison with the results of standard specimens are shown in Figure 12. As depicted, a general reduction in lifetime was found for CRB as a consequence of the introduction of the notch. A reduction of about four orders of magnitude of the fatigue lifetime at ε_{max} of 50% was recorded. Furthermore, in contrast to the results of unnotched axisymmetric dumbbells, failure was observed even at 20% of maximum (nominal) strain. The fitting power law from the statistical analysis of the results, performed through the ASTM E739–10 was found to be:

$$\varepsilon_{max} = 119 \cdot N_f^{-0.24}. \tag{5}$$

Moreover, the variations of both the normalized maximum force and crack length during the test with CRB geometry were analyzed and reported in Figure 13a. It is worth noting that the machine reached such high strains with a delay; since a stable deformation was observed after a transient period of eight cycles, the maximum force was attained after nine cycles. Considering the cylindrical symmetry of the samples, the crack length was approximated as the projection of the actual radial crack. In addition, the reported crack length was considered as the sum of the crack lengths observed on both sides of the specimen in the camera record (see the picture in Figure 13b). To have a proper measurement of the crack evolution, more cameras would be needed; however, this approximation is considered sufficiently accurate to monitor the evolution of the specimen's ligament section. As depicted in Figure 13a, the larger crack increase was observed at about 30 cycles, a time at which an abrupt variation of the maximum force was also recorded; nevertheless,

a smaller crack length increase was present even before this stage. In actuality, the crack starts to grow immediately after the application of the load—at the ninth cycle after stable deformation is reached. On the other hand, in unnotched specimens, the microscopic crack growth occurred after initiation.
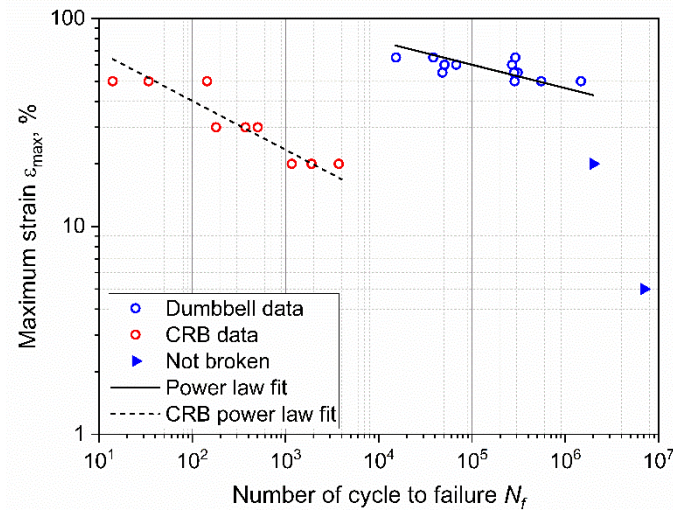

Figure 12. Wöhler curve obtained from axisymmetric dumbbell specimens (blue) and CRB (red) of CB filled NBR at a frequency of 4 Hz and a load ratio R_ε of 0.5. The fitting power laws of the axisymmetric dumbbell specimen (continuous line) and of CRB (dashed line) were obtained using ASTM E739–10.
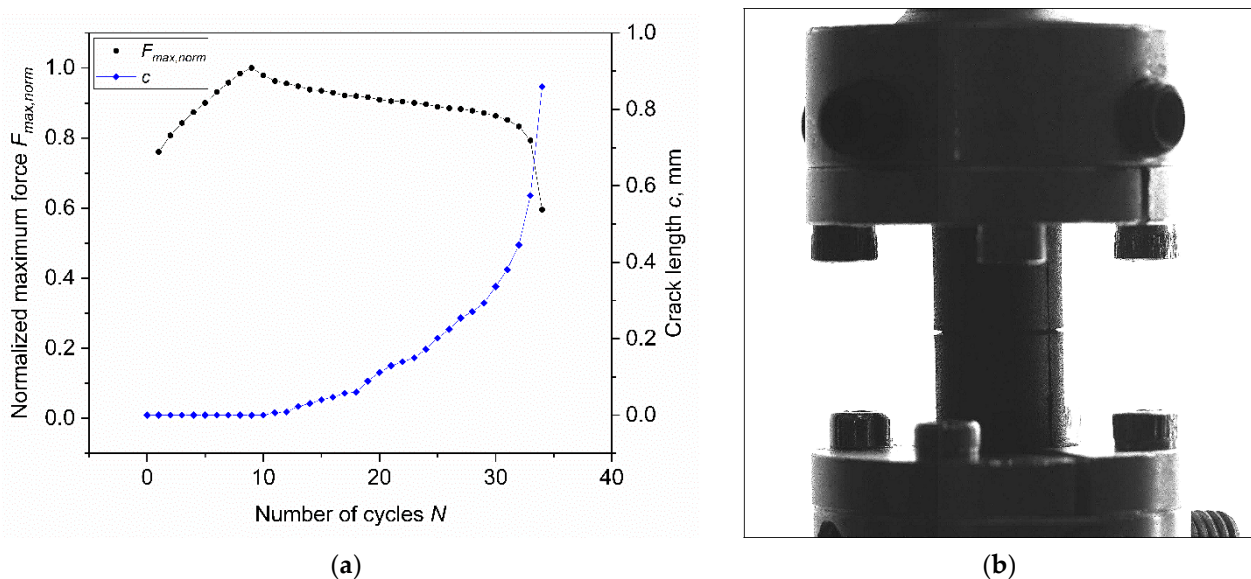

(**a**)　　　　　　　　　　　　　(**b**)

Figure 13. (**a**) Normalized maximum force (circles) and crack length (diamonds) against number of cycles for CRB specimens obtained from axisymmetric dumbbell specimens of CB filled NBR. (**b**) Picture of the tested CRB at $N = 30$; on both sides, the crack opening can be recognized. The test was performed at the maximum strain of 50% at a frequency of 4 Hz and a load ratio R_ε of 0.5.

3.4. Fracture Surface Analysis of the Cracked Round Bar Specimens

Additionally, the fracture surfaces of the CRB specimen were analyzed and a representative example is reported in Figure 14. There are several similarities in the failure mechanism when compared with the unnotched kind in Figure 9. In addition to the region of radial notching, the fracture surfaces of CRBs also displayed the three aforementioned regions of initiation, fatigue striation, and catastrophic failure. Moreover, even in this case, the fatigue striations show increasing distances moving from the initiation region, and in correlation

with the increasing crack length reported in Figure 13a. Overall, these results suggest that a similar damage mechanism is maintained, and that the introduction of the artificial notch is equivalent to a specimen with a larger initial defect in an unnotched specimen.
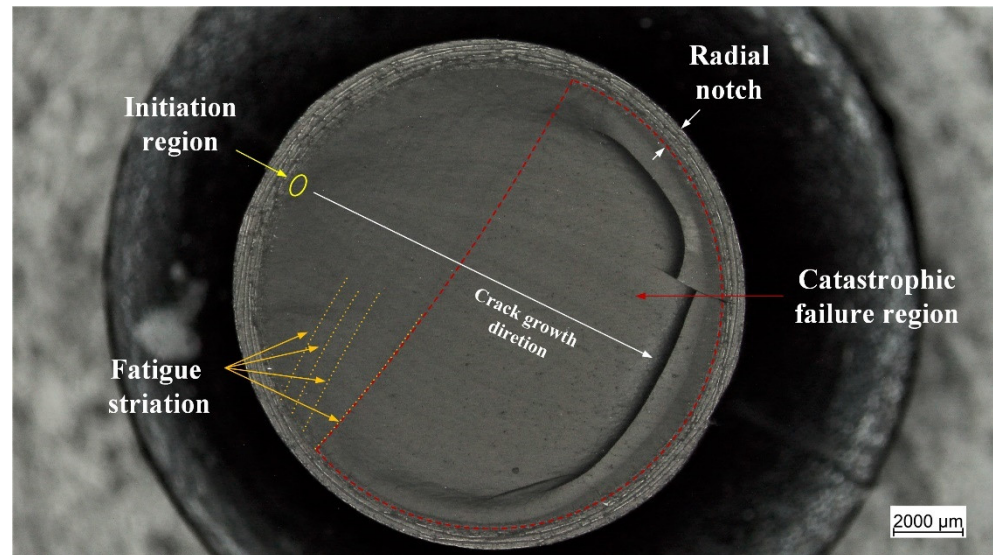

Figure 14. Light microscope picture of the fracture surface of a notched axisymmetric dumbbell specimen (CRB) of CB filled NBR after fatigue testing. At the specimen edge the radial notch can be observed, and a further three regions are displayed: initiation region (yellow), fatigue striation (orange)—corresponding to macroscopic fatigue crack growth—and catastrophic failure (red). The test was performed at a frequency of 4 Hz and a load ratio R_ε 0.5.

3.5. Defect Size Assesment

As already mentioned, the fatigue lifetime can be correlated with the crack growth by considering the initial size of defects that cause fatigue failure. In fact, by considering the defect size c_0, it is possible to connect the failure of the material to defects and inhomogeneities naturally present in the material.

In order to obtain the value c_0, the integration of the crack growth characteristic is required. Generally, the fatigue crack growth of rubbers within the stable regime can be described using the Paris law [5]:

$$\frac{dc}{dN} = CG^m, \tag{6}$$

where dc/dN represents the crack growth rate, G represents the tearing energy, and C and m are materials constants. For small cracks, the energy release rate (i.e., tearing energy) can be factored into strain energy density and crack size [2] and its estimation can be given by:

$$G = 2 \cdot k(\lambda) \cdot W \cdot c, \tag{7}$$

where W is the strain energy density and c is the crack length; $k(\lambda)$ is a function of the stretch ratio [72]. In actuality, Equation (7) represents the tearing energy for single edge notch specimens [3]; nevertheless, it is a good approximation for small cracks in terms of initial defects. Moreover, the strain energy density W was evaluated considering the area under the loading curve by numerical integration of hysteresis data as:

$$W = \int \sigma \cdot d\varepsilon = \int \frac{F}{A} \cdot \frac{ds}{s} = \frac{1}{V} \int_{s_{min}}^{s_{max}} F \cdot ds. \tag{8}$$

where σ is the engineering stress, ε is the engineering strain, F is the force, A the resistant area of the specimen, s is the displacement, s_{min} and s_{max} are the minimum and the maximum displacements, respectively, and V is the volume of the specimen. By combining Equations (6) and (7), and integrating the number of cycles for failure, N_f, can be obtained:

$$N_f = \frac{1}{(m-1)\cdot C(2kW)^m} \cdot \left(\frac{1}{c_0^{m-1}} - \frac{1}{c_f^{m-1}}\right). \tag{9}$$

Assuming that the initial defects size c_0 is much smaller than the final crack length c_f, this last contribution can be neglected, obtaining:

$$N_f = \frac{1}{(m-1)\cdot C(2kW)^m} \cdot \frac{1}{c_0^{m-1}}. \tag{10}$$

This equation can be used to calculate the number of cycles to failure as a consequence of the growth of a pre-existing defect with the dimension c_0. Alternatively, Equation (10) can be reversed to evaluate the effective critical defect size from which the failure originated. It is worth noting that for the evaluation of the overall lifetime, this approach for elastomers often neglects the initiation time; however, this is justified considering what was found through the analysis of the evolution of defects during fatigue, which investigated for filled polychloroprene rubber (CR) through μ-CT [31,32], and for filled natural rubber (NR) through SEM analysis [28,29]. It was shown that cracks are initiated in the early stages of fatigue tests and that the number of defects mainly increase within the first 10% of fatigue life. In the successive stages, the initiated defects slowly increased in size, whereas the number of cracks is more stable: it constantly increases but with a lower rate of nucleation. Therefore, the majority of the lifetime of rubbers is governed by crack growth and the initiation time can be neglected.

The effective critical defect size c_0 was calculated by reversing Equation (10) and using the number of cycles to failure N_f, as reported in Figure 3. The values of k and W were calculated for the corresponding strain levels. In particular, the strain energy density for each specimen was evaluated through Equation (8) at the beginning of the test. As for the coefficients m and C of the Paris law, these were evaluated from the data and the fatigue master curve shifting procedure was previously reported in [35]. In that work, fatigue crack growth characteristics at different temperatures (and at the same frequency and load ratio as in the work presented here) were analyzed, and a fatigue master curve based on the temperature dependence of the loss modulus was constructed. Using this procedure, horizontal shift factors were evaluated for the temperatures measured during the testing of axisymmetric dumbbells, allowing for the calculation of m and C for each test, while accounting for the influence of temperature on these parameters. An overview of all the values used for the calculation of c_0 are reported in Table 1. Using these parameters, the effective critical defect sizes were calculated, and the values at different strains are reported in Figure 15. As depicted, the values c_0 were found to be in the range between 4 and 14 μm for the different maximum strains. The values of the critical defect size are similar, regardless of the applied strain level: this points towards the conclusion that the defect size is an intrinsic value related to the material. The reason for the different degrees of dispersion in the results at different strains was mainly related to the large scattering of the fatigue data at the same strain values (see Table 1). Due to the independence of the size on the strain, it is possible to consider the mean value for all specimens: the effective critical defect size c_0 was 9 ± 3 μm.

Table 1. Overview of the values used to calculate the critical defect size with the reversion of Equation (10). The values of the number of cycles to failure are the same as reported in Figure 3.

| ε_{max} (%)	N_f	W (kJ/m^3)	k (λ)	T (°C)	m	C
50	1,472,620	715	2.38	47.4	3.7	1.26×10^{-14}
	551,975	817	2.38	52.7	3.7	1.91×10^{-14}
	286,860	814	2.38	50.5	3.7	1.62×10^{-14}
55	48,181	948	2.33	57.4	3.7	2.69×10^{-14}
	308,772	1000	2.33	56.4	3.7	2.45×10^{-14}
	283,510	971	2.33	55.0	3.7	2.24×10^{-14}
60	67,622	1072	2.29	56.2	3.7	2.45×10^{-14}
	269,073	1103	2.29	57.0	3.7	2.57×10^{-14}
	130,393	1099	2.29	52.9	3.7	1.91×10^{-14}
65	291,859	1267	2.26	61.7	3.7	3.63×10^{-14}
	15,318	1222	2.26	60.3	3.7	3.24×10^{-14}
	38,475	1288	2.26	63.7	3.7	4.17×10^{-14}
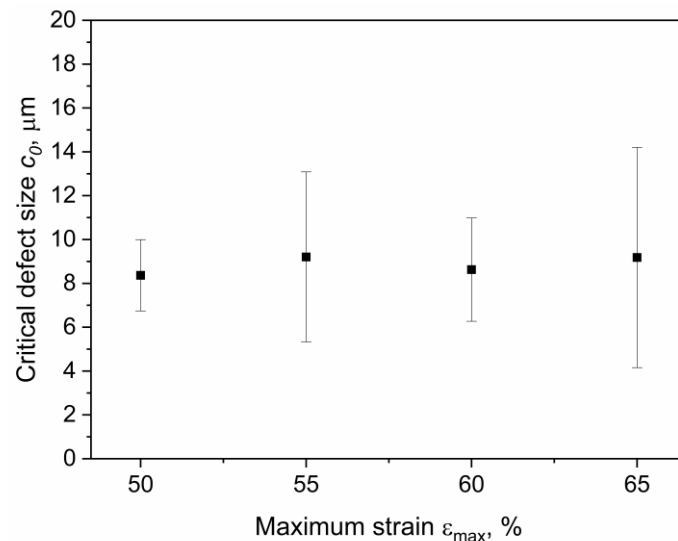
Figure 15. Critical defect size c_0 at different strains evaluated from fatigue data using Equation (10). The fatigue tests were implemented on axisymmetric dumbbell specimens of CB filled NBR at a frequency of 4 Hz and a load ratio R_ε of 0.5.

Moreover, the initial defect size of the axisymmetric dumbbell specimens was evaluated through the reconstruction of μ-CT (Figure 16a). From the reconstructed volume, naturally present defects have been identified (Figure 16b) and their volumes have been determined. In order to have a direct comparison with the critical defect size c_0, the cavities have been approximated as spheres and their radii have been calculated. The particle size distribution is displayed in Figure 16c, in which the relative frequency for each value of the particle radius is reported. As depicted, the dimensions of detected cavities were of few μm, between 1 and 24 μm. It is important to stress that considering the temperature influence on crack growth parameters strongly affects the calculation of the defects' dimensions; however, a very good agreement between CT data and the back-calculation from CT measurements is obtained. Indeed, the defect size distribution indeed vanishes above 8–10 μm, which corresponds quite well with the value of c_0 of 9 μm previously identified (see inset of Figure 16c).
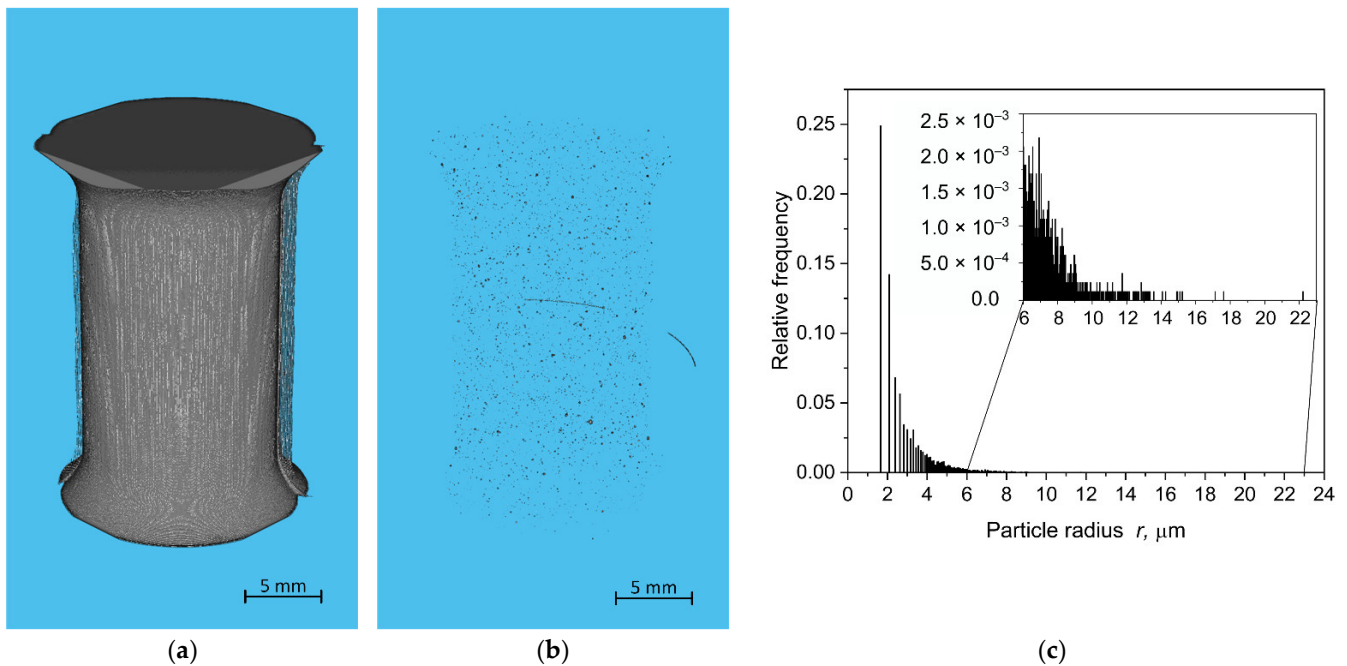
Figure 16. (**a**) Volume reconstruction of an undamaged (i.e., not yet loaded and cycled) axisymmetric dumbbell specimen obtained from μ-CT. (**b**) Cavity distribution in the reconstructed volume obtained from μ-CT with a connectivity equal to 26. (**c**) Particle size distribution considered as the spherical radius of the cavities.

In addition, further observations could be made by calculating the lifetime based on the evaluated defects. In fact, Equation (10) was used to estimate the lifetime for the two interrupted tests. More specifically, the average c_0 (9 μm) was used as the initial defect size, and the calculated fatigue life for the maximum strains of 5% and 20% were of 3.5×10^{12} and 2.9×10^8, respectively. The results are well above the number of cycles at which the tests were stopped (7×10^6 and 2×10^6, respectively). The details concerning the parameters used for the calculation are reported in Table 2.

Table 2. Overview of the values used to calculate the number of cycles to failure for interrupted tests using Equation (10).

ε_{max} (%)	W (kJ/m^3)	k (λ)	T (°C)	m	C	$N_{f,calc}$
5	16	2.88	26.2	3.7	2.24×10^{-15}	3.5×10^{12}
20	187	2.68	31.6	3.7	3.55×10^{-15}	2.9×10^8

Similarly, fatigue lifetime predictions were calculated considering the mean values of c_0 and the minimum and maximum values of particle radius found by μ-CT (so 1.7 and 22.2 μm, respectively). Some approximations have been made in the calculations. In particular, the linear relation between the strain energy density W and maximum strain (reasonable in the strain range between 50 and 65%) was considered, which resulted in the following equation:

$$W = -757,142 + 31,014 \cdot \varepsilon_{max}. \tag{11}$$

The values of k were calculated at the different strains, whereas the material coefficients m and C were estimated through the aforementioned temperature shifting procedure. A linear relation between temperature and maximum strain was considered:

$$T = 21.3 + 0.62 \cdot \varepsilon_{max}. \tag{12}$$

Therefore, the fatigue lifetime predictions were calculated using Equation (10), and these results were then compared with the experimental fatigue results described in the previous section. These results illustrate the impact of initial defect size. As depicted in Figure 17, when considering the minimum and maximum value of particle size, the fatigue predictions show a broad spectrum spanning across three orders of magnitude. Of course, the calculations using the average c_0 give values similar to the experimental data and to the power law fit (Equation (1)): these have been included to illustrate the typical scatter in the data.
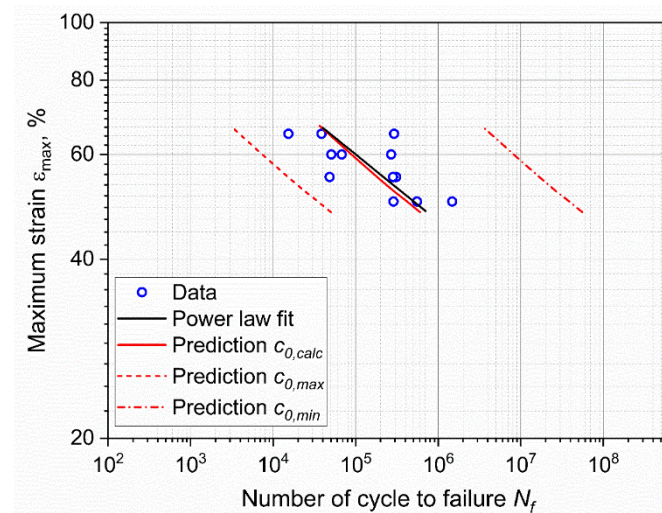
Figure 17. Comparison between fatigue data and the calculated fatigue lifetimes for the calculated defect size ($c_{0,calc}$), and the maximum and minimum sizes evaluated from μ-CT ($c_{0,max}$ and $c_{0,min}$, respectively).

3.6. Correlation of the Results Based on J-Integral

Finally, a non-linear J-integral hyperelastic model for the CRB has been developed. This energetic approach has the advantage of being applied in order to describe materials that show non-linear mechanical behavior, and it is useful for comparing different geometries. In particular, the J-integral was evaluated as [73]:

$$J = \frac{F^2}{\pi(r_{out} - a)^2} \cdot f\left(\frac{a}{r_{out}}\right), \tag{13}$$

where F is the force, r_{out} the external radius of the CRB, a is the size of notch in the CRB, and $f(a/r_{out})$ is a geometric factor found by the FEM simulation as:

$$f\left(\frac{a}{r_{out}}\right) = 11.190\left(\frac{a}{r_{out}}\right)^4 - 3.766\left(\frac{a}{r_{out}}\right)^3 - 1.072\left(\frac{a}{r_{out}}\right)^2 + 3.615\left(\frac{a}{r_{out}}\right) + 0.012. \tag{14}$$

Equation (13) was used to compute J_{max} and J_{min} using F_{max} and F_{min}, respectively. The difference between J_{max} and J_{min} was then used to compare the CRB results with those of standard dumbbell samples. The J-integral of the axisymmetric dumbbell was evaluated using Equation (7); in fact, J can be approximated as the energy release rate G [60]. The values of J for dumbbell specimens were evaluated using the calculated c_0 and the strain energies reported in Table 1. The considered forces were those measured at the beginning of the test. An overview of the data used for the evaluation of J is reported in Table 3. The J-integral as a function of number of cycles to failure for both geometries is plotted in Figure 18. A unique fitting curve was found for both geometries; this demonstrates that independently of the specimen geometry, it is possible to evaluate the fatigue lifetime based on J-integral. Although this J-integral formulation and its applicability still need to be verified on different geometric parameters and materials, it seems to be a promising

candidate for extending fracture mechanic tools for the fatigue assessment of elastomers with reduced testing times.

Table 3. Overview of the values used to calculate the J-integrals for CRB using Equation (13).

E_{max} (%)	N_f	a (mm)	r_{out} (mm)	F_{max} (N)	F_{min} (N)	J (J/m^2)
	3724	0.47	7.19	526	129	120
20	1899	0.69	7.26	556	157	200
	1165	0.86	7.24	540	145	251
	371	1.00	7.09	702	178	554
30	504	0.85	7.29	720	190	433
	180	0.84	7.36	757	206	452
	14	0.64	7.19	1002	213	638
50	144	0.62	7.08	973	229	594
	34	0.71	7.19	841	200	498
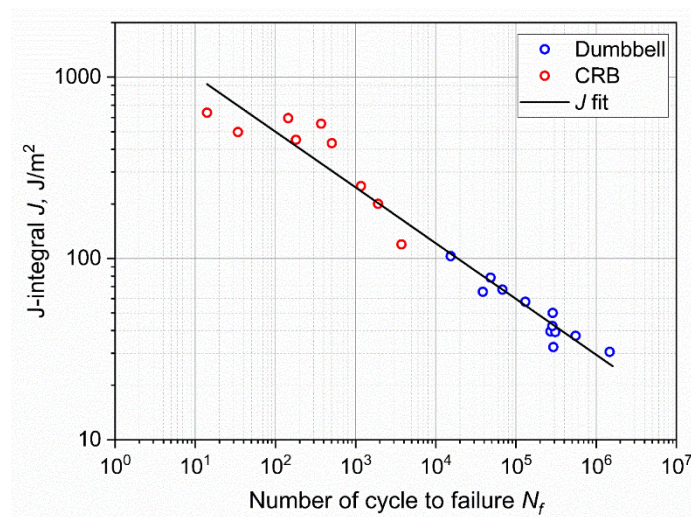
Figure 18. Wöhler curve in terms of the J-integral for axisymmetric dumbbell (blue) and CRB (red) specimens. A unique fitting line was found correlating the two geometries.

4. Conclusions

The fatigue behavior of a carbon black filled NBR was investigated in the presented work. Fatigue measurements were performed on axisymmetric dumbbell specimens and also on CRB specimens (i.e., axisymmetric dumbbells with a circumferential notch). The number of cycles to failure was measured for both sets, and Wöhler curves were constructed. Although the recorded points were considerably scattered, the results could be described with a power law.

The results of the axisymmetric dumbbell specimens were investigated in more detail through the analysis of temperature variations, hysteresis, secant, dynamic moduli, stored and dissipated energies, and the normalized force peaks. In general, all the observed values largely varied in the early stages of fatigue (approximately up to 2500–3000 cycles), but they stabilized with a lower degree of variation up to the failure of the specimens, suggesting a slow crack growth process. Even though these variations evidenced a continuous and progressive accumulation of relaxation and damage, a clear distinction between initiation and propagation was not observed.

Additional details could be obtained by further investigations considering a fracture mechanics approach. The fracture surfaces featured initiation areas from which evident fatigue striations originated from. Similar aspects of the fracture surfaces were found for axisymmetric dumbbells with a circumferential notch. These results suggested similarities in the damaging mechanism and that the notch can be represented as a larger defect. As

expected, the introduction of a notch led to a reduction in fatigue life up to four orders of magnitude.

Moreover, the fatigue life of dumbbells was correlated to the defect size by integrating the crack growth characteristic and taking into account the effect of temperature, obtaining values that were independent on the strain level. The evaluated defect size was then compared with the defect sizes analyzed through X-ray microtomography, confirming similar dimensions and a good accuracy of the calculations.

Finally, through the evaluation of the J-integral, it was possible to link the fatigue life of unnotched and notched axisymmetric dumbbells, evidencing a geometry independency of the J-integral formulation. This formulation for notched axisymmetric dumbbells may represent a new tool for the investigation of accelerated fatigue in elastomers.

Supplementary Materials: The following supporting information can be downloaded at: https://www.mdpi.com/article/10.3390/ma15113745/s1, Figure S1: Comparison of Wöhler curves considering N_i and N_f.

References

1. Ellul, M.D. Mechanical fatigue. In *Engineering with Rubber: How to Design Rubber Components*, 3rd ed.; Gent, A.N., Ed.; Hanser Publications: Cincinnati, OH, USA, 2012.
2. Mars, W.V.; Fatemi, A. A literature survey on fatigue analysis approaches for rubber. *Int. J. Fatigue* **2002**, *24*, 949–961. [CrossRef]
3. Gent, A.N.; Lindley, P.B.; Thomas, A.G. Cut growth and fatigue of rubbers. I. The relationship between cut growth and fatigue. *J. Appl. Polym. Sci.* **1964**, *8*, 455–466. [CrossRef]
4. Lake, G.J.; Lindley, P.B. Cut growth and fatigue of rubbers. II. Experiments on a noncrystallizing rubber. *J. Appl. Polym. Sci.* **1964**, *8*, 707–721. [CrossRef]
5. Lake, G.J.; Lindley, P.B. The mechanical fatigue limit for rubber. *J. Appl. Polym. Sci.* **1965**, *9*, 1233–1251. [CrossRef]
6. Fielding-Russell, G.S.; Rongone, R.L. Fatiguing of rubber-rubber interfaces. *Rubber Chem. Technol.* **1983**, *56*, 838–844. [CrossRef]
7. Young, D.G. Dynamic property and fatigue crack propagation research on tire sidewall and model compounds. *Rubber Chem. Technol.* **1985**, *58*, 785–805. [CrossRef]
8. Royo, J. Fatigue testing of rubber materials and articles. *Polym. Test.* **1992**, *11*, 325–344. [CrossRef]
9. Lake, G.J. Fatigue and fracture of elastomers. *Rubber Chem. Technol.* **1995**, *68*, 435–460. [CrossRef]
10. Choi, I.S.; Roland, C.M. Intrinsic defects and the failure properties of cis-1,4-polyisoprenes. *Rubber Chem. Technol.* **1996**, *69*, 591–599. [CrossRef]

11. Mars, W.V.; Fatemi, A. Fatigue crack nucleation and growth in filled natural rubber. *Fatigue Fract. Eng. Mater. Struct.* **2003**, *26*, 779–789. [CrossRef]

12. Zarrin-Ghalami, T.; Fatemi, A. Fatigue life predictions of rubber components: Applications to an automobile cradle mount. *Proc. Inst. Mech. Eng. Part D J. Automob. Eng.* **2012**, *227*, 691–703. [CrossRef]

13. Zarrin-Ghalami, T.; Fatemi, A. Material deformation and fatigue behavior characterization for elastomeric component life predictions. *Polym. Eng. Sci.* **2012**, *52*, 1795–1805. [CrossRef]

14. Kim, H.J.; Song, M.W.; Moon, H.I.; Kim, H.; Kim, H.Y. Fatigue life prediction of a rubber material based on dynamic crack growth considering shear effect. *Int.J. Automot. Technol.* **2014**, *15*, 317–324. [CrossRef]

15. El Yaagoubi, M.; Juhre, D.; Meier, J.; Kröger, N.; Alshuth, T.; Giese, U. Lifetime prediction of filled elastomers based on particle distribution and the J-integral evaluation. *Int. J. Fatigue* **2018**, *112*, 341–354. [CrossRef]

16. Gehrmann, O.; El Yaagoubi, M.; El Maanaoui, H.; Meier, J. Lifetime prediction of simple shear loaded filled elastomers based on the probability distribution of particles. *Polym. Test.* **2019**, *75*, 229–236. [CrossRef]

17. Guo, H.; Li, F.; Wen, S.; Yang, H.; Zhang, L. Characterization and Quantitative Analysis of Crack Precursor Size for Rubber Composites. *Materials* **2019**, *12*, 3442. [CrossRef] [PubMed]

18. El Maanaoui, H.; Meier, J. Lifetime prediction with temperature dependence for EPDM and NR elastomers based on fatigue crack growth mechanical measurements and filler distribution. *Polymer* **2021**, *228*, 123909. [CrossRef]

19. Andena, L.; Rink, M.; Frassine, R.; Corrieri, R. A fracture mechanics approach for the prediction of the failure time of polybutene pipes. *Eng. Fract. Mech.* **2009**, *76*, 2666–2677. [CrossRef]

20. Le Cam, J.-B.; Huneau, B.; Verron, E.; Gornet, L. Mechanism of fatigue crack growth in carbon black filled natural rubber. *Macromolecules* **2004**, *37*, 5011–5017. [CrossRef]

21. Mars, W.V.; Fatemi, A. Nucleation and growth of small fatigue cracks in filled natural rubber under multiaxial loading. *J. Mater. Sci.* **2006**, *41*, 7324–7332. [CrossRef]

22. Saintier, N.; Cailletaud, G.; Piques, R. Crack initiation and propagation under multiaxial fatigue in a natural rubber. *Int. J. Fatigue* **2006**, *28*, 61–72. [CrossRef]

23. Hainsworth, S.V. An environmental scanning electron microscopy investigation of fatigue crack initiation and propagation in elastomers. *Polym. Test.* **2007**, *26*, 60–70. [CrossRef]

24. Le Cam, J.-B.; Toussaint, E. The mechanism of fatigue crack growth in rubbers under severe loading: The Effect of Stress-Induced Crystallization. *Macromolecules* **2010**, *43*, 4708–4714. [CrossRef]

25. Weng, G.; Huang, G.; Lei, H.; Qu, L.; Nie, Y.; Wu, J. Crack initiation and evolution in vulcanized natural rubber under high temperature fatigue. *Polym. Degrad. Stab.* **2011**, *96*, 2221–2228. [CrossRef]

26. Le Cam, J.-B.; Huneau, B.; Verron, E. Fatigue damage in carbon black filled natural rubber under uni- and multiaxial loading conditions. *Int. J. Fatigue* **2013**, *52*, 82–94. [CrossRef]

27. Le Cam, J.-B.; Huneau, B.; Verron, E. Failure analysis of carbon black filled styrene butadiene rubber under fatigue loading conditions. *Plast. Rubber Compos.* **2014**, *43*, 187–191. [CrossRef]

28. Huneau, B.; Masquelier, I.; Marco, Y.; Le Saux, V.; Noizet, S.; Schiel, C.; Charrier, P. Fatigue crack initiation in a carbon black-filled natural rubber. *Rubber Chem. Technol.* **2016**, *89*, 126–141. [CrossRef]

29. Marco, Y.; Huneau, B.; Masquelier, I.; Le Saux, V.; Charrier, P. Prediction of fatigue properties of natural rubber based on the descriptions of the cracks population and of the dissipated energy. *Polym. Test.* **2017**, *59*, 67–74. [CrossRef]

30. Federico, C.E.; Padmanathan, H.R.; Kotecky, O.; Rommel, R.; Rauchs, G.; Fleming, Y.; Addiego, F.; Westermann, S. Cavitation Micro-mechanisms in Silica-Filled Styrene-Butadiene Rubber Upon Fatigue and Cyclic Tensile Testing. In *Fatigue Crack Growth in Rubber Materials: Experiments and Modelling*; Heinrich, G., Kipscholl, R., Stoček, R., Eds.; Springer: Cham, Switzerland, 2020; ISBN 978-3-030-68919-3.

31. Marco, Y.; Le Saux, V.; Calloch, S.; Charrier, P. X-ray computed μ-tomography: A tool for the characterization of fatigue defect population in a polychloroprene rubber. *Procedia Eng.* **2010**, *2*, 2131–2140. [CrossRef]

32. Le Saux, V.; Marco, Y.; Calloch, S.; Charrier, P. Evaluation of the fatigue defect population in an elastomer using X-ray computed micro-tomography. *Polym. Eng. Sci.* **2011**, *51*, 1253–1263. [CrossRef]

33. Euchler, E.; Bernhardt, R.; Schneider, K.; Heinrich, G.; Tada, T.; Wießner, S.; Stommel, M. Cavitation in Rubber Vulcanizates Subjected to Constrained Tensile Deformation. In *Fatigue Crack Growth in Rubber Materials: Experiments and Modelling*; Heinrich, G., Kipscholl, R., Stoček, R., Eds.; Springer: Cham, Switzerland, 2020; ISBN 978-3-030-68919-3.

34. Schieppati, J.; Schrittesser, B.; Wondracek, A.; Robin, S.; Holzner, A.; Pinter, G. Effect of mechanical loading history on fatigue crack growth of non-crystallizing rubber. *Eng. Fract. Mech.* **2021**, *257*, 108010. [CrossRef]

35. Schieppati, J.; Schrittesser, B.; Wondracek, A.; Robin, S.; Holzner, A.; Pinter, G. Temperature impact on the mechanical and fatigue behavior of a non-crystallizing rubber. *Int. J. Fatigue* **2021**, *144*, 106050. [CrossRef]

36. *ISO 18489:2015*; Polyethylene (PE) Materials for Piping Systems—Determination of Resistance to Slow Crack Growth under Cyclic Loading-Cracked Round Bar Test Method, 2015, 23.040.20 Plastics Pipes; 23.040.45 Plastics fittings (18489). ISO: Geneva, Switzerland, 2015.

37. Moroni, G.; Petrò, S. A Discussion on Performance Verification of 3D X-Ray Computed Tomography Systems. *Procedia CIRP* **2018**, *75*, 125–130. [CrossRef]

38. Tagliabue, S.; Andena, L.; Nacucchi, M.; de Pascalis, F. An image-based approach for structure investigation and 3D numerical modelling of polymeric foams. *J. Polym. Res.* **2021**, *28*, 75. [CrossRef]

39. Otsu, N. A threshold selection method from gray-level histograms. *IEE Trans. Syst. Man Cybern.* **1979**, *9*, 62–66. [CrossRef]

40. Andena, L.; Caimmi, F.; Leonardi, L.; Nacucchi, M.; de Pascalis, F. Compression of polystyrene and polypropylene foams for energy absorption applications: A combined mechanical and microstructural study. *J. Cell. Plast.* **2019**, *55*, 49–72. [CrossRef]

41. Najman, L.; Schmitt, M. Watershed of a continuous function. *Signal. Process.* **1994**, *38*, 99–112. [CrossRef]

42. ANSYS Inc. ANSYS Help Release 2022 R1. Available online: https://ansyshelp.ansys.com (accessed on 31 January 2022).

43. Wöhler, A. Wöhler's experiments on the strength of metals. *Engineering* **1867**, *4*, 160–161.

44. *E739-10*; Practice for Statistical Analysis of Linear or Linearized Stress-Life (S-N) and Strain-Life (e-N) Fatigue Data. ASTM International: West Conshohocken, PA, USA, 2015.

45. Ruellan, B.; Le Cam, J.-B.; Jeanneau, I.; Canévet, F.; Mortier, F.; Robin, E. Fatigue of natural rubber under different temperatures. *Int. J. Fatigue* **2019**, *124*, 544–557. [CrossRef]

46. Schieppati, J.; Schrittesser, B.; Wondracek, A.; Robin, S.; Holzner, A.; Pinter, G. Impact of temperature on the fatigue and crack growth behavior of rubbers. *Procedia Struct. Integr.* **2018**, *13*, 642–647. [CrossRef]

47. Schieppati, J.; Schrittesser, B.; Wondracek, A.; Robin, S.; Holzner, A.; Pinter, G. Heat build-up of rubbers during cyclic loading. In Proceedings of the 11th European Conference on Constitutive Models for Rubber (ECCMR 2019), Nantes, France, 25–27 June 2019.

48. Gent, A.N.; Scott, K.W. Dynamic mechanical properties. In *Engineering with Rubber: How to Design Rubber Components*, 3rd ed.; Gent, A.N., Ed.; Hanser Publications: Cincinnati, OH, USA, 2012.

49. Ferry, J.D. *Viscoelastic Properties of Polymers*, 3rd ed.; Wiley: New York, NY, USA; Chichester, UK, 1980; ISBN 978-0-471-04894-7.

50. Hertzberg, R.W.; Manson, J.A. *Fatigue of Engineering Plastics*; Academic Press: New York, NY, USA; London, UK, 1980; ISBN 0123435501.

51. Alshuth, T.; Abraham, F.; Jerrams, S. Parameter Dependence and Prediction of Fatigue Properties of Elastomer Products. *Rubber Chem. Technol.* **2002**, *75*, 635–642. [CrossRef]

52. Kim, W. Fatigue life estimation of an engine rubber mount. *Int. J. Fatigue* **2004**, *26*, 553–560. [CrossRef]

53. Abraham, F.; Alshuth, T.; Jerrams, S. The effect of minimum stress and stress amplitude on the fatigue life of non strain crystallising elastomers. *Mater. Des.* **2005**, *26*, 239–245. [CrossRef]

54. Kim, J.; Jeong, H. A study on the material properties and fatigue life of natural rubber with different carbon blacks. *Int. J. Fatigue* **2005**, *27*, 263–272. [CrossRef]

55. Kim, H.; Kim, H.-Y. Numerical life prediction method for fatigue failure of rubber-like material under repeated loading condition. *J. Mech. Sci. Technol.* **2006**, *20*, 473–481. [CrossRef]

56. Woo, C.S.; Kim, W.D. Fatigue lifetime prediction methodology of rubber components. In *High Performance Structures and Materials IV, Proceedings of the HPSM 2008, Algarve, Portugal, 13–15 May 2008*; de Wilde, W., Brebbia, C.A., Eds.; WIT Press: Southampton, UK, 2008; pp. 285–293; ISBN 9781845641061.

57. Woo, C.-S.; Kim, W.-D.; Kwon, J.-D. A study on the material properties and fatigue life prediction of natural rubber component. *Mater. Sci. Eng. A* **2008**, *483-484*, 376–381. [CrossRef]

58. Woo, C.-S.; Kim, W.-D.; Lee, S.-H.; Choi, B.-I.; Park, H.-S. Fatigue life prediction of vulcanized natural rubber subjected to heat-aging. *Procedia Eng.* **2009**, *1*, 9–12. [CrossRef]

59. Abraham, F.; Alshuth, T.; Jerrams, S. Dependence on mean stress and stress amplitude of fatigue life of EPDM elastomers. *Plast. Rubber Compos.* **2013**, *30*, 421–425. [CrossRef]

60. El Yaagoubi, M.; Juhre, D.; Meier, J.; Alshuth, T.; Giese, U. Tearing energy and path-dependent J-integral evaluation considering stress softening for carbon black reinforced elastomers. *Eng. Fract. Mech.* **2018**, *190*, 259–272. [CrossRef]

61. El Yaagoubi, M.; El Maanaoui, H.; Meier, J. New fatigue test sample: Lifetime prediction of carbon black filled elastomers based on the probability distribution of particles. *Polymer* **2020**, *208*, 122973. [CrossRef]

62. Meier, J.; Robin, S.; Ludwig, M.; El Yaagoubi, M. Influence of Filler Induced Cracks on the Statistical Lifetime of Rubber: A Review. In *Fatigue Crack Growth in Rubber Materials: Experiments and Modelling*; Heinrich, G., Kipscholl, R., Stoček, R., Eds.; Springer: Cham, Switzerland, 2020; ISBN 978-3-030-68919-3.

63. Zahnt, B.A. Ermüdungsverhalten von Diskontinuierlich Glasfaserverstärkten Kunststoffen—Charakterisierungsmethoden, Werkstoffgesetze und Struktur-Eigenschafts-Beziehungen. Ph.D. Thesis, Montanuniversität Leoben, Leoben, Austria, 2003.

64. Pinter, G.; Ladstätter, E.; Billinger, W.; Lang, R.W. Characterisation of the tensile fatigue behaviour of RTM-laminates by isocyclic stress–strain-diagrams. *Int. J. Fatigue* **2006**, *28*, 1277–1283. [CrossRef]

65. Berer, M.; Major, Z.; Pinter, G.; Constantinescu, D.M.; Marsavina, L. Investigation of the dynamic mechanical behavior of polyetheretherketone (PEEK) in the high stress tensile regime. *Mech. Time-Depend. Mater.* **2014**, *18*, 663–684. [CrossRef]

66. Tong, X.; Chen, X.; Xu, J.; Zheng, Y.; Zhi, S. The heat build-up of a polymer matrix composite under cyclic loading: Experimental assessment and numerical simulation. *Int. J. Fatigue* **2018**, *116*, 323–333. [CrossRef]

67. Gent, A.N. Elasticity. In *Engineering with Rubber: How to Design Rubber Components*, 3rd ed.; Gent, A.N., Ed.; Hanser Publications: Cincinnati, OH, USA, 2012.

68. Arbeiter, F.; Schrittesser, B.; Frank, A.; Berer, M.; Pinter, G. Cyclic tests on cracked round bars as a quick tool to assess the long term behaviour of thermoplastics and elastomers. *Polym. Test.* **2015**, *45*, 83–92. [CrossRef]

69. Wang, C.; Stiller, T.; Hausberger, A.; Pinter, G.; Grün, F.; Schwarz, T. Correlation of Tribological Behavior and Fatigue Properties of Filled and Unfilled TPUs. *Lubricants* **2019**, *7*, 60. [CrossRef]

70. Wang, C.; Hausberger, A.; Berer, M.; Pinter, G.; Grün, F.; Schwarz, T. An investigation of fretting behavior of thermoplastic polyurethane for mechanical seal application. *Polym. Test.* **2018**, *72*, 271–284. [CrossRef]

71. Frank, A.; Freimann, W.; Pinter, G.; Lang, R.W. A fracture mechanics concept for the accelerated characterization of creep crack growth in PE-HD pipe grades. *Eng. Fract. Mech.* **2009**, *76*, 2780–2787. [CrossRef]

72. Greensmith, H.W. Rupture of rubber. X. The change in stored energy on making a small cut in a test piece held in simple extension. *J. Appl. Polym. Sci.* **1963**, *7*, 993–1002. [CrossRef]

73. Scibetta, M.; Chaouadi, R.; Van Walle, E. Fracture toughness analysis of circumferentially-cracked round bars. *Int. J. Fract.* **2000**, *104*, 145–168. [CrossRef]